RADAR

Research Archive and Digital Asset Repository

OXFORD BROOKES UNIVERSITY

Silane surface modification of boron carbide in epoxy composites

David D. S. Rodrigues (2013)

https://radar.brookes.ac.uk/radar/items/346c2ce6-cadb-4612-a666-e796b852ddeb/1/

WWW.BROOKES.AC.UK/GO/RADAR

Silane Surface Modification
of Boron Carbide
in Epoxy Composites

by David D S Rodrigues

OXFORD BROOKES UNIVERSITY

Science & Technology Facilities Council

Oxford Brookes University

A thesis submitted in partial fulfilment of the requirements of
the award of Doctor of Philosophy
September 2013

ABSTRACT

Boron carbide (BC) is used as a radiation absorber in the nuclear industry and particle physics experimentation. BC parts are generally manufactured through a sintering process, which limits the size and shape of components and imparts high cost. On the other hand, a polymeric matrix composite (PMC) with high BC content can be easily obtained through a moulding process, providing lower cost parts whilst accommodating increased complexity of geometry and size. Despite the importance of BC in industry, only a few studies have been carried out on epoxy PMCs containing only small amounts of BC. The lack of adhesion exhibited between BC and resin led to limited mechanical strength and durability. Hence, silane surface modification of BC particles was conducted with γ−glycidoxypropyltrimethoxysilane (GPS) as an aqueous solution to attain an 80%wt BC-epoxy PMC with improved strength and durability. Surface analysis on BC, and physical-chemical characterisation, mechanical testing and durability studies on the PMCs were conducted to better understand the effect of silane treatment and parameters (pH, %GPS). Fourier Transform Infrared (FTIR) and X-ray Photoelectron Spectroscopy (XPS) confirmed boron oxide and hydroxyl groups on the native surface which can offer a means of attachment to the silane. Surface modification was more evident using higher GPS concentrations in pH5-7 solutions. These parameters were found to strongly affect the silane layer structure (crosslinking, density, thickness and coverage). Also, IR bands corresponding to B-O-Si were evident which are typically found on borosilicate glass. Increased hydrophobicity and adhesive wettability confirmed by sessile drop method, led to PMCs with higher density, lower porosity and reduced water permeability. Mechanical testing by means of three-point bending (3PB), Iosipescu and double v-notch (DVN) tests demonstrated correlations between strength improvement and the various surface modifications and physical-chemical characterisation. This was supported by SEM of the PMC failure surfaces, showing enhanced adhesion through distinguishable layers of epoxy and small BC particle clusters, remaining attached to the larger particles. This was due to a better adhesive wetting and stronger interfacial bonding. Optimal mechanical properties and durability were generally obtained using 0.5-1%GPS in pH5 solutions due to the combination of high initial strength and lower reductions in strength after ageing (water immersion).

Keywords: Boron Carbide; Silane Treatment; Surface Analysis; Epoxy; Composite; Mechanical Strength; Durability.

ACKNOWLEDGMENTS

Finally, I would like to thank Carla and all my family for their unconditional love and support throughout this project.

CONTENTS

LIST OF SYMBOLS AND ABREVIATIONS

Al	Aluminium
^{10}B	Boron isotope
B	Boron element
B_4C / $B_{12}C_3$	Boron carbide
B_2O_3	Boron oxide
C	Carbon element / Diamond
Ca	Calcium element
$C_3H_8O_3$	Glycerol
CH_2I_2	Diiodomethane
Fe	Iron element
H_2O	Water
HBO_2	Oxoborinic acid
H_3BO_3	Boric acid
HNO_3	Nitric acid
H_2SO_4	Sulphuric acid
He	Helium element
$K^{10}BF_4$	^{10}B potassium fluoroborate salt
Li	Lithium element
Na	Sodium element
Ni	Niquel element
O	Oxygen element
Si	Silicon element
SiC	Silicon carbide

α	Degree of conversion
γ	Interfacial tension
θ	Contact angle
π_a	Open Porosity
ρ	Density
Φ	Work function of the spectrometer
$+$	Lewis acid component
$-$	Lewis base component
%wt	Percentage by weight
D	Diffusion coefficient
d	Thickness of silane layer
E'	Storage modulus
E''	Loss modulus
E_u	Energy applied onto the surface with corona discharge
F	Load
f_{GPS}	Percentage of surface covered by silane layer
G_a	Gibbs free energy
h	Height of the test specimen
hv	Energy of radiation source
I	Intensity of the XPS peaks
M_S	Maximum moisture uptake
M_t	Moisture uptake

m	mass
n	Number of passes over substrate surface area, with corona discharge
L	Length of the corona electrode
pH	activity / concentration of the hydrogen ion, $(-\log_{10}[H^+])$
phr	Parts per hundred resin
P	Permeability coefficient
R_{tr}	Rupture strength
s	Span distance
t	Shear strength
t_{xy}	Tensile strength
$\tan\delta$	Loss factor $(=E''/E')$
T_g	Glass transition temperature
v	Treatment velocity of the substrate versus energy source
W_a	Work of Adhesion
w	Width of the test specimen

2k	Two-component
3PB	Three-Point Bending
AAMS	N-(2-aminoethyl)-aminopropyltrimethoxysilane
AB	Lewis acid-base component
AHEW	Amine Hydrogen Equivalent Weigh
APES	Aminopropyltriethoxysilane
ARXPS	Angle Resolved X-Ray Photoelectron Spectroscopy
ATR	Attenuated Total Reflectance
ATSDR	Agency for Toxic Substances and Disease Registry
BC	Boron Carbide
BE	Binding energy
BN	Boron Nitride
BS	British Standard
BSE	Back Scattering Electron
CAGR	Compounded Annual Growth Rate
CAS	Chemical abstracts service division of the American Chemical Society
CDT	Corona Dischage Treatment
CRCWI	Cooperative Research Centre for Wood Innovations
CSIRO	Commonwealth Scientific and Industrial Research Organisation
CT	Coatings Technology
DMA	Dynamic Mechanical Thermal Analysis
DGEBA	Diglycedyl Ether Bisphenol-A
DGEBF	Diglycedyl Ether Bisphenol-F
DTGS	Deuterated Triglycine Sulfate
DVN	Double V-Notch
ECN	Epoxy Cresol Novolac
EDX	Energy Dispersive X-ray Spectroscopy
EIS	Electrochemical Impedance Spectroscopy
EP	Epoxy
EPN	Epoxy Phenol Novolac
EEW	Epoxy Equivalent Weight
FPL	Forest Products Laboratory (sulfuric acid/sodium dichromate etching for Al)
FTIR	Fourier Transform Infrared spectroscopy

FT-NMR	Fourier Transform Nuclear Magnetic Resonance Spectroscopy
GPS	Glycidyloxypropyl-trimethoxysilane
HDPE	High density polyethylene
HIP	Hot Isostatic Pressing
HP	Hot Pressing
HPA	Hummel Polymers and Additives
HTPB	Hydroxyl-terminated polybutadiene
HV	Vickers Hardness Number
IMFP	Inelastic Mean Free Path
IR	InfraRed
ISIS	Pulsed neutron and muon source at the Rutherford Appleton Laboratory
ISO	International Organization for Standardization
IUPAC	International Union of Pure and Applied Chemistry
KE	Kinetic Energy
LDPE	Low Density Polyethylene
LW `	Lifshitz-van der Waals / dispersive component
MSDS	Material Safety Data Sheet
MMC	Metal Matrix Composite
MPS	Methacryloxypropyltrimethoxysilane
MTES	Methyltriethoxysilane
MW	Molecular weigth
OM	Optical Miscroscopy
OR	Alkoxy group of the silane
PCS	Photon Correlation Spectroscopy
PDMS	Polydimethysiloxane
PMC	Polymer Matrix Composite
PMMA	Poly(methyl-methacrylate)
PP	Polypropylene
PSA	Pressure Sensitive Adhesive
PTFE	Polytetrafluoroethylene
PVC	Polyvinyl chloride
PVDF	Polyvinylidene fluoride
RAIR	Reflection-Absorption Infrared Spectroscopy
RAL	Rutherford Appleton Laboratory
RH	Relative Humidity
SE	Secondary electron
SCA	Silane Coupling agent
SEM	Scanning Electron Microscopy
SFE	Surface Free Energy
SICOR	SIlane-on-CORona
SIMS	Ion Mass Spectrometry
STFC	Science and Technology Facilities Council
TEPA	Tetraethylenepentamine
TEM	Transmission Electron Microscopy
ToF	Time-of-Flight
TOFA	Tall-oil Fatty acids reaction products
TPO	Thermoplastic Polyolefin
UHMWPE	Ultra-high molecular weight polyethylene
UK	United Kingdom
VP	Variable pressure

VTES	Vinyltriethoxysilane
XPS	X-ray Photoelectron Spectroscopy
XRD	X-ray Diffraction
X	Organofunctional group of the silane
Y	Propylene chain of the silane

LIST OF FIGURES

LIST OF TABLES

CHAPTER 1 – INTRODUCTION

1.1 Background

ISIS is one of the UK's major scientific research facilities, located at the Rutherford Appleton Laboratory (RAL) and operated by the Science and Technology Facilities Council (STFC). This facility has the brightest spallation neutron source in the world, which uses muon spectroscopy and neutron scattering to study the structure and behaviour of materials (STFC 2009). The neutrons are created by the impact of accelerating protons with a heavy tungsten metal target which are channelled through guides, or beamlines, to penetrate the matter, being only deflected from the nuclei of atoms. The statistical accumulation of the deflected neutrons at different positions and the loss or gain of energy can provide information on the structure and dynamic behaviour of the material, at a microscopic scale ranging from the subatomic to the macromolecular. However, neutrons are a dangerous form of radiation and consequently the target and beamlines must be heavily shielded.

Boron carbide (BC) is a non-oxide ceramic material with the ability to absorb neutrons without forming long lived radio nuclides. Hence, it is used by RAL as a neutron absorber and shielding material, both to protect humans and sensitive instruments from stray neutron radiation. BC is typically employed in highly sensitive instruments where size is limited (e.g. space applications), due to its specific high neutron absorption/low scattering cross-sections of ^{10}B isotope and relatively low production cost. This material is also distinctive due to its high hardness, being only behind that of cubic boron nitride and diamond. Other properties include low thermal conductivity, low susceptibility to thermal shock failure, high chemical resistance and high brittleness (Thévenot 1990, Bigdeloo and Hadian 2009, Toumanov 2003). Neutron absorber and shielding parts can be produced using the solid state sinter process. This involves heating the boron carbide powder in a furnace to a specific temperature just below its melting point where upon the particles adhere to each other (Toumanov 2003). BC is also one of the most difficult materials to sinter due to its covalent nature, low mobility, high melting point, high hardness and brittle

character (Thévenot 1990, Wang *et al.* 2005, Zakhariev *et al.* 2009).

Recently, the global demand for BC has been healthy increasing in matured regions such as US, Japan and Europe, with the former as the leading global producer and the latter showing the greatest compounded annual growth rate (CAGR). Boron carbide and boron nitride markets are expected to show a growth of 3.1 thousand metric tonnes per year by 2017, despite the lower demand within the metal and minerals industry due to the impact of the global economic recession. This demand results mainly from the material, automotive, heavy, and aerospace industries. The initial growth will be from the outcome of newer production processes and methods used in end-use industries of fibreglass, ceramics, electronic device, refractory coatings and others. Other markets, especially in China, Turkey, Russia and Chile are also expected to show sustainable growth as a result of the high cost from labour and waste treatment (Global Industry Analysts 2012).

An alternative to sintered boron carbide is a high BC content epoxy polymeric matrix composite, made through a moulding process to obtain lower cost parts with increased complexity of geometry and size (Suresha *et al.* 2009). Epoxy resins are widely used as coatings, structural adhesives and polymeric matrix composites (PMC). They are probably the most versatile family of thermosetting polymers exhibiting an attractive combination of properties (processing, mechanical, chemical, thermal) and excellent adhesion to different materials (Table 4.1). For a low cost PMC using moulding process, the resin must have: low viscosity (350–1500 cP); suitable working time (1–2 hour); room temperature cure; reduced shrinkage (0.00010–0.0051 in/in); no pressure required; good mechanical strength, such as, flexural (~70 MPa), tensile (~50 MPa) and shear (~30 Mpa); Young modulus of approximately $1 - 2$ GPa; glass transition temperature above service conditions (23℃); and resistance to water and radiation. All properties that were taken in consideration for the selection of the adhesive are described in Table 4.5. These polymers have good durability to aggressive environments, such as, exposure to gamma rays and neutron radiation (Okuno 2005, Huang *et al.* 2011, Huang *et al.* 2012). Hence, these resins are highly valued by nuclear and aerospace industries. The resin can exist in several forms (bisphenol-A, bisphenol-F and phenol/cresol NOVOLAC) and is primarily used in combination with a curing agent for both cold- and hot-setting. During this process the resin is crosslinked and a three-dimensional and insoluble network is obtained. The final properties of the cured material results from the nature of resin and curing agent, the cure process, degree of conversion and crosslinking and other factors (Petrie 2000).

1.2 Research Needs

Polymeric matrix composites are increasingly replacing conventional engineering materials due to the ability to tailor properties for a specific application. PMC consist of a reinforcement embedded in a resilient polymetomadas emric matrix (resin). The reinforcement is generally fibres, metallic strands, filaments or particles bonded together with polymer resins. These materials are normally sheet or fibre-wound forms dispersed in a thermosetting or thermoplastic resin. The function of the polymer is to bond the reinforcement together and transmit the load between them. The composites are built up from a complex interplay of physical and chemical factors that occur at the interface or interphase region between the resin and the inorganic material (Plueddemann 1991). These factors (e.g. chemical nature, size, shape, dispersion, orientation), as well as, the reinforcement and resin determines the macroscopic properties of the composite, such as, physical and mechanical strength, wear resistance, coefficient of expansion, concentration gradients and durability (Petrie 2000, Silva and Ochsner 2007, Avella *et al.* 2001). When micro or nanoparticles are used in PMC, they can be incorporated into the resin using a mechanical process in order to disperse them in the matrix and avoid agglomeration. Generally, the process requires the use of high shear rates or a high intensity ultrasonic liquid processor (Wang *et al.* 2001, Rodgers *et al.* 2005, Bhattacharya *et al.* 2008). The amount of particles used in the polymer matrix is also a key parameter to obtain a material with a range of properties required for a specific application (Abenojar *et al.* 2009a, Abenojar *et al.* 2009b). Furthermore, the morphology of the particles can have a great influence on the strength of the composite, acting as stress concentrators and micro-crack initiators or crack stoppers (Abenojar *et al.* 2009a, Abenojar *et al.* 2009b, Shi *et al.* 2006). However, composites can be costly to make and their long-term properties are not easy to predict. Regardless of the potential of the PMC, many companies and government agencies only use them in a limited number of well-proven applications.

Despite the importance of boron carbide in the industry, only a few studies have been performed, typically using small amounts of BC as a filler in epoxy resins. These composites have also been used as a neutron shielding material on the outside of nuclear reactors to prevent stray radiation escaping, and in various components of neutron spectrometers, such as, shielding blocks, bricks, beam narrowers and stoppers (Huang *et al.* 2011, Huang *et al.* 2012, Pugh and Hendy 1985). Some attempts have also been made

to obtain a PMC reinforced with boron carbide particulate for ballistic armour applications. An epoxy resin was used as a binder, wherein the BC powder exhibits a particle size distribution in which some of the particles exhibit a particle size of 100 μm or more and some have a particle size of 50 μm or less (Canfer and Robertson 2010). Furthermore, a study was conducted to evaluate the effects on the curing and mechanical properties of the BC-Epoxy composite using small particle concentrations and different size distributions (Abenojar *et al.* 2009b). In this case the BC acted as an accelerator or retardant in the cure depending on the amount and size of the particles, without affecting the degree of conversion. However, a shift in the glass transition temperature to lower values was observed due to changes in the crosslinking. The particles tend to deposit and agglomerate due to the low viscosity of the resin. The use of smaller amounts of BC particles has led to an increase of bending strength. Nevertheless, the poor adhesion between the BC and epoxy was demonstrated during wear tests. Another study also evaluated the behaviour of BC particulate filled epoxy composites as a three-body abrasive wear material, using different amounts of filler and under diverse loads and abrading distances (Suresha *et al.* 2009). Improved performance of the composites was achieved using low amount of boron carbide in epoxy, as a result of a more uniform dispersion of filler and better adhesion between the matrix and the BC. Whereas, agglomeration of the matrix and poor adhesion was observed with an higher amount of BC. Therefore, the lack of adhesion exhibited between BC and the epoxy resin leads to a composite with limited mechanical strength and durability. In addition in the last decade, these composites have been more frequently exposed to even harsher environments (Wang *et al.* 2006a, Wang *et al.* 2006b), such as, extreme temperature high-speed, high radiation and high-erosion, etc.

1.3 Hypotheses

Silane coupling agents (SCA) are one means of chemical treatment used to enhance adhesion between a polymer and an inorganic material, by modifying the filler surface and the bonding process at the interface. The result is a chemical bridge between the materials with higher hydrophobicity to prevent moisture penetration, better transfer of stress from the resin to the filler, more efficient dispersion of the filler and reduction of the apparent viscosity of the uncured system. Silane treated products can therefore exhibit improved performance and durability (Plueddemann 1991, Abenojar *et al.* 2009a). The success of the silane treatment is highly dependent on a number of preparation and application

parameters. These include solution pH, silane concentration, nature of the solvent, hydrolysis time, application method, drying time/temperature and time lag between surface treatment and bonding. The hydrolysis and condensation are affected by the hydrolytic stability of the silane in solution, which depends greatly on the nature of the solvent, pH and silane concentration. Furthermore, these processes are dynamic and consequently they depend on the age of the solution. Also, it has been observed that the performance of the final composite is generally improved when only a small concentration of coupling agent is used (0.01 to 2%). Drying time and temperature will affect the degree of the oligomerisation and crosslinking of the silane and, as a result, the final properties of the composite (Abel *et al.* 2006, Parker and MacLachlan 2000, Matisons 2009, Ishida and Miller 1984, Tesoro and Wu 1991). Despite the considerable amount of experience in the use of silanes as coupling agents, most, if not all, current employment is based on empirically determined procedures. Indeed, the most effective preparation and application procedures, as well as, the mechanisms by which the silanes promote bond strength and durability are not fully understood.

Extensive research has been conducted to improve bond strength between glass fibre and the resin in reinforced polymer composites. SCA was then successfully used to enhance metal-adhesive bonding. Previous investigation have suggested that a metal–oxygen–silicon bond is formed on silane treated steel, iron and aluminium surfaces (Van Ooij 2000, Franquet *et al.* 2003, Hu *et al.* 2006). In the case of boron carbide no studies using silanes have been reported, despite its importance to the industry.

1.4 Objectives

In this work, a novel approach of surface treatment for BC was conducted using SCA in a attempt to enhance adhesion to epoxy and other properties, and to improve our knowledge of silane technology. A research project was conducted to understand the relationships between the silane treatment parameters and the modified surface chemistry of the BC. Moreover, the interfacial adhesion between the epoxy resin and the silanised ceramic material was investigated through mechanical and durability testing of a BC particle-epoxy polymeric matrix composite (BC-epoxy PMC). The use of corona was considered both as a standard surface treatment for the BC and also prior to silane application in an attempt to promote attachment for the SCA and increase its effectiveness. The experimental investigation was conducted as a function of the surface conditions (as received and corona

treated), treatment conditions (solution pH and silane concentration) and environment conditions (standard atmosphere and immersion in water). The objectives within the scope of this study were:

1. Review of surface treatment technology, silane coupling agents and surface chemistry analysis methods;

2. Study the effect of the various silane treatment parameters on the BC particle surface chemistry;

3. Conduct physical-chemical characterisation of the BC-epoxy PMC and its components;

4. Evaluate the effect of different silane treatments on the mechanical properties of the PMC;

5. Evaluate the durability of the proposed BC-epoxy PMC;

6. Analyse and define the adhesion phenomena on the ceramic surface in the composite matrix;

7. Define the optimal silane treatment conditions for the BC-epoxy PMC explored in aims (3), (4), (5) and (6).

1.5 Outline of Thesis

The thesis is composed of eight chapters which can be organised in three major parts: Literature review; Experimental and analytical research; Discussion, conclusions and further recommendations.

Part 1 – Literature review

Chapter 2 describes the main review of the research which focus on adhesion theories, silane coupling agents, surface treatments and their combinations in order to promote adhesion and other properties.

Chapter 3 gives a insight of BC as an advanced material for industry, chemical composition and structure, surface chemistry, synthesis, bulk properties, limitations for the manufacturing components and consequently the use as composites.

Chapter 4 presents detailed information about the importance of the epoxy adhesives for polymer matrix composites, type of resins and curing agents, formulations, cure

mechanisms, and properties required for moulding process.

Part 2 – Experimental and analytical research

Chapter 5 describes details of the materials (boron carbide, epoxy adhesive and silane coupling agent), surface treatments conditions (silane solutions and corona discharge), surface analysis techniques for the BC (FTIR, Wettability, XPS, SEM/OM), characterisation methods for the adhesive and composites (DMA, FTIR, Wettability, Bulk Density, Open Porosity, Water Absorption, Mechanical Testing, Weathering, SEM) and finally the experimental program involved in this research work.

Chapter 6 presents the most relevant results from: elemental, physical-chemical, surface free energy and morphological characterisation of the untreated/treated BC to evaluate the silane surface modification; chemical, cure kinetics, rheological and wettability studies of the adhesive to better understand its behaviour on the manufacture process and mechanical properties of the composites; physical-chemical, mechanical characterisation and environmental durability studies of the PMCs and constituent materials.

Part 3 – Discussion, Conclusions and Further work

Chapter 7 gives an empirical correlation of the research data that was presented in the previous chapters, in particular between the BC surface properties provided from the various silane treatments and the physical-chemical properties, mechanical strength and durability of the epoxy PMCs.

Chapter 8 presents the main conclusions of the research and proposes future recommendations related to evaluation of the chemistry, enhanced adhesion and hydrophobicity of the BC surface with the various silane treatments, and to the performance and durability of the silanised composites.

CHAPTER 2 – ASPECTS OF ADHESION

2.1 Introduction

Epoxy adhesives are widely used in structural bonded joints and polymeric matrix composites (PMC) for advanced applications. In the case of PMC, the reinforcement is embedded in a resilient resin. Therefore, the mechanical strength of the composite is directly related to the bond nature between the materials, known as adhesion. This can be defined as the attraction between two materials or more usefully as the energy required to separate them and create two separate interfaces (Kinloch 1987).

The interface or surface can be defined together as the plane where a sudden change of the physio-chemical properties (composition, density, structure or orientation) occurs over a distance (Hudson 1998). Generally, the term interface is normally used when two condensed phases are present (liquid-liquid, liquid-solid and solid-solid), whereas surface is usually applied to solid-vapour or liquid-vapour phases. On the other hand, the interphase is a phase with a specific thickness and distinct physical-chemical properties which has been formed from interactions occurring between the two phases. In this work, it is defined as the transition zone between the substrate surface (reinforcement) and bulk properties of the adhesive (resin) (Silva and Ochsner 2008).

Adhesion is perceived as a simple concept but actually covers a variety of processes that occur when materials are brought in contact. Consequently, different theories have been proposed reflecting the complexity of the phenomena (Schultz and Nardin 2003, Peterson 2005). Some of these are described in this work to fully understand the phenomena and to predict the performance and durability of a PMC. In particular, these include adhesive rheology, flow and deformation of the reinforcement, surface chemistry and wetting, mechanics and certain degradation processes.

2.2. Adhesion Theories

Several adhesion theories have been proposed reflecting the complexity of the phenomena. These include mechanical interlocking, interdiffusion or interpenetration, electrostatic, physisorption (dispersive), chemisorption (chemical bonding) and thermodynamic (Comyn 1997, Adams 2005). More typically, an individual mechanism can not fully explain the phenomena on its own and more likely there are several mechanisms contributing simultaneously to adhesion.

Mechanical interlocking suggests that the phenomena results from the penetration and keying of the adhesive into the surface irregularities of the substrate. Interlocking can be improved by increasing the surface roughness and therefore interfacial area. The surface topography plays an essential role in this mechanism, which explains the most significant bonding process on materials, such as, wood, textiles, and on some anodised metals and alloys (Allen 2005, Kinloch 1987). Good adhesion strength is attained through this mechanism, and is most effective when the applied force is perpendicular to the interface (Packham 2005).

The interdiffusion theory describes adhesion between different polymers, where their chains intermingle after contact at molecular level, eliminating the initial boundary. Thus, chain mobility and compatibility of the polymers are essential. The former can be promoted with temperature increase, solvents or plasticising agents, and the latter results from the chemical structure and specific interactions between the polymers. Nevertheless, this mechanism is rarely applicable due to the lack of solubility of the polymer chains (Comyn 2006).

The electrostatic theory proposes that attraction forces between two materials in contact result from the transfer of electrons from one to the other and the formation of an electrical double layer (Pocius 2002). This theory may only be applied to a few specific systems, due to the fact that most polymers are insulators (Comyn 1997).

The adsorption theory is generally accepted as the most important mechanism, and is always present to some extent (Warson and Finch 2001). This theory suggests that attractive forces arise from the interatomic and intermolecular interactions between the adhesive and substrate (Comyn 1997, Kinloch 1987). This mechanism can be differentiated into physisorption or chemisorption if the type of interactions are secondary forces or

chemical bonds, respectively (Allen 2005).

Secondary forces are weak and arise from the intimate contact between the molecules with slightly positive or negative charge regions (dipoles), known as van der Waals forces and hydrogen bonds. The former includes the Keesom, Debye and London forces. Hydrogen bonds result from Keesom forces between a hydrogen (slight positive charge) and a more electronegative atom (oxygen, nitrogen and fluorine). Also, acid-base interactions may occur when the donation of an electron pair from one molecule (Lewis base) to the other (Lewis acid) is possible. Physiorption is always present to a degree and plays a major contribution to the bond strength of polymeric systems, specially, when intimate interfacial contact is observed (Kinloch 1987).

Chemisorption theory suggests the formation of a covalent or ionic bond between the surface atoms or molecules of the substrate and adhesive, i.e., at the interface (Comyn 1997). This bond is shorter and stronger when compared to a secondary bond, as a result of the atoms or molecules of the two materials sharing or swapping electrons (Table 2.1). Thus, surfaces must to be in close proximity in order to react and maintain their chemical bond (Comyn 2006). Unfortunately, chemisorption is not commonly found when adhesives are involved, most of their interactions being polar or secondary valence bond in nature (Butt 2008).

Table 2.1 Chemical bonds length and energy (Kinloch 1987, Butt 2008, Comyn 2006, Kurmi and Sedha 2008).

Chemical bond		Length (nm)	Energy (kJ/mol)
Primary	Ionic	0.2 – 0.3	600 – 1100
	Covalent	0.1 – 0.2	60 – 710
	Metallic	0.3 – 0.5	10 – 650
Donor – acceptor	Brønsted acid – base interactions	–	≤ 1000
	Lewis acid – base interactions		≤ 80
Secondary	Hydrogen bonds	0.2	
	- involving fluorine		≤ 40
	- excluding fluorine		10 – 25
	van der Waals forces	0.4 – 0.5	
	- dipole – dipole (Keesom)		4 – 20
	- dipole – induced dipole (Debye)		< 2
	- dispersion (London)		0.08 – 40

The chemisorption and thermodynamic theories are closely related. Both rely upon chemical alterations of the surface, the former with the modification of the composition

and the latter with the change in the wettability or surface tension parameters (Chehimi et al. 2003).

Thermodynamic theory is extensively used in adhesion technology to evaluate molecular interactions at the interface. The adhesive generally behaves as a liquid during the bonding process and flows on the substrate surface, known as wetting. This phenomena can be defined as "macroscopic manifestations of molecular interactions between liquids and solids in direct contact at the interface between them" (Berg 1993). Good wetting is the ability of a liquid to spread spontaneously over a solid surface, which is absolutely essential for the molecules to be close enough to interact at nanoscale distance, and consequently achieve optimum adhesion. The wetting depends mostly on the surface tension of the liquid (γ_L) and the surface free energy (SFE) of the solid (γ_S). These properties are bulk thermodynamic parameters and do not explain the type of molecular interactions occurring between the phases involved. The work of adhesion, W_a, is the decrease of Gibbs free energy per unit area required to separate reversibly two phases initially in contact to form two new surfaces. This property indicates how the different types of intermolecular forces contribute to adhesion between condensed phases. In the case of a solid and liquid, W_a is defined by Dupré (Eq. 2.1) as the work required to separate a unit area of the solid-liquid interface (Packham 2005).

$$W_a = -\Delta G_a = \gamma_S + \gamma_L - \gamma_{SL} \tag{2.1}$$

Where G_a is the Gibbs free energy, γ_S and γ_L is the surface tension of the solid and the liquid, and γ_{LS} is the interfacial tension solid-liquid.

Several methods were proposed to determinate W_a and explain the molecular interactions that occurs at the interface (Good 1993, Comyn 1997). More recently, these interactions have been differentiated by dispersive or secondary forces (van der Waals) and accept-donor electron pair interactions (e.g. Lewis acid-base) (Berg 1993, Comyn 2006, Awaja *et al.* 2009). These interactions can be investigated by measurement of contact angles of a drop of liquid resting on the substrate, i.e., between the solid-liquid interface and liquid-vapour surface (Butt 2008).

2.3 Adhesion Promotion

The use of a suitable adhesive and application procedures, combined with a suitable surface treatment of the substrate, are essential to obtain good initial bond strength. Although a good knowledge of adhesives and application methods are a solid base in this field, the treatment of the substrate surface is very important or even essential in order to promote better adhesion for the real case. Surface treatments can range from a simple solvent cleaning to a complex multiple step procedure based on mechanical, physical or chemical processes. These procedures can remove contaminates, weak boundary layers, change the surface topography (Petrie 2006a) and modify the surface chemistry of the substrate. One of the most common physical processes is corona discharge, which is a variation of the plasma treatment that has been used to improve the adhesion on substrates with low or non-polar SFE through morphological and chemical modification. Nevertheless, long-term adhesive bonding is more difficult to attain, especially on the intended service life, and the use of coupling agents are required to overcome this situation. Generally, these compounds improve adhesion and promote water-resistant bonding by modifying the surface chemistry and consequently the interactions across the interface (Butt 2008). These agents illustrate an example of the chemiorption theory with the formation of covalent bonds between the coupling agent with both adhesive and substrate (Baker *et al.* 2002, Plueddemann 1991).

2.4 Silane Coupling Agents (SCA)

Silanes coupling agents are commonly used to improved strength and durability of adhesive joints and reinforced polymer matrix composites (PMC). Amino organofunctional silane was developed specifically to improve adhesion between glass-fibre reinforcements and phenolic resins in PMC (Plueddemann 1991). Methacrylate and vinyl organofunctional silanes were also formulated to overcome poor adhesion between glass-fibre and polyester resins. Great effort was conducted to understand the chemistry, adhesion mechanisms and the practical concepts behind the silane technology, which was mostly related to glass-fibre reinforced polyester and epoxy matrix composites (Plueddemann 1991). Further work was done to exploit interfacial water resistance provided by the silane coupling agent (SCA) to minimise the drastic loss of the adhesive strength of polymer systems when exposed to high moisture environments, as reported at that time by some studies (Ishida and Koenig 1978). Thus, other applications started to emerge with the development of new SCAs

incorporated in different polymer systems as adhesion promoters, release agents and corrosion protection for metal substrates (Plueddemann 1991). Phosphoric and chromium based treatments were intensively used at that time by the industry to improve corrosion resistance of metal substrates. However, high toxicity and carcinogenicity of these compounds represented too big a risk to public health and to the environment (ATSDR 2012, Adams 2005). Hence, extensive research was undertaken in the development of an alternative and more environmental-friendly silane surface treatments. Today, SCAs are largely used to improve corrosion resistance and adhesion between metals and polymers (Palanivel *et al.* 2003, van Ooij and Zhu 2006, Ferreira *et al.* 2004, van OoiJ 2004). Moreover, several SCAs have been developed since to obtain high strength polymer composites for intense applications and to improve bonding between adhesives and coatings to inorganic substrates, such as, glass, silicon minerals, metals, etc.

SCAs are normally used as an additive, primer or surface treatment according to the application approach. When incorporated as additives into the adhesive formulation, they are able to migrate to the interface, react with the inorganic substrate and form a stronger bond with the resin (Petrie 2006a, Comyn 2006, Abel and Watts 2009). However, the most effective approach is to promote adhesion directly onto the substrate through surface treatment, despite the requirement of an additional bonding procedure step (Bieleman 2008, Petrie 2006a, Cognard 2006). The SCA is normally applied directly as a solution onto the substrate. Improved adhesion is attained prior to adhesive bonding through modification of the substrate surface chemistry, where one end of the silane molecule is bonded to the inorganic material and the other is available to react with the polymer phase (Baker *et al.* 2003, Petrie 2006a, Plueddemann 1991). This dual reactivity of hybrid organic-inorganic silane structure can be tailored to provide chemical bridging between the adhesive and substrate, increased interfacial resistance to moisture and other chemical species, enhanced wettability and rheology, a stronger interphase of the inorganic and organic boundary layers, a more effective transfer of stress from the resin to the inorganic material, improved dispersion of the reinforcement in the matrix and reduced apparent viscosity of the system (Plueddemann 1991, Petrie 2006a, Baker *et al.* 2003).

2.4.1 Structure

A SCA is a silicon-based monomer possessing organic and inorganic functionality with generic name of organofunctional trialkoxysilane. The generic chemical structure is $Y_{(4-n)}$-Si-$(OR)_n$ (n = 1, 2, 3 or 4) where Si is the silicon in the centre of the molecule, OR is an hydrolysable alkoxy group, and Y is an non-hydrolysable organofunctional group. In our case, a trialkoxy silane (n = 3) was used, possessing the structure as shown in Fig. 2.1. The Y group is generally composed of an alkyl section and a reactive organic group that bonds to a specific resin (-$CH_2CH_2CH_2$-R'), where R' is a vinyl -$HC=CH_2$, amino -NH_2, chloride -Cl, isocyanate -NCO, epoxy -$CHOCH_2$ or mercapto -SH group. The hydrolysable alkoxy group enables attachment to the inorganic substrate in order to achieve the coupling effect, through methoxy -OCH_3, ethoxy -OC_2H_5, or acetoxy -$OCOCH_3$ groups. A silane molecule with bi-functional groups can form covalent bonds between the polymer and inorganic material, acting as a chemical bridge (Plueddemann 1991, Petrie 2006a, Comyn 1997). Selection of the SCA is generally accomplished by assuming the direct reaction and the formation of a covalent bond between the substrate and adhesive.
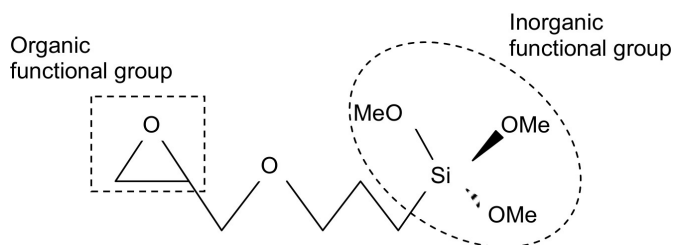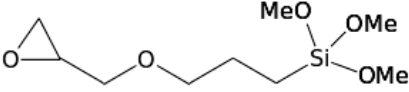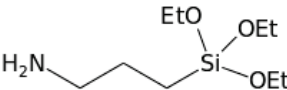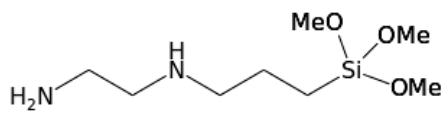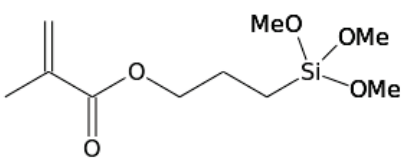
Figure 2.1 Chemical structure of an organosilane (Dow Corning 2005, Sigma-Aldrich 2010).

Therefore, several SCA are commercially available for a specific application by matching chemical reactivity of the organofunctional group, solubility of the alkoxy groups, structural characteristics (e.g. alkyl section), and possibly the thermal stability of the silane with the same parameters of the polymer structure (Plueddemann 1991, Cognard 2006). Generally, the initial approach is to select one coupling agent suitable within predicted categories as shown in Table 2.2, assuming a direct bond between the two materials.

Table 2.2 Structures and names of some commercially available silane coupling agents (Comyn 2006).

Functional Group	Structure and Name	CAS No.	Compatible Resin
Epoxy	γ-glycidoxypropyltrimethoxysilane (γ-GPS)	2530-83-8	Epoxy Phenolic
Amino	γ-aminopropyltriethoxysilane (γ-APES)	919-30-2	Nylon Epoxy Phenolic Melamine
	N-(2-aminoethyl)-aminopropyltrimethoxysilane (AAMS)	1760-24-3	Epoxy Phenolic Melamine
Methacryl	γ-methacryloxypropyltrimethoxysilane (γ-MPS)	2530-85-0	Styrene Polyester

2.4.2 Solution and Surface Reactions

An SCA must first hydrolyse and condensate in order to promote adhesion between the organic and inorganic material. Initially, the alkoxy groups convert to reactive acidic silanol groups ($\equiv$SiOH) with the formation of a free alcohol as a by-product (reaction 2.1). This process occurs during the preparation of the silane as an aqueous or alcohol-water solution, or by direct reaction with the residual water on the inorganic surface.

$$(2.1)$$
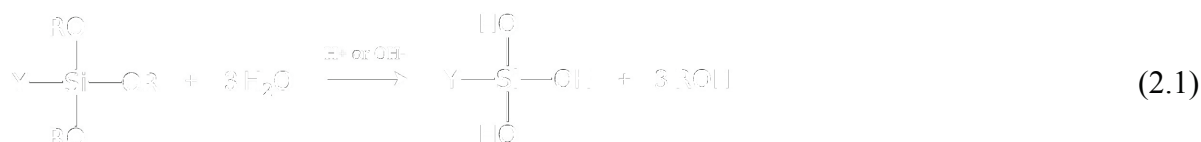
This process involves three steps, which become faster as the steric hindrance experienced by the water molecule decreases with the conversion of the alkoxy to hydroxyl groups in silane structure (Chambers *et al.* 1993). After hydrolysis, the silanol groups react with

adjacent silane molecules in solution to form dimers through either water (dehydration) or alcohol condensation according to the reaction 2.2.

$$(2.2)$$

$$(2.3)$$
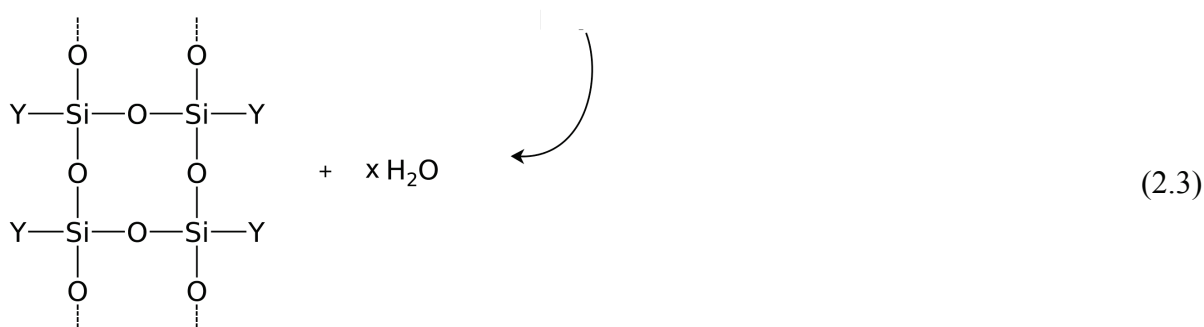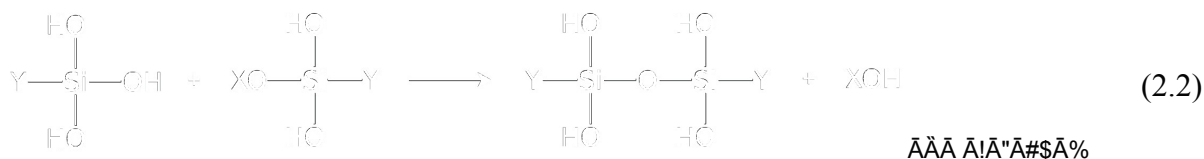
The dimers can also condense to higher molecular weight species (oligomers) possessing a branched hydrophobic structure (reaction 2.3) as a result of the formation of known as a siloxane bonds (–Si-O-Si–). When in contact with the substrate, the hydrolysed species interact with the hydroxyl groups present on the inorganic surface through hydrogen bonding. Through a condensation reaction, a covalent bond is probably formed between the silane and inorganic substrate (reaction 2.4), together with the release of water as a side product (Palanivel *et al.* 2003, Zhu and van Ooij 2004). Thus, this process is more effective on substrates with more hydroxyl groups on the surface.

$$(2.4)$$
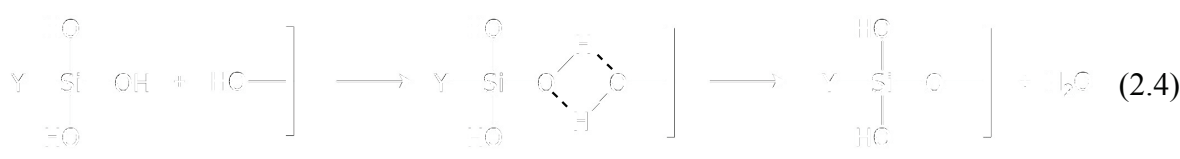
The condensation of the hydrolysed molecules on an inorganic surface result in the formation of a branched molecular structure (Fig. 2.2) that can range from a monolayer (one molecular thickness) to a multilayer structure. The latter exhibits a more or less tight polysiloxane network that becomes more diffuse away from the surface (van Ooij *et al.* 2006, Zhu and van Ooij 2004). Heating is applied to avoid the reversible process of the hydrolysis and to promote the formation of the polysiloxane network on the surface.
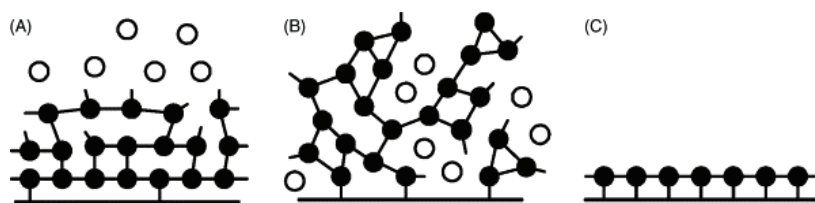
Figure 2.2 Schematic illustration of (a) multilayer, (b) three-dimensional polymerisation and (c) monolayer of silane on surfaces. ● – chemically or ○ – physically adsorbed molecules (Kudo *et al.* 2008).

Ideally, a well defined oriented monolayer should provide the best results, i.e., a one molecular thickness coating (Fig. 2.2c) which bulk properties does not affect the overall performance of the system. Normally, a thicker film (50 to 100 nm) is obtained with the silane molecules more or less randomly oriented (Fig. 2.2a,b). This fact is related to most silanes possessing a relatively short alkyl chain in their chemical structure. In the case of γ-GPS, the silane typically adsorbs in the form of a multilayer structure (Fig. 2.2a) consisting of between 5 and 25 molecular layers on the surface, along with approximately 50% of the organofunctional groups oriented outward (Kinloch and Watts 2006). Despite the stronger covalent bonds formed across the interface through silane molecular bridging, a thicker and more open film (Fig. 2.2b) may lead to cohesive failure of a weak polysiloxane network, as well as, water penetration through the structure, hydrolysis of the siloxane bonds and interfacial disbonding (Kinloch and Watts 2006, Honkanen *et al.* 2011, Xu 2004). Moreover, the morphology of polysiloxane structure and type of interaction with the substrate depends on several application parameters used for the silane solution. (Van Ooij and Sabata 1991).

2.4.3 Application Parameters

The effectiveness of the treatment depends on the structure and functionality of the silane, nature of the resin and the substrate surface (system), application parameters, and adhesion mechanisms involved during bonding process. Nevertheless for a particular system and silane, the efficiency of the surface treatment is highly dependent on a number of application parameters. The hydrolysis and condensation are affected by the hydrolytic stability of the silane in solution, which depends greatly on the solvent nature, pH values and silane concentration (Ishida and Miller 1984, Miller and Ishida 1986, Naviroj *et al.*

1984, Graf et al. 1984, Plueddemann 1991). Furthermore, these processes are dynamic and consequently they depend on the age of the solution (hydrolysis time). It has been observed that the final properties of the system are generally improved when a small concentration of the silane is used. These factors, as well as, pH and drying time/temperature, will affect the degree of the oligomerisation and crosslinking of a particular silane and as a result the final properties of the composite. Also, the time elapsed between surface treatment and bonding was found to influence the durability of the system due to the deterioration in silane surface 'activity' during storage conditions (Abel *et al.* 2006, Parker and MacLachlan 2000, Matisons 2009). Thus, no one set of optimised parameters can be universally applied to achieve optimum strength and durability for all types of substrates and resins. Despite the considerable amount of experience in the use of silane coupling agents for adhesion promotion, most if not all, their current employment is based on empirically determined formulations and application procedures. Therefore, the most efficient application methods, along with the mechanisms by which these agents enhance the bond strength and durability, are not fully understood (Abel *et al.* 2006). Hence, surface analysis has been used as a driving tool to characterise the surface chemistry and topography of the substrates, and to identify the interaction mechanisms promoted by an SCA at the interface (Riekerink *et al.* 2001). Furthermore, several mechanical test methods have been used to determine the adhesive bond strength and durability of silane treated systems, which are critical to predict the lifetime of a structure or composite in service environments.

An early review of studies on silanes to improve adhesion in inorganic reinforced PMCs concludes that optimum application conditions for the treatment correspond to maximum hydrolysis of the silane and minimum condensation of the hydrolysed species (Tesoro and Wu 1991). Extent and kinetics of these processes were found to be affected by the solvent nature, pH value, ageing time, and silane concentration and structure. The reviewed studies agreed that molecular bridging of an SCA is theoretically achieved by the formation of a siloxane bond on the substrate surface and the interaction of the organofunctional group with the resin through chemisorption or other adhesion mechanism. Also, other important factors were considered important to take into account during the silane treatment, such as, microstructure, morphology and mechanical properties of the interphase regions.

Another work has showed that the type and number of alkoxy groups in the structure will determine the silane solubility and amount of water required to achieve full hydrolysis (Miller and Berg 2003). Silane treatments were performed on glass beads for a reinforced thermoplastic polymeric matrix (polyvinyl butyral). Two different sets of silanes were used, each with a similar organofunctional group but different number of alkoxy groups. Mechanical and wettability tests showed that di- and tri-alkoxy silanes provided a more effective surface modification and superior adhesion strength than that of mono-alkoxy structures due to the higher number of reactive groups available to interact with the inorganic material. Moreover, research has showed that the length of the alkyl section between the silicon (Si) atom and the organofunctional group (X) also affects the hydrolysis (Xie *et al.* 2010). In the case of a methacrylatealkylsilane in acetone-water solution at pH4, the hydrolysis rate decreased 20 fold changing a methyl to a propyl section (Fig.2.3). The shorter length promotes higher reactivity of methoxy groups as a result of the stronger electron interaction between the methacrylate (X) and the Si atom, known as the "α-effect" of silanes. This effect can also justify the higher reactivity of the α-aminoalkyl silanes, where the interaction between the free electron pair of the nitrogen and Si atom weakens the Si-O-Me bonds.

| (a) | (b) | (c) |
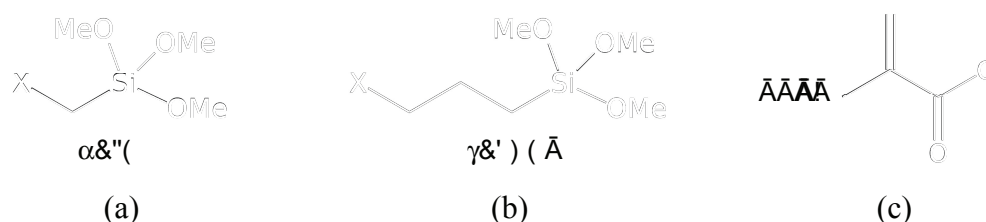
Figure 2.3 (a) α-methacryloxymethyl-trimethoxy silane, (b) β-methacryloxypropyl-trimethoxy silane, and (c) methacrylate group, X.

Also, different alkyl-substituted trialkoxysilane in water-acetone solutions and a 2.5% γ-GPS in aqueous solution were studied by means of Fourier transformation infrared spectroscopy (FTIR) and titration (Xue *et al.* 1991). The hydrolysis rate was higher with more acidic solutions (pH3.5 and pH4), smaller alkoxy groups, and also (but less evident) with smaller alkyl sections when in the presence of the organic solvent. In contrast, the condensation was slower for moderate acidic solutions (pH4). Also, a decrease in concentration of the epoxy groups was confirmed as a result of the interactions with water and silanol group. The former was affected by the solution pH and exhibited a slightly faster rate as result of the excess of water present in solution. This fact results from the

hydrolysis being a equilibrium process as showed by reaction 2.5. According to the Chatelier's principle, the system in a aqueous solution shifts towards the hydrolysis of the silane to counteract the high concentration of water and establish a new equilibrium.

(2.5)

Optimal application parameters for improved adhesion on aluminium using 1% γ-MPS aqueous solution at pH 4 were investigated through Attenuated Total Reflectance (ATR) and Reflection-Absorption Infrared (RAIR) FTIR (Pantoja *et al.* 2009). The hydrolysis and condensation was evaluated through the characteristic bands attributed to Si–O–C, Si–OH and Si–O–Si vibration modes. Hydrolysis times between 45 and 60 minutes promoted the highest amount of Si–O–Al bonds. Notably, a complex relationship was found between the hydrolysis, and immersion / drying time in order to optimise the silane treatment.

The effect of the application parameters on hydrolysis, condensation and molecular structure of γ-GPS on aluminium was investigated by means of Fourier-Transform Nuclear Magnetic Resonance (FT-NMR), Raman IR and FTIR (Bertelsen and Boerio 1999, Bertelsen and Boerio 2001). Hydrolysis was very rapid in a 1% γ-GPS deuterium oxide solution (34 min) and more slowly in a 25% of silane in aqueous solution (45–60 min). A faster process was achieved (15–30 min) by lowering the solution pH. In contrast, the condensation process was slow in a 10% γ-GPS aqueous solution (20 h). Silane films showed a lower water content and higher crosslinking with an increase in the drying temperature. Unfortunately, oxidation/degradation of the epoxy ring to a carbonyl group was also confirmed. This process was more evident at 180ºC, leading to a decrease of the epoxy rings available to bond with the adhesive and probably to a less effective silane treatment.

The adsorption of a 1% γ-GPS aqueous solution on FPL-etched aluminium was investigated by means of FTIR grazing-angle (Underhill *et al.* 1998). The presence of chemisorbed and physisorbed species on the surface was confirmed at the Si–O–X region of the spectra, with the latter more present at higher pH. Hydrolysis time and solution pH had no effect on the amount of the adsorbed species on the surface, which was only

affected by the silane concentration. Hence, the proposed adsorption mechanism did not involve the direct interaction of silane with the aluminium but with adventitious carbon found on all surfaces.

A different adsorption mechanism was observed in the absence of water with a 2% γ-GPS methanolic solution applied on a iron substrate (Davis and Watts 1996). X-ray photoelectron spectroscopy (XPS) identified the existence of a thin uniform layer on the surface (1.7 nm of thickness). Whereas, Time-of-Flight Secondary Ion Mass Spectrometry (ToF-SIMS) confirmed the presence of a more complex and randomly orientated polysiloxane structure and the formation of Fe-O-Si covalent bond. This indicates that a discrete layer, directly bonded to the iron surface, is covered with different silane fragments. The adsorption mechanism resulted in the direct interaction of the non hydrolysed silane with hydroxyl on the oxidised metal surface with the release of an alcohol as side product of the condensation. This counteracted the general understanding of silane chemistry at the fine.

The strength and durability of epoxy and polyurethane adhesive bonded joints on aluminium, mild steel, stainless steel and glass substrates was investigated using various silane types and two application methods (Walker 1991). The treatments provided the highest increase of strength when applied as solution to the metals substrates. In contrast, the addition of silane into the adhesive formula was only effective for the glass substrates. In the case of the epoxy adhesives, the γ-GPS was generally the best treatment for metals, whereas its addition in the epoxy itself only promoted a small increase in bond strength. Furthermore, the treated adhesive joints on metal and glass showed a significant improvement of their bond durability when exposed during 15 weeks to 100%RH at 21°C.

Another work was undertaken to evaluate the durability of mild steel adhesive bonded joints (Gledhill et al. 1990). Adhesive joints were immersed in water at 60°C for 1500 hours. The untreated aged joints suffered approximately 85% decrease of their initial bond strength. In contrast, limited degradation was exhibited by the treated adhesive joints. Optimal durability was achieved using a dilute silane aqueous solution with neutral pH, mixed during 30 to 90 minutes for hydrolysis, applied on the steel substrate and left to dry at 20°C. It was found that the type of silane affects the solution pH and the use ethanol/water based solution had no effect on the durability. Moreover, immersion time and drying temperature contributed only marginally to an increase in durability.

More recently, the effect of multiple silane solution parameters was investigated on the durability and failure mechanisms of aluminium bonded joints using a epoxy adhesive (Abel *et al.* 2006). A γ-GPS aqueous and water/methanol solution was applied on a aluminium alloy substrate. The durability was evaluated using Boeing wedge joint apparatus at 96%RH and 50ºC. A complex interaction between the silane concentration and solution pH was found. The best durability was achieved using 1% γ-GPS in a pH5 aqueous solution after one hour of hydrolysis time and a maximum of 7 days for bonding. However, the drying temperature provided no significant improvement on the overall durability of the bonded joint. The surface characterisation was conducted by means of microscopy, XPS and SIMS showing interphase failure processes in the aluminium oxide-silane diffusion zone.

Optimum conditions of a silane treatment were also investigated on aluminium adhesive joints subject to cryogenic environments (Kim *et al.* 2010a). Single-lap shear tests and wettability measurements showed higher strength and SFE when 1% γ-GPS in a pH5 aqueous solution. The treated joints exhibited an increase in shear strength of 20% and 45% when compared to an acetone cleaned joint with and without mechanical abrasion, respectively. Moreover, optical microscopy (OM) and XPS on the failure surfaces of the treated joints showed different extents of cohesive failure from the epoxy adhesive, which became more predominate with the increase of adsorption of the silane.

Despite the extensive research previosly described, a clear understanding of the ideal application conditions are very difficult to attain on the reactions of silanes in solution, polysiloxane structures and interactions on the surface This is due to the multiplicity and complexity of variables presented in each study, e.g., substrate, resin, silane, application parameters and properties required (service conditions).

2.4.4 Substrate

Extensive research has been undertaken to enhance the bond between glass fibre and an epoxy resin in reinforced polymeric composites. Silanes were then successfully applied to improve metal-adhesive bonding (Adams 2005). Surface analysis on treated aluminium (Abel *et al.* 2000, Abel *et al.* 2004, Abel and Watts 2009, Rattana *et al.* 2002, Rattana *et al.* 2006, Kim *et al.* 2010a), steel (Ferreira *et al.* 2004, Van Schaftinghen *et al.* 2004) and zinc (Van Ooij and Sabata 1991, Bexell and Olsson 2001), have suggested the formation of

metal–oxygen–silicon (M-O-Si) bonds (Plueddemann 1991, Tesoro and Wu 1991, Palanivel *et al.* 2003, Zhu and van Ooij 2004). This is related to the different concentrations of hydroxyl groups on the surface according to the native chemistry of the substrate (Abel *et al.* 2004). The metal surface undergoes oxidisation and hydration in the presence of humidity, which leads to the formation of hydroxyl groups. These groups will then react with silane and form a siloxane bond (Abel *et al.* 2000), which has already been established through improved bond strength and hydrolytic stability (Pluedemann 1991) and later confirmed by SIMS analysis (Abel *et al.* 2004). However, the mechanisms pertaining to silane treatment on metals are beyond the scope of the present work.

In the case of boron carbide no studies using silanes with epoxy resins have been reported, despite the importance of this material to the industry. Nevertheless, previous research seemed to indicate that silane coupling agents could improve the adhesion between BC and an epoxy matrix. BC powder was treated with γ-aminopropyltriethoxysilane (γ-APES) to enhance compatibility with silicone coatings (Xu and Jia 2007). The surface chemistry was conducted through wettability tests and FTIR. Optimal wettability was attained when treated with 5%wt. γ-APES (in relation to the BC) and left to dry at 80°C for 3 hours, resulting in a increase in the contact angle with water from 76º up to 92º. The spectra of treated BC showed a peak attributed to the Si-O stretching mode at 1100-1000 cm^{-1}, confirming the adsorption of the silane on BC. Also, improved mechanical properties and corrosion resistance were confirmed with the treated BC reinforced silicone matrix coating through mechanical testing, SEM and EIS.

Other research was also conducted to modify the surface chemistry of boron and boron compounds with silane coupling agents or in combination with other treatments. Boron (B) fibres treated with plasma or/and silane treatment were investigated to obtain optimal bond strength in epoxy matrix composite (Brack *et al.* 2005). The fibres were subjected to plasma using different atmospheres (argon, oxygen and de-ionised water) and/or silane treatment. The latter was attained by immersion of the BC in 1%wt. γ-GPS aqueous solution during 10 minutes. The mechanical tests confirmed an increase in the adhesion between the fibre and the epoxy resin, especially when the plasma process was applied to the surface prior to silane treatment. Surface chemistry analysis performed through XPS, TOF-SIMS and OM demonstrated direct correlation with the pull-out mechanical tests. It was reported that the plasma treatment increased the boron-oxygen containing species (B_2O_3 and other sub-oxide species) on the fibre surface, providing attachment for the silane

coupling agent (B-O-Si). Also, a very weak peak corresponding to a B-O-Si ion fragment was found despite the lack of evidence of the mechanism attachment. Improved adhesion was also confirmed with a locus of failure changing from interfacial to the epoxy interphase and ultimately fibre breakage.

Furthermore, surface chemistry and structural characteristics of the BC nanoparticles were investigate as a system for T cell-guided boron neutron capture therapy (Mortensen *et al.* 2006). Ball milling (200 rpm, 12 to 144 hours) was performed with the particles in various atmospheres (air, nitrogen or argon) and their surfaces were investigated using Transmission Electron Microscopy (TEM), Photon Correlation Spectroscopy (PCS), XPS, X-ray Diffraction (XRD), FTIR, and other chemical analysis. The milled material exhibited a more homogeneous/spherical shape, reduced size distribution and overall negatively charged surface. The latter is believed to be a result of boronic surface groups due to the presence of boric acid (Fig. 2.4), which acts as a Lewis acid by accepting a hydroxyl ion, OH^-, in order to form a tetrahedral borate ion, $B(OH)_3^-$.
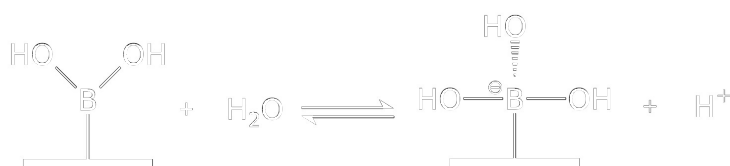
Figure 2.4 Surface charging mechanism of a BC nanoparticle in aqueous solution (Mortensen *et al.* 2006).

These hydroxyl groups could provide an attachment for silane coupling agents and consequently an increase in bond strength (Plueddemann, 1991) as described in the previous section.

Other work reported the synthesis and thermal characterisation of poly-borosiloxanes (PBS) to be used as polymeric precursors for the protection of carbon fibres in ceramic matrix composites (Siqueira *et al.* 2007). The preparation of PBS involved the hydrolysis of methyltriethoxysilane (MTES) or vinyltriethoxysilane (VTES) and condensation of the hydrolysed species with a boric acid in solution (reactions 2.6-2.8). After complete dissolution, a clear solution was obtained, cast for gelation, and finally left to dry at 60ºC for 10 days. FTIR spectra confirmed the presence of borosiloxane bonds (B-O-Si) from the crosslinked trigonal BO_3 units in the polymeric structure. These bonds can be easily formed according to the following reactions:

$$=B–OH \quad + \quad ≡Si–OR' \quad → \quad =B–OR' \quad + \quad ≡Si–OH \qquad (2.6)$$

$$=B–OH \quad + \quad ≡Si–OH \quad → \quad =B–O–Si≡ \quad + \quad H_2O \qquad (2.7)$$

$$=B–OH \quad + \quad ≡Si–OR' \quad → \quad =B–O–Si≡ \quad + \quad R'–OH \qquad (2.8)$$
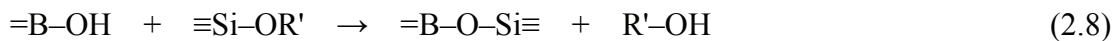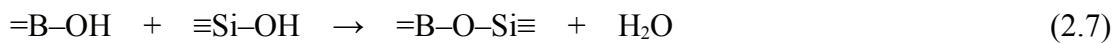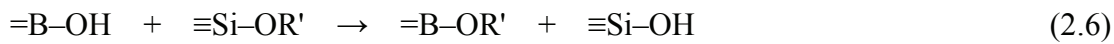
Additional studies have used silane coupling agents to increase adhesion of epoxy adhesives on not to dissimilar materials to boron carbide, such as silicon carbide (SiC) and diamond (C) particles. A silane coupling agent was used to improve the adhesion of micro scale SiC particles (6 and 12%wt.) in a reinforced epoxy composite (Abenojar *et al.* 2009a). The non bonded particles inside the matrix act as crack initiators, decreasing the mechanical strength and wear resistance of the composite. The ceramic particles were treated with 3%wt. γ-GPS aqueous solution (pH 4, hydrolyse for 60 minutes) during 30 minutes and dried in a vacuum oven at 100ºC for 12 hours. Mechanical testing conducted on treated specimens showed increased strength by means of three-point bending (3PB) test. SEM conducted on the fracture surfaces displayed a silane coated particle with a slight shape modification. It was suggested this may reduce the risk of stress concentration and crack initiation. Moreover, the treatment improved adhesion between the reinforcement and matrix, which consequently increased the composite strength.

Also, a silane was applied on SiC particles to improve their interaction and dispersion in an epoxy matrix (Zhou *et al.* 2008). The effect of treatment was evaluated on thermal conduction mechanisms of a low filler content (8.6 and 14%vol.) PMC. The native surface was remove by a rinse in hydrofluoric acid (HF) and then oxidised in atmosphere of air at 900ºC to obtain a very thin silicon dioxide layer (10 to 140 nm). Silane treatment was conducted prior and after oxidation of the particles by immersion in a 3%wt or 10%wt. (in relation to micro- or nano- particles) of γ-APES ethanol solution at 60ºC for 30 minutes and drying at 110ºC for 60 minutes. Particles without silane treatment were found to be unevenly dispersed and agglomerated. FTIR showed silane covalently bonded to the SiC particles and a higher crosslinked SiC/resin three-dimensional network which led to composites with higher thermal conductivity, specially when oxidised nanoparticles were used for reinforcement.

Another work evaluated the effect of the silane treatment of SiC nano and micro- particles on the impact strength of a reinforced epoxy composite (Kavitha *et al.* 2012). Particles were treated with γ-APES in a acetone-water solution and dried at 60ºC for 6h and at 120ºC for 8 hours. A low viscosity room temperature cure epoxy resin in order to obtained

an 1.5%wt SiC-epoxy composite through a moulding process. The impact strength of the composite was higher with the incorporation of the nano-particles. Even higher strength was achieved by the treated composites as a result of the improved particle dispersion and bonding. FTIR confirmed surface chemical modification of the particles with the presence of the silane amine groups required for molecular bridging between the SiC and epoxy resin. Sedimentation method, TEM and SEM confirmed a great improvement of the particle dispersion in the resin with silane treatment. Moreover, the failure surfaces showed that the reinforcement leads to toughening of the epoxy and better bonding.

Chemical modification of a diamond (C) surface was conducted to increase compatibility with polytetrafluoroethylene (PTFE) (Tsubota *et al.* 2005). This was carried out in order to obtain a pre-coated nickel(Ni)/silanised diamond composite plate with higher water resistance and wear resistance, provided by the hydrophobic polymer coating and the super-hard material, respectively. Diamond micro-particles were oxidised in an acid solution (H_2SO_4 and HNO_3), washed with water and dried. Finally, the powder was treated with (tridecafluoro-1,1,2,2-tetrahydrooctyl)triethoxysilane in toluene solvent at 100ºC for two hours and vacuum dried. A suspended silanised diamond particle aqueous solution was used for the Watts Ni plating bath. Modification of the surface chemistry was confirmed by means of XPS, FTIR and a wettabilitty test on the untreated and silanised powder. Diamond content in the deposited Ni plate was proportional to the amount of particle suspended in the Watts Ni bath. Unsurprisingly, wear resistance improved with the incorporation of particles, regardless of their surface treatment and content in the composite.

2.5 Silane Coupling Agent And Corona Discharge (SICOR)

Some materials exhibit a surface chemistry that makes them difficult to adhesively bond or to be silane treated, such as polyethylene, polypropylene and other polyolefins. The inert hydrocarbon nature of their surfaces does not provide organofunctional groups, which could react with the silane by hydrogen or covalent bonds. To achieve satisfactory bonding, combinations of physical and chemical surface treatments can be used to enhance adhesion between the reinforcement and the matrix, and thus obtain a higher strength PMC. The synergistic effect from this combination results in a more effective modification of the surface chemistry in order to improve adhesion (Gutowski *et al.* 2005).

A process known as "SICOR" for SIlane-on-CORona was developed by W.S. Gutowski,

from CSIRO Polymer Surface Engineering Group in Melbourne. A two-step surface chemistry modification is conducted to overcome the low adhesion of some paints, adhesives, inks, coatings and pressure sensitive adhesives (PSA). In addition, the SICOR process does not involve the use of environmentally hazardous solvents or primer ingredients (aromatic and chlorinated), which were previously required for the surface treatment of these materials. Initially, the substrate is oxidised with the Corona Discharge Treatment (CDT) to create reactive sites on the inert substrate surface, such as hydroxyl, carbonyl and carboxyl groups.

CDT has been used to improve the adhesion and wettability of adhesives and coatings on materials with low and non-polar SFE (Cognard 2006). Despite the development of alternative treatments, CDT remains the primary surface treatment for various polymers due to it being a simple, reliable and fast surface treatment (Markgraf 2000, Palm 2007). CDT is a variation of plasma treatment through the application of a high frequency/voltage discharge in air at atmospheric pressure, by initiating a non-equilibrium cascade process which lead to the formation of electrons at high temperature in a partially ionised gas at room temperature (Pocius 2002, Hoeben 2000). The air is decomposed through a variety of gas-phase reactions to form different energetic species, such as, ozone, oxygen, ions, radicals, photons and electrons (Fig.2.5). When in contact with a substrate these species provoke morphological and chemical modification of the substrate surface. The former suggests an increase in roughness and subsequently, in surface area on which the adhesive can adhere better. The chemical modification leads to a higher polar nature of the treated surface resulting from the formation of oxide species (Fig.2.5). These result from the reactions between charged oxygen species in the air and the substrate molecules, such as, hydroxyl, carboxyl or carbonyl groups (Cognard 2006).

Figure 2.5 Energetic species formed in the air and on the surface during corona discharge process.

CDT can also clean the surface by breaking up deposited contaminants, such as, oils from the manufacture process of metals, into lower molecular species (Palm 2007). It can also increase the crosslinking of the polymer surface (Ebnesajjad 2008). CDT can be a very complex process, where its effectiveness and uniformity depend on a significant number of substrate, atmosphere and application parameters. The former is related with the chemistry and surface topography, and substrate geometry, i.e., distance between the surface and electrode. The absence of a special chamber makes the CDT a low cost and high-speed treatment for large surface areas, but also limits the process to the local air atmosphere chemistry and environment conditions, e.g., temperature and relative humidity. In addition, application parameters must be studied for a specific material and geometry in order to optimise the process, such as, power output, treatment time, air thickness and flow-rate, corona reactor design, substrate temperature and cooling rate, and treatment age decay (Tuominen et al. 2010, Pocius 2002, Uehara 1999, Neyman 2003). The latter is associated to the short-time effect of the CDT, which requires that the adhesive bonding should be carried out immediately after the discharge (Hartshorn 2009). Nevertheless, effectiveness of the treatment for specific substrate, atmosphere and corona reactor design is mostly affected by the power output and treatment time. These parameters define the energy applied onto the surface, E_u, by the following equation.

$$E_u = \frac{P \cdot n}{L \cdot V}$$

(2.9)

Where P is the power output of the corona discharge expressed in watts; n is number of passes over substrate surface area, L is the length of the corona electrode expressed in millimetres, v is the treatment velocity of the substrate versus energy source in mm/s ($V = d / t$, d is the electrode width and t is treatment time) (Gutowski *et al.* 2002a). In order to achieve adhesion promotion, a minimum energy must be supplied onto the surface to initiate the oxidation, whereas, an excessive level can lead to the degradation of the substrate and to the formation of a weak boundary layer as a result of the high presence of low molecular weight species on the surface (Sapieha *et al.* 1993). Moreover, the effectiveness of the CDT can be increased by feeding liquids or oxygen-containing gases into the system (Pocius 2002, Kinloch 1987, Lieberman and Lichtenberg 2005).

Nevertheless, these reactive sites only promote better adhesive wettability through polar

interactions between the substrate and adhesive molecules at the interface, which is only effective for less demanding or short-term applications. Thus, a second step is conducted through a silane treatment, where the reactive groups on the surface provide attachment to the silane through chemisorption or other adhesion mechanisms. The adsorbed silane improves bond strength and durability through the formation of a hydrophobic chemical bridge between the adhesive and substrate/reinforcement (Gutowski *et al.* 1993, Gutowski *et al.* 1999a, Gutowski *et al.* 2002a, Gutowski 2003, Gutowski *et al.* 2003, Frazer 2001).
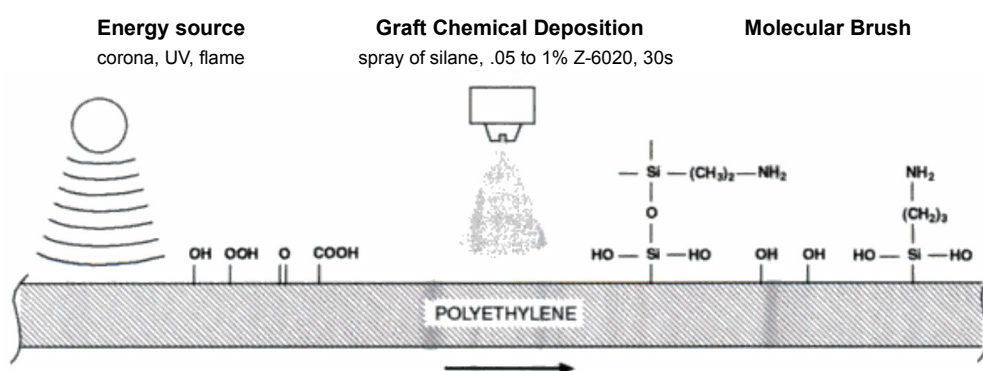
Figure 2.6 Schematic representation of the different steps of the SICOR process on polyethylene (Gutowski *et al.* 2002a).

The SICOR provides a simple process to incorporate onto the substrate surface a great variety of molecular structures with the desired organofunctional groups as shown in Fig. 2.6. In the second step of the process, the material can be immersed or sprayed with the diluted silane aqueous or alcohol solution followed by a drying period using a oven, infrared element or hot air gun (Gutowski *et al.* 2002a). A wide rage of engineering and automotive thermoplastic polyolefin (TPO) substrates are treated using the combined surface treatment with various structural adhesives, sealants, pressure sensitive adhesives (PSA) and paints (Gutowski and Pankevicius 1993, Gutowski *et al.* 2002a, Gutowski *et al.* 2002b). The SICOR process was shown to promote adhesion of epoxy resins on polypropylene (PP) and high density polyethylene (HDPE) substrates, and ultra-high molecular weight polyethylene (UHMWPE) fibres. The result is a significant increase in the lap-shear strength for PP and HDPE, and a higher interlaminar fracture strength and flexural modulus for the fibres. SEM analysis showed a shift from one of a purely adhesive to a highly cohesive-in-fibre failure after SICOR treatment. XPS analysis confirmed the presence of the silane amine groups on the fibre surface treated with SICOR. Enhanced

adhesion was also achieved using polyurethane, methacrylate and cyanoacrylate adhesives on low density polyethylene (LDPE), UHMWPE, HDPE and PP substrates (Gutowski *et al.* 1993, Gutowski *et al.* 2002a, Gutowski *et al.* 2002b). The former showed a strength increase similar or even higher compared to plasma treatment, superior by 200% compared with the CDT alone and more than 300% compared with a polyolefin primer. HDPE and PP exhibited a significant but less evident lap-shear strength improvement from CDT to SICOR whereas UHMWPE exhibited the highest increase with the combined process. FTIR, XPS and wettability tests on the LDPE surface showed chemisorbed and physisorbed γ-APES with the latter form being removed from the outermost layer of the polysiloxane structure after immersion in water. Also, the bond durability of adhesives, sealants and coatings on these SICOR-treated materials is similar to that with chlorinated primers and even better compared to that with flame or ammonia plasma treatment (Gutowski *et al.* 1999a, Gutowski *et al.* 2002b). The SICOR process also improves the shelf life of TPOs, resulting in a consistent lap shear strength and a pure cohesive failure within the cyanoacrylate adhesive bondline up to 360 days of storage in air prior to bonding (Gutowski *et al.* 1999b, Gutowski *et al.* 2000, CRCWI 2002). This compares well against ammonia plasma treated PP materials, which go through an abrupt strength decrease and fully cohesive failure within 6 hours of shelf time. SICOR was also extended to other polymers and metal which resulted in a enhanced strength and a change from adhesive to a mostly cohesive failure within the sealant, even when immersed in water for 7 days at room temperature. This worked particularly well for polyvinylidene fluoride (PVDF), polyvinyl chloride (PVC), stainless steel and organic-dye anodised aluminium substrates. SICOR has also provided a viable on-line surface treatment to overcome the lack of bond strength and durability under high humidity or wet exposure of adhesives and PSA on timber and wood-based products (Gutowski *et al.* 2005, CRCWI 2003). This was particularly evident with some Australian hardwood substrates that exhibit higher concentration of bulk phenolic and surface lipophilic extractives on the surface (Widsten *et al.* 2006, CRCWI 2004). Higher bond strength was achieved with the SICOR process using a one-component polyurethane structural adhesive on spotted gum, sugar gum, blackbutt and mountain ash treated timber (CRCWI 2005).

A three-step process was also developed to attain optimal bonding between poly(methyl-methacrylate) (PMMA) and polydimethysiloxane (PDMS) substrates by combining oxygen plasma, silane (5% v/v γ-APES aqueous solution, 85ºC) and corona

treatment (Kim *et al.* 2010b). Wettability tests showed a decrease of the water contact angle on PMMA from the untreated (70º), plasma (55º) to silanised (9º) surface. Optimal tensile strength was attained with plasma prior to silane treatment. XPS analysis confirmed surface oxidation after plasma, higher silane adsorption, and activation of the siloxane layer after CDT by the substitution of the amine groups to hydroxyl radicals.

CHAPTER 3 – BORON CARBIDE

3.1 Introduction

Boron carbide (BC) is a non-oxide ceramic that was originally discovered in 1883 as a by-product of reactions involving metal borides. Despite this, its chemical formula has only been known since 1934 (Karaman 2007). BC possesses an interesting combination of chemical and mechanical properties which are difficult to obtain from other materials, such as low density, super-hardness, high melting point, good resistance to critical and complex environments, excellent thermal and electrical properties, and good neutron absorption and shielding ability (Table 3.1). Thus, there is a high demand for BC in advance applications, and recently for new applications (Thevenot 1990, May *et al.* 1997, Ahn 2005, Lee and Speyer 2003, Abenojar *et al.* 2009b, Abenojar *et al.* 2011, Suri *et al.* 2009).

Table 3.1 BC keys properties and applications.

Key Properties	Applications
High hardness	Abrasive for cutting, blasting, polishing and lapping applications
Low density	Anti-ballistic armour plates/tiles (vehicle and body/personal armour)
Wear resistance Low friction coefficient High elastic modulus	Slurry pumping and grit blasting nozzles high-pressure water jet cutters, automotive components, padlocks, ceramic tooling and dies, precision toll parts, evaporating boats for materials testing, mortars and pestles, scratch and wear resistant coatings, dressing diamond tools, cermet and metal matrix composites.
Good nuclear absorption	Stray radiation absorption and shielding in the nuclear industry. Control rod and shutdown pellets in nuclear reactors/power plants.
Good chemical resistance Refractory properties	Chemically inert, good resistance to acids (hydrofluoric, chromic and nitric acid), oxygen (passivation) and chlorine. Additive for magnesia-carbon, silicon carbide and other materials to enhance the high temperature oxidation resistance. Solid Fuel for ducted rockets (HTPB/BC based propellants). High temperature electronic devices and Be/Be alloy replacement in aerospace applications.

The relatively low production cost of the BC and high neutron absorption cross section of the boron element make this ceramic material one of the most used as neutron absorber and shielding to protect humans and instruments from stray radiation, sensors, neutron poison, control/shutoff rods and containing material in the industry (Huang *et al.* 2012). This is related to the specific high thermal neutron absorption/low scattering cross-section of the boron (752 barn), as consequence of the presence of ^{10}B (3837 barn) isotope in the natural element form (20% ^{10}B + 80% ^{11}B). The main ^{10}B(n, α)^{7}Li neutron capture reaction between the boron isotope and neutron result in the formation of stable non-radioactive isotopes, such as lithium ($_2$Li^7) and helium ($_2$He^4) isotopes (Chaudhari *et al.* 2011, Abenojar *et al.* 2009b).

$$(94\%) \; ^{10}\text{B} + \text{n} \rightarrow \; ^{7}\text{Li}^{*}(0.84 \text{ MeV}) + \; ^{4}\text{He} (1.47 \text{ MeV}) + \gamma \, (0.48 \text{ MeV}) \quad\quad (3.1)$$

$$(6\%) \; ^{10}\text{B} + \text{n} \rightarrow \; ^{7}\text{Li} (1.02 \text{ MeV}) + \; ^{4}\text{He} (1.78 \text{ MeV}) \quad\quad\quad\quad (3.2)$$
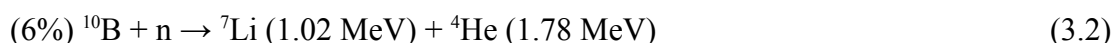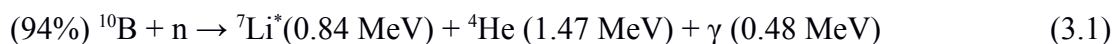
Also, a much less probable neutron capture reaction may occur in the presence of fast neutrons (E > 1.2MeV) with the formation of helium and tritium ($_1$H^3). This absorption ability is not only suitable for applications at the low neutron energy range but also at higher energies, as a result of the monotonic decrement of ^{10}B cross section with the neutron energy. The ability is satisfactory across the entire neutron energy spectrum, which makes BC a very effective absorber or shielding material in the intermediate and fast energy range (Subramanian 2010).

Other interesting property is the high hardness of the BC which is only surpassed by the cubic boron nitride and diamond (Zakhariev *et al.* 2009). Thus, BC is extensively used as ballistic shielding material as result of its extraordinary hardness, high elastic modulus and low density (Lee and Yoo 2001). Various studies have been conducted over the last decades on BC using different conditions to evaluate its performance, in particular the response to shock loading (Dandekar 2001, Dandekar *et al.* 2008, Grady 1994, Savio *et al.* 2011). Also, BC not only exhibits an extraordinary hardness at high temperatures (up to 1873°C) when compared with other refractory materials but also is the hardest material which can be produced economically in high quantities (Zakhariev *et al.* 2009). In the case of the BC, high hardness is related to more localised covalent bonds and higher inter-atomic electron density (Reynaud 2010). Several works showed that the BC hardness increases with the carbon content until reaching the edge of the homogeneity range at

approximately 20% (Werheit 2007). The hardness suffers a step decrease due to the formation of the carbon phase in the BC solid solution (Domnich *et al.* 2011).

3.2 Composition and Structure

BC exhibits a disordered composition ranging from 91.2% to 80% ($B_{10.4}C \rightarrow B_4C$) of boron, in which the latter is the rarely achieved theoretical stoichiometric ratio. Typically, BC composition is richer in boron, ranging from B_4C to $B_{6.5}C$, similar to that showed in Table 3.2 (Pierson 1992). The substitution of carbon atoms within the molecular structure by boron atoms results in a single-phase regime exhibiting a wide variation of composition as exhibited in the Fig. 3.1 (Reynaud 2010, Hong, 2012, Thevenot 1990).

Table 3.2 Typical chemical and elementary composition of the synthesised BC.

Compound / Element	Content (%)
Boron (B) + Carbon (C)	94.0 – 98.5
Boron (B, min.)	74.0 – 79.0
Carbon (C, max.)	17.0 – 24.0
Boron oxide (B_2O_3)	0.1 – 1.0
Iron (Fe)	0.2 – 0.5
Silicon (Si)	0.1 – 0.3
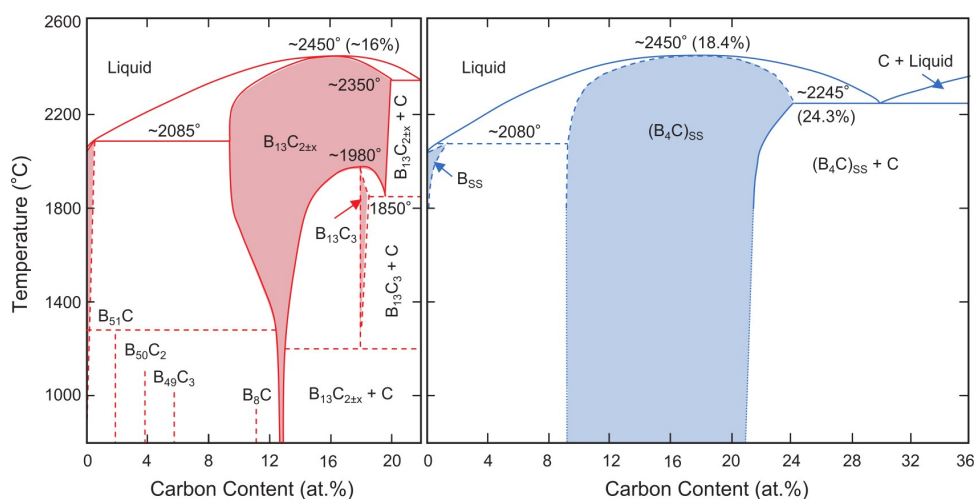
Figure 3.1 Boron-carbon phase diagram of the BC depicting $B_{13}C_2$ or B_4C as the stable phase (Domnich *et al.* 2011).

BC exhibits generally a rhombohedral structure, composed by icosahedra units and a linear three-atom inter-icosahedral chain (Fig. 3.2). The icosahedra is a regular polyhedron with 20 identical equilateral triangular faces, 30 edges and 12 equivalent vertices, forming a cage of 12 atoms with an I_h symmetry. However, BC icosahedra units are distorted from ideal symmetry due to the presence of polar and equatorial crystallographic sites. The former corresponds to the six atoms of the icosahedron that are directly bonded to atoms in neighbouring icosahedra and the latter corresponds to the other six atoms that are linked to the inter-icosahedral chain. The icosahedra units and the three-atom chains are located respectively at the nodes and along the (111) axis of a rhombohedral Bravais lattice, $R\bar{3}m$ space group (Bigdeloo and Hadian 2009, Lazzari et al. 1999).
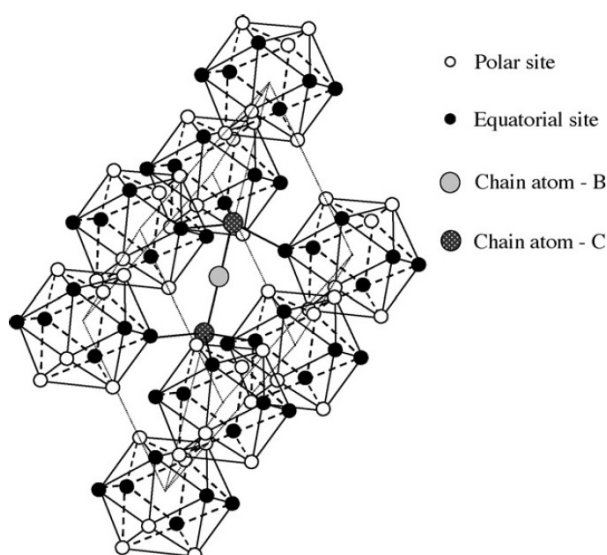
Figure 3.2 Boron carbide structure, $B_{12}C_3$ (Lazzari et al. 1999).

The BC structure exhibits mainly four bond types as a result of hybridisation of the valence electrons from the ground state of the carbon and boron atoms (Table 3.3), more specifically, highly delocalised intra-icosahedra sp^2 bonds, π bonds from the inter-icosahedron sp hybrids, three-atom chain π characteristic double resonant bonds and finally the bond between the three-atom chain carbon and the icosahedra boron atom at the equatorial site. Nevertheless, the bonding within the structure can change by alterations in the stoichiometric composition or by the presence of additives or contaminants and consequently affecting the physical-chemical and mechanical properties of BC (Reynaud 2010, Domnich *et al.* 2011).

Table 3.3 Electronic configurations and orbital coordination for the boron and carbon.

Element	Atomic radius (nm)[*]	Electro-negativity	Electronic state	Orbital		
				Configuration	**Coordination**	**Angle (°)**
C	0.077	2.5	Ground $1s^2 2s^2 2p^2$	↑↓ ↑↓ ↑ ↑ $1s$ $2s$ $2p_x$ $2p_y$ $2p_z$	–	–
			Hybrid $1s^2(sp^3)^4$	↑↓ ↑ ↑ ↑ ↑ $1s$ sp^3 sp^3 sp^3 sp^3	Tetrahedral	~109.5
B	0.088	1.8	Ground $1s^2 2s^2 2p^1$	↑↓ ↑↓ ↑ $1s$ $2s$ $2p_x$ $2p_y$ $2p_z$	–	–
			Hybrid $1s^2(sp^2)^3$	↑↓ ↑ ↑ ↑ $1s$ sp^2 sp^2 sp^2	Trigonal planar	120.0

* Note: tetrahedral configuration sp^3

The rhombohedral structure can possess different boron contents, such as, $(B_{11}C)CBC$ with one carbon atom staying at a polar site of the icosahedral unit, $(B_{12})CBC$ with no carbon in the icosahedral unit or even with a higher substitution of the carbon atoms with boron atoms in the icosahedral unit and linear chain (Pierson 1996, Conde *et al.* 2000). The increase of carbon content in rhombohedral BC will result in small changes of the lattice parameters due to the atom radius of carbon being smaller than that of boron, resulting in a slightly smaller unit cell structure (Table 3.4). Therefore, localized phases with varying composition may exist in a single material (Jimenez *et al.* 1999, Mauri *et al.* 2001).

Table 3.4 Lattice parameters and unit cell volume of BC as a function of carbon content, reference to hexagonal structure (Pierson 1996).

Carbon content (at%)	Lattice parameters (nm)		Unit cell volume (nm³)
	a	*c*	
20.2[*]	0.55991[*]	1.20740[*]	3.27809[*]
19.2	0.59950	1.20707	3.27763
19.6	0.56030	1.20802	3.28440
18.7	0.56032	1.20909	3.28745
16.0	0.56152	1.21411	3.31525
12.3	0.56286	1.21748	3.34039
9.3	0.56438	1.21750	3.35851
8.1	0.56440	1.21731	3.35818

* Note: $B_{12}C_3$

Other structures in the BC can also be found, such as, tetragonal ($B_{50}C_2$, $B_{50}C$, $B_{48}C_3$, $B_{51}C$, $B_{49}C_3$) and orthorhombic (B_8C). The latter is metastable, more difficult to synthesise and its physical properties are not well known (Velamakanni 2009). The boron content depends on the reactions used for the BC synthesis as well on the temperature and pressure at which this process occurs (Sun et al. 2009).

3.3 Synthesis

BC can be synthesized into a form of fine black powder or coarse black glossy crystals as a result of the different preparation methods, such as, the carbothermal reduction of boron oxide (B_2O_3), boric acid (H_3BO_3) and borax ($Na_2B_4O_7$), the direct solid-solid reaction of constituent elements (C and B) and the magnesiothermal reduction of boron oxide in the presence of carbon (Yanase et al. 2009, Bigdeloo and Hadian 2009, Thevenot 1991). The BC synthesis reactions through carbothermal and magnesiothermal reduction are showed in the the Eq.3.3-3.5 and 3.6, respectively.

$$2\,B_2O_3 \;+\; 7\,C \;\;\underset{1400°C}{\overset{heat}{\longrightarrow}}\;\; B_4C \;+\; 6\,CO \tag{3.3}$$

$$4\,H_3BO_3 \;+\; 7\,C \;\;\underset{1700°C}{\overset{heat}{\rightleftharpoons}}\;\; B_4C \;+\; 6\,CO \;+\; 6\,H_2O \tag{3.4}$$

$$4\,B \;+\; C \;\;\underset{1200-1950°C,\,0.01\,Pa}{\overset{heat}{\rightleftharpoons}}\;\; B_4C \tag{3.5}$$

$$2\,B_2O_3 \;+\; 6\,Mg \;+\; C \;\;\underset{1400°C}{\overset{heat}{\longrightarrow}}\;\; B_4C \;+\; 6\,MgO \tag{3.6}$$
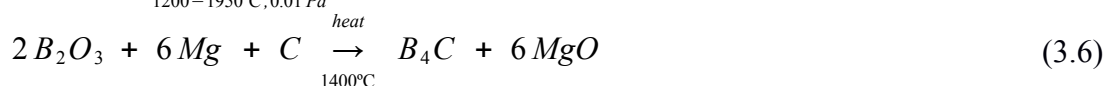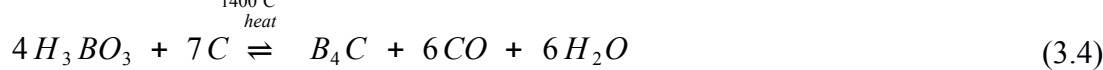
The latter reaction (Eq. 3.6) is unsuitable for high pure powder production due to the presence of magnesium by-products, such as MgB_2, which are extremely difficult to remove even with repeated hot acids treatments (Patnaik 2003, Toumanov 2003). Moreover, the synthesis without free carbon (C) is difficult since BC is in equilibrium with this element ($B_nC \rightleftharpoons B_nC + C$, $4 < n < 10$). Thus, the most used process in the industry is carbothermic reduction of boric acid or boron oxide with carbon black (Eq. 3.3 and 3.4) in an electric arc furnace at a temperature over 1750 to 2000°C, despite the formation of an graphite phase (Table 3.5) and reduced yield of BC as result of evaporation losses (Suri *et al.* 2009, Subramanian *et al.* 2010).

Table 3.5 Synthesis conditions and phases obtained for the BC.

Stoichiometry (B/C)	Temperature (°C)	Phases
4	≤ 1600	B_4C (amorphous)
4	1800 – 1850, 3h	B_4C (rhombohedral) + Graphite
> 4	1800 – 1850, 3h	B_4C (rhombohedral) + B_8C (orthorhombic) + Graphite

The synthesised product is then mechanically milled to a fine powder with the required size mesh and purified through chemical and thermal oxidation to remove the excess non-reacted carbon and contamination compounds from the grinding media (Alizadeh *et al.* 2004, Jung *et al.* 2004). The purification can be achieved by stirring the powder in an aqueous process with hydrochloric acid and heat for the dissolution of the impurities (Subramanian *et al.* 2010). The various steps involved in the production of BC by carbothermal reduction are represented as a flow chart in the Fig. 3.3.
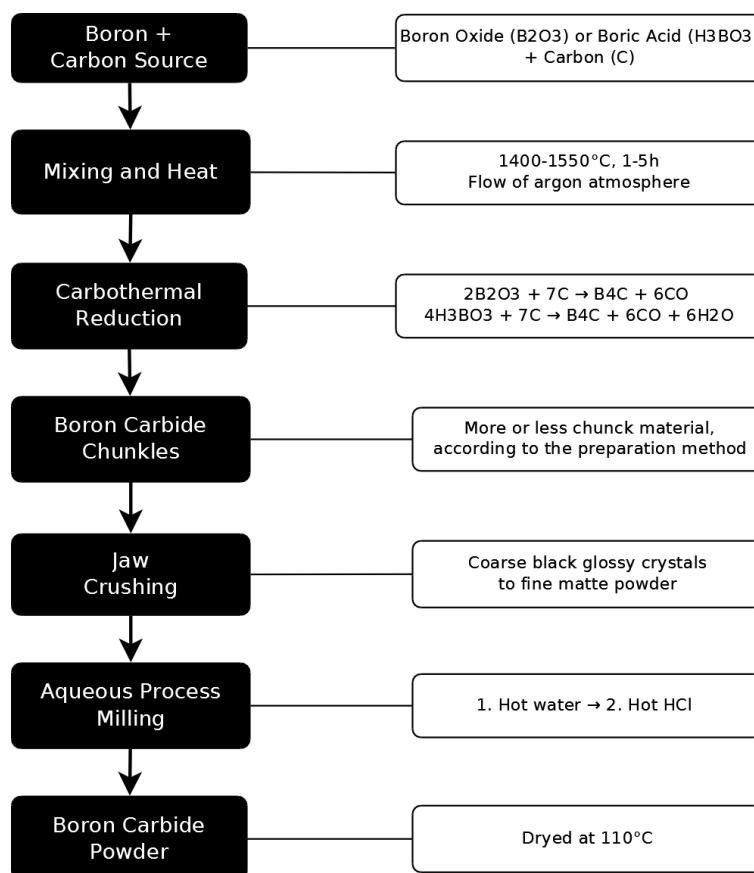
Figure 3.3 Flow chart of the commonly used BC production process (Subramanian *et al.* 2010).

3.4 Components

The BC components are typically obtained by pressureless sintering of the synthesised product through cold compaction and heating of the milled powder in a furnace just below its melting point until the particles adhere to each other (Toumanov 2003). However, BC is difficult to sinter and requires temperatures above 2000°C to obtain a high density and avoid the formation of second-phase graphite, which affect greatly the mechanical properties of BC (Subramanian *et al.* 2010, Suri *et al.* 2009, Ohji and Singh 2009). Improved density can be achieved through the activation of the synthesised powder using a combination of physical and chemical methods (Thévenot 1991). A high energy milling process is used to enhance the BC reactivity in order to reduce the particle size to submicron dimensions, change the size distribution, alter the particle shape, modify the surface activity and disperse the agglomerates (Kelly and Spottiswood 1982, Summers 1983, Suryanarayana 2001, Mortensen *et al.* 2006). BC with a density close to 90% of the theoretical value can only be attained with a smaller particle size distribution and higher temperature as shown in Table 3.6 (Suri *et al.* 2009, Subramanian *et al.* 2010).

Table 3.6 Density of the pressureless BC using different particle size and temperature (Roy *et al.* 2006).

Particle size (µm)	Temperature (°C)	Density, ρ (%)
2.0 / 0.8 / 0.5	2225	80 / — / —
	2275	80 / — / 81
	2300	— / 87 / 85
	2325	85 / 88 / —
	2375	87 / 93 / 90

Additives can also be mixed with BC powder to decrease temperature and pressure of the sintering process as well as to increase the density of the components. These compounds are generally transition metals (Al, Mg, Ni, Fe, Co, Cu), metalloids (B, Si), carbides (Be$_2$C, SiC), oxides (ZrO$_2$, TiO$_2$) and others (AlF$_3$, TiB$_2$, W$_2$B$_5$ and C) (Chen *et al.* 2005, Singhal and Sing 2006). Industry normally uses small doses of carbon (1 to 5%wt) or boron (1 to

3%wt), and more recently carbides to improve the pressureless sintering and BC properties (Table 3.7). However, the use of additives can also induce other reactions and the formation of a second phase precipitation, which may affect fracture toughness, strength and hardness of the sintered ceramic components (Roy et al. 2005; Skorokhod and Krstic 2000; Sano *et al.* 2009). Hence, it's essential to control and identify the new phases formed during sintering.

Table 3.7 Density of the BC with different additives (Roy *et al.* 2006).

Additives	Temperature (°C)	Density, ρ (%)
none / 5% ZrO_2	2275	80 – 81 / 93
none / 1% C / 3% C	2325	85 – 88 / 91 / 90
none / 5% TiB_2	2375	87 – 90 / 82

Higher density is only achieved through hot pressing (HP) and hot isostatic pressing (HIP) sintering process. These have been use to overcome the low sinterability and to achieve high mechanical performance, as a result of the near full theoretical density (up to 95%) and pure single-phase form obtained for the BC. The heat and pressure applied to the material from all directions with isostatic process removes internal voids and microporosity through a combination of plastic deformation, creep, and diffusion bonding. This leads to the reduction of microshrinkage and consolidation of material. These sintering processes generally require lesser additives than the pressureless one in order to obtain higher density and strength (Sano *et al.* 2009, May *et al.* 1997).

3.4.1 Manufacture Limitations

BC components are typically manufactured using HP and HIP sintering as a batch process. Initially, the synthesised powder is compacted into a hot pressing die and exposed under vacuum or argon atmosphere to very high temperature and pressure. This fact is related to the BC being one of the most difficult materials to sinter due to its covalent nature, high melting point, low mobility, solid-solid reaction kinetics and high vapour pressure (Suri *et al.* 2009, Subramanian *et al.* 2010).

BC does not melt congruently showing temperature variations in the reaction zone with the liquid state becoming increasingly rich in carbon. The material must be solidified at a rate

so that no equilibrium can be established between the solid and liquid state. Hence, the solidified material can exhibit non-uniform composition with a second-phase graphite, which affect greatly the mechanical properties of BC. Therefore, the final density is difficult to control and temperatures above 2000°C are required to improve the efficiency of the transport mechanisms, such as grain-boundary and volume diffusion (Ohji and Singh 2009). The highest density with approximately 93% of theoretical value, is only achieved with a very fine BC powder. These powders possess a high surface area on which a thin boron oxide layer is formed. This limits the densification process. The oxide must be eliminated before sintering by adding an amorphous carbon source and heating the BC to temperatures above 1300ºC. Thus, the high temperatures used in the manufacturing process requires expensive graphite tooling and special furnaces (Singhal and Sing 2006). The inner surfaces of the graphite mould must be coated with boron nitride (BN) to prevent reactions and consequent damage of the BC components and hot pressing die. Also, the load necessary to attain the desirable pressure (20 to 40 MPa) increases with the size of the ceramic component. Thus, expensive and very large loading equipment is necessary, limiting the size and production volume of the components, and their geometry is also essentially restricted to blocks, plates or cylindrical forms (Sano *et al.* 2009, May *et al.* 1997). Generally, the components are machined to obtain a specific geometry and size through an expensive and time consuming process. This is associated with high brittleness and hardness showed by the BC, as result of the strong covalent bonds present in its crystal lattice (Zakhariev *et al.* 2009). The brittleness can be reduced by doping with transition and post-transition metals, such as titanium, zirconium and aluminium, which become partially dissolute in the BC (Makarenko et al. 1977, Lipp et al. 1966). Nevertheless, sintered components tend to be machined in their undensified state, since it requires diamond surface grinder and cutting tools using several passes and slow removal rates. Large components are typically obtained by applying pressure to an entire stack of sintered plates. After densification, the HP component generally is oversized in order to remove material down to the required shape and dimensions or to be cutt into small tiles. Beside being time consuming, this process causes cracks on the surface, leading to superficial and sub-surface damage of the components. Yields are greatly dependent on the tile geometry, being generally higher when cut into square-shape blocks from one larger sintered component. Different geometries are attained by cutting and removing the excess material to the desirable shape, resulting in even lower yields and higher costs (Sano *et al.* 2009, May *et al.* 1997, Campbell *et al.* 2008).

3.5 Composites

Despite the high technological importance of BC as an advanced material, its use is surprisingly limited, due to the complexity and high cost associated with the sintering process required to attain components. This has led to alternative solutions such as the inclusion of synthesised BC into metallic (MMC) and polymeric (PMC) matrix composites for nuclear, military, aerospace and automotive applications (Jung and Kang 2004). The reinforcement (e.g. chemical nature, size, shape, dispersion, orientation) and matrix (e.g. resin, hardener, curing cycle, degree of conversion and crosslinking) determines the macroscopic properties of the composite, such as, physical and mechanical strength, wear resistance, coefficient of expansion, concentration gradients and durability.

3.5.1 Metal Matrix (MMC)

MMC normally involves the exploitation of aluminium (Al) alloys as a matrix due to their low density, diverse composition, low melting temperature, flexible processability, heat treatment capability, strength and plasticity (Alizadeh *et al.* 2011, Kommel and Kimmari 2006, Jung and Kang 2004). Also, liquid aluminium exhibits reasonable reactivity with BC, making the production of these composites more feasible (Jung and Kang 2004). The main reaction products at the interface of the BC-Al composites are AlB_2 and Al_3BC, the volume fractions of which are proportional to the interaction time between the two materials (Kouzeli *et al.* 2002). BC nanoparticles are generally incorporated into metal matrices in low to medium concentrations (4 to 50%wt) to provide a shorter sintering time, lower residual aluminium content, and improved mechanical and thermal properties when compared with conventional Al-alloys, such as strength, fracture toughness, stiffness, hardness and heat resistance (Gorshenkov *et al.* 2012, Kouzeli *et al.* 2002, Vogt *et al.* 2009, Kommel and Kimmari 2003, Kommel and Kimmari 2006). These properties depend not only on the stoichiometric ratios of the initial material but also on the adhesion between them, which is proportional to the wettability of liquid aluminium on the ceramic surface (Kommel and Kimmari 2006, Shorowordi *et al.* 2003). Long process times and high temperatures are generally required to attain good wetting. An infiltration method using aluminium at high temperature and high vacuum, and the addition of titanium compounds can increase the wettabilitty of the aluminium liquid on BC (Jung and Kang 2004,

Halverson *et al.* 1989). Nevertheless, it remains difficult to obtain the full density of the MMC either through conventional or novel manufacturing methods (Powder Metallurgy, Hot Isostatic Pressing, Quasi-Isostatic Forging, Metal Infiltration, Self-Propagating High-Temperature Synthesis), which are normally time, energy, and cost consuming (Kommel and Kimmari 2006).

3.5.2 Polymer Matrix (PMC)

On the other hand, BC reinforced PMC can be produced using less demanding methods using a wide range of polymers, such as, polyethylene, propylene, phenolic resin, epoxy, silicone (Hayun *et al.* 2008) or combination of resins (Gopalani *et al.* 2009).

Polyethylene matrices have been used with small additions of BC (2%wt.) as an absorbing material or combined with others (8 to 30%wt.) to produce components for neutron shielding applications (Harrison *et al.* 2008, Kaloshkin *et al.* 2012). Despite polyethylene composites reinforced boron and boron compounds are widely being used as neutron shielding materials, although these polymers possess limited strength, poor heat resistance and low durability to neutron radiation (Okuno 2005). Also, these composites have been more frequently exposed to even more harsh environments during the last decade, such as, extreme temperature high-speed, high radiation and high-erosion, etc. (Wang *et al.* 2005, Wang *et al.* 2006a, Wang *et al.* 2006b).

Meanwhile, various approaches have been conducted to exploit epoxy resin composites reinforced with BC for neutron shielding, abrasive resistance and military ballistic protection. Some attempts have been made to obtain a PMC reinforced with BC particles for ballistic protection due to the high hardness and low density of the BC. An epoxy resin was used as a binder, wherein the BC powder exhibits a particle size distribution in which some of the particles possess a size of 100 µm or more and some have a particle size of 50 µm or less (Canfer and Robertson 2010). Also, an epoxy matrix composite with 75%wt BC has been developed as lightweight armour system. PMC was manufactured through compression moulding at 170°C, which allows components to be much from any shape (Naebe *et al.* 2011). Good multi-hit tolerance, scalability and effectiveness against a wide range of fragment simulating projectiles (5.56 mm to larger calibre) was achieved without the addition of external reinforcement. Hence, the composite is potentially effective for protection against anti-personnel to anti-vehicle calibre threats. A PMC have also been

used as a neutron shielding material on the outside of nuclear reactors to prevent stray radiation escaping, and in various components of neutron spectrometers, such as, shielding blocks, bricks, beam narrowers and stoppers (Abenojar *et al.* 2009b, Huang *et al.* 2012, Pugh and Hendy 1985). A neutron protection epoxy film reinforced with BC was investigated on the shielding, shear strength, hardness, impact resistance, adhesion and flexibility properties and durability (Huang *et al.* 2011, Huang *et al.* 2012). Various types/combinations of curing agents, particle size distributions and film thickness were used. Radiation shielding was more effective when the film thickness was above 300 μm. Strength and durability was higher when a combination of two cure agents (aromatic tertiary amine and modified flexible low crosslinking polyamide resin) and 30%wt. of BC was used. Another study, also evaluating the behaviour of BC particles filled epoxy composites as a three-body abrasive wear material, using different amounts of filler (average size 15 μm) and under diverse loads and abrading distances (Suresha *et al.* 2009). It demonstrated improved performance of the composites using low amounts of BC (10%wt) in epoxy. This was reported to be a result of a more uniform dispersion of filler and better adhesion between the matrix and the BC. Agglomeration of the particles and poor adhesion to epoxy was observed with higher amounts of BC (15 to 20%wt).

The influence of BC addition on the cure kinetics, viscoelastic and mechanical properties of a room temperature amine cure DGEBA epoxy resin has been conducted using different particle size distributions and concentrations (7 to 23 μm, 6 to 12%wt BC) (Abenojar *et al.* 2009b). In this case the BC acted as accelerator or retardant in the cure depending on the amount and size of the particles, without affecting the degree of conversion. However, a reduction in the glass transition temperature (T_g) was observed, reportedly due to changes in crosslinking. The particles tended to deposit and agglomerate due to the low viscosity of the resin. The use of smaller amounts of BC particles led to an increase in bending strength. Nevertheless, poor adhesion between the BC and epoxy was demonstrated during wear tests.

A good knowledge of degradation mechanisms and their effect on the long-term properties of these composites are essential to attain a stronger confidence from industry for their use in high demanding applications. The degradation mechanisms and changes in the physical, rheological and mechanical properties of a aged epoxy coating reinforced with 6%wt. BC (7 and 23μm) were evaluated when exposed to a high moisture and temperature environment (50% and 95% RH at 60°C) (Abenojar *et al.* 2011). The degree of

degradation and plasticisation was proportional to the amount of absorbed water, which depends on the moisture to which the composite was exposed. Structural relaxation was lower for the aged material subject to both humidity and temperature, compared with similar species exposed only to high temperature. Hence, the effect of the temperature was evident, providing a higher T_g and improved bending strength. In contrast, diminished strength was obtained with exposure to high humidity and temperature. Full recovery or even higher values was observed in some cases after a drying process. Only partial weight loss was confirmed through gravimetry and FTIR. Wear resistance decreased with humidity exposure, which was more evident in PMC than that of the pure epoxy coating. Nevertheless, exposure to low moisture and high temperature led to improved strength, reportedly as a result of plasticisation in the composite (1%wt. absorbed water).

Regardless of the potential of these composites, they are built up from a complex interplay of physical and chemical factors that occur at the interface or interphase region between the matrix and the inorganic material (Plueddemann 1991, Jun *et al.* 2011, Abenojar *et al.* 2009b). In the previous cases, a lack of adhesion exhibited between BC and the epoxy resin and the agglomeration / sedimentation of the particles lead to composites with limited mechanical properties and durability. Hence, understanding of the native surface chemistry of BC is critical to improve adhesion, dispersion and water resistance through silane modification.

3.6 Surface Chemistry

BC particles have been incorporated into ceramic matrix composites and in protective layers deposited on the surface of C/C composites to improve their resistance to oxidation (Naslain *et al.* 2004, Smeacetto *et al.* 2002). The latter is related to the low oxidation resistance of the boron, BC and boride species, specially when exposed to high temperatures, which lead to the formation of a oxide film that act as a oxygen diffusion barrier and consequently to the passivation of the material to protect (Smeacetto *et al.* 2002). The processes and extent of the BC oxidation have been widely investigated showing that strongly depends on the composition and morphology of the material as well of the environmental conditions, such as, atmosphere, flow, temperature and pressure. Several studies have been conducted showing the different processes that participate in the oxidation of ceramic and powdered BC, such as, the diffusion of the elements (boron, carbon and oxygen) in the bulk and through the oxide film, chemical reactions between the

material and atmosphere species, and finally the vaporisation and transport of the reaction products (Steiner 2005). The theoretically possible reactions that BC may suffer when exposed to an air atmosphere are listed below, involve mainly the oxygen and/or water species and the formation of boron oxide (B_2O_3) as may reaction product. This fact is related to all reactions (Eq. 3.12-3.17) possess a negative Gibbs energy, despite the first being the most favourable even at lower temperatures (Li and Qiu 2007).

$$B_4C\,(s)\; +\; 4\,O_2\,(g)\; \rightleftharpoons\; 2\,B_2O_3\,(s)\; +\; CO_2\,(g) \qquad\qquad (3.12)$$

$$B_4C\,(s)\; +\; 7/2\,O_2\,(g)\; \rightleftharpoons\; 2\,B_2O_3\,(s)\; +\; CO\,(g) \qquad\qquad (3.13)$$

$$B_4C\,(s)\; +\; 8\,H_2O\,(g)\; \rightleftharpoons\; 2\,B_2O_3\,(s)\; +\; CO_2\,(g)\; +\; 8\,H_2\,(g) \qquad\qquad (3.14)$$

$$B_4C\,(s)\; +\; 7\,H_2O\,(g)\; \rightleftharpoons\; 2\,B_2O_3\,(s)\; +\; CO\,(g)\; +\; 7\,H_2\,(g) \qquad\qquad (3.15)$$

$$B_4C\,(s)\; +\; 6\,H_2O\,(g)\; \rightleftharpoons\; 2\,B_2O_3\,(s)\; +\; C\,(s)\; +\; 6\,H_2\,(g) \qquad\qquad (3.16)$$

$$B_4C\,(s)\; +\; H_2O\,(g)\; \rightleftharpoons\; 2\,B_2O_3\,(s)\; +\; CH_4\,(g)\; +\; 4\,H_2\,(g) \qquad\qquad (3.17)$$
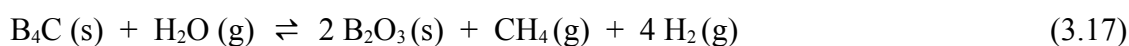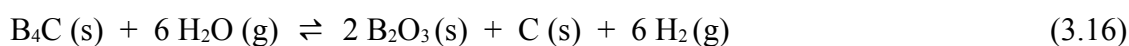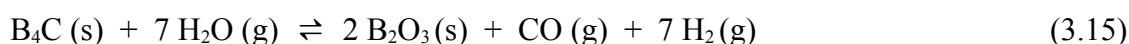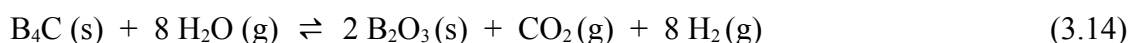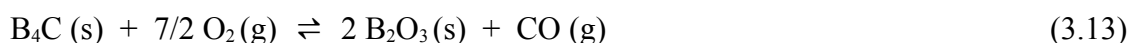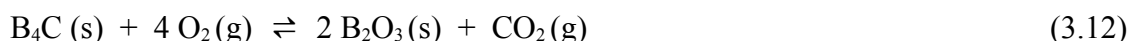
Moreover, the oxidation of the BC can be explained as a two stage process (Eq. 3.18-3.19) where the boron oxide can react with the water vapour present in the air to form boron acid species, such as oxoborinic acid (HBO_2) and boric acid (H_3BO_3) (Steinbrück 2005, Rybakov 1995).

$$B_2O_3\,(s)\; +\; H_2O\,(g)\; \rightarrow\; 2\,HBO_2\,(l) \qquad\qquad (3.18)$$

$$B_2O_3\,(s)\; +\; 3\,H_2O\,(g)\; \rightarrow\; 2\,H_3BO_3\,(l) \qquad\qquad (3.19)$$

The oxidation of the BC components in an air atmosphere was studied showing a near-parabolic process with the formation of B_2O_3, HBO_2 and H_3BO_3 (Efimenko *et al.* 1987). Also, the formation of a very thin film of B_2O_3 was observed in oxygen atmosphere at approximately 550ºC. The formation rate was directly proportional to the exposed temperature and limited by the diffusion of boron, oxygen and carbon elements from the bulk to the surface at temperatures inferior to 1200ºC. On the other hand, at higher temperatures the vaporisation rate of the oxide surpass the oxidation rate of the BC (Li and Qiu 2007). Another study of the oxidation process with wet and dry air at temperatures above 900ºC was also conducted showing a weight loss and the formation of BO or HBO_2 as main products (Sato *et al.* 1988).

In contrast, the BC powder exhibited a lower initial oxidation temperature and faster rate

as a result of the higher surface area, specially when the ceramic material is in a wet air atmosphere. However, the oxidation rate with dry air surpasses that with wet atmosphere at temperatures above 700ºC. This is related with B_2O_3 film formed on the BC surface that inhibits the oxidation process in water, leading to a linear and non-linear oxidation kinetics in dry and wet atmosphere, respectively (Litz and Mercuri 1963). A different work conducted with submicron BC powder at room temperature showed a slow oxidation process in wet air with the formation of film composed by boron oxide (B_2O_3), oxoborinic acid (HBO_2) and boric acid (H_3BO_3) species (Matje and Schwetz 1988). Also, the oxidation behaviour of micron BC powder in air was evaluated showing that the degree is strongly dependent on particle size and temperature. The kinetics in static air showed a limited/controlled rate law by the oxygen diffusion through the B_2O_3 layer. However, the evaporation of boron oxide at high temperature changes the oxidation process (Li and Qiu 2007). Another work was done to predict the thickness of the oxide film at equilibrium through the development of a parametric model for the simulation of BC oxidation at high temperatures. The rate was calculated by the convective transport of the gaseous reaction products showing it strongly depends on the atmosphere and flow conditions This fact is the result of the transport process being the slowest step in the BC oxidation, in particularly the removal of the boric acid from the surface (Steiner 2005). Furthermore, surface chemistry and structural characteristics of the BC nanoparticles were investigated after ball milling in various atmospheres (Mortensen *et al*. 2006). The milled material exhibited a overall negatively charged surface which is believed to be a result of boronic surface groups due to the presence of boric acid, which acts as a Lewis acid by accepting a hydroxyl ion, OH^-, in order to form a tetrahedral borate ion, $B(OH)_3^-$.

CHAPTER 4 – EPOXY ADHESIVES

4.1 Introduction

Epoxy (EP) resins were probably found in early 1900s by the Russian chemist Prileschajev through the reaction between olefins and peroxybenzoic acid. However, research for mass production of the resin through epichlorohydrin only started in 1927. Bisphenol-A based epoxy resin was achieved in 1936 by two chemists, P. Castan and S.O. Greenlee, which during the late 1930s applied several patents based on their work. Later, the synthesis process was licensed by the Swiss company Ciba-Geigy, which in 1946 commercialised the first epoxy resin. Ciba epoxy business was sold in the late 1990s and at the present is now the Huntsman Advanced Materials (Irfan 1998).

EP resins are probably the most versatile family of thermosetting polymers with a very interesting combination of properties which makes them to be extensively exploited as coatings, structural adhesives and composite materials for advanced applications. They exhibit exceptional mechanical, chemical and thermal properties, and excellent adhesion to a wide range of materials such as glass, metal, timber, concrete, fibres, etc (Table 4.1). Moreover, epoxy resins have demonstrated good durability to aggressive environments, such as, exposure to gamma rays and neutron radiation (Okuno 2005, Zhang *et al.* 2008, Huang *et al.* 2011, Huang *et al.* 2012). Hence, they are highly valued by nuclear, aerospace and military applications. Epoxy adhesives are generally 100% solid one- (1k) or two- (2k) component system, i.e., resin and curing agent. Different types and stoichiometry of components, with or without the incorporation of fillers and other additives, can be used to formulate an adhesive with tailored properties before and after the cure process (Mailvaganam 1997, Irfan 1998). Also, the final properties of the cured material results from the preparation, application and cure processes, degree of polymerisation, crosslinking and other factors (Okuno 2005, Abenojar *et al.* 2009b] .

Table 4.1 Typical properties of a generic epoxy resin (Petrie 2006, International Association of Plastics Distribution 2008, ULIDES 2013).

Properties[*]	Nominal Value	Test Method
PHYSICAL		
Specific Gravity (g/cm^3)	0.65 – 1.77	ASTM D1505
Apparent Density (g/cm^3)	1.02 – 1.61	ASTM D1895
Mix Viscosity (cP)	65.0 – 23600	ASTM D2393
Moulding Shrinkage – Flow (in/in)	0.00010 – 0.0051	ASTM D955
Water Absorption (%), 24h / saturation	0.06 – 0.41 / 0.20 – 0.87	ASTM D570
TIME		
Shelf Life (weeks)	24 – 54	-
Pot Life (min)	1.0 – 6500	-
Demould Time (min)	0.54 – 270	-
Post Cure Time (hr)	0.50 – 7.7	-
MECHANICAL		
Tensile Modulus (GPa)	0 – 18 (~2.4)	ASTM D638
Tensile Strength (MPa)	28 – 90	ASTM D638
Tensile Elongation (%), Yield / Break	0.4 – 7.9 / 0.6 – 21	ASTM D638
Flexural Modulus (GPa)	0 – 12	ASTM D790
Flexural Strength (MPa)	90 – 145	ASTM D790
Compressive Modulus (GPa)	0 – 3	ASTM D695
Compressive Strength (MPa)	23 – 174	ASTM D695
Shear Strength (MPa)	7 – 53	ASTM D732
Notched Izod Impact (J/m)	11 – 64	ASTM D256
Durometer	69 – 93	ASTM D2240
Lap Shear Strength (MPa)		ASTM D1002
Aluminium / Stainless steel, Acid etch	19 / 49	
THERMAL		
Deflection T Under Load (ºC)	24 – 480 (1.8 MPa)	ASTM D648
Max. Continuous Use T (ºC)	70 – 180	ASTM D794
Glass Transition T (ºC)	133 – 228 /52 – 171	ASTM E1356 / DSC
CLTE - Flow (m/m/°C)	6 – 92 x 10^{-6}	ASTM D696
Thermal Conduct. (Btu·in/hr/ft2/°F)	0.4 – 6.0	ASTM C177

[*] nominal value at 23ºC when the temperature is not defined

4.2 Epoxy Resins

Epoxy resins contain a three-membered cyclic ether group with a equilateral triangle structure generally known as 1,2-epoxide, oxirane or epoxy group. These resins can be present in different forms in the adhesives formulation, more specifically, bisphenol-A, bisphenol-F and phenol/cresol NOVOLAC (Table 4.2) and is primarily used in combination with a curing agent for cold-setting and hot-setting. They are the most widely used epoxy resins in the industry due to their bi- or multi-functionality. Other monofunctional compounds are only used as reactive diluents, viscosity modifiers, or adhesion promoters (Petrie 2006b).

Table 4.2 Chemical structure, functionality and CAS number of the different epoxy resins (O'Donoghue *et al.* 2003).

Epoxy resin	Structure	Functionality	CAS number
Bisphenol-A (DGEBA)		1.9	1675-54-3
Bisphenol-F (DGEBF)		2.1	2095-03-6
Phenol NOVOLAC (EPN)		2.6 - 3.5	28064-14-4
Cresol NOVOLAC (ECN)		2.7 - 5.4	29690-82-2

The most widely used epoxy resin is diglycidyl ether of bisphenol-A (DGEBA), which is normally the reaction product between epichlorohydrin and bisphenol-A (Fig. 4.1). DGEBA possesses excellent properties that are mostly related to its chemical structure, where: bisphenol-A moiety provides toughness, rigidity and good performance at high temperature; the ether linkages promote chemical resistance; the alkyl section gives flexibility; and hydroxyl and epoxy groups provide the reactivity and excellent adhesion.
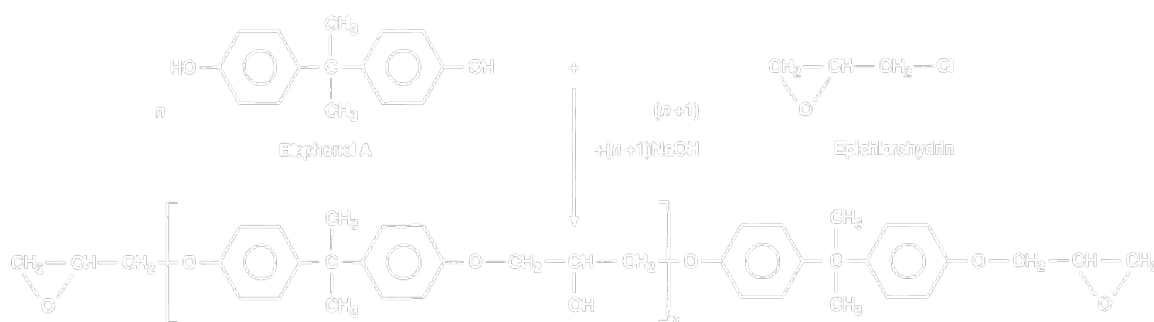
Figure 4.1 Synthesis reaction of bisphenol-A based epoxy resin, DGEBA (Irfan 1998).

Diglycidyl ether of bisphenol-F (DGEBF) resins result from the reaction between epichlorohydrin and bisphenol-F. The latter is composed of an isomers mixture with

ortho-ortho, ortho-para and para-para bonds, whereas bisphenol-A is mainly composed of para-para bonds (Comyn 1997). The DGEBF is typically incorporated into an adhesive formulation to lower its viscosity and tendency for DGEBA resins to crystallise when exposed to temperature cycles. The former modification facilitates the addition of fillers, improved workability, and to easily remove entrapped air/voids due to the lower viscosity. Epoxy phenol NOVOLAC (EPN) resins are obtained by reacting an excess of phenols with formaldehyde in the presence of an acidic catalyst. EPN resins have high epoxy functionality, which depend on the initial number of phenolic hydroxyl groups and extent to which they react with the epichlorohydrin. These high-viscosity liquids or semi-solids are normally used as modifiers in DGEBA adhesive formulations to improve crosslink density that provides excellent mechanical and electrical properties, mouldability, and thermal and chemical resistance properties. Other types of resins can also be incorporated into the epoxy adhesives, such as, glycidyl ether of tetraphenolethane and aliphatic and cycloaliphatic resins (Petrie 2006b).

The molecular structure of the resin affects the chemical, mechanical and thermal properties of the adhesive. The resin molecular-weight and the number/location of the reactive sites in the structure (functionality) defines the kinetics of the cure process, and degree of polymerisation and crosslinking. Generally, low-molecular-weight epoxies are more reactive and form denser crosslinked network even, at lower temperature. Thus, resins are selected according to the processing requirements and final properties of the cured adhesive in service conditions (Table 4.3).

Table 4.3 Chemical, mechanical and thermal properties of the epoxy resins (O'Donoghue *et al.* 2003).

Propriety	Lower		Higher
Functionality	DGEBF	DGEBA	NOVOLAC
Chain length	DGEBF	DGEBA	NOVOLAC
Crosslink density	DGEBA	DGEBF	NOVOLAC
Glass transition temperature, T_g	DGEBA	DGEBF	NOVOLAC
Chemical resistance	DGEBF	DGEBA	NOVOLAC
Hardness	DGEBA	DGEBF	NOVOLAC
Flexibility	NOVOLAC	DGEBF	DGEBA

4.3 Curing Agents

There are present a great variety of curing agents with different chemical nature and structures, providing a wide range of processing and final properties to the adhesive for different applications. They are normally ammonia derivatives, mercaptans, phenolic resins and anhydride and carboxylic acids (Petrie 2006b, Comyn 1997). The ammonia derivatives are the most diverse and widely used family of curing agents, which includes amines and polyamides. Amine compounds can be defined as primary, secondary or tertiary, according to the number of substituted hydrogen atoms in the ammonia by an alkyl or aromatic group, respectively (Hara 1990). An overview of the various ammonia derivatives and their influence on the properties of epoxy adhesives is shown in Table 4.4.

Table 4.4 Epoxy adhesive properties influenced by commercial derived amine curing agents (Air Products 2001a).

Property	←													→
Colour/Chromatic stability	Weak	5		1	**2**		7	4		6		3		Excellent
Viscosity	High	1		7	6	5		**2**			3	4		Low
Lifetime	Short	7	6	4	(5)		6		1		**2**	(5)		Long
Low temperature cure	Weak	**2**		1		6	3		4			5	7	Good
Aesthetics	Matte	6		**2**		1		7	3			4	5	Gloss
Flexibility	Moderate	7	6		5		4	3		**2**		1		Excellent
Adhesion	Moderate	5	6		3		7		4	**2**	1			Excellent
Acid resistance	Moderate	1		**2**		7	6		4	3		5		Excellent
Solvent resistance	Weak	**2**		1		5		4	3			7	6	Very good
Water resistance	Very good	5		7	6		4	3		**2**		1		Excellent

Note: curing agent and respective commercial name; 1–Polyamide, Ancamide 350A; **2–Amideamine, Ancamide 506**; 3–Cycloaliphatic-A, Ancamide 1618; 4–Cycloaliphatic-MB, Ancamide MCA, 5–Aromatic, Ancamide TL/TLS; 6–Aliphatic-A, Ancamide 1608; 7–Aliphatic-MB, Ancamide 1856; A–adduct type; MB–Mannich base type.

During the cure process, the liquid resin becomes progressively more viscous to form a more or less amorphous high- molecular-weight cross-linked three-dimensional solid with good adhesive and cohesive strength. This exothermic process is mainly conducted by polyaddition in the presence of a curing agent (Fig. 4.2a and 4.2b) or homopolymerisation reaction via a catalyst. The former mechanism leads to the formation of a heteropolymer structure, which is made-up of epoxy resin molecules linked together via the reactive sites of the curing agent. In contrast, the homopolymerised network is only composed of epoxy resins linked together by their own reactive sites (Petrie 2006b). Nevertheless, the cure is

essentially conducted by ring-opening polymerisation, without the formation of side products, which leads to a low shrinkage of the resin during the cure process and consequently to a reduced internal stress of the crosslinked adhesive.

4.4 Formulation

Hence, the selection of the curing agent and respective stoichiometry used in the formulation are critical to the final crosslinked structure, affecting the mechanical properties of the cured adhesive. In the case of amine compounds, recommended stoichiometry is determined by well-established procedures (Irgan 1998). Generally, stoichiometry between the epoxy group and amine hydrogen is 1:1 (up to 50%wt.) to ensure complete polymerisation and consequently maximum product stability (Petrie 2006b). Despite not ensuring a full degree of polymerisation and consequently sacrificing some properties, other stoichiometries can be used to promote another properties which are more relevant for a particular application, such as, higher elastic modulus, increased density, superior hardness, greater brittleness, lower T_g, decreased chemical resistance to solvents and humidity, etc. Formulations ranging from a more balanced to richer curing agent stoichiometry normally present a more open structure, as result the of the initial stages, or full process, being dominated by polyaddition reactions (Fig. 4.2a and 4.2b) (Petrie 2006b). This stoichiometry provides faster cure, better mechanical strength and lower water resistance (O'Donoghue *et al.* 2003). Also, enhanced deformation capacity of the cured material is related to these structures suffer plasticisation being typically more prone to absorb moisture from the surroundings. However, the adhesive strength is not affected because no resin recrystallisation and homopolymerisation occurs at these stoichiometries (d'Almeida *et al.* 2003). Whereas, formulations richer in resin lead to the full consumption of curing agent reactive sites and steric hindrance of the tertiary amine (Fig. 4.2c) resulting in a more compact, brittle and rigid macromolecular structure with better heat and environmental resistance. This is mainly attributed to the recrystallisation and homopolymerisation of unreacted epoxy monomers (Fig. 4.2d and 4.2e), with the latter forming mostly step like structures (Chiao 1990). Non stoichiometric formulations may result from the false assumption that mass and volume are directly interchangeable, despite the amine curing agent and epoxy resin density ranging from 0.92 to 0.98 and 1.15 to 1.20 g/cm^3, respectively (Paint & Coating Industries 2006).
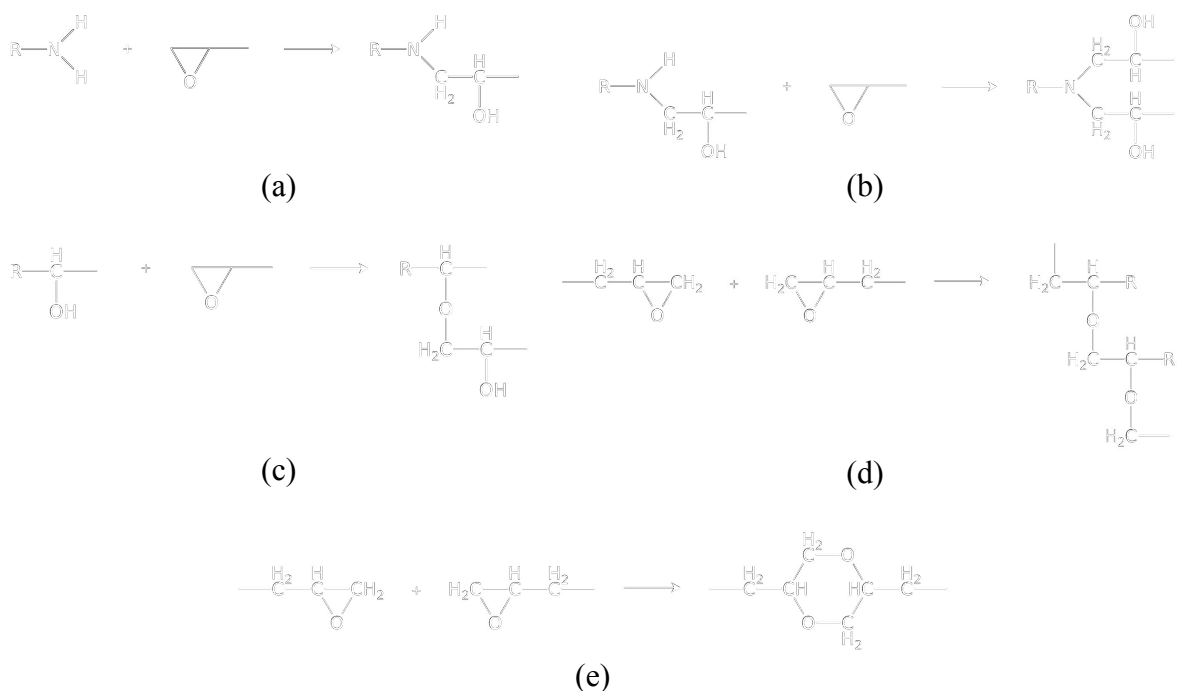
Figure 4.2 Cure mechanisms of an epoxy resin by: polyaddition with (a, b) a primary amine; (c) nucleophilic attack through the hydroxyl groups generated from the reactions a and b; (e) homopolymerisation with the formation of the p-dioxane ring structure or (d) step like structure (d'Almeida *et al.* 2003).

Heat cure and catalysts are generally considered for one-component (1k) epoxy adhesives, i.e. a resin premixed with a curing agent only soluble at high temperatures. The catalyst function is to initiate homopolymerisation without making part in the crosslinked structure. Moreover, most commercial epoxy adhesives contain other compounds, like flexibilisers, tougheners, diluents, fire-retardants, fillers, thixotropic agents, adhesion promoters, foaming agents, pigments, etc. They are incorporated into the adhesive formulation to obtain tailored properties for a specific application, such as, specific density, rheology/thixotropy, fire resistance, peel strength, impact resistance, toughness, deformation/brittleness, shrinkage, cost, adhesion and aesthetics (Petrie 2006b).

4.5 Properties for Moulding Process

The use of the adhesive as a binder for reinforced polymeric matrix composites (PMC) depends on the manufacturing process, compatibility with reinforcement, properties and life-time required under service conditions. In the scope of this work, an adhesive suitable for moulding of PMC was used taking in consideration most of the properties required for open or close moulding (Table 4.5).

Table 4.5 Adhesive properties suitable for mould manufacturing process of PMC
(Crosslink Technology 2012, Biron 2004).

Stage	Property	Description
Processing	Limitations	Considerations on the available equipment, type of moulding (hand or automated), cure (room or high temperature), mould geometry and size, presence of fillers or reinforcement (particles, fibres, etc.).
Preparation	Low viscosity	Ensure an effective wettability / dispersion of the reinforcement and an low mixed viscosity. Pre-heated components result in a reduced viscosity.
	Room temperature	Easier, simpler and low cost process.
	Low reactivity	Provide medium to long pot-life, similar to the required working time (for each 10ºC rise in temperature → 50% reduction of the pot-life).
	No to low pressure	No pressure to low pressure for an easier, simpler and low cost process.
Cure	Temperature	Preferentially close to room temperate for an easier, simpler and low manufacturing process.
	Time	Slow cure system / low exotherm to avoid the release of heat in a short-time time period, specially when using large amounts for moulding.
	Shrinkage	Low shrinkage to minimise the internal stress and obtain dimensionally stable parts (use of a high content of filler/reinforcement particles).
	100% solids No volatiles	Avoid the formation of bubbles in the matrix from solvents or volatile side-products formed during cure (use of vacuum to remove bubbles).
Service	Adhesion	Good adhesion to the an wide range of materials, specially considering within the scope of this work.
	Good mechanical behaviour	High mechanical strength for structural applications. Flexibility for better stress distribution as result of the applied loads, and distinct mechanical and thermal expansion characteristics of the embedded materials.
	Thermal-stability	Loss of the PMCs mechanical properties as a result of the α-relaxation of the adhesive's macromolecular structure (T_g) must be avoided at temperatures lower than those observed under service conditions.
	Durability	Provide the performance required during life-time service. Good resistance to chemicals, temperature and radiation.

The moulding process is a low cost process to obtain finished parts without the requirement of special equipment. However, this is a slow process only suitable for low volume production of PMC parts. Nevertheless, this is a flexible technique which allow the use of other polymer systems, embed reinforcements and encapsulate electronic components or assemblies (Crosslink Technology 2012).

The literature review in the previous three chapters has shown that:

- Limitations of the sintered BC components restricts their use for radiation shielding;

- Low content BC-epoxy PMC have been investigated for other applications;

- Lack of adhesion to epoxy resin and agglomeration of the BC particles resulted in PMCs with limited mechanical properties and durability;

- SCAs represent an efficient means of surface modification to promote adhesion, particle dispersion and bonding durability with epoxy resins;

- Silane solution parameters and surface chemistry of the material strongly affect the effectiveness of the SCA;

- Oxidation and hydration of the BC surface in atmospheric air have eventually an important role in the interaction with the SCA;

- Epoxy resins are used by the nuclear industry due to their properties for moulding process and service conditions.

Despite the importance of BC to the industry and extensive research using SCA, no studies have been reported to enhance adhesion and bonding durability of BC to epoxy resins. This investigation was conducted to demonstrate that enhanced adhesion, particle distribution and bonding durability can be attained by silane modification, and finally to obtain a high content BC-epoxy PMC with improved properties through moulding process for radiation shielding. Hence, an experimental programme was undertaken in this work, involving various materials and methods which are described in the next chapter.

CHAPTER 5 – METHODOLOGY

In an attempt to enhance our knowledge of silane coupling agents, an experimental investigation was conducted to evaluate the relationships between various treatments on BC surface chemistry, and the resulting performance and durability of a BC-Epoxy PMC. In this chapter, three sections provide information of the materials, surface treatments and methods employed. This allows a better understanding of the experimental programme and data acquired in this work. The first section describes relevant properties of the materials, and the composition and manufacturing process of the PMC. Also, detailed information can be found on the procedures used for the silane and corona treatment. Finally, a short review and experimental conditions for each methods are given in this chapter. The experimental programme comprises: surface treatment and analysis of the BC, physical-chemical characterisation of the materials and composite; manufacturing process, mechanical strength and artificial ageing of the PMC (Fig. 5.1).

5.1 Materials Employed

The materials used in this study were an epoxy adhesive, a wetting agent, BC and a silane coupling agent. The BC consisted of a high-purity powders and sintered blocks, which were added to the composite epoxy formulation and used as a surface model to evaluate the surface chemistry, respectively. The adhesion promotion and surface modification to the BC was established through the use of a silane coupling agent.

5.1.1 Epoxy Adhesive

In this work, a low- viscosity molecular-weight 2k epoxy adhesive was used in the manufacturing of the PMC, possessing most of the properties described in the section 4.5. Also, a wetting additive was incorporated in the adhesive formulation to improve wettability, dispersion of the BC particles in the matrix and to reduce mixed viscosity (Table 5.1).
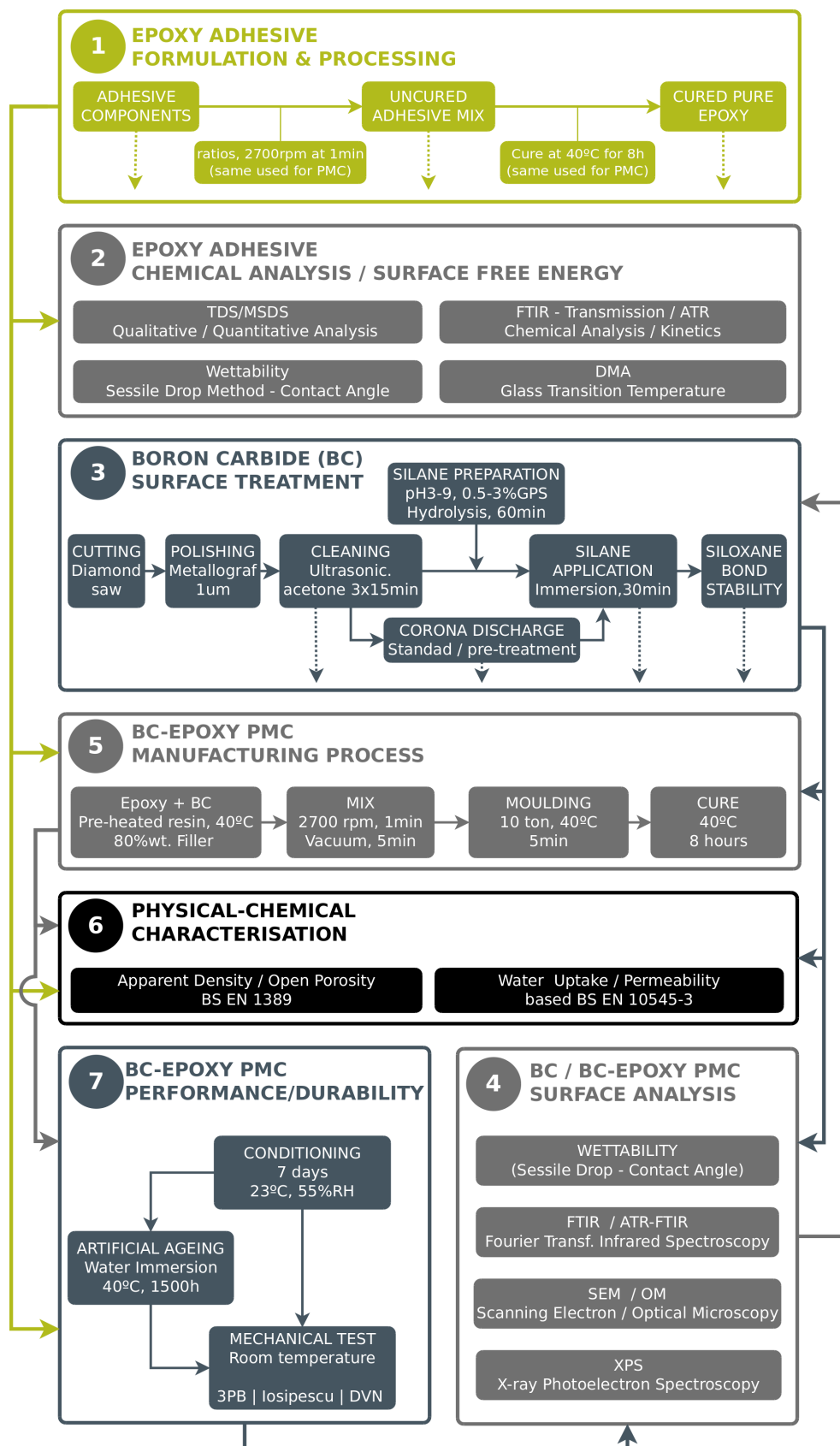
Figure 5.1 Flowchart depicting the characterisation of the materials and PMC characterisation, surface treatment and analysis of the BC, manufacturing process and evaluation of the performance and durability of the BC-Epoxy PMC.

Table 5.1 Reference and composition of each component of the adhesive (Bitrez 2007, Bitrez 2009, Air Products 2001b, Air Products 2004, Air Products 2008, BYK 2008, BYK 2011a, BYK 2011b).
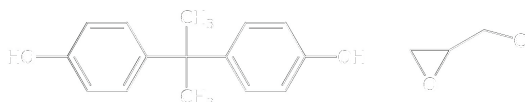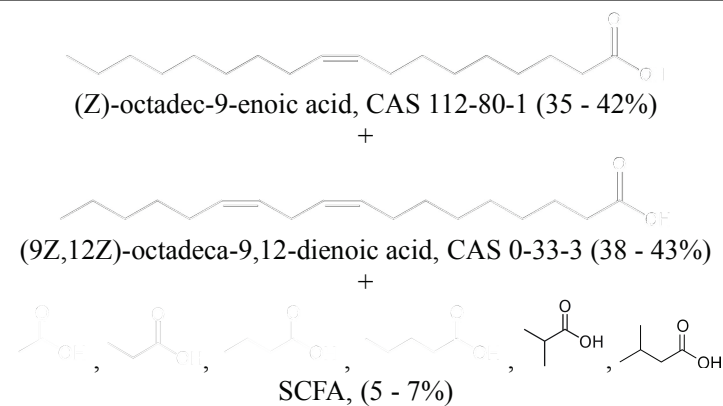
Component	Reference	Composition	wt%
Epoxy resin (100%)	Bitrez Arapox 60-600	Bisphenol-A epichlorohydrin resin, MW<700	100
Curing agent (100%)	Air Products Ancamide 506	Fatty acids, tall-oil, reaction products (TOFA[*]) with Tetraethylenepentamine (TEPA)	>85
		3,6,9- Triazaundecamethylenediamine	<15
Wetting agent (100%)	BYK-W980	2-butoxyethanol and xylene	20
		polyamine amide salt	80

[*] consists mostly of oleic and linoleic acid with small amount of short chain fatty acids, SCFA (Kjellin and Johansson 2010)

The resin of the adhesive is a diglycidyl ether of bisphenol-A (DGEBA) which is commonly used as the primary chemical building block for the broad spectrum of epoxy adhesives. The adhesive formulation includes an general purpose room temperature curing agent, such as tetraethylenepentamine (TEPA). This aliphatic polyamine curing agent when combined with standard unmodified liquid epoxy DGEBA resin offers a low viscosity, medium pot-life and room temperature cure adhesive. Aliphatic polyamines also provide high chemical and solvent resistance and enhanced physical properties to the applied system (Dow Chemical 2009a, Dow Chemical 2009b). A plasticiser is also in the adhesive formulation, an epoxidised tail oil fatty acid. The reactive epoxy groups present allow the plasticiser to be resin compatible and non migrating. These compounds provide a small degree of resiliency to a normally rigid system, depending on the component's functionality and molecular nature. Thus, they help to reduce stresses caused by shrinkage during cure or by different thermal expansion rates between the adhesive and the substrate (Petrie 2006b, Huntsman 2009). A wetting additive, BYK-W980, was used to improve wettablity, and reduce adhesive viscosity and air trapped in the matrix so that a higher filler loading of the BC was possible. Despite the use of SCA to improve adhesion, this wetting agent was still employed to confer the other desirable characteristics. This wetting agent is suitable for epoxy resins with carbonate fillers according to information provided in the manufacturer's technical data sheet.

The chemical structure and name according to International Union of Pure and Applied Chemistry (IUPAC) for the the different compounds present in the components of adhesive is summarised in Table 5.2.

Table 5.2 Structure and name of the compounds present in the adhesive formulation (Air Products 2001b, Air Products 2004, Air Products 2008, Bitrez 2007, Bitrez 2009, BYK 2011a, BYK 2011b, BYK 2008).

Composition	Compound Structure and Name
Bisphenol-A epichlorohydrin resin CAS 25068-38-6	4,4'-(2,2-Propanediyl)diphenol - 2-(chloromethyl)oxirane (1:1)
TOFA with tetraethylenepentamine CAS 68953-36-6	(Z)-octadec-9-enoic acid, CAS 112-80-1 (35 - 42%) + (9Z,12Z)-octadeca-9,12-dienoic acid, CAS 0-33-3 (38 - 43%) + SCFA, (5 - 7%) = TOFA, CAS 61790-12-3 *N*-(2-aminoethyl)-*N*'-{2-[(2-aminoethyl)amino]ethyl}ethane-1,2-diamine CAS 112-57-2
3,6,9-Triazaundecamethylenediamine CAS 112-57-2	*N*-(2-aminoethyl)-*N*'-{2-[(2-aminoethyl)amino]ethyl}ethane-1,2-diamine
2-butoxyethanol CAS 111-76-2	
polyamine amide salt	X – R – NH - [- CO – R' – CO – NH – R – NH -]$_n$ – H Generic molecular structures

The main properties of each component used in the adhesion formulation were obtained from the manufacturers data sheets and compiled in Appendix A (Table A.1). The cure process starts as soon as the resin and cure agent are mixed together, producing an exponential increase in the viscosity and mechanical properties of the adhesive. After cure, the adhesive exhibits good mechanical behaviour, adhesion, strength and stiffness. Some of these values were provided by manufacturers (Table 5.3).

Table 5.3 Adhesive physical-chemical properties before and after cure (Air Products 2001b).

Stage	Properties	
Before cure	Mixed viscosity @25°C (cP)	1400
	Gel time @25°C (min)	385
	Thin film set time @25°C (h)	23
After cure	Density (g/cm3)	1.12
	Vickers hardness (GPa)	0.27
	Tensile strength (MPa)	47.4
	Tensile modulus (GPa)	2.0
	Tensile elongation at Break (%)	4.9
	Flexural strength (MPa)	73.4
	Flexural modulus (GPa)	1.4
	Heat deflection temperature (°C)	58
	Lap shear strength (MPa)	22.9 (mild steel)

Experimental procedure

The procedure used in the preparation and cure of adhesive (Fig. 5.2) was conducted according to the conditions recommended in the manufacturer's technical data sheet to ensure optimum mechanical properties of pure adhesive and BC-Epoxy PMC specimens (Air Products 2001b). The stoichiometry used was 54 parts by weight of the curing agent (Amine Hydrogen Equivalent Weight, AHEW=105) with 100 parts of resin (Epoxy Equivalent Weight, EEW=189), which is in agreement with the theoretical value obtained according to the Eq. 5.1 (Air Products 2003).

$$phr \text{ of Curing Agent } = \frac{AHEW \text{ of Curing Agent}}{EWW \text{ of Resin}} \cdot 100 \qquad (5.1)$$

```
┌──────────────────┐        ┌────────────────────────────────────┐
│ Homogenisation   │────────│ Each component individually homogenised │
└──────────────────┘        └────────────────────────────────────┘
        │
        ▼
┌──────────────────┐        ┌────────────────────────────────────┐
│ Addition         │────────│ 1. Pre-heated epoxy resin @40ºC (65%wt) │
└──────────────────┘        │ 2. Hardener (35%wt)                   │
        │                   └────────────────────────────────────┘
        ▼
┌──────────────────┐        ┌────────────────────────────────────┐
│ Mixing           │────────│ 1. Hand mix carefully with a spatula  │
└──────────────────┘        │ 2. Speed mix, 1min @ 2700 rpm         │
        │                   └────────────────────────────────────┘
        ▼
┌──────────────────┐        ┌────────────────────────────────────┐
│ Addition         │────────│ Wetting agent, +1.5%wt                │
└──────────────────┘        └────────────────────────────────────┘
        │
        ▼
┌──────────────────┐        ┌────────────────────────────────────┐
│ Mixing           │────────│ 1. Hand mix carefully with a spatula  │
└──────────────────┘        │ 2. Speed mix, 1min @ 2700 rpm         │
        │                   └────────────────────────────────────┘
┌─────────────┐     ▼
│ BC-Epoxy PMC│ ┌──────────────────┐  ┌────────────────────────────────────┐
│ Manufacturing│ │ Moulding        │──│ Applied carefully to minimize the retention │
└─────────────┘ └──────────────────┘  │ of air bubbles in the matrix         │
        │                   └────────────────────────────────────┘
        ▼
┌──────────────────┐        ┌────────────────────────────────────┐
│ Cure             │────────│ 8 hours @ 40ºC                        │
└──────────────────┘        └────────────────────────────────────┘
        │
        ▼
┌──────────────────┐        ┌────────────────────────────────────┐
│ Characterisation │────────│ Adhesive's physico-chemical properties │
└──────────────────┘        └────────────────────────────────────┘
```

Figure 5.2 Procedure used in the preparation and cure of the epoxy adhesive.

5.1.2 Boron Carbide

Boron carbide material used in this work was in powder form and sintered block, both supplied by PI-KEM Limited, Tamworth, England. The powder consisted of a high-purity three-particle-size, which was added to the formulation of the epoxy matrix composite. A sintered block was used as a surface model to evaluate the effect the various treatments had on the SFE and wettability of BC. This provided better understanding of the treatment's influence on the viscosity of the uncured mixture, and density, open porosity, water permeability, mechanical properties and durability of the PMC. According to the scope of this work, select properties of the BC are summarised in the Table 5.4. Additional information relative to the nomenclature, identifiers, and chemical and electrical properties of the ceramic material is shown in Appendix A (Table A.2).

Table 5.4 Boron carbide formula, CAS number and properties (Pierson 1992, Pierson 1996, Thevenot 1990, Suri *et al.* 2009, Aoqui *et al.* 2002).

General	IUPAC	Boron carbide
	Formula	B_4C
	CAS number	12069-32-8
Physical properties	Density (g/cm3)	2.48 - 2.52 (solid)
	Specific gravity	2.51
	Solubility in water	Insoluble
	Crystal structure	Rhombohedral / Orthorhombic
	Apparent porosity (%)	< 3
Mechanical properties	Vickers Hardness (GPa)	27.5 – 34.3
	Modulus of Elasticity (GPa)	352 – 455
	Flexural strength (MPa)	330 – 400
	Compressive strength (MPa)	1400 – 3400
	Poisson's ratio	0.16 – 0.21
	Fracture toughness (MPa.m$^{\frac{1}{2}}$)	3.0 – 3.5
	Tensile modulus (GPa)	440 – 470
	Tensile strength (MPa)	350
Thermal properties	Coef. of thermal expansion (/ºC)	$5.0 – 5.6 \times 10^{-6}$ (20 - 1000ºC)
	Conductivity (W/m/K)	20 – 92 (20ºC)
	Specific heat (J.K^{-1}.kg^{-1})	950 (25°C)
	Max. working temperature (ºC)	600 (oxidising atmosphere)
		2000 (reducing atmosphere)
	Neutron capture cross-section (barn)	600 – 750
	Upper continuous use temperature (ºC)	600 – 800

5.1.2.1 Particles

BC particles with a high purity and different grit designations were used in the composite formulation. Some information relative to the mesh size distribution, elemental and chemical composition and mixing ratio used for various grit sizes is summarised in Table 5.5. These ratios were used for the composite formulation in agreement with current practice employed by RAL/STFC.

Table 5.5 Grit type, size distribution, and elemental/chemical concentrations of the boron carbide particles (PI-KEM 2011l, Choudhury *et al.* 2007).

Properties		F60	F360	F1200
Grit type		macro	micro	micro
Mesh size average*, d50 (μm), Max (d3) – Min (d94)		250 300 – 210	23 40 – 12	3 7 – 1
Elemental concentration (%wt.)	B	77.0	76.5	74.5
	C	21.4	22.2	22.9
	Fe	> 0.15	> 0.20	> 0.20
	O	> 1.00	> 1.00	> 1.00
	N	> 1.00	> 1.00	> 1.00
	Si	> 0.15	> 0.15	> 0.15
Chemical concentration (%wt.)	B_4C	97.1	96.7	93.5
	B_2O_3	> 0.50	> 0.20	> 0.20
Mixing ratio (%wt.)		22.9	27.4	49.6

* by photosedimentometer.

5.1.2.2 Sintered Material

Square sintered block samples with dimensions of 12 x 25 x 6 mm (Pi-KEM 009XP9258) were used as a surface model to evaluate the effect of the treatments on the SFE or wettability of the boron carbide (Fig. 5.3). The instrumentation and procedure used during the polishing is shown in appendix A (Table A3) and Fig. 5.4, respectively.

(a)   (b)   (c)
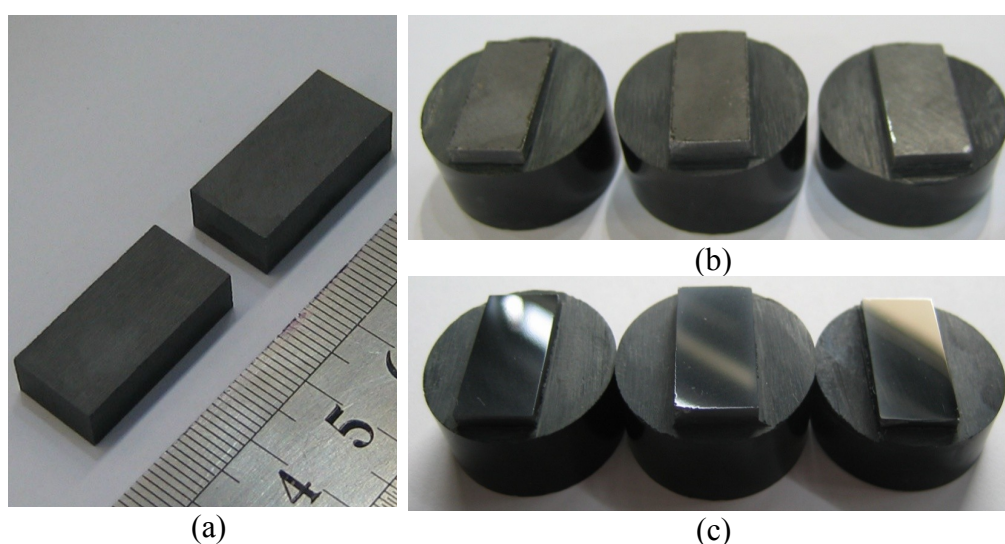
Figure 5.3 Sintered BC samples (a) as received, (b) before and (b) after surface polishing.

The surface polishing was initially conducted to remove the roughness and potentially

some contamination resulting from the cutting process (Fig. 5.4).

| Cutting | Sintered B4C cutted with a diamond saw
samples with 25 x 12 x 6mm3 |

| Grinding - 1st stage | Disc: MD-Piano 600 \| Surface speed: 370rpm
Pressure: 20N/sample \| Lubricant: Water
Holder speed:65rpm \| time: 2min/cycle \| Direction >> |

| Grinding - 2nd stage | Disc: MD-Allegro \| Surface speed: 370rpm
Pressure: 30N/sample \| Lubricant: DiaPro Allegro 9um
Holder speed:65rpm \| time: 2min/cycle \| Direction >> |

| Polishing - 1st Stage | Disc: MD-Dac \| Surface speed: 370rpm
Pressure: 20N/sample\| Lubricant: DiaPro Dac 3um
Holder Speed:65rpm \| time: 5min/cycle \| Direction >> |

| Polishing - 2nd Stage | Disc: MD-Dur \| Surface speed: 370rpm
Pressure: 20N/sample \| Lubricant: DiaPro Nap B 1um
time: 3min/cycle \| Direction >< |

| Cleaning | Ultrasonicated in acetone (3×15 minute/cycle)
Holder speed:65rpm \| Grade solvents were employed |

| Silane surface Treatment | γ –glycidoxypropyltrimethoxysilane
(0.5/1.0/3.0 % w/w) in aqueous solution pH=3/5/7 |

| Wettability test | Chemical and energy surface characterization
Contact angle, Sessile drop method |

* - The surface was cleaned with an cotton cloth (1st- DI-water+detergent, 2nd- DI-water and 3rd- Isopropanol) and analised with an microscope during all procedures and each stage was repeated until a regular surface was obtained

Figure 5.4 Polishing procedure used on the surface of the sintered BC.

5.1.3 Boron Carbide-Epoxy Composite

The composites were fabricated according to the mixing ratios of the materials (Table 5.6) and based on the manufacture process (Fig. 5.6) used by STFC. Although a different mix process and an additional degassing stage were used in this work. Once exposed to the appropriate surface treatment, the particles were incorporated in the pre-heated adhesive and then mixed using a Speedmixer DAC 150FVZ-K at 2700 rpm for 1 minute. The mechanical blending was conducted to assure a uniform mixture and effective dispersion of the particles. After this stage, the mixture was degassed and poured into stainless steel moulds (designed for the mechanical test specimens) as shown in Fig. 5.5. Finally, the composites were compressed under a stress of 10 MPa (Instron Universal Test Machine) and left to cure at 40°C for 8 hours. Test specimens of the pure epoxy resin were also made for comparison using the same manufacturing process.

Table 5.6 Content of the materials used for the manufacture of the composite.

Material	Component	Content (%wt.)	Total content (%wt.)
Epoxy adhesive	Resin	12.9	20.2
	Curing agent	7.0	
	Wetting agent	0.3	
BC particles	F1200	39.6	79.8
	F360	21.9	
	F60	18.3	
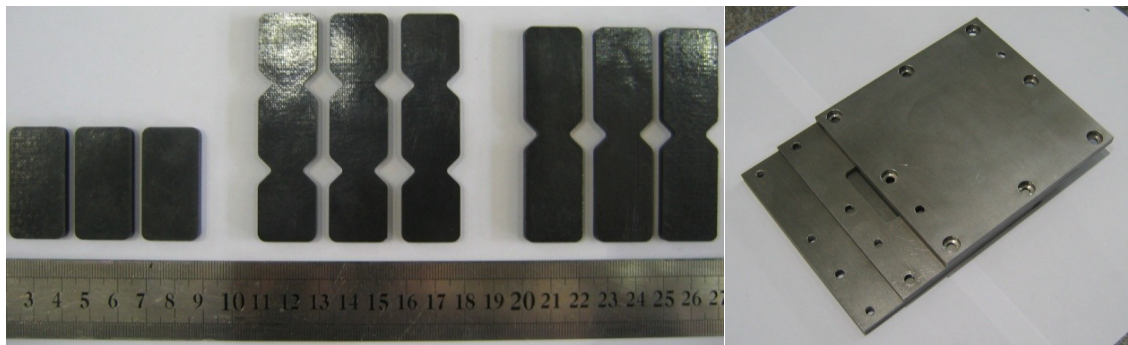
Figure 5.5 Moulds used for the manufacture of the BC-epoxy PMC test specimens.

Addition	Boron carbide with different grit sizes 18.3/21.9/39.6 parts (w/w) of F60/F360/F1200
Mixing	Hand mix carefully with a spatule
Addition	Pre-heated epoxy resin @ 40ºC, 12.9 parts (w/w)
Mixing	Hand mix carefully with a spatule
Addition	Hardener and wetting agent 7.0/0.3 parts (w/w) @ 23ºC
Mixing	1. Hand mix carefully with a spatule 2. Speed mix, 1min @ 2700rpm
Degassing	Boron carbide and epoxy mixture, 5min in vacuum
Moulding	1. Pour small bits from the borders to the centre 2. Apply some pressure with a spatule Obtain a homogeneous material without trapped air
Pressure	Apply high pressure and temperature in an autoclave (5min@10ton,40ºC)
Cure	40ºC, during 8 to 10 hours

Figure 5.6 Manufacturing process of the BC-epoxy PMC.

5.2 Surface Treatments

In this work, two surface treatments were employed to the BC for improved adhesion in the epoxy composite, more specifically a silane coupling agent (SCA) and corona discharge treatment (CDT).

5.2.1 Silane Coupling Agent (SCA)

A short carbon chain silane with an epoxy functional group, γ-glycidyloxypropyl-trimethoxy-silane, (Sigma 440167, Sigma-Aldrich Company Ltd., United Kingdom) was used as an aqueous solution to immerse the boron carbide particles prior to the manufacture of the composite (Fig. 5.7). Additional information relative to the nomenclature, general and physical-chemical properties of the silane is summarised in the Table A.4.
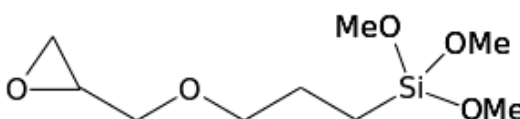
Figure 5.7 γ-glycidyloxypropyl-trimethoxysilane (GPS) molecule structure.

<u>Experimental procedures</u>

The preparation and application procedure of the silane solution on the BC particles and sintered square blocks was based on Abenojar *et al.* 2009a and manufacturer's technical data sheet to ensure a more effective surface treatment and to identify the optimum conditions. Various studies reported in section 2.4.3 showed the significant influence of the solution pH and silane concentration on the efficiency of the surface treatment. Therefore, the optimum conditions for the silane treatment were investigated using different pH values (pH3, pH5, pH7 and pH9) and concentrations (0.5, 1.0, and 3.0%wt. GPS). The silane solutions were prepared using deionised water ($0.0 - 0.1$ µS, Hanna Instruments HI 98308) and pH adjusted (Jenway pH Meter 3050) with acetic acid (10%vol.) or sodium hydroxide (0.1M). BC was immersed in fresh silane solutions (1 hour of hydrolysis, 550 rpm) for 30 minutes, followed by a drying time at 105ºC for 12 hours (Fig. 5.8). A gel of the condensed silane was also obtained using a high concentrated GPS aqueous solution (30%wt., pH5) and analysed with FTIR spectroscopy (Johnsen *et al.* 2003).
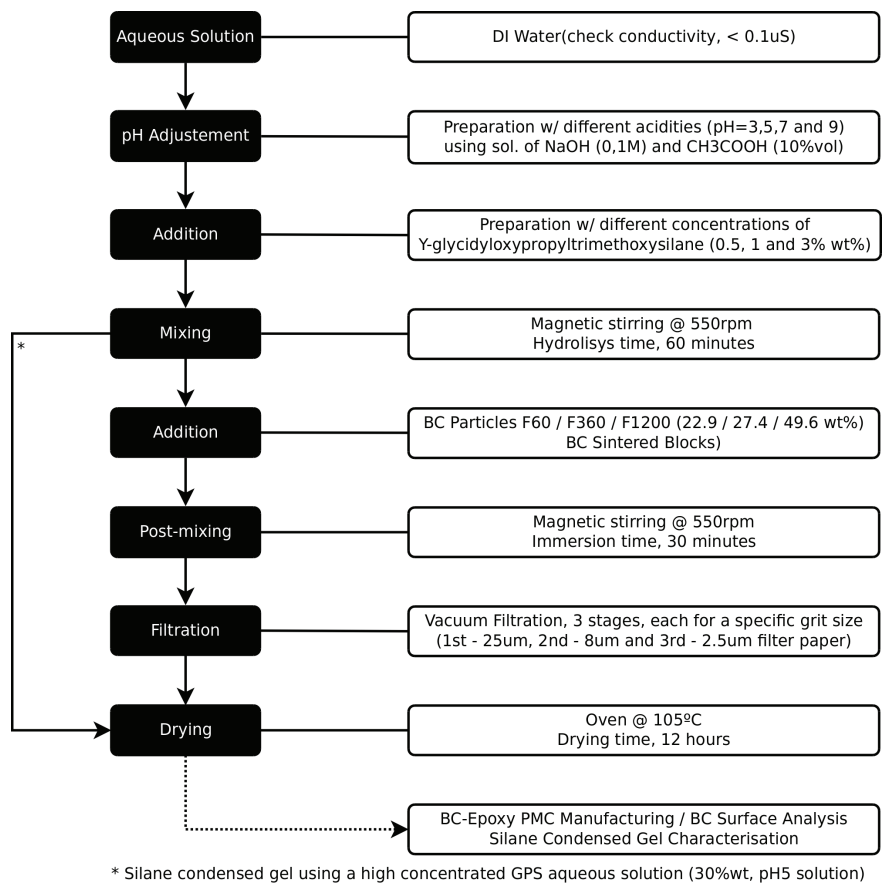
Figure 5.8 Surface treatment procedure of the BC with silane coupling agent.

5.2.2 Corona Discharge Treatment (CDT)

The use of corona discharge treatment (TANTEC HV 05-2) was considered both as the only treatment and also prior to silane application to promote the formation of boron-oxygen species. The discharge (58 kJ/m^2) was applied on the BC inside thin PTFE envelopes ($2 \times 70 \text{ } \mu m$, one for each grit size) with an area of $210 \times 145 \text{ mm}^2$ (Fig. 5.9).The discharge was applied seven times (forward $\leftrightarrow$ backward) at a constant rate (~1.2 m/min) in each direction of the envelope and from side to side. In order to ensure a more effective treatment, the envelope was shaken every time that the direction or side was changed. The distance between the electrode and the envelope was kept constant, corresponding to a dielectric barrier thickness of 2.5 mm.

| (a) | (b) |
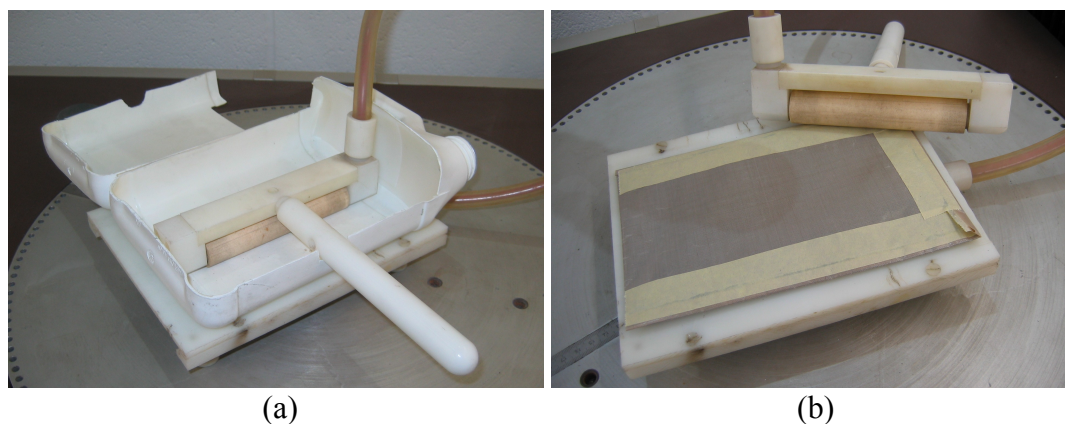
Figure 5.9 Corona discharge treatment apparatus for the BC particles with (a) box and (b) PTFE envelope(final) approach.

5.3 Methods

The effect of silane treatments on the BC was evaluated through surface analysis. This was accomplished by elemental, chemical, surface free energy (SFE) and morphological characterisation of the untreated and treated BC using Fourier Transform Infrared Spectroscopy (FTIR), X-ray Photoelectron Spectroscopy (XPS), Wettability tests and Optical and Scanning Electron Microscopy (SEM). Also, chemical characterisation, kinetics, rheological and wettability studies of the adhesive were carried out to better understand the behaviour on different treated BC surfaces before, during and after the cure process of the PMC. These were conducted through FTIR, Dynamic Mechanical Thermal Analysis (DMA) and Sessile Drop method. Physical-chemical characterisation was done with the determination of bulk density, open porosity and water permeability of the PMC and constituent materials, using gravimetric methods. The mechanical properties and durability of the PMC was determined through three-point-bending (3PB), Iosipescu, and double v-notch (DVN) tests, before and after exposure to artificial ageing (immersion in water). Finally, the topography and failure modes analysis of the fracture surface of the composites was conducted by SEM.

5.3.1 Surface Analysis

5.3.1.1 X-ray Photoelectron Spectroscopy (XPS)

X-ray Photoelectron Spectroscopy (XPS) is a relatively non-destructive surface analysis method that provides elemental percentage composition, functional group identification,

and depth profiling/imaging. In this technique, an electromagnetic radiation source (hv) emits monochromatic X-ray photons that irradiate the surface of interest (<100 Å), which leads to the emission of photoelectrons from the surface atoms. These photoelectrons are then separated according to the kinetic energy (KE) and concentration/counts using the energy analyser and detector of the spectrometer. The energy and counts are related to the valence states and molecular environments, and to the number of atoms with a specific energy level. Thus, the binding energy of the photoelectron can be expressed as:

$$BE = hv - KE + \Phi \qquad\qquad (5.2)$$

Where BE is the binding energy of the photoelectron, hv is the energy of X-ray source , KE is the kinetic energy of the photoelectron, and Φ is the work function of the spectrometer.

The qualitative and semi-quantitative analytical information is represented by a XPS spectrum where the photoelectron counts are represented as a function of their binding energy. The low resolution of XPS survey spectrum exhibits various peaks located at characteristic energies in the full range of the binding energy generally 1000 eV wide, which represent the various elements present in the surface. The characteristic binding energy and intensity of the peak is related to the unique electronic configuration of the element and its concentration within the surface, respectively. The high-resolution spectrum of each element, normally 20 eV wide, shows small shifts of the binding energy as a result of an electron of the atom being influenced by the nearest neighbour group of atoms. Hence, XPS allows the identification and quantification of the functional groups present at the surface. The depth distribution of an element or functional group within the surface can also be attained through angle resolved XPS (ADXPS), using different grazing take-off angles to intensify the signal fraction from surface species (Ratner and Castner 2009). Recently, this technique has been used to conduct image mapping of the elemental or functional groups distribution of silanes present on the the surface (Bexell 2003). XPS has been extensively used in the research of silane and adhesive technology to identify the substrate surface chemistry, evaluate the adsorption of the silane coupling agents and to evaluate the failure modes of adhesive joints (Kinloch *et al.* 2006, Abel *et al.* 2004, Abel *et al.* 2006, Abel and Watts 2009, Rattana *et al.* 2002, Brack *et al.* 2005).

Experimental Procedure

Elemental and chemical analysis was performed on the untreated and silane treated BC particles using a Sigma Probe spectrometer (Thermo VG Scientific, East Grinstead, U.K.) equipped with Monochromatic AlKα source and a hemispherical analyser, according to the experimental conditions and spectra parameters indicated in Table 5.7. Surface elemental and chemical analyses were attained from the high resolution spectra using Shirley background fitting, followed by curve-fitting and assignment of the peaks. The charge correction was made by indexing the energy of C1s electron of adventitious surface carbon to its characteristic level of 285.0 eV. The stoichiometry and full width at half maximum (FWHM) were considered in the fitting.

Table 5.7 XPS experimental conditions used on the untreated and silanised BCparticles.

Instrumentation	Samples	Experimental conditions
Thermo VG Scientific Sigma Probe spectrometer	BC F360 particle Untreated / Silanised	Survey spectra: pass energy 100 eV, step 0.4 eV, range 1350 to 0 eV
Monochromatic AlKα source (*hv* = 1486.6 eV)	Aluminium crucibles fixed on a glass substrate	High resolution spectra: pass energy 20 eV, step 0.2 eV
Thermo Advantage software v4.84 Build 02812		B1s, C1s, O1s, Si2p Na1s, Ca2p, N1s, Fe2p
Mechanical Engineering Sciences Surrey University		Spot size: 1 mm x 3 mm take off angle: 90°

Using the Beer–Lambert principle, the average thickness of the silane layer was estimated by assuming a uniform and homogeneous film across the surface (Watts and Wolstenholme, 2003, Abel *et al.* 2000). Hence, two equations (Eq. 5.3 and 5.4) were considered for the B1s and Si2p signals.

$$I_{B1s}^d = I_{B1s}^\infty \cdot e^{-\left(\frac{d}{\lambda_{B1s} \cdot \sin\theta}\right)} \tag{5.3}$$

$$I_{Si2p}^d = I_{Si2p}^\infty \cdot \left[1 - e^{-\left(\frac{d}{\lambda_{Si2p} \cdot \sin\theta}\right)}\right] \tag{5.4}$$

Where I_{B1s}^d is the intensity of B1s electrons from the BC attenuated by a silane layer, *d* is the thickness of the GPS layer, expressed in nanometre (nm), I_{B1s}^∞ is the intensity of B1s

electrons from an infinitely thick and clean BC substrate, θ is the electron take-off angle relative to the sample surface (90º), λ_{B1s} is the inelastic mean free path (IMFP) or attenuation length of the B1s electrons (nm), I^{d}_{Si2p} is the intensity of Si2p electrons from the silane layer, I^{∞}_{Si2p} is the intensity of Si2p electrons from an infinitely thick GPS layer and , λ_{Si2p} is the inelastic mean free path (IMFP) or attenuation length of the Si2p electrons (2.5 nm). In the case of a very thin GPS layer, the thickness can be determined only from Si2p signal by solving the Eq. 5.4 to:

$$d = -\lambda \cdot \sin\theta \cdot \ln\left(1 - \frac{I^{d}_{Si2p}}{I^{\infty}_{Si2p}}\right) \tag{5.5}$$

Also, the composition of the silanised BC particles was also evaluated with the determination of the percentage of surface covered by GPS layer (f_{GPS}) using Eq. 5.6, followed by the calculation of the elemental concentration for the uncovered, $\%X_{BC}$, and silanised fractions, $\%X_{GPS}$.

$$f_{GPS}(\%) = \left(1 - \frac{\%B}{\%B_0}\right) \cdot 100 \tag{5.6}$$

Where $\%B_0$ and $\%B$ are the boron percentage on the untreated and silane treated BC surface, respectively. Hence, from $\%B/\%B_0$ ratios it was possible to determine the elemental percentages from the non-covered BC fractions. Consequently, elemental contribution of the silane layer ($\%C_{GPS}$, $\%O_{GPS}$) was also determined through Eq. 5.7.

$$\%X = \%X_{BC} + \%X_{GPS} \ \wedge \ \%X_{BC} = \left(\frac{\%B}{\%B_0}\right) \cdot \%X \ \Leftrightarrow \ \%X_{GPS} = \left(1 - \frac{\%B}{\%B_0}\right) \cdot \%X \tag{5.7}$$

Where $\%X$ is the total element percentage, and $\%X_{BC}$ and $\%X_{GPS}$ are the element percentage from the non-covered and covered surface fractions, according to the silane treatment parameters.

5.3.1.2 Fourier Transform Infrared Spectroscopy (FTIR)

Fourier Transform Infrared spectroscopy (FTIR) is a interferometric technique used to obtain chemical bond information for qualitative and quantitative surface analysis. The basis of the method is to measure the fractions of the absorbed radiation for each frequency of the IR spectrum after the incident beam interacts with the sample and excites vibrations of the molecular bonds. The raw data is simultaneously collected for a wide spectral range and converted through a mathematical process (Fourier transform) into a spectrum, where the absorbed IR radiation is represented as a function of the frequency, in units of wavelength or wavenumber. The absorption for a specific molecular fragment exhibits distinctive frequencies and is not largely affected by the rest of the structure. These fragments are known as functional groups and exhibit characteristic IR absorption bands in the spectrum. Importantly, the spectrum must be subtracted from absorptions introduced by the atmosphere present in the optical pathway (background) in order to obtain the unique spectrum with characteristic IR bands of the sample (Pemble 2009).

Each IR spectrum consists of three regions: 4000-1300 cm^{-1} that gives information about the compound functional groups; 1300-900 cm^{-1} normally known as the fingerprint region; 900-650 cm^{-1} called the aromatic region. The presence of bands in the latter region does not necessarily come from the aromatic compounds. However, the absence of strong absorption in the 910-650 cm^{-1} region usually indicates the lack of aromatic character. The high and low frequency regions are the most important for a preliminary analysis, with the former region usually being the easier to interpret (Pemble 2009). The interpretation of a vibrational spectrum involves three steps: identifying the functional groups present by their characteristic absorption bands; relating them to molecules which have those functional groups; and matching the compound spectrum with others from libraries (reference spectrum).

FTIR is intensively used to analyse the surface chemistry of silane treated solid and other forms of samples (particles, fibres, fillers, etc.) (Miller and Ishida 1986, Bertelsen and Boerio 1999, Bertelsen and Boerio 2001, Pantoja *et al.* 2009, Zhou *et al.* 2008, Shukla *et al.* 2008; Lu *et al.* 2008, Deflorian *et al.* 2008, Underhill and DuQuesnay 2006, Rider 2006, Johnsen *et al.* 2003, Eaton *et al.* 2001). It is particularly suited for highly IR absorbent materials. Also, depth profile can be attained by changing the incidence angle or crystal material, which possess different optical densities.

Experimental Procedure

In the scope of this work, two FTIR sampling techniques were used for the chemical analysis according to the type of sample to be analysed and the information required (Table 5.8), more specifically, through transmittance and Attenuated Total Reflectance (ATR-FTIR).

Table 5.8 FTIR Instrumentation, sampling techniques and experimental test conditions.

Instrumentation	Sampling techniques	Experimental test conditions
Perkin Elmer FT-IR Spectrum 65 Spectrum v10 software Deuterated Triglycine Sulfate (DTGS) detector	Transmittance (FTIR)	4000-400 cm^{-1}, 32 scans, resolution 4 cm^{-1}. Adhesive/KBr pellet (1:100 w/w) BC F1200/KBr pellet (1:500 w/w) ~ 0.250 mg, 5 min at 10 tons, ~1mm thickness
Hummel Polymers and Additives (HPA) and Coatings Technology (CT) libraries	Attenuated Total Reflectance (ATR-FTIR)	4000-650 cm^{-1}, 32 scans, resolution 4 cm^{-1}, ATR correction. Adhesive (film w/ 200 μm) BC F1200 particles

The cure kinetics of the adhesive was also studied at room temperature through ATR-FTIR, by spreading a small drop of fresh epoxy adhesive mixture over the diamond crystal and collecting a spectrum every 5 minutes for 15 hours. The chemical reactions and concentration level of the species involved in the curing process of the epoxy resins was controlled to determine the degree of conversion (α) of the epoxy for a particular time (t). In this case, it can be described as a two step process, whereby an oxirane group reacts with a primary amine that results in a secondary amine (Fig. 4.2a). The latter also reacts in the second step with another oxirane to form a tertiary amine (Fig. 4.2b). Thus, the concentration of the species involved was quantitatively assumed by the area of the absorption of the assigned bands, according to the Lambert Beer's law. IR spectra confirmed that the C-H bonds of the aromatic ring were not involved in the cure with the area of the corresponded band ($Abs_{1035cm-1}$) not being affected during time, and as a consequence it was used as a reference. Whereas, the area of the band assigned to the oxirane ($Abs_{915cm-1}$) decreased during the cure. Hence, characteristic bands of the C-H stretching in the aromatic ring of the bisphenol were monitored to determine α as a function of time using Eq. 5.8.

$$\alpha = \left[1 - \frac{\left(\dfrac{Abs_{915cm^{-1}}}{Abs_{1035cm^{-1}}} \right)_t}{\left(\dfrac{Abs_{915cm^{-1}}}{Abs_{1035cm^{-1}}} \right)_{t=0}} \right] \times 100 \tag{5.8}$$

5.3.1.3 Wettability Test (Sessile Drop)

The wettability test exploits a thermodynamic approach to characterise solid surfaces through the determination of surface free energy (SFE) components, which depends on the interfacial intermolecular forces occurring between the solid and liquid phases. The test provides information on the contact effectiveness between adhesive and substrate in order to attain optimal adhesion for a specific system. Generally, better wettability is achieved with higher SFE solids on which a lower SFE liquid spreads easily on the substrate surface. However, wettability must be considered as only one of the factors that contribute to overall adhesion. Various techniques have been developed to obtain the solid SFE indirectly through the measurement of force, dimension, pressure, volume and other properties, e.g. Wilhelmy plate method, capillary rise, captive bubble method and sessile drop (Hearn 2010). These techniques demonstrate a high sensitivity to the immediate surface chemistry of the solid (3 to 10 Å of depth), despite not providing information about the functional groups present on the surface (Johnston and Ratner 1996).

The sessile drop method is the most used wettability technique to determine the SFE of a solid by directly measuring the contact angle between a drop of a probe liquid deposited ideally on a clean, homogeneous, smooth, flat and non-deformable solid surface. In this work, the surface was polished to 1 μm finish but the final surface roughness, R_a, was not measured. The contact angle is obtained between the tangent plane of liquid and solid surface with the system at thermodynamic equilibrium, using digital image analysis of the drop profile. Hence, this method is very simple and straightforward with minimum substrate preparation and a use of at least two probe liquids on the surface of interest in a air atmospheric environment. The contact angles are affected by experimental factors such as the purity of the probe liquids, drop size and age, and environmental conditions, such as, air temperature and moisture. Other factors may affect the contact angle, specially when a liquid advances or recedes over a non-ideal surface, as a result of the roughness, porosity,

chemical heterogeneity, reorientated polarity or contaminates on the substrate surface (Comyn 2006, Butt 2008, Good 1993).

Experimental Procedure – Boron Carbide

The sessile drop method was used to determinate the SFE of the BC and adhesive, along with the nature of the interactions occurring on the ceramic material with the different surface treatments applied in this study. Deionised water and diiodomethane were used to obtain the polar (*AB*) and dispersive (Lifshiz–van der Waals, *LW*) components of the solid SFE. A third probe liquid (glycerol) was also used to determine the electron acceptor and donor fractions from the polar component, which corresponds to the Lewis acid (+) and base (-) interactions between the liquid and BC surface (Table 5.9).

Table 5.9 Surface free energy components of the various probe liquids (Comyn 2006).

Probe Liquids	Liquid surface tension (mJ/m^2)				
	Total γ_L	Dispersive γ_L^{LW}	Polar γ_L^{AB}	Lewis acid γ_L^+	Lewis base γ_L^-
DI-Water, H_2O	72.8	21.8	51.0	25.5	25.5
Diiodomethane, CH_2I_2	50.8	50.8	0.0	0.0	0.0
Glycerol, $C_3H_8O_3$	64.0	34.0	30.0	3.9	57.4

A liquid drop was formed at a constant rate to a specific volume and then deposited on the boron carbide surface in order to measure the respective contact angle, *θ*, according to the experimental conditions shown in Table 5.10.

Table 5.10 Wettability instrumentation and experimental test conditions.

Instrumentation	Experimental test conditions
Kruss DSA10 Control Unit	Temperature: 23 ± 2°C
Kruss DSA 10 MK2 TC1	Method: Sessile Drop
Falcon Video Capture PCI Card	Baseline: Manual w/ line fitting
	Contact angle detection: tangent methods 1/2
Drop Shape Analysis Software v1.80.0.2	(Polynomial)
ImageJ v1.45s w/ Low Bond Axisymmetric	Drop volume: 5 µm
Drop Shape Analysis plug-in	Rate: 6.32 µl/minute
	Drop age: 30 seconds
Joining Technology Research Centre,	Measurements: 5-7 per probe liquid/substrate
Oxford Brookes University	Probe liquids: DI-Water, Diiodomethane and
	Glycerol

The experimental values were used in the van Oss, Chaudhury and Good equation (Eq. 5.9) to calculate the SFE of the BC in terms of the dispersive, Lewis acid and base, and polar (Eq. 5.10) components (Good 1993).

$$\gamma_L \cdot (1+\cos\theta) = 2 \cdot \left(\sqrt{\gamma_S^{LW} \cdot \gamma_L^{LW}} + \sqrt{\gamma_S^+ \cdot \gamma_L^+} + \sqrt{\gamma_S^- \cdot \gamma_L^-} \right) \qquad (5.9)$$

$$\gamma^{AB} = 2 \cdot \sqrt{\gamma^+ \cdot \gamma^-} \qquad (5.10)$$

Where γ_L is the surface tension liquid-vapour, γ_S is the surface tension solid-vapour interface, θ is contact angle, and *LW, +, -* and *AB* are superscripts for the dispersive, Lewis acid, Lewis base and polar components, respectively.

| (a) | (b) |
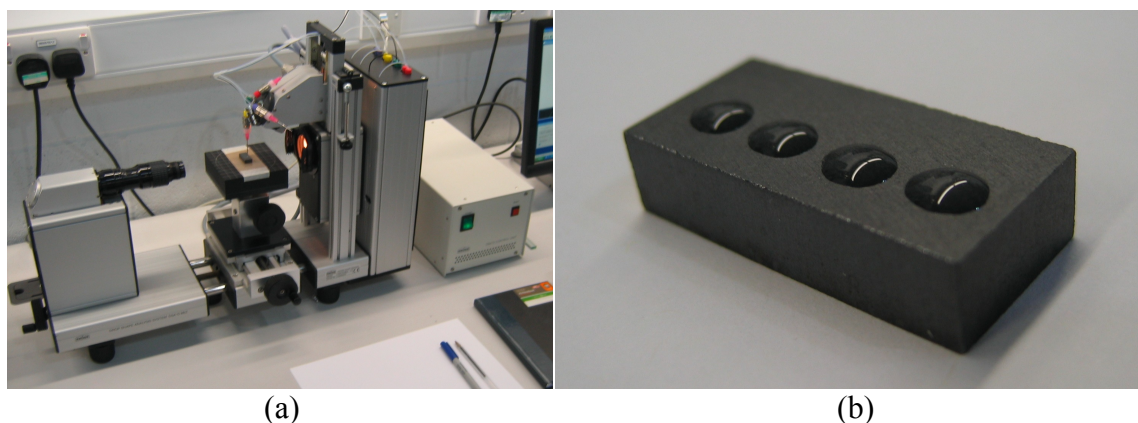
Figure 5.10 Wettability test conducted with (a) contact angle goniometer on (b) BC with different surface treatments.

Experimental Procedure – Epoxy adhesive

The effect of the silane treatment on the wettability of the adhesive was also evaluated to better understand its influence on the viscosity of the uncured BC-epoxy mixture, density/porosity of the cured mixture and short-/long-term mechanical properties of the composite. Some research carried out with cured adhesives showed that the SFE depends not only on the epoxy systems studied but also on the methods and test conditions used as shown in the Appendix A (Table A.5). However, in the case of the SFE for the uncured epoxy adhesives there has been none reported in the literature. Hence, the contact angle of the adhesive on the treated ceramic material was measured and compared with the theoretical values (θ_T) determined using the SFE of the silanised BC and uncured adhesive

(Eq. 5.11).

$$\theta_T = \arccos\left[(2/\gamma_L)\cdot\left(\sqrt{\gamma_L^{AB}\cdot\gamma_S^{AB}}+\sqrt{\gamma_L^{LW}\cdot\gamma_S^{LW}}\right)-1\right]$$

(5.11)

Where γ_L is the SFE of the uncured adhesive, γ_S is the SFE of untreated/treated BC, θ_T is contact angle of the adhesive on the BC surface, and *LW* and *AB* are superscripts for the dispersive and polar components.

The SFE of the uncured adhesive was obtained by measuring the contact angle on a series of substrates with different polar/dispersive component ratios, such as, polyethylene, polycarbonate, polyvinylidene chloride, Zytel HTN (35% glass reinforced high performance polyamide resin), BC and glass.

(a)	(b)
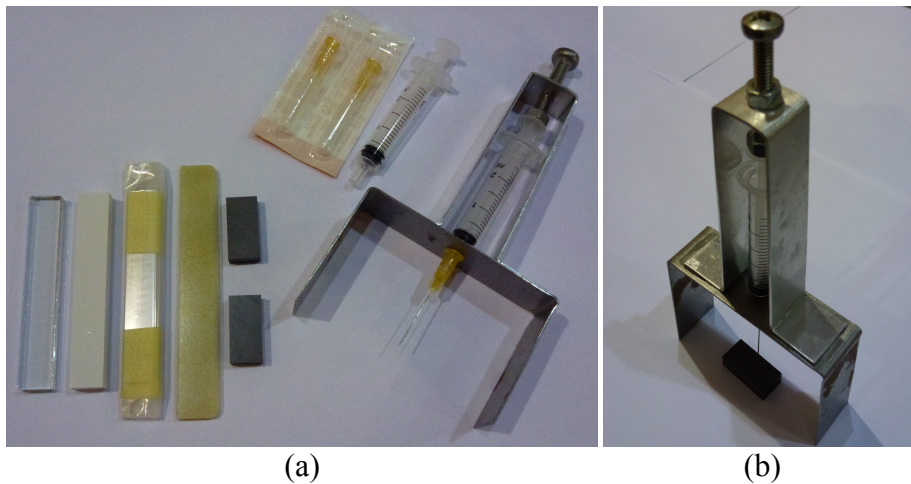
Figure 5.11 Wettability test of the adhesive (a) on various substrates using (b) specific fixture for sessile drop method.

Their SFE components were acquired using the same procedure applied for the BC. The SFE of the uncured adhesive was obtained by plotting the cosine θ_{exp} against the polar/dispersive components ratio of the different substrates (Eq. 5.12).

$$\underbrace{\left(\frac{1+\cos\theta_{exp}}{2\cdot\sqrt{\gamma_S^{LW}}}\right)}_{y}=\underbrace{\left(\frac{\sqrt{\gamma_L^{AB}}}{\gamma_L}\right)}_{m}\cdot\underbrace{\left(\sqrt{\frac{\gamma_S^{AB}}{\gamma_S^{LW}}}\right)}_{x}+\underbrace{\left(\frac{\sqrt{\gamma_L^{LW}}}{\gamma_L}\right)}_{b}$$

(5.12)

Where γ_L is the SFE of the uncured adhesive, γ_S is the SFE of substrate, θ_{exp} is contact angle of the adhesive on the substrate surface, and *LW* and *AB* are superscripts for the dispersive and polar components, *x* and *y* are the values used for the plot, and *m* and *b* are the slope and intercept of the resulting plot.

The polar and dispersive SFE components of the uncured adhesive were determined using the slope and intercept of the resulting plot (Eq. 5.13 and 5.14), and subsequently used to obtain its theoretical contact angle on the untreated and silane treated BC surface through Eq. 5.11.

$$\gamma_L^{AB} = \frac{m^2}{(m^2 + b^2)^2} \tag{5.13}$$

$$\gamma_L^{LW} = \frac{b^2}{(m^2 + b^2)^2} \tag{5.14}$$

5.3.1.4 Scanning Electron Microscope (SEM)

Scanning electron microscopy (SEM) is an important non-destructive high resolution microscopic technique to obtain micrographs of the morphology and topography of the sample surface. Some advantages of the electron over light microscopy is a much higher magnification (>100,000X) and depth of field (>100X).

In this technique, a high-energy incident beam is focused on the surface of the sample, which is created by accelerating electrons in a vacuum (10^{-5} to 10^{-7} Torr) from a thermal emission source or field emission cathode until they reach energies between 0.1 to 50 KeV. The electrons are focused onto the sample by a series of electromagnetic lenses. This primary electron beam scans, in a raster pattern, the sample surface, and in doing so a variety of signals are produced from interactions with the topmost region of the surface to some micrometers in depth. The outcome is the emission of elastic and inelastic scattered electrons, electromagnetic radiation and heat. The emitted electrons are then collected by a general scintillator or a solid-state detector.

The inelastic scattered or low-energy secondary electrons (<50 eV) are collected from each probed area of the surface. This information is then electronically collected, processed and displayed as a high-resolution SEM micrograph. The contrast of the micrograph depends on the amount of generated secondary electrons that reaches the detector, which is related

to the angle of incidence and accelerating voltage of the primary electron beam, surface morphology and chemistry, element composition, sample crystallography and local charging effect on the probed surface. The elastic or high-energy backscattered electrons emitted from deeper in the surface can also be used to show contrasts according to the elemental composition of the sample. This contrast/brightness in a backscattered electron micrograph is proportional to the mean atomic number of a region over the sample surface.

Also, X-ray radiation is generated when the excited electrons return to an inner shell orbital as a result of the inelastic collisions between the primary electrons and the sample. SEM can be combined with an Energy Dispersive X-ray Spectrometer (EDX) to provide also qualitative and quantitative elemental information on the sample (O'Connor *et al.* 2003).

Experimental Procedures

Morphological studies of the untreated/silanised BC particles and the topography analysis of the fracture surface of the BC-epoxy composites were conducted to observe the effect of the surface treatment on the particles, according to experimental conditions presented in the Table 5.11.

Table 5.11 SEM Instrumentation, sampling and experimental test conditions.

Instrumentation	Samples	Experimental conditions
S-3400N Type I HITACHI, Japan PC-SEM software Life Science Oxford Brookes University	BC-Epoxy composite cut // to the failure surface, 4mm height, uncoated and fixed on carbon impregnated double sided adhesive tape on aluminium pin-type stubs	Secondary Electron (SE) Back Scattering Electron (BSE) Pressure: variable pressure (VP) Accelerating voltage: 10-15 keV Magnification: x70 – 1500 Working distance: 10 - 15 mm
JSM-6480LV JEOL, Japan JEOL/EO Version 1.1 Begbroke Science Park Oxford University	BC particles Untreated: F60, F360 and F1200 Silanised: F1200 uncoated and fixed carbon impregnated double sided adhesive tape on aluminium pin-type stubs	Secondary Electron (SE) Back Scattering Electron (BSE) Pressure: variable pressure (VP) Accelerating voltage: 10 keV Magnification: x60 – 5000 Working distance: 9 - 10 mm

5.3.2 Material Characterisation

5.3.2.1 Bulk Density/Open Porosity

The first physical property of the composite studied was the bulk density (ρ_b, kg/m^3). This property is related to the density of the adhesive and BC, as well as their concentration in the formulation. However, the density of a high content BC composite with a specific particle size distribution and concentration depends also on its porosity (π_a, %), e.g. the amount of air trapped in the matrix, which is related to the adhesive's wettability on the BC surface and the the actual processing of the composite (mix mode, temperature, degassing and pressure). This translates to (a) the adhesive's ability to replace the surrounding gas phase layer of the particle and (b) the mechanism by which a more uniform particle dispersion and reduced air entrapment is achieved. The adhesive's ability to wet the BC depends on its surface chemistry, which can change when the BC is treated with silane solutions or corona discharge. Therefore, the bulk density ρ_b (Eq. 5.15) and open porosity π_a (Eq. 5.16) of the composite were determined based on standard BS EN 1389:2003, using five test specimens per surface treatment and manufacturing process (Table 5.12).

$$\rho_b = \frac{m_1}{m_3 - m_2} \cdot \rho_L \tag{5.15}$$

$$\pi_a = \frac{m_3 - m_1}{m_3 - m_2} \cdot 100 \tag{5.16}$$

Where m_1 is the mass of the dry test specimen, m_2 is the apparent mass of the immersed test specimen, m_3 is the mass of the soaked test specimen and ρ_L is the bulk density of the immersion liquid.

Table 5.12 Instrumentation, sampling and experimental test conditions for determination of the bulk density and open porosity.

Instrumentation	Samples	Experimental Conditions
Analytical balance: Sartorius (10^{-4} g resolution)	BC Sintered square blocks (12 x 25 x 6 mm)	Conditioning: Air , 23°C, 55% RH, 7 x 24h
Environmental test cabinet: Weiss Gallenkamp FE300H R40 Vacuum cabinet and pump	Pure adhesive, BC-Epoxy PMC (20 x 15.5 x 4.5 mm)	Immersion: DI-Water, 0.1μS, pH6-7, 23°C, 1h
	five specimens per material	Vacuum: 740 – 760 mmHg

5.3.2.2 Water Absorption

The durability of the PMCs is related to well-known degradation mechanisms, which mostly concern water penetration into the system via diffusion or capillary action through the polymer matrix, migration along the interface and absorption through porous reinforcements (Barraza *et al.* 2003, Chow *et al.* 2007). Regardless of the transport mechanism involved, they lead to interfacial debonding and consequently to poor stress distribution between the matrix and reinforcement (Dawood and Rizkalla 2010, Iglesias *et al.* 2002). Free volume and hydroxyl groups present in the polymer structure also allow the water molecules to diffuse and form hydrogen bonds, which lead to plasticisation, swelling and hydrolysis of the matrix (Kinloch 1987, Davis 2003). Swelling induces dimensional instability and increases the composite internal stresses (Barraza *et al.* 2003). Plasticisation leads to plastic deformation as a result of a higher mobility of the polymer's network elements from the weakening of the interchain bonds. Both effects lower the T_g and are generally considered quasi-reversible processes (Chiang and Fernandez-Garcia 2003). Whereas, microcracking and hydrolysis normally cause permanent damage in the polymer structure, particularly when the fracture mechanism is mostly controlled by strain concentrations around the microcavities and microcracks (Chen et al. 2002), and by promoting even further water diffusion within the matrix. Nevertheless, all these processes result in the degradation of the mechanical, physical, thermal and chemical properties of the composite (Thwe and Liao 2002, Dhakal *et al.* 2007, Ray 2006). The degradation is directly proportional to the amount of absorbed water (Abenojar *et al.* 2011), which depends on the reinforcement (nature, size and concentration), resin's nature and wettability, manufacturing process and external factors, such as, temperature (Ahmad *et al.* 2011, Ray 2006), relative humidity, oxygen concentration and exposure time (Huang and Sun 2007). Hence, the water absorption process is critical to investigate particularly when structural applications and long-term service conditions are considered (Tang *et al.* 2005, Real *et al.* 2006). Therefore, a study was carried out to understand the effect of the silane treatment on water transport mechanisms within the matrix and at the BC-epoxy interface.

Moisture uptake

The evaluation of the moisture absorption of the pure adhesive, sintered BC and composite at room temperature was based on EN ISO 10545-3:1997. Three specimens per material (50 x 50 x 4.5 mm) were dried in an oven and cooled in a desiccator before obtaining the

initial mass. After immersion, the specimens were taken at different time intervals from the water to obtain its mass and determine the moisture absorption (M_t) according to Eq. 5.17.

$$M_t(\%) = \frac{m_t - m_0}{m_0} \cdot 100 \qquad (5.17)$$

Where m_0 and m_t are respectively the mass (g) of the test specimen before and after immersion.

Water Permeability

The water absorption behaviour can also be quantified using a diffusion coefficient, which is a measure of the water's ability to penetrate through the composite segments. The diffusion mechanism of a chemical species from a high to a low concentration region can be based on the concept that its flow rate through a unit area per unit time is proportional to the concentration gradient normal to the area surface, i.e., Fick's first law (Eq. 5.18).

$$J_x = -D \cdot \frac{dc}{dx} \qquad (5.18)$$

Where J_x is the diffusion flux of a substance in one spacial direction across a plane of unit area in unit time (mol.m^{-2}.s^{-1}), c is the concentration (mol.m^{-3}), x the space coordinate normal to the plane, and D is the diffusion coefficient (m^2.s^{-1}). However, most diffusion processes are non- steady state as a result of the flux variations with time in all spacial directions across a volume element, which can be represented by Fick's second law in Cartesian coordinates (Eq. 5.19).

$$\frac{dc}{dt} = D \cdot \left[\frac{d^2c}{dx^2} + \frac{d^2c}{dy^2} \frac{d^2c}{dx^2} \right] \qquad (5.19)$$

For an isotropic thin film absorbing a liquid, the diffusion into the edges can be ignored and consequently the equation can be simplified to a one spacial direction diffusion through an infinite plate (Eq. 5.19).

$$\frac{dc}{dt} = D \cdot \frac{d^2c}{dx^2}$$

(5.20)

The Fickian diffusion model is based on the cooperative movement of the liquid molecules into the volume element without considering the molecule-molecule interactions. The diffusion coefficient can be determined by following the water uptake as a function of time, considering one-dimensional moisture absorption of the composite sample with thickness h immersed in water with both sides under invariable environmental conditions. Normally, the moisture uptake exhibits initially a linear increase followed by the slow down of absorption rate until reaching a plateau stage, corresponding to the saturation of the sample. This behaviour is mathematically expressed by the fraction of water uptake at time t (M_t) and at equilibrium saturation (M_∞), and diffusion coefficient constant (D) (Crank 1979).

$$\frac{M_t}{M_\infty} = 1 - \frac{8}{\pi^2} \sum_{j=0}^{\infty} \frac{\exp\left[-(2j+1)^2 \pi^2 \left(\frac{Dt}{h^2}\right)\right]}{(2j+1)^2}$$

(5.21)

The fraction at the initial stage of the absorption process ($M_t / M_\infty < 0.6$) can be simplified and rearranged to obtain the diffusion coefficient D, which can be calculated from a plot of moisture uptake versus square root of time (Eq. 5.22).

$$\frac{M_t}{M_\infty} = \frac{4}{\pi^{1/2}} \left(\frac{Dt}{h^2}\right)^{1/2} \Leftrightarrow D = \pi \left(\frac{h}{4 M_\infty}\right)^2 \left(\frac{M_t}{t^{1/2}}\right)^2$$

(5.22)

The water permeability coefficient (P) was also determined for all composites and constituent materials to evaluate the effect of the silane treatments on water passage through the matrix and interface (Sreekala *et al.* 2002, Ahmad *et al.* 2011), according to the following equation:

$$P = M_\infty \cdot D$$

(5.23)

5.3.2.3 Dynamic Mechanical Analysis (DMA)

DMA provides information on the viscoelastic behaviour of the polymeric materials during first order thermodynamic transitions (melting and crystallisation), pseudo second order (glass transition) and secondary transitions. This technique involves the application of a small oscillatory/sinusoidal mechanical stress/strain to a solid or viscous liquid, and measuring its response as a function of temperature or frequency (Fig. 5.12). This deformation can be achieved in different manners, such as, bending, torsion, shear, compression and tension (Sandler 1998).

(a)   (b)   (c)

Figure 5.12 Representation of the (a) applied sinusoidal stress, (b) material response or strain and (c) phase lag between applied stress and material response.

A perfectly elastic solid material responds proportionally, according to Hooke's law, and in phase ($\delta = 0°$) to the applied sinusoidal stress (Fig. 5.13a). However, a delay in the response or phase lag from the material ($0° < \delta < 90°$) is observed when the internal molecular motions of the polymer chains occur at the same frequency range of the imposed stress or deformation. Hence, the material responds viscoelastically by exhibiting characteristics of both solids and liquids, (Fig. 5.13b). Whereas, in an ideal Newtonian fluid (Fig. 5.13c), the stress will be proportional to the strain rate but out of phase ($\delta = 90°$) (Sandler 1998).
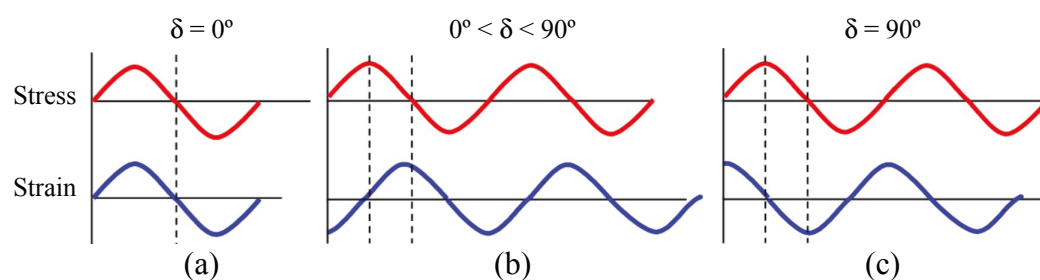
Figure 5.13 Material response to the sinusoidal stress by exhibiting an (a) elastic, (b) viscoelastic and (c) viscous behaviour.

The behaviour of the material is evaluated through the determination of a real and imaginary component of the complex modulus (E^*), which corresponds respectively to the sum of the storage (E') and loss (E'') moduli. The first component is related to the purely elastic behaviour with the storage of the mechanical energy into potential energy and the latter component is associated to the viscous behaviour when energy is dissipated as heat resulting from the imposed deformation (Fig. 5.14). The ratio of the dissipated energy to maximum potential energy stored during a cycle is called loss or damping factor (tanδ = E''/E').
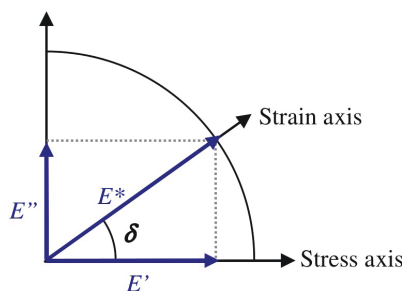
Figure 5.14 Vectorial representation of storage modulus (E'), loss modulus (E'') and tanδ.

Normally, viscoelastic properties of amorphous polymers are studied within a temperature range of -150 to 600ºC. The increase of the temperature at a controlled rate leads to the polymer reaching its glass transition, i.e., through a change from elastic, to viscoelastic-rubber and finally to viscous-fluid behaviour (Fig. 5.15).
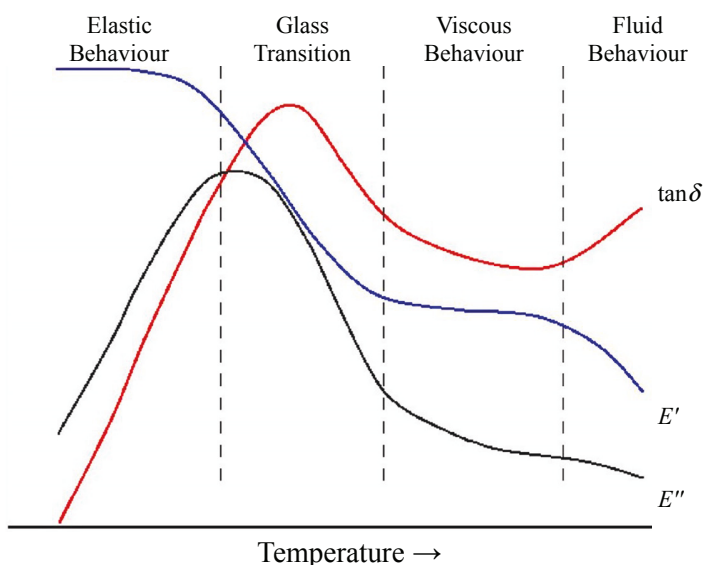
Figure 5.15 Storage (E') modulus, loss (E'') modulus, and loss factor (tanδ) as a function of the temperature, for typical amorphous polymer.

A high conversion of the mechanical energy, provided by the applied sinusoidal stress, to heat is observed during the glass transition of the material. This results from the micro-Brownian motion of the chain segments within the polymer molecular structure (intramolecular), similar to those observed in a vibrating string, and from the cooperative motion of the segments with the neighbour chains (intermolecular). Hence, amorphous polymers undergo from a "rigid" glass state to viscoelastic-fluid state as temperature increases, as a consequence of the intra- and inter- molecular interactions that leads to α-relaxation of the material (Menczel 2009). Therefore, the glass transition temperature (T_g) is determined by the maximum value of the tanδ as a function of temperature (Fig. 5.15), in the region near the highest values of the loss modulus, E'' (Abenojar *et al.* 2009b). Thus, DMA was conducted to determine E' and T_g of the epoxy adhesive used in the composite formulation in order to understand better its mechanical behaviour and the effect of the water temperature on the degradation mechanisms, according to the experimental conditions shown in the Table 5.13.

Table 5.13 Instrumentation, sampling and experimental conditions for DMA testing.

Instrumentation	Sampling technique	Experimental conditions
Triton Technology, Tritec 2300 DMA Universal Analysis 2000 software	Dimensions: 40 x 5-10 x 4.5mm Cure: 8h at 40ºC	Thermal profile: 20 to 100 °C (3ºC/min) Test frequency: 1 Hz
Calibration and set-up for Dual cantilever testing	Conditioning: Air, 7 x 24h at 23ºC, 50%RH.	T_g determined through the raw data plot to find peak tan δ

5.3.3 Mechanical Testing

The mechanical properties of the composite were obtained under different stresses to evaluate whether or not the surface treatments were enhancing initial adhesion strength and bond durability between BC reinforcement and epoxy matrix, using various pH values and silane concentrations. In addition, mechanical testing data was correlated with that of the surface analysis and physical characterisation to obtain the optimal silane treatment conditions. Therefore, three test methods were assessed using the instrumentation and experimental conditions described in Table 5.14.

Table 5.14 Mechanical testing set-up, methods and specimen description.

Set-up	Test method (based on)	Specimens description
Universal testing machine, Nene Instruments Ltd, UK	Three-point bending (BS EN ISO 3325:1999)	40 x 20 x 4 mm [*/**]
Deltalab-Nene Test Software issue 6.6 v7	Iosipescu (BS EN 12289:2005)	76 x 20 x 4 mm [**]
5 KN load cell, calibrated Cross-head speed: 1mm/min Compression mode	Double v-notch, DVN (non-standard)	80 x 20 x 4 mm [**]

* span distance: 22.5mm, load diameter: 6mm, support diameter: 2 mm
** notch angle/depth: 90°/4.5mm

Three specimens were moulded to the required geometry for each test method in order to calculate the strength of the epoxy adhesive and composites with different surface treatments (Fig. 5.16). The load data and cross-head displacement curves for each specimen, all showed a linear deflection behaviour before maximum load was reached with the failure of specimen.

(a) (b)

(c)
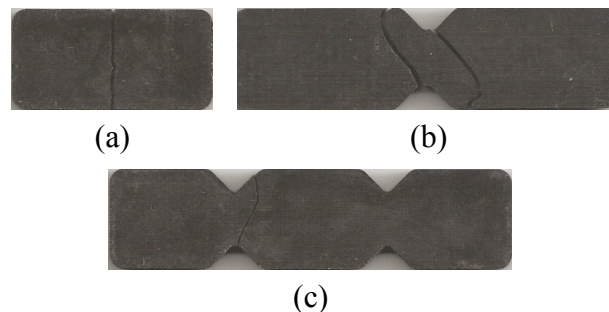
Figure 5.16 Characteristic failure modes of the PMCs for the (a) three point-bending, (b) Iosipescu and (c) double v-notch test methods.

5.3.3.1 Three-Point-Bending (3PB)

The three-point-bending (3PB) test is commonly used to evaluate the "pure" flexural stress-strain response of brittle materials and composites under transverse load (static mode). This versatile method provides an ease way to prepare and test materials, despite its high sensitivity to the specimen and loading geometry and strain rate. The specimen comprises a short-beam geometry of uniform thickness, width and length, based on the BS EN ISO 3325:1999 standard (Fig. 5.17a). The specimen was supported at both ends on two

cylinders with its centre aligned at the midpoint between supports (Fig. 5.17b). The load was applied in the centre of the specimen until fracture and the maximum value was registered as a measure of the apparent shear strength of the material (Fig. 5.17c).

(a)	(b)	(c)
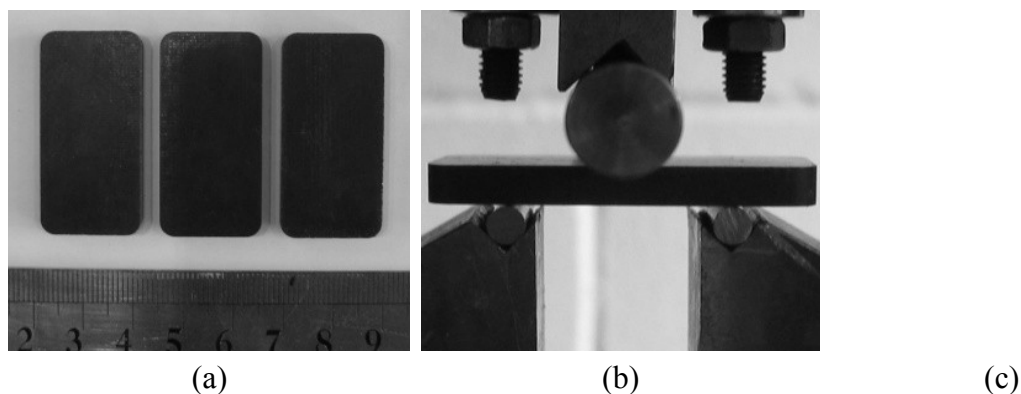
Figure 5.17 Three point bending (a) BC-Epoxy composite specimens, (b) test set-up and (c) configuration, the external force diagram, the shear-force diagram, and the bending moment diagrams along the longitudinal axis of the specimen.

In practice, this results in a contribution of both shear and axial tensile stress that depends on ratio between the supports (span distance, s) and transverse area ($A = w \cdot h$, where w is the width of the specimen and h the depth) (Roche *et al.* 1991). A high ratio ($s/A > 10$) would provide more suitable information about the flexural properties of the material, whilst a low ratio ($s/A = 4.5$) would provide a shear dominant contribution (transverse rupture strength, R_{tr}, MPa) that is calculated according to Eq. 5.24. In the case of this study, a s/A ratio of 0.3 was obtained according to the test specimens and testing set-up.

$$R_{tr} = \frac{3 \cdot F \cdot s}{2 \cdot w \cdot h^2} \tag{5.24}$$

Where F is the maximum load observed during the test (N), w is the measured width of the test specimen (mm) and h is the measured height of the test specimen between the notch tips (mm).

5.3.3.2 Iosipescu

The Iosipescu shear test was initially develop by Nicolai Iosipescu for isotropic materials (Iosipescu 1967) and later for the use in unidirectional PMC (Walrath and Adams 1983,

Odegard and Kumosa 2000) and anisotropic composites (Manhani *et al.* 2007). The Iosispecu test has been the most widely used in material science since that time, despite the first standard based on this test method having been published only in 1993 (ASTM Standard D5379-98).

The Iosipescu specimen comprises two parts of a beam separated by a pair of v-notches located at the lower and upper edges in the midpoint of the specimen length (x-axis, Fig. 5.18a), with a geometric dimension based on the BS EN 12289:2005. The specimen is pushed against the back of the fixture and centred along the x-axis with the help of a small diameter rod of the fixture located below the lower v-notch. After alignment, each part of the specimen is then fixed to one of each half of a special fixture, where one sets directly and freely on the base of the testing machine and the other is fixed to the cross-head and moves parallel to the plane x,y (Fig. 5.18b). The displacement between the two halves result in two force couples, one for each part of the specimen, with the formation of two opposite bending moments and consequently a pure shear stress along the loading axis (y-axis) is generated in the region between the notches as exhibited in the Fig. 5.18c.

| (a) | (b) | (c) |
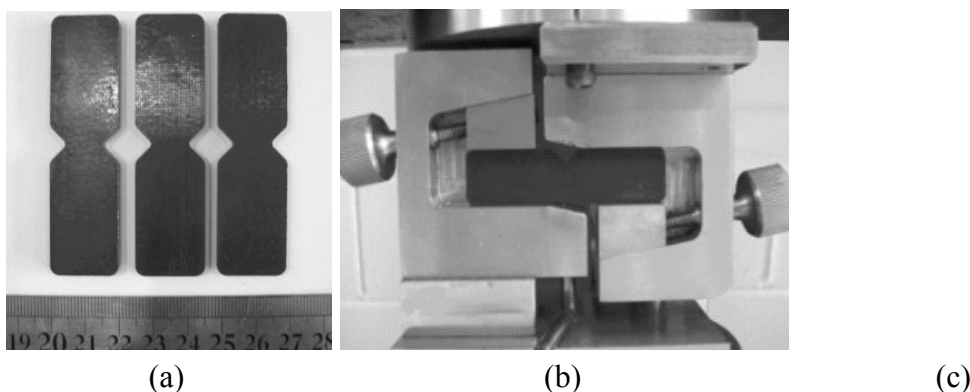
Figure 5.18 Iosipescu shear test (a) BC-Epoxy composite specimens, (b) test set-up and (c) Loading configuration, and shear-force and the bending moment diagrams.

In this work, the composite tensile strength, t_{xy}, was obtained using the Iosipescu test, despite this method been initially performed to measure shear strength. In this test, an unexpected failure was formed between the notch section at 45° to the longitudinal axis of the beam and perpendicular to the lateral surface of the v-notchs (Fig. 5.16b). This characteristic failure mode is generally observed with brittle-isotropic materials and is the result of a pure tensile stress state located close to the notch tip (Manhani *et al.* 2007, Parmenter and Milstein 1998). Thus, this test was therefore used to determinate the tensile

strength of the boron carbide epoxy composite using Eq. 5.25.

$$t_{xy} = \frac{F}{w \cdot h}$$

(5.25)

Where F is the maximum load observed during the test (N), w is the measured width of the test specimen (mm) and h is the measured height of the test specimen between the notch tips (mm). This provided a vertical crack, initiating from the notch tip.

5.3.3.3 Double v-notch (DVN)

A non-standard mechanical approach was used to measure the shear strength of the composite, which will be referred in this work as the double v-notch (DVN) test. The test specimen comprises of a three part beam separated by two pairs of v-notches located at the lower and upper edges in each third of the specimen length (x-axis, Fig. 5.19a). The specimen is pushed against the back of the fixture, aligned along the x-axis with centre part at the unsupported area, and fixed and supported at both end parts with the help of a small diameter rod. After alignment, each part of the specimen is then fixed to one of each half of a special fixture, where one sets directly and freely on the base of the testing machine and the other is fixed to the cross-head and moves parallel to the plane x,y (Fig. 5.19b). The load is applied over the full length of the centre part of the specimen and stress along the loading axis (y-axis) is generated in the section between the notches (Fig. 5.19c). The maximum load was used to determinate of the shear strength of the composite, which was calculated according to Eq. 5.26.

$$t = \frac{F}{2 \cdot w \cdot h}$$

(5.26)

Where F is the maximum load observed during the test (N), w is the measured width of the test specimen (mm) and h is the measured height of the test specimen between the notch tips (mm). This provided a vertical crack, initiating from the notch tip.

(a)   (b)   (c)
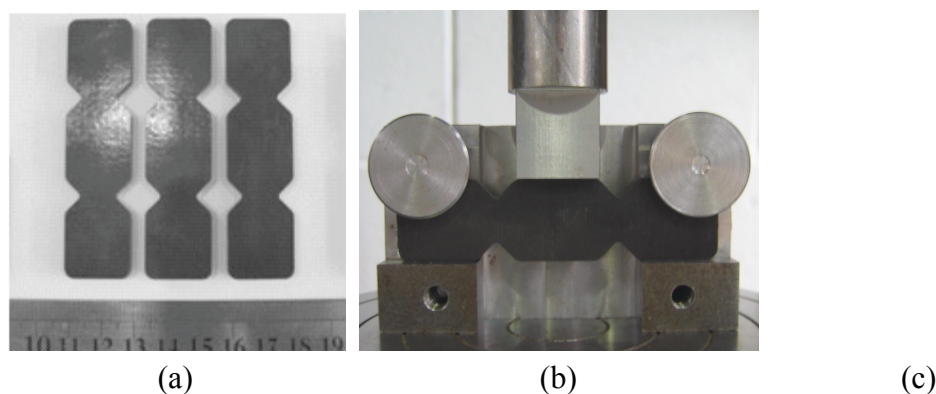
Figure 5.19 Double v-notch shear test (a) BC-Epoxy composite specimens, (b) test set-up and (c) Loading configuration, and shear-force and the bending moment diagrams.

5.3.4 Ageing Conditions – Water Immersion

The hydrothermal ageing of PMCs was investigated to provide a better understand of the effect of the silane treatment on ageing mechanisms and consequently on durability, particularly through the loss of strength as a result of the debonding process at the interface region caused by the water when the materials are exposed to immersion. The water uptake of the aged epoxy neat resin and BC-Epoxy composites was obtained, and their mechanical properties determined through 3PB, Iosipescu and DVN tests (Table 5.15). The ageing process was conducted by immersion in deionised water at 40ºC without sustained load for a period of time of 2 months (1400-1500 hours). Three specimens were used for each composite with a specific surface treatment and mechanical test method. Before immersion, the mass of the test specimens was obtained after conditioning for 7 days. The specimens were periodically visually examined for evidence of failure / debonding occurrence during immersion.

Table 5.15 Instrumentation, sampling and conditions used for the ageing and mechanical testing of the pure adhesive and BC-Epoxy composites.

Instrumentation	Samples	Conditions
Environmental test cabinet: Weiss Gallenkamp FE300H R40	Epoxy neat resin	Conditioning: Air , 23ºC, 55% RH, 7 x 24h
Analytical balance: Sartourius (10^{-4} g resolution)	BC-Epoxy composite Untreated , Silanised (pH= 3, 5, 7, 9; %wt.= 1, 3%)	Immersion / Ageing: Di-Water, 0.1µS, pH6-7, 40ºC
Oven: Gallenkamp Sanyo OMT	Moulded for the test Three specimens per material	Mechanical testing: 3PB, Iosipescu, DVN

An expanded matrix of the various methods, materials and types of BC surfaces used during this experimental programme is shown in Table 5.16.

Table 5.16 Expanded matrix of the methods, materials and surfaces involved in the experimental investigation.

Study	Method	Material	Surface			
			Untreated	**Corona**	**Silane**[*]	**SICOR**[**]
Surface Analysis	DSA	BC, Epoxy	✓	✓	✓	-
	FTIR	BC, Epoxy	✓	✓	✓	-
	XPS	BC	✓	-	✓	-
	OM	BC	✓	-	-	-
	SEM	BC, PMC	✓	✓	✓	-
Kinetics	FTIR	Epoxy	-	-	-	-
Rheology	DMA	Epoxy	-	-	-	-
Physical – Chemical	Density	BC, Epoxy, PMC	✓	✓	✓	-
	Porosity		✓	✓	✓	-
	Water permeability		✓	✓	✓	-
Mechanical	3PB	PMC, Epoxy	✓	✓	✓	✓
	Isopescu		✓	✓	✓	✓
	DVN		✓	✓	✓	✓
Durability	Water immersion	Epoxy, PMC	✓	✓	✓	-

* 0.5, 1 and 3 %wt GPS in pH3, pH5, pH7 solutions
** 1 %wt GPS in pH7 solution after corona treatment

CHAPTER 6 – EXPERIMENTAL RESULTS

In this chapter, the effects of various surface treatments employed on BC to improve adhesion and other properties of the epoxy composite are presented. These include the experimental results of the surface analysis conducted on the BC, physical-chemical characterisation of the composite and its constituent materials, mechanical testing and environmental durability studies carried out on the pure adhesive and PMC, and an investigation of the failure surfaces after testing.

6.1 Adhesive Characterisation

Chemical, cure kinetics, rheological and wettability studies were conducted on the epoxy adhesive in order to better understand its behaviour as a liquid during the manufacturing process and as a binder on the mechanical properties of the PMC at service conditions.

6.1.1 Chemical studies (FTIR)

The chemical characterisation of the adhesive's components, uncured mix and cured material was determined by matching the spectra of the samples with that available from digital libraries and by identifying the functional groups and respective various vibration modes from the characteristic frequency tables available in literature.

6.1.1.1 Components

The matching method allowed the main components of the epoxy adhesive to be identified using matching percentage between the spectra of the sample and of the references from the digital libraries (Table 6.1). The resin was identified as a diglycidyl ether of bisphenol-A (Epoxy resin, Bisphenol-A, HPA Index No. 66), the curing agent as a polyamine amide (Polyamine amide, dimer fatty acid, HPA Index No. 107), and the wetting agent as a long chain polyglycol ester (Fatty acid polyglycol ester, HPA Index No. 781). The best matching spectrum for each component is shown in the Fig. 6.1.

Table 6.1 Best matching commercial products from library and value for the adhesive components and cured product.

Adhesive Component	Matching Product		
	Commercial name	**IR library***	**Match value (%)**
Resin	Epoxy resin, Bisphenol-A	HPA	87.0
	Ciba 6010	CT	88.6
	DER 331	CT	88.6
Curing agent	Polyamine amide, dimer fatty acid	HPA	92.0
	Genamid 151	CT	97.2
	Ancamine 220	CT	96.0
Wetting agent	Fatty acid polyglycol ester	HPA	90.0
	BYK Anti-Terra U	CT	93.7
	Deplastol	CT	92.8

* HPA – Hummel Polymers and Additives ; CT - Coating Technology.
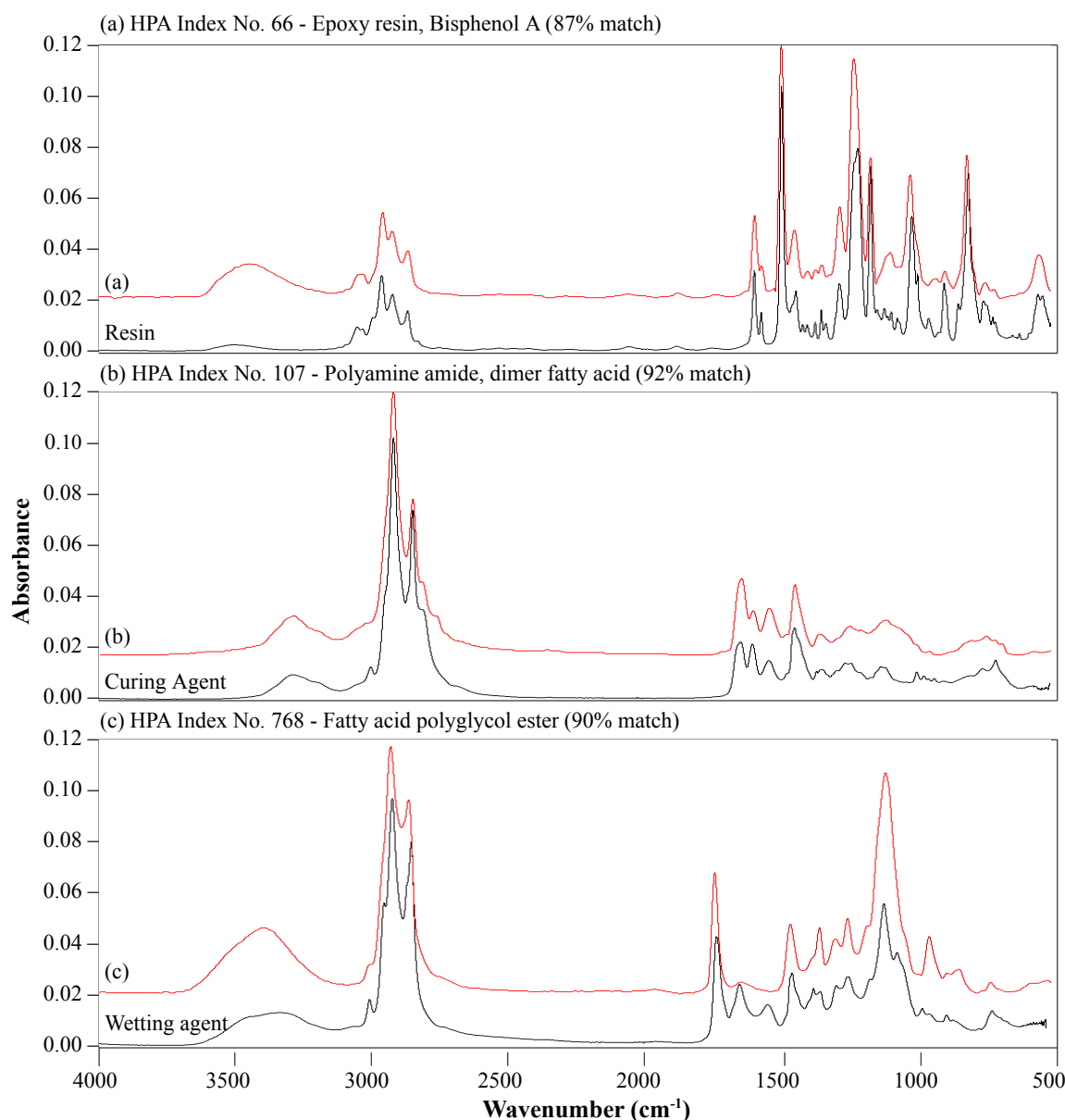
Figure 6.1 Best match spectra obtained from the libraries for the (a) resin, (b) curing agent and (c) wetting agent used in the adhesive formulation.

The resin is a highly versatile and general purpose unmodified basic liquid epoxy resin, showing a spectrum with a match value of 94% and 92.6% when compared to that from HPA and CT libraries, respectively. According to the literature and material safety data sheet (MSDS) of the matched products, the resin is based on the reaction of bisphenol-A and epichlorohydrin. It is used in cold or heat cured systems for improved properties such as chemical resistance and glass transition temperature for PMC (Hunstman 2006, Dow Chemical 2009, Penn and Wang 1998).

The curing agent was identified as mixture of polyamine amide and dimer fatty acids, which reference spectra from HPA and CT exhibited an match value of 92% and 96-97%, respectively. It can be used as a modifier for lower viscosity and longer pot life and high solids systems with good appearance, mechanical properties and high chemical resistance for industrial coatings, concrete primers, sealers, flooring, and grouts (Irfan 1998, BASF 2013, Flick 1993). Other properties promoted by this curing agent on epoxy adhesives can be found in Table 4.4. A similar product by the same manufacture (Ancamine 220) was found in the library, composed of a polyamide based on c-18 unsaturated fatty acid dimers with TETA and TOFA (Air Products 2008).

The wetting agent was identified from the HPA library with a match value of 90% as a fatty acid polyglycol ester. Nevertheless, a better match was attained from the CT library with a value of 93.7% for BYK Anti-Terra U and 92.8% for Deplastol. The former is a salt of unsaturated polyamine amides and lower molecular weight acidic polyesters normally used as a standard wetting and dispersing additive for solvent-borne and solvent-free systems to prevent flooding/floating, reduce viscosity and avoid thixotropy (BYK 1998, BYK 2009). Deplastol is a polyethylene glycol /polyether glycol ethoxylated lauric acid product from Henkel used as a viscosity reducer (Ash and Ash 1993). Alkoxylated oils and fatty acids or alkyl polyglycol esters are present in several non-ionic surfactants products generally used as wetting, emulsifying, softening, lubricating and dispersing agents for domestic and industrial applications (Elementis Specialities 2012).

Further characterisation was done through the interpretation of spectra by assigning bands to the vibration modes of the functional groups. The resin, curing agent, wetting and adhesive spectra were grouped for a better identification of the frequencies. The functional group characteristic wavenumber, intensity and vibrational modes were assigned to most of the bands in the spectra of the adhesive's components, and cured and uncured products.

The symbols and abbreviations used are *v* for the stretching vibrational modes, δ for the bending vibrational modes, ρ for the rocking vibrational modes, and subscript letters are *s* for symmetric, *as* for asymmetric, *ip/op* for in/out of plane vibrations, *r* for rocking and *sc* for scissor. Also, the intensity and geometry of the characteristic bands corresponded to: *vs* for very strong, *s* for strong, *m* for medium, *w* for weak, *vw* for very weak, *v* for variable, and *b* for broad (Table 6.2-6.5).
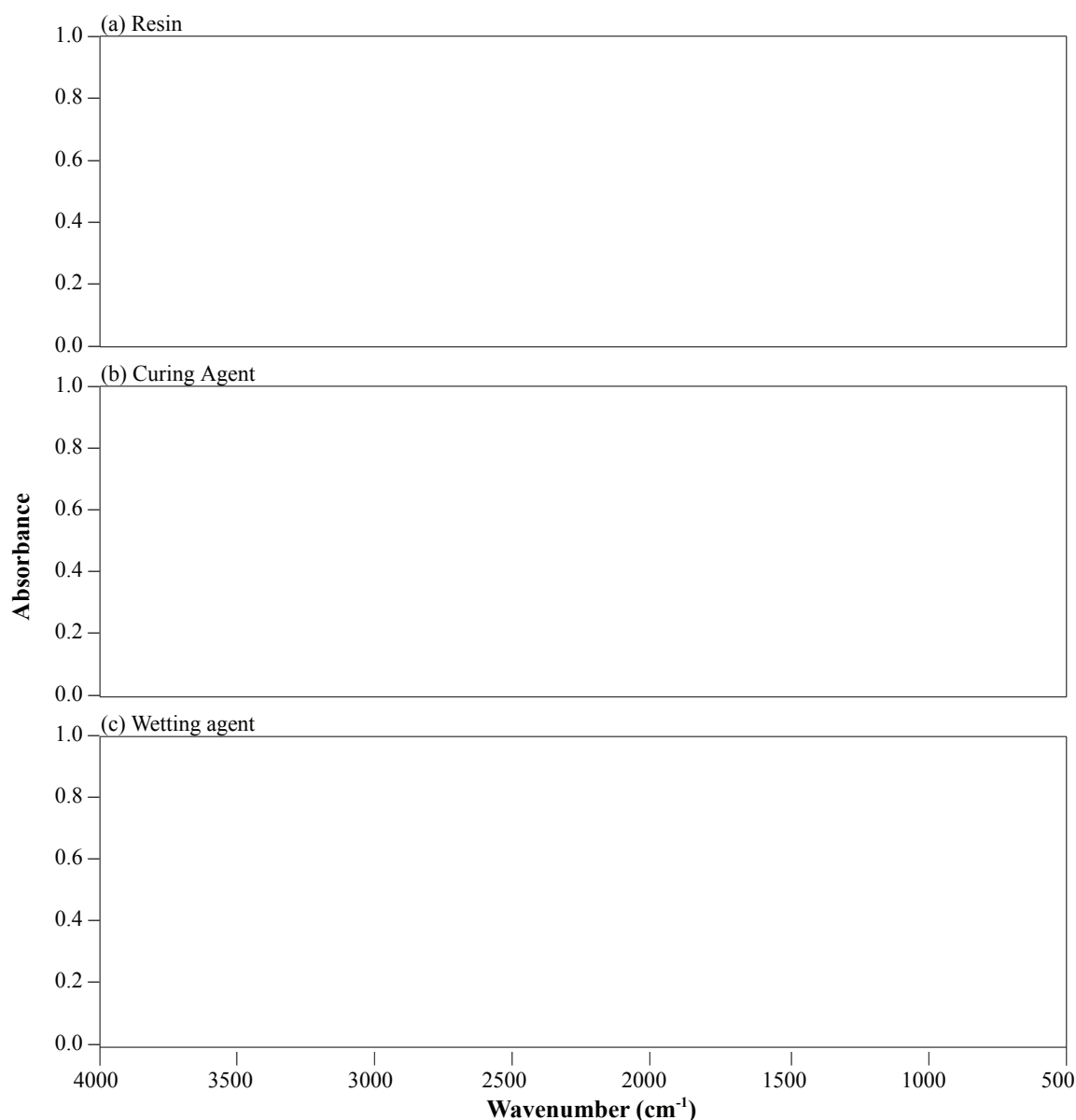
Figure 6.2 Spectra obtained from the samples of the (a) resin, (b) curing agent and (c) wetting agent used in the adhesive formulation.

Table 6.2 Characteristic bands of the functional groups present in the spectrum of resin.

Band no.	Intensity	Wavenumber (cm^{-1})	Functional group
1	*w, b*	3600-3200 (3505)	ν_s O-H
2,3	*vw*	3100-3000 (3056, 3037)	ν C-H Aromatic
4	*w-m*	2975-2950 (2966)	ν_{as} CH$_3$ Aliphatic
5	*w-m*	~2930 (2927)	ν_{as} CH$_2$ Aliphatic
6	*w-m*	2885-2865 (2872)	ν_s CH$_3$ Aliphatic
7	*w-m*	2870-2840 (2852)	ν_s CH$_2$ Aliphatic
8,9	*w*	(2063, 1890)	δ_{op} C-H p-subs. Aromatic hydrocarbon groups
10,11	*v*	1625-1590 (1606, 1581)	ν C=C Aromatic
12	*s*	~1506 (1507)	ν C-C para-substituted Aromatic
13	*m*	1490-1440 (1455)	δ_{sc} CH$_2$
14,15	*m*	1390-1365 (1384, 1362)	δ_s C-H, C(CH$_3$)$_2$
16	*w-m*	(1296)	ρ_t CH$_2$
17	*s*	1270-1230 (1229)	ν_{as} C-O-C Aryl ethers (Aromatic)
18	*s*	~1190 (1181)	ν C-C between p-Aromatic
19	*w*	1150 – 1040 (1107)	ν C-O Alcohol
20	*s*	~1035 (1032)	ν_s C-O-C Aryl ethers (Aromatic)
21	*w*	920-910 (914)	ν_{as} Oxirane, Epoxy ring
22	*m*	830-820 (826)	δ_{op} C-H para-substituted Aromatic
23	*vs*	860-780 (770,736)	δ_{op} C-H Aromatic
24	*m*	730-710 (725)	ρ_r CH$_2$

The FTIR spectrum of the resin (Fig. 6.2a) shows a high aromatic content compound possessing alcohol and epoxy functionalities, with bands (Table 6.2) assigned to: alcohol groups by O-H stretching at 3505 cm^{-1} and C-O stretching at 1107 cm^{-1}; aliphatic by several C-H stretching modes in the region 2975-2840 cm^{-1}, bending at 1455cm^{-1} and rocking at 725 cm^{-1}; aromatic (p-aromatic) by C-H stretching at 3056 and 3037 cm^{-1}, C=C stretching at 1606 and 1581 cm^{-1} (strong at 1507 cm^{-1}) and C-H bending at 740 and 736 cm^{-1} (medium at 826 cm^{-1}); oxirane or epoxy ring group by asymmetric stretching band at 914 cm^{-1}; aryl ethers by C-O-C stretching at 1229 and 1032 cm^{-1}; hydrocarbon groups bonded to or between p-aromatic by C-H stretching at 1890 and 1384 or 1360 cm^{-1}.

Table 6.3 Functional groups characteristic bands present in the spectrum of the curing agent.

Band no.	Intensity	Wavenumber (cm^{-1})	Functional group
1	*s, b, v*	3500-3300 (3288)	ν_s N-H, Amine
2	*w-m*	3100-3000 (3005)	δ N-H overtone
3	*s*	~ 2930 (2922)	ν_{as}CH$_2$ Aliphatic
4	*s*	2870-2840 (2852)	ν_sCH$_2$ Aliphatic
5	*m*	1690-1640 (1654)	ν C=O, δ N-H Amide I
6	*m*	1650-1580 (1611)	δ_{sc} N-H, Amine
7	*w-m*	1560-1500 (1551)	ν C-N, δ N-H Amide II
8	*m*	1490-1440 (1456)	δ_{sc} CH$_2$
9	*w*	(1375,1361)	δ CH$_3$
10	*w*	~1271 (1272), 1229−1301 (1251)	δ CH$_2$ or ν C-N δ_{ip} N-H Amide III
11	*w*	1170-1140 (1141)	δ_s CCH or ρ_t CH$_2$
12	*w*	910-665 (769)	δ N-H wag
13	*w*	730-710 (722)	ρ_r CH$_2$

The curing agent (Fig. 6.2b) is a compound of mostly aliphatic nature with primary and secondary amine, and amide groups. The spectrum features bands (Table 6.3) attributed to: amine groups by the N-H stretching at 3288 cm^{-1}, bending at 1611 cm^{-1} and wagging at 769 cm^{-1}; aliphatic CH$_2$ by two strong stretching modes at 2922 and 2852 cm^{-1}, bending at 1455 cm^{-1} and rocking at 722 cm^{-1}; amides from the combined C=O and N-H vibrations modes at 1654, 1551 and 1251 cm^{-1}. Most of the vibration modes in the spectrum are due to stretching and deformation modes of N-H bonds of secondary amines and amides groups. This is related to the presence of a broader band and a shoulder at the region 3500-3300 cm^{-1}. In contrast, primary amines generally exhibit two well defined stretching modes. Also, a weak band at 3005 cm^{-1} was attributed to the overtone of the N–H bending band of secondary amines (Reichenbächer and Pop 2012). Furthermore, a band located at 1654 cm^{-1} is typically only from C=O stretching of amides due to mesomerism of the R-(C=O)-N< group.

Table 6.4 Functional groups characteristic bands present in the spectrum of the wetting agent.

Band no.	Intensity	Wavenumber (cm^{-1})	Functional group
1	*b, v*	3600-3200, 3500-3300 (3288,3212)	ν_s O-H, ν_s N-H
2	*w*	3100-3000 (3000)	δ N-H overtone
3	*s*	~ 2930 (2922)	ν_{as} CH$_2$ Aliphatic
4	*s*	2870-2840 (2852)	ν_s CH$_2$ Aliphatic
5	*m-s*	1750-1735 (1735)	ν C=O Ester, Aliphatic
6	*m*	1690-1640 (1649)	ν C=O, δ N-H Amide I
7	*m*	1590-1510 (1548)	ν C-N, δ N-H Amide II
8	*m-s*	1490-1440 (1458)	δ_{sc} CH$_2$
9		1378, 1354	δ CH$_3$
10	*m*	(1294)	ρ_t CH$_2$
10,11	*m*	~1271 (1272), 1301- 1229 (1250)	δ CH$_2$ or ν C-N, δ_{ip} N-H Amide III
12,13	*m-s*	1300-1000 (1120, 1072)	ν C-O Alcohol, Ester
14	*m*	730-710 (723)	ρ_r CH$_2$

The wetting agent is mostly of an aliphatic nature with different functional groups, such as, amide, ester and alcohol groups (Fig. 6.2c). The FTIR spectrum exhibits bands (Table 6.4) which result from: combinations of N-H and C=O vibration modes typically assigned to amides at 3500-3300, 1649, 1548 and 1250 cm^{-1}; aliphatic C-H stretching, bending, twisting and rocking modes at 2922, 2852, 1458, 1378, 1354, 1294 and 723 cm^{-1}; C=O and C-O (one stronger and broader than the other) stretching at 1735, 1120 and 1072 cm^{-1}.

6.1.1.2 Uncured and cured adhesive

The interpretation of the spectrum was also conducted on the adhesive in its uncured and cured form (Fig. 6.3) by assigning the bands present in each spectrum to the vibration modes of the functional groups (Table 6.5).
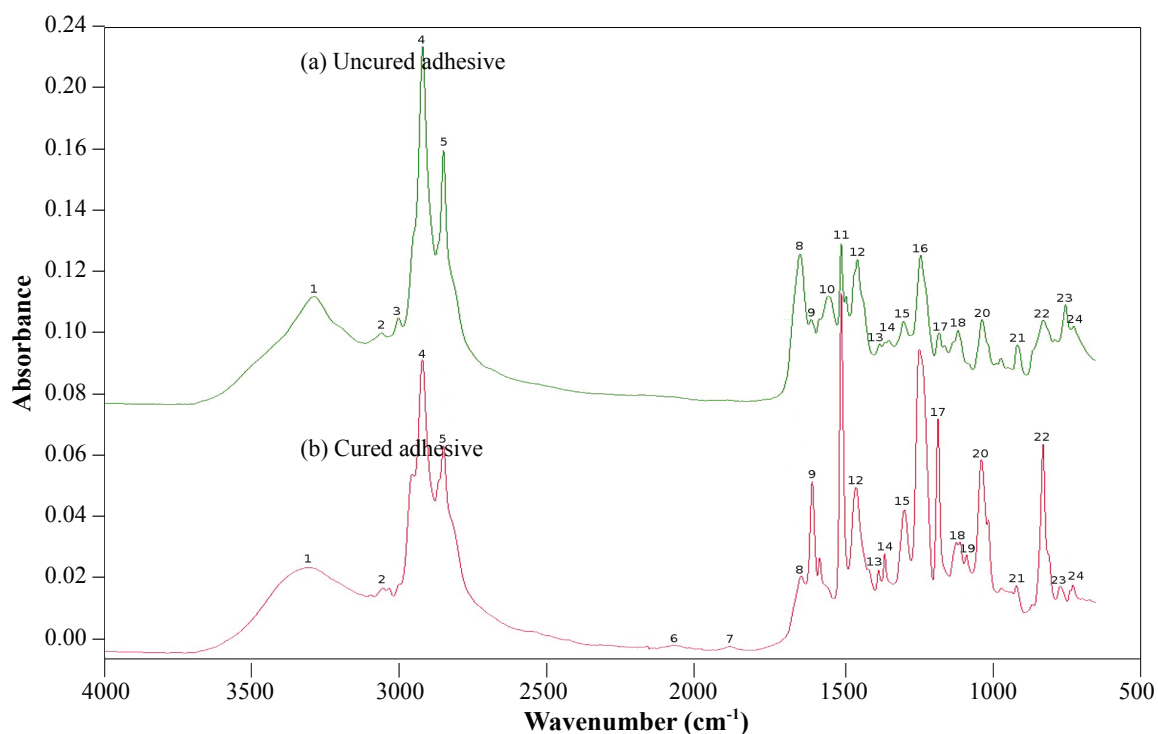
Figure 6.3 Spectra obtained from the samples of the (a) uncured and (b) cured adhesive.

Table 6.5 Functional groups characteristic bands present in the spectra of the adhesive.

Band no.	Intensity	Wavenumber (cm^{-1})		Functional group
		Uncured	**Cured**	
1	*s, b, v*	3600-3200, 3500-3300 (3289)	(3300)	ν_s O-H, ν N-H
2,3	*m-w*	3100-3000 (3058, 3037)	(3057, 3037)	ν_s C-H Aromatic
4,5	*s*	~ 2930, 2870-2840 (2923, 2853)	(2924, 2853)	ν_{as}, ν_s CH$_2$
6,7	*vw*	(2072, 1886)	(2075, 1886)	$\delta_!$ C-H p-subs. Aromatic hydrocarbon groups
8	*m-s*	1650-1560 (1647)	(1644)	ν C=O, δ N-H Amide I
9,10	*m*	1625-1590, 1590-1575 (1610, 1583)	(1606)	ν C=C Aromatic
11	*s*	(1509)	(1508)	ν C-C p-subs. Aromatic semicircle
12	*m-s*	1490-1440 (1455)	(1458)	$\delta_{"\#}$ CH$_2$
13, 14	*m*	1390-1365 (1377, 1350)	(1382, 1391)	δ_s C(CH$_3$)$_2$
15	*m*	(1297)	(1296)	$\rho_\$$CH$_2$
16	*s*	1270-1230 (1241)	(1244)	ν_{as} C-O-C Aryl ethers (Aromatic)
17	*m*	~1190 (1180)	(1181)	ν C-C between p-aromatic
18	*m*	1150 – 1040 (1114)	(1107)	ν C-O Alcohol
19,20	*m*	~1086, ~1035 (1077, 1036)	(1085, 1035)	$\delta_{\%!}$C-H Aromatic
21	*w-m*	920-910 (915)10	(916)	ν_{as} Oxirane, Epoxy ring
22	*m*	830-820 (828)	(826)	δ_{op} C-H para-substituted aromatic
23	*m*	860-780 (751)	(768)	$\delta_!$ C-H Aromatic
24	*m*	730-710 (722)	(720)	δ_r CH$_2$

The adhesive in the uncured and cured form, exhibits a spectra with most of characteristic bands which were previously assigned to epoxy resin and the curing agent, such as, aromatic and oxirane groups in the former and amine and amide in the latter. The main differences between the two adhesive spectra are the reduction or even removal of some of the bands as a result of the epoxy ring opening mechanism during cure, particularly, N-H stretching (band no.1) with a presence of a bold band due to O-H stretching at the same region, C=O stretching from the amide (band no.8); the asymmetric stretching from oxirane group (band no.21).

6.1.2 Cure kinetic studies (FTIR)

The cure kinetics of the adhesive was studied at room temperature through FTIR spectroscopy, by monitoring the bands assigned to the oxirane ($Abs_{915cm-1}$) and C-H bonds of the aromatic ring ($Abs_{1035cm-1}$) as a function of time (Fig. 6.4). The latter band was used as a reference due to these bonds not being involved in the cure.
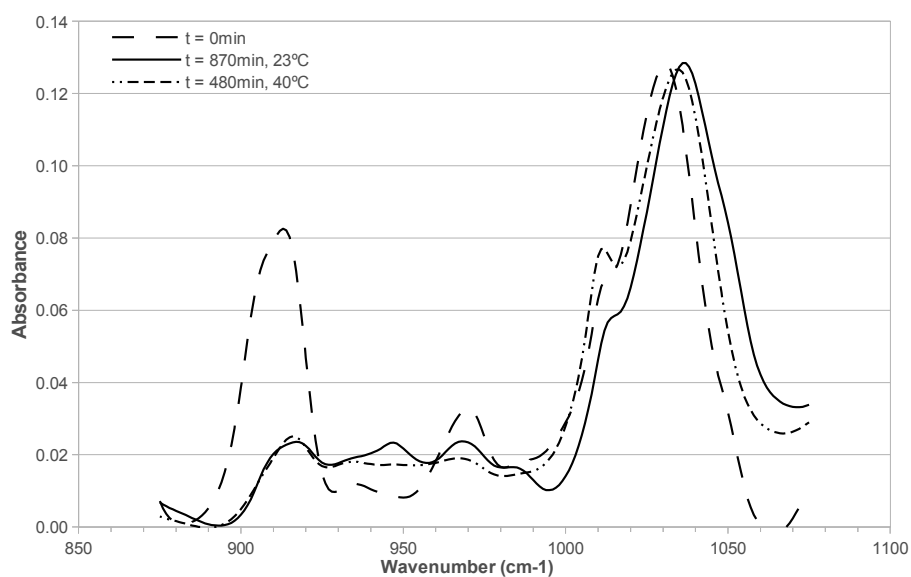
Figure 6.4 Spectra of the epoxy adhesive in the wavenumber range from 875 to 1075 cm^{-1}, before cure (0h), after 15h at 23ºC and 8h at 40ºC of cure.

The monitoring of the cure through the band at 915 cm^{-1} was not simple due to other bands being present in the same region, in particular when the absorption of the oxirane band decreases as that of the other band located at approximately 948 cm^{-1} increases. Furthermore, both bands suffered a small shift to higher frequencies from 913 to 915 cm^{-1} and from 1031 to 1035 cm^{-1} for the epoxy ring and C-H bonds, respectively. These may

lead to some deviations at the final stage of cure when the concentration of oxirane groups is reduced. The ratio of both areas ($Abs_{915cm-1}/Abs_{1035cm-1}$) was used to determine α as a function of time using Eq. 5.8.
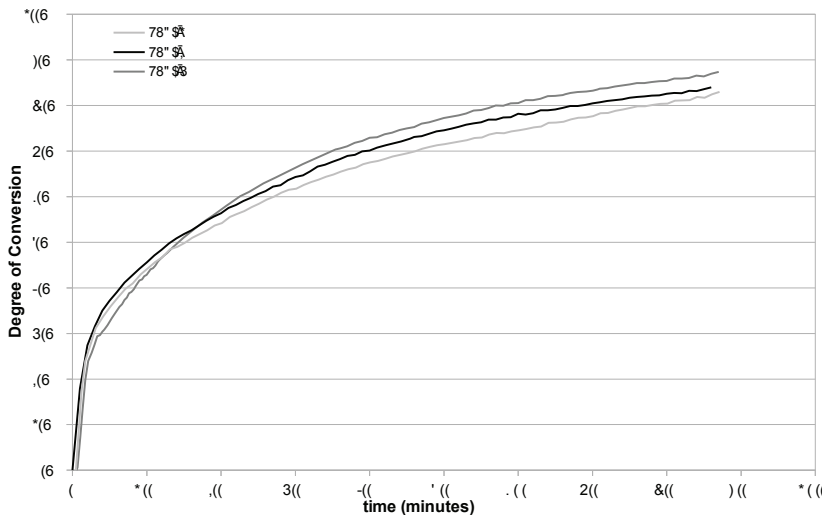
Figure 6.5 Epoxy adhesive kinetics using degree of conversion as a function of the time of cure at 23°C.

Nevertheless, the cure of the epoxy adhesive showed three distinct stages of conversion (Fig. 6.5). A faster reaction in the first 30 minutes up to 30%, followed by a progressively slower cure rate until approximately 75% is reached at 500 minutes and finally by a slowly linear increase to values between 83 and 87%. The adhesive exhibited an average α of 85% after 870 minutes at 23°C. This value is similar to that obtained by the same adhesive (α = 84%) with a cure process at 40°C for 8 hours, the same cure-regime used for the manufacturing process of the BC-Epoxy PMC. However, the full conversion requires more time in both cases according to MSDS of the curing agent, which specifies a typical full cure schedule of 7 days at ambient temperature. Also, it is important to take into consideration that BC particles seem to act as cure accelerators or retardants during the first 60 minutes of the process, depending on their size (7 and 23 μm) and concentration (6 and 12%wt.) in the epoxy adhesive (Abenojar *et al.* 2009b).

6.1.3 Rheological studies (DMA)

Dynamic mechanical thermal analysis was conducted to study the influence of the adhesive's viscoelastic properties on the performance and durability of polymeric matrix composite. This is directly related to the mechanical strength and chemical resistance of the polymer matrix to stress and aggressive species from the surroundings, i.e., to the molecular structure and cross-linking of the adhesive. These characteristics provide some spacing, free volume and degree of freedom for the motion of small groups and chain segments of polymer network or for other molecules from surroundings to penetrate through the adhesive matrix. This is particularly more evident with relaxation of the network as temperature increases to values near the glass transition of the adhesive (T_g). The T_g is generally used as a parameter to indirectly determine mechanical behaviour, average lifetime and chemical degradations during service conditions (Abenojar *et al.* 2009b).

The glass transition temperatures can be obtained from either the maximum value of the tan δ curve or mid-point of the transition in log E' (Fig. 6.6). The former provided the higher value (60.7 ± 0.7ºC) compared to that acquired from the storage modulus (53.8 ± 0.2ºC). Furthermore, the epoxy adhesive used for the composite exhibited a modulus of 1.1 ± 0.1 GPa at 25ºC.
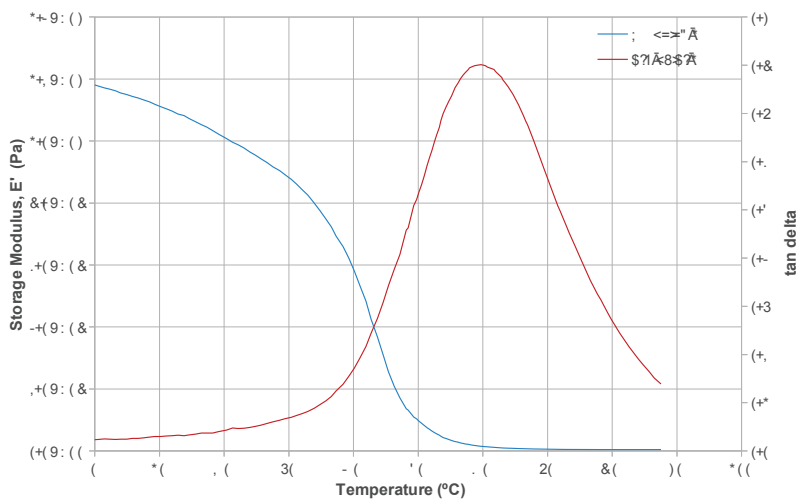
(a)
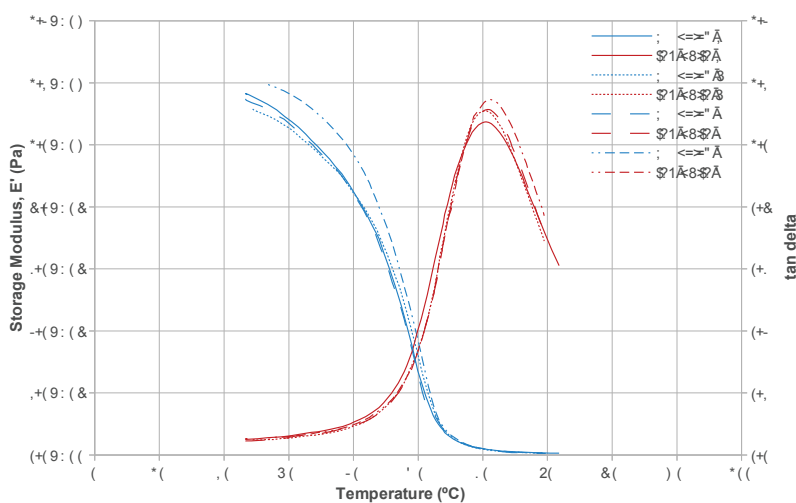
(b)
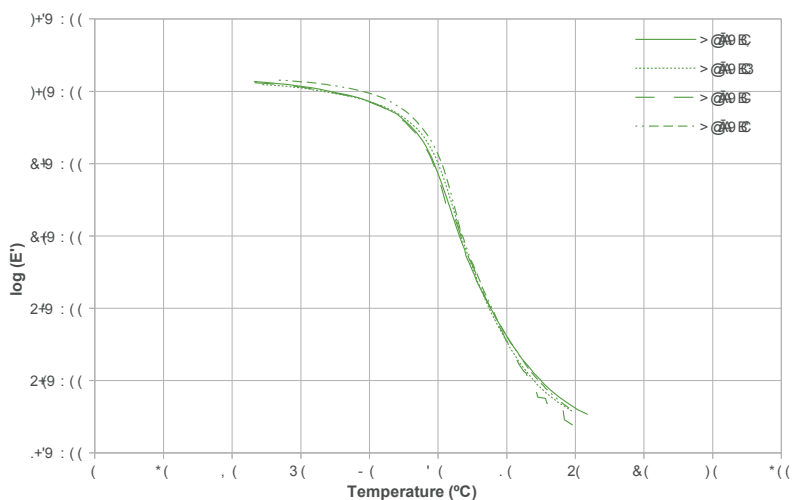
(c)

Figure 6.6 DMA curves of the epoxy adhesive, (a) tan δ and storage modulus for the full temperature range, and (b) tan δ and storage modulus and (c) log E' from 25 to 70ºC.

6.1.4 Wettability studies (Sessile Drop)

The surface free energy (SFE) of the uncured adhesive was obtained by measuring the contact angle (θ) on a series of substrates. Their polar and dispersive energy terms were determined (Table 6.6) using the same procedure applied to the boron carbide (Table 5.10, Eq. 5.9-10). The experimental SFE values for the various substrates are consistent with that reported in literature (Maitz *et al.* 2006, Smith 2009).

Table 6.6 Contact angles of the probe liquids and surface free energy on various substrates.

Substrate	Contact angle, θ (°, degrees)			Surface free energy (mJ/m²)			
	H_2O	CH_2I_2	$C_3H_8O_3$	γ_S^{LW}	γ_S^{AB}	γ_S^+	γ_S^-
Polyethylene	95.6 ± 0.9	51.4 ± 1.3	76.6 ± 1.8	33.5	0.7	0.3	0.4
Polycarbonate	75.0 ± 1.7	29.5 ± 1.7	58.8 ± 0.3	44.4	3.1	4.9	0.5
PVC	68.8 ± 2.1	30.3 ± 1.5	53.4 ± 2.4	44.1	5.0	7.7	0.8
Zytel HTN[*]	64.1 ± 2.3	41.0 ± 1.4	44.1 ± 1.1	39.3	9.7	8.3	2.8
Glass 1	48.0 ± 2.5	38.5 ± 1.5	36.0 ± 0.8	40.4	14.1	21.4	2.3
BC, 1 μm finish	51.0 ± 1.7	48.0 ± 1.0	31.0 ± 1.5	35.4	18.9	16.3	4.9
Glass 2	37.3 ± 1.5	44.0 ± 1.1	30.0 ± 1.4	37.5	19.0	31.0	2.3
Cured Epoxy[**]	75.6 ± 2.5	42.0 ± 2.3	62.6 ± 1.9	38.6	3.7	6.4	0.5
GPS Gel[***]	64.0 ± 3.0	28.0 ± 1.6	45.0 ± 2.3	45.0	7.4	8.2	1.7

[*] Zytel HTN51G35HSL NC010, 35% glass reinforced, heat stabilised, lubricated high performance polyamide resin, [**] Adhesive formulation used in the BC-Epoxy composite; [***] GPS gel prepared according to section 5.2.1.

The energy terms of the uncured epoxy were acquired using Eq. 5.12 and plotting the calculated polar/dispersive component ratio of various substrates and respective contact angles of the adhesive (θ_{exp}) on the same solids (Table 6.7).

Table 6.7 Adhesive contact angle on the various substrates and correspondent plot data values.

Substrate	θ_{exp} (°, degrees)	x, $\left(\sqrt{\gamma_S^{AB}/\gamma_S^{LW}}\right)$	y, $\left(1+\cos\theta_{exp}\right)/2\cdot\sqrt{\gamma_S^{LW}}$
Polyethylene	54	0.1409	0.1372
Polycarbonate	35	0.2647	0.1365
PVC	36	0.3373	0.1366
Zytel HTN	45	0.4962	0.1363
Glass 1	43	0.5920	0.1363
Glass 2	48	0.7122	0.1359
Boron Carbide	52	0.7101	0.1358

The polar and dispersive components were determined through the slope and intercept values from linear regression (Fig. 6.7) using Eq. 5.13 and 5.14. The uncured epoxy possessed a polar and dispersive component of 0.01 mJ/m² and 53.07 mJ/m², respectively. These SFE terms were then used to determinate the theoretical contact angle of the adhesive on the several BC surfaces indicated in section 6.2.3 (Table 6.9). It was found that the adhesive suffered a decrease in SFE after cure with a small increase of the polar component (γ_S^{AB} = 3.70 mJ/m², γ_S^{LW} = 38.59 mJ/m²).
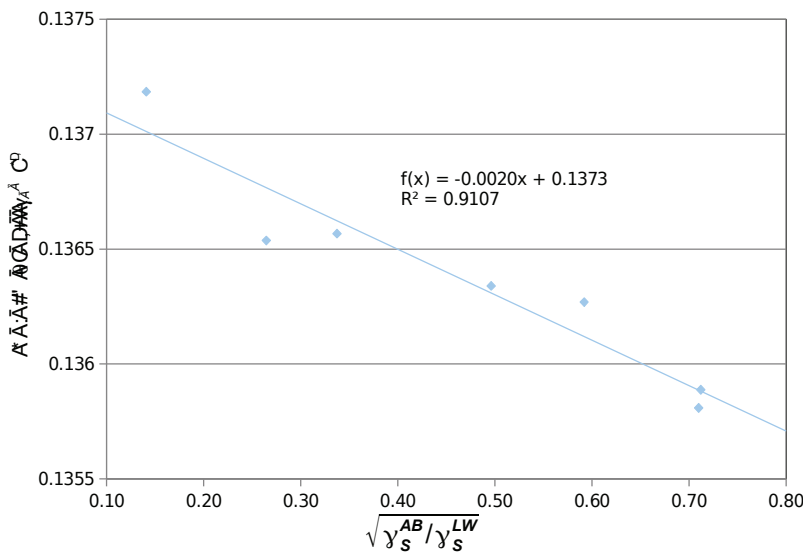
Figure 6.7 Determination of the dispersive and polar fractions of the surface free energy of the uncured adhesive.

6.2 Boron Carbide Characterisation

Morphological, elemental and chemical characterisation of the BC are essential to understand the modification of its surface chemistry and free energy, which could consequently have a direct effect on adhesion, performance and durability of the PMCs.

6.2.1 Morphology (OM and SEM)

Morphological studies of the untreated and silane treated BC particles were conducted through OM and SEM to observe the effect of the surface treatment on the particles. Particle sizes of around 350–100 µm were found for F60, 45-9 µm for F360 and 8-1 µm for F1200 (Fig. 6.8), with the former exhibiting a wider distribution than that specified by

the manufacturer (section 5.1.2). The BC particles generally exhibited smooth, rippling and gradual concentric fractures (conchoidal), which are normally observed in brittle materials exhibiting little or no cleavage. Small fissures were also observed propagating outwards from the centre of the fractures.

(a)

| x5 | x50 | x100 |

(b)

| x5 | x50 | x100 |

(c)

| x5 | x50 | x100 |

Figure 6.8 Optical microscopy of BC particles for the grit size of (a) F60, (b) F360 and (c) F1200.

SEM micrographs of F60 and F360 particles showed a greater extent of this type of fractures (Fig. 6.9a, 6.9b), whilst the F1200 tended to exhibit more rounded, polygonal-type shapes with less sharp edges as a result of faceted fractures (Fig. 6.9c). To summarise, most of the particles possessed a plate-like shape with relatively sharp and thin edges.

(a)　　　　　　　　　　　　　　　(b)

(c)　　　　　　　　　　　　　　　(d)
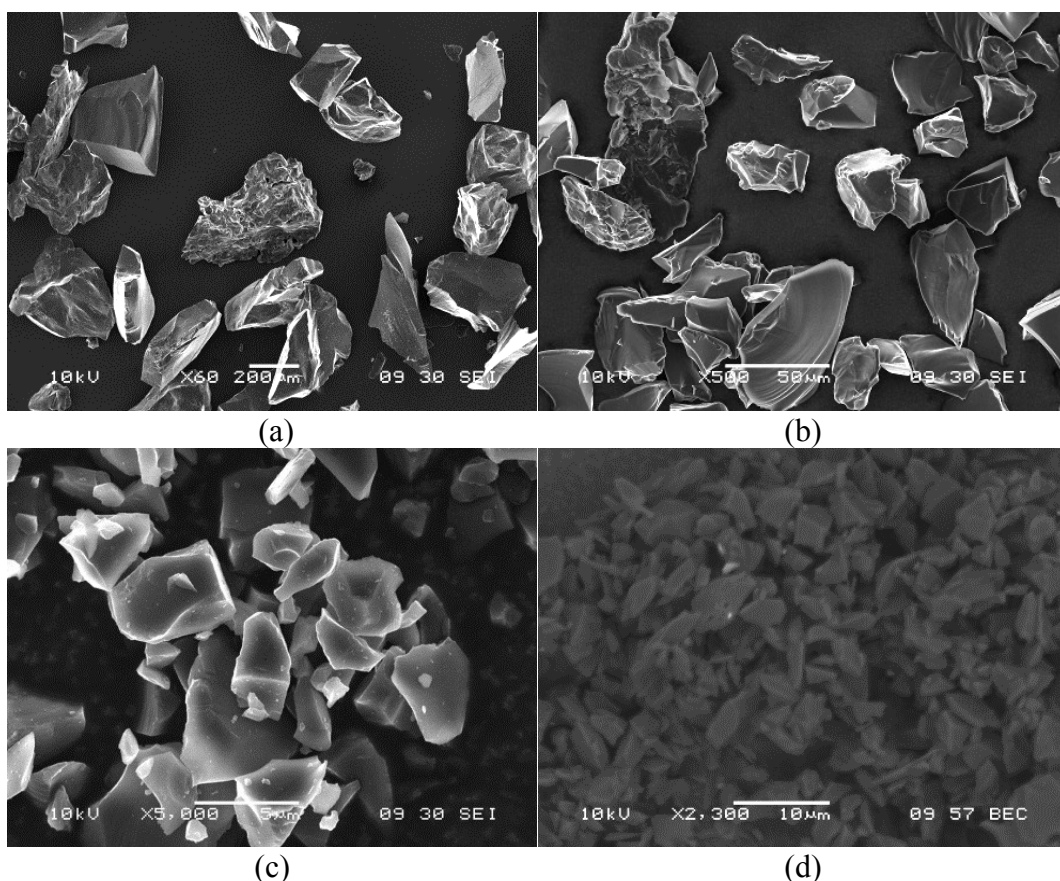
Figure 6.9 Scanning electron microscopy with secondary electrons, SE, on (a) F60 (b) F360 and (c) F1200 and with back scattering electrons, BSE, on (d) F1200.

Elemental analysis showed a boron/carbon ratio lower than suggested from the stoichiometry of the BC (4:1). This was not unexpected given the possible substitution of the two elements in the C-B-C chain linked to $B_{11}C$ icosahedra clusters, located along the main diagonal of the BC rhombohedral structure. Higher ratios would be the result of the presence of regions of β-rhombohedral boron (Mortensen *et al.* 2006, Ghosh *et al.* 2007, Mondal and Banthia 2005).

The untreated BC particles also exhibited small amount of contamination, confirmed by the noticeable lighter spots visible in Fig. 6.9d using back scattering electron analysis. These result from higher atomic number elements, such as iron, sodium and calcium. Also, the silane treated BC material showed a lighter surface and smoother edges as a result of interaction of the electrons with the silane layer (Fig. 6.9c).

6.2.2 Chemical Analysis (FTIR)

FTIR spectroscopy was carried out on untreated BC as a baseline to compare the effect of various surface treatments (Fig. 6.10-11 and Table 6.8).

6.2.2.1 Untreated BC

The spectra of the untreated particles (Fig. 6.10a) shows two strong characteristic bands at 1542 and 1074 cm^{-1}, which were attributed to the characteristic vibration modes of the central atom located in three-atom chain/diagonal (C–B–C) and B–C stretching of the icosahedral BC cell unit (Ghosh *et al.* 2007, Rodríguez *et al.* 2004). The broad form of the former can be as a consequence of other vibration modes (B–C, C–C and BC clusters), indicating the existence of more amorphous materials and higher disordered structures (Rodríguez *et al.* 2004). Also, the presence of free icosahedral B$_{12}$ molecules is confirmed through a band located at 842 cm^{-1} (Ghosh *et al.* 2007). Moreover, the bands at 3458 (broad), 1435 (strong) and 703-624 cm^{-1} (three, weak) were attributed to the O–H and B–O stretching and B–O–H deformation vibrations, respectively (Rodríguez et al. 2004, Kakiage *et al.* 2012, Mondal and Banthia 2005).

6.2.2.2 Corona treated BC

In corona treated samples, FTIR indeed confirmed the higher presence of boron hydroxyl and oxide groups (Fig. 6.10b) through an increase in absorbance of the bands at 3458 (broad), 1435 (strong) and 703-624 (three, weak) cm^{-1}, assigned to O–H and B–O stretching, and B–OH deformation vibrations. Also, bands from aliphatic C-H stretching were observed at 2958, 2921 and 2852 cm$^{-1.}$.

Table 6.8 Functional groups characteristic bands present in the spectra.

Sample	Band no.	Intensity[*]	Wavenumber (cm^{-1})	Functional group[*]
Untreated BC	1	*w*	3458	ν_a(O-H)
	2	*m-s*	3458	ν(C-B-C)
	3	*w-m*	1435-1404	ν(B-O)
	4	*s*	1074	ν(B-C)
	5	*w-m*	842	free icosahedral B$_{12}$
	6	*w-m*	701	ν(B-OH)
Non-hydrolised silane	7,8	*m*	2942-2840	ν_{as}(C–H) CH$_3$ CH$_2$
	9	*w-m*	1466	δ_{sc}(C-H) CH$_2$
	10	*w*	1339	ρ or δ(C-H) CH$_3$
	11	*w*	1254	ν_s(epoxy ring)
	12	*m*	1191	ν(CH$_2$-O-CH$_2$)
	13	*s*	1075	ν_{as}(Si-O-CH$_3$)
	14	*w-m*	909	ν_{as}(Epoxy ring)
	15	*m*	815	ν_s(Si-OCH$_3$)
	16	*m*	777	*w*(C-H), CH$_2$
Silane condensed gel	17	*b, m*	3390	ν_{as}(O–H) SiOH
	18,19	*m*	2934, 2870	ν(C–H) CH$_2$
	20	*w*	1724	ν(C=O) Epoxy, oxidation
	21	*w-m*	1646	δ_s(Si-OH)
	22	*m*	1198	ν(CH$_2$-O-CH$_2$)
	23	*m-s*	1091	ν(Si-OH)
	24	*m-s*	1008	ν_{as}(Si-O-Si)
	25	*m*	907	ν_{as}(Epoxy ring), ν_a(Si-OH)
Silanised BC	26	*b,m*	3669	ν_{as}(O–H) SiOH, free OH
	27,28	*m*	2981,2889	ν(C–H) CH$_2$
	29	*w-m*	1626	ν(C-B-C), d(O–H) SiOH
	30,31	*w-m*	1473,1462	δ_{sc}(C-H) CH$_2$ or O-CH$_2$
	32	*s*	1392	ν(B-O-Si)
	33	*m*	1250	ν_s(Epoxy ring)
	34	*s*	1152	ν(Si-OH)
	35	*m-s*	1095	ν(B-C), ν_a(Si-O-Si)
	36	*m*	966	ν(Si-OH)
	37	*m*	941	ν(B-O-Si)
	38	*w*	879	ν(B-O-Si)
	39	*w*	850	free icosahedral B$_{12}$,Si-O-Si

* Symbols and abbreviations: *b* – broad; *w* – weak; *m* – medium; *s* – strong; *v* – stretch; *δ* – bend; *w* – wag; *sc* – scissor; *s* – symmetric; *as* – asymmetric.
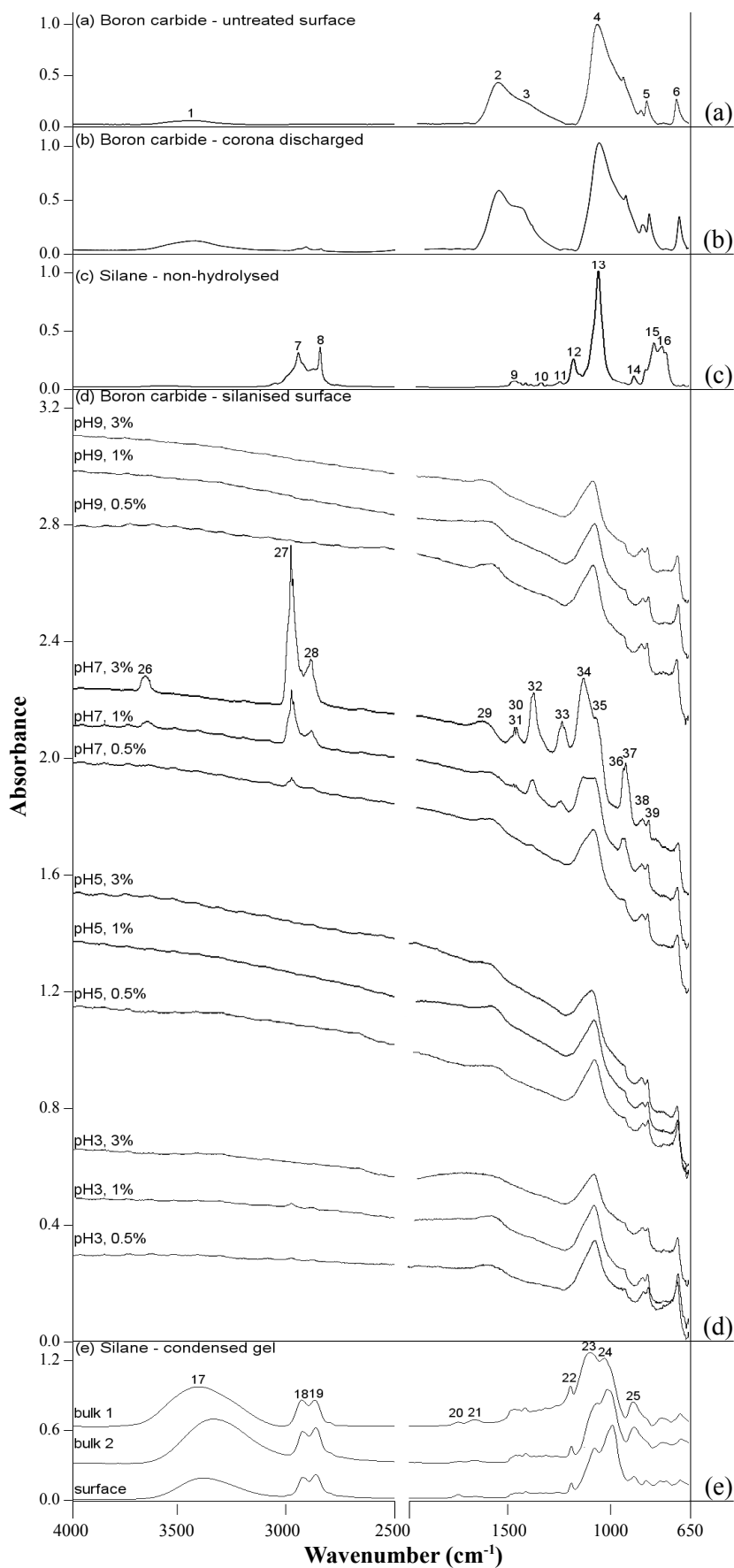
Figure 6.10 FTIR spectra of the (a) untreated, (b) corona discharged and (d) silanised BC, and of the (c) non-hydrolysed and (d) condensed gel form of the silane.

6.2.2.3 Silane treated BC

To better understand the effect of the various silane treatments on the surface of the BC, the spectra of the non-hydrolysed and condensed gel form of the silane were acquired and respective characteristic bands were assigned (Fig. 6.10, 6.11 and Table 6.8). The non-hydrolysed silane (Fig. 6.10c) showed bands assigned to the aliphatic C–H stretching at 2942 and 2840 cm^{-1}, CH_2–O–CH_2 stretching at 1191 cm^{-1} and Si–O–CH_3 stretching at 1075 cm^{-1} and epoxy ring at 1254 and 909 cm^{-1} (Bertelsen and Boerio 2001, Johnsen *et al.* 2006, Parker and Maclachlan 2000, Xue *et al.* 1991). Whereas, the silane gel (Fig. 6.10e) exhibited a broad band at 3390 cm^{-1} as a result of the presence of the silanol group (Si–OH). This group was also confirmed by the vibration modes of the SiOH at 1646, 1091 and 907 cm^{-1}, indicating that the silane was fully hydrolysed using the pH5 aqueous solution (Johnsen *et al.* 2006, Kurth *et al.* 1994). The increase of intensity of band at 1091 cm^{-1} is in agreement with the higher absorbance showed by the other vibration modes attributed to the silanol group. Additionally, the condensation reaction was observed with the appearance of a strong band at 1008 cm^{-1}, which was assigned to the Si-O-Si stretching of the cross-linked silane as an outcome of the high GPS concentration used to obtain the gel. A weak band located at 1724 cm^{-1} was assigned to carbonyl group (C=O) stretching vibration (Bertelsen and Boerio 2001).

The surface treatments on BC consisted of using various aqueous solutions with different pH values and silane concentrations. The solution pH clearly showed an influence on the surface chemistry of the treated BC (Fig. 6.10d, 6.11), with an increase in surface modification going from the most acidic to neutral solution**.** The GPS concentration also affects the number of silanol groups available to react on the surface, and the extension of the condensation process through silane cross-linking and/or the formation of bonds on the ceramic surface. These can be confirmed by the intensity increase of the bands attributed to the silanol vibration modes (3669–3638, 1151 and 964 cm^{-1}) and Si–O–Si stretching (1075 cm^{-1}) with the increase of silane concentration using pH5 and pH7 solutions (Kurth *et al.* 1994, Rider 2006, Hanoosh and Abdelrazaq 2009). A small shift of these bands to a higher frequency can be related to distortions and rotations of the Si-O bonds as a result of the pressure applied to promote contact between the silanised BC particles and ATR crystal (Fiedrich and Weidler 2010). Finally, multiple bands of medium (1392–1382 and 968–942 cm^{-1}) and lower (684–675 cm^{-1}) intensity were found on the surface of the BC treated with pH7 solution, which were attributed to the stretching and bending vibrations of the

borosiloxane bond (B–O–Si) (Nolan *et al.* 2000, Muralidharan *et al.* 2004, Mansour *et al.* 2007, Wróblewska *et al.* 2010, Orhan *et al.* 2008).
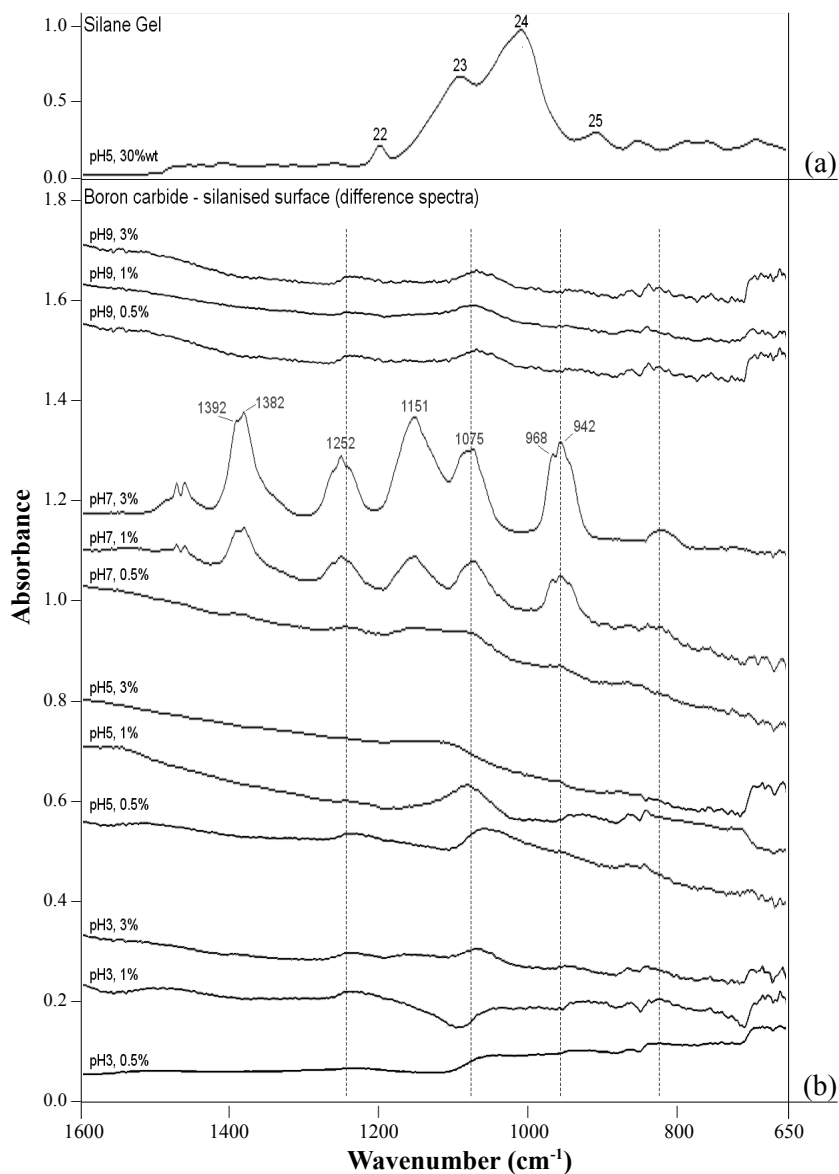
Figure 6.11 FTIR fingerprint region of the (a) silane gel spectra and (b) difference spectra between the silanised and untreated boron carbide surface.

6.2.3 Surface Free Energy (Sessile Drop)

Contact angle measurements were conducted using probe liquids and uncured epoxy on BC to obtain the surface free energies and to predict the wettability of the resin on the various treated surfaces.

6.2.3.1 Influence of solution pH and GPS concentration

The SFE of the untreated BC was 52.5 mJ/m^2, exhibiting a high dispersive component (γ_S^{LW}= 33.7 mJ/m^2, γ_S^+ = 16.5 mJ/m^2, γ_S^- = 5.4 mJ/m^2), as shown in Fig. 6.12 and in the Appendix A (Table A.6). The BC with corona treatment exhibited an increase in the SFE to 64.6 mJ/m^2 mainly as a consequence of a higher Lewis acid component (γ_S^+ = 44.8 mJ/m^2). Hence, a decrease of the contact angle was observed with more polar liquids, e.g. water dropped from 51° to 7.3°, as shown in Appendix A (Table A.7). The effect of solution pH and silane concentration on the SFE of the BC was also investigated in terms of their dispersive, Lewis acid and base components. The silane treated BC exhibited a lower SFE, depicted by a decrease in the Lewis acid component from 16.5 to 2.1 mJ/m^2. On the other hand, the dispersive component increased from 33.7 to 38.7 mJ/m^2, particularly when lower pH values (3 and 5) and higher concentrations (1-3%GPS) were employed. This led to a decrease in contact angle for the pure dispersive liquid (di-iodomethane) from 51° to 42°.
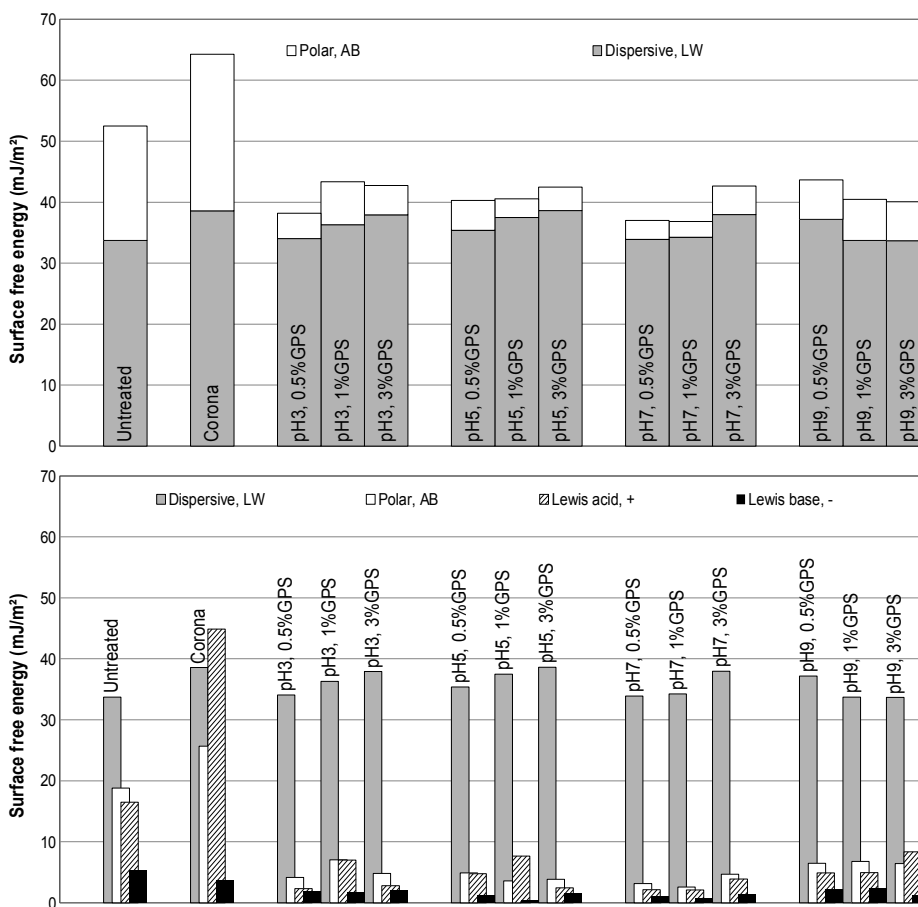
Figure 6.12 Surface free energy values for the BC treated with different pH and silane concentrations.

6.2.3.2 Influence of post-treatment time delay

The effect of the treatment age was also investigated on the SFE of the silane treated BC (Fig. 6.13). Previous work has shown that an increase of post-treatment time results in a decrease of the strength /fracture energy of adhesive joints (Abel *et al.* 2006). Hence, sessile drop tests were conducted on the treated BC using 3%GPS with the different pH values to determine the SFE components and their changes as a function of the post-treatment time (23ºC, 50%RH) and to confirm if the layer will remains 'active' prior to bonding with the adhesive. A small increase of the polar component was observed with time mainly as a result of the lewis acid component, which was more evident with the pH3 solution.
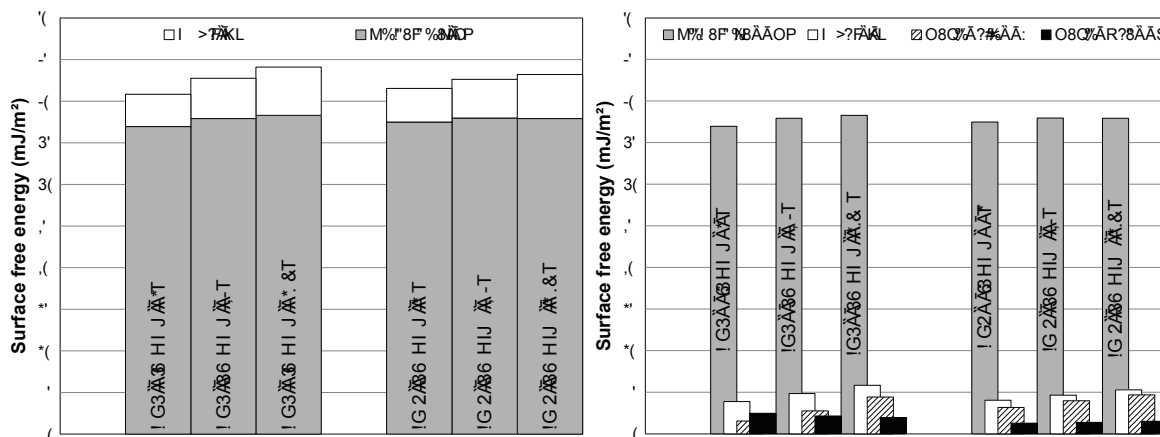
Figure 6.13 Surface free energy components of the silane treated BC with various post-silane treatment time delay.

6.2.3.3 Influence of surface treatment on adhesive wettability

To determine if the SFE changes observed with the surface treated BC were likely to affect the adhesive's wettability, the contact angle of the uncured adhesive on silanised BC was measured using 3%GPS with the different pH values. Furthermore, these experimental contact angles (θ_{exp}) were compared with theoretical values (θ_T) which were determined by using the SFE components of the BC and uncured epoxy adhesive in Eq. 5.11 (Table 6.9)

Table 6.9 Experimental and theoretical adhesive contact angle on the BC.

Surface treatment	Contact angle (º, degrees)	
	θ_{exp} (sessile drop)	θ_T (Eq. 5.11)
Untreated	51.5 ± 0.8	50
Corona	45.0 ± 2.9	40
pH3, 3%GPS	46.0 ± 1.7	47
pH5, 3%GPS	46.7 ± 1.4	44
pH7, 3%GPS	47.8 ± 2.5	46
pH9, 3%GPS	51.5 ± 0.9	46
GPS gel	38.0 ± 1.6	32

The theoretical values showed good agreement with the measured adhesive contact angles for the various treated/untreated surfaces. It was also noted that the gelation of the adhesive affected its wettability with an increase of contact angle on BC surface from 50 to 55°, specifically 15 minutes after mixing the resin with the curing agent.

6.2.4 Elemental / Chemical Analysis – X-ray Photoelectron Spectroscopy (XPS)

A typical XPS survey spectra of the untreated and silane treated BC particles are shown in Fig. 6.14 and in Appendix A (Fig. A.1), respectively. The native chemistry of BC particles presented boron (B), carbon (C), oxygen (O) as the main elements, with some traces amounts of calcium (Ca) and sodium (Na). In the case of the silane surface, the main elements were boron, carbon, oxygen and silicon (Si). Also, some trace amounts of calcium were found when lower concentrations of GPS were used.

Figure 6.14 Survey or wide spectra of the untreated BC surface.

6.2.4.1 Elemental Analysis

The elemental analysis of the BC surfaces were attained from the B1s (183.5 – 198.5 eV), C1s (277.5 – 292.5 eV), O1s (524.5 – 539.5 eV), Si2p (95.5 – 110.5 eV), Na1s (1064.5 – 1079.5 eV), Ca2p (342.5 – 357.5 eV), N1s (396.5 – 410.05 eV) and Fe2p (702.0 – 732.0 eV) high resolution spectra using Shirley background fitting. Surface composition for the untreated and silane treated BC surface, using different solution pH and concentrations of GPS, is summarised in Table 6.10 and Fig. 6.15.

Table 6.10 XPS elemental analysis for the untreated and silane treated BC (atomic %).

Surface treatment	%B	%C	%O	%Si	%Ca	%Na	%N	%Fe
Untreated [*/**]	58.83	22.11	17.97	–	0.52	0.58	–	–
pH3, 0.5% GPS	53.65	25.6	18.21	1.67	0.25	–	0.50	0.13
pH3, 1% GPS	48.09	29.72	18.83	3.29	0.37	–	–	–
pH3, 3% GPS	29.26	24.82	36.17	9.75	–	–	–	–
pH5, 0.5% GPS	49.06	28.67	18.56	3.27	0.43	–	–	–
pH5, 1% GPS	41.31	31.63	22.06	4.43	–	–	–	–
pH5, 3% GPS	14.02	44.58	32.06	9.33	–	–	–	–
pH7, 0.5% GPS	47.23	29.59	19.67	3.23	0.28	–	–	–
pH7, 1% GPS	40.99	32.29	22.23	4.20	0.29	–	–	–
pH7, 3% GPS	10.97	47.04	32.81	9.18	–	–	–	–
pH9, 0.5% GPS	47.66	29.66	19.12	3.26	0.30	–	–	–
pH9, 1% GPS	47.64	28.69	19.69	3.65	0.33	–	–	–
pH9, 3% GPS	23.66	39.67	29.48	6.97	–	–	–	–

* Mortensen *et al.* 2006: %B 58.8 | %C 24.9 | %O 14.6 | %Si 0.5 | %N 1.0 | %Ca 0.1
** Choudhury *et al.* 2007: %B 71.0 | %C 19.0 | %O 1.0 | %Si 0.3 | %N 2.0 | %Fe 0.3

The untreated surface was composed of 59% boron, 22% carbon and 18% oxygen with trace amounts (~0.5%) of calcium and sodium, showing an elemental ratio of approximately 3:1:1. A similar surface composition was found on BC nanoparticles (%B 59, %C 25, %O 15) with some trace amounts of nitrogen, silicon and calcium (Mortensen *et al.* 2006). Whereas, other experimental investigations showed compositions with B/C near 4:1 (Choudhury *et al.* 2007, Zhou *et al.* 2007) that correspond to a more single phase crystalline structure without oxides located in the bulk of the material (Jacobsohn *et al.* 2004).

In the case of the silane treated BC, boron was the major element for 0.5% and 1% of GPS (Fig. 6.15), whereas, the 3% GPS solutions provided surface compositions with carbon as the main element. An exception was found with pH3 solutions, which led to a surface composition with oxygen as the main component.
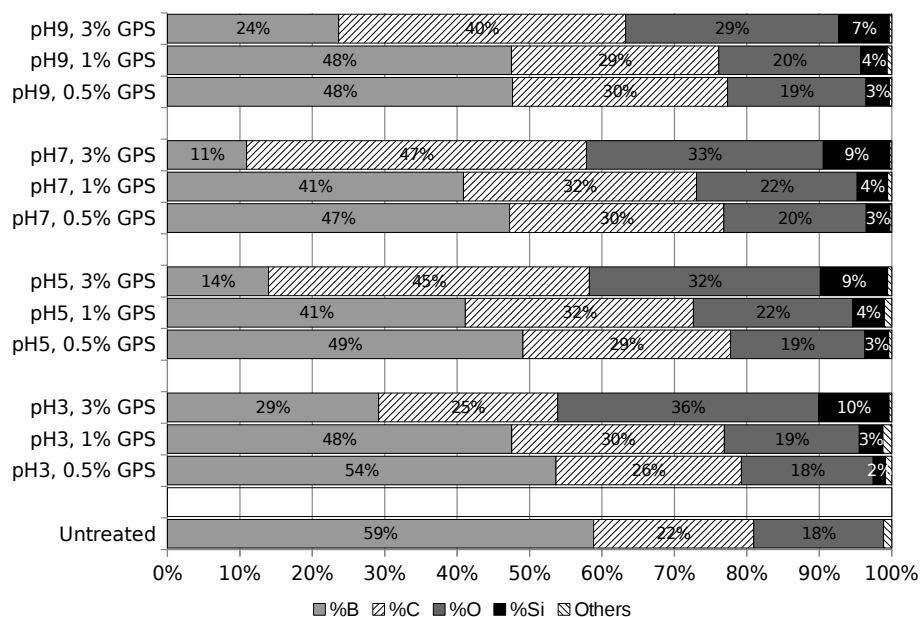
Figure 6.15 Representation of the elemental composition on the untreated and silane treated BC.

The elemental composition as a function of the silane concentration (Fig. 6.15-16) showed that %B decreased as %Si, %O and %C increased. The highest increase and decrease were found for %C and %B, respectively. This was particularly clearer as the concentration of GPS increased from 1 to 3% GPS. Generally, the elemental composition of the silane treated BC when compared to that of the untreated particles showed an increase according to the following order: C > Si > O for 0.5-1% GPS and C > O > Si for 3% GPS. The elemental composition on the treated BC was also evaluated as a function of solution pH (Fig. 6.16). In the case of the 0.5%GPS solutions, elemental variations were greater as pH increased, i.e., a reduction in %B, and an increase of %Si, %C and %O. Similar behaviour was found using 1-3%GPS solutions up to pH7 but reduced variations at pH9. A decrease of %O as pH increased was observed with the highest concentration of silane. Generally, the greatest variations in the full range of silane concentrations were exhibited with pH5-7 solutions. The depletion in %C and %O was particularly evident for 3%GPS in pH3 solution by showing a %Si of 10%. This was unexpected and may be associated to an inaccurate relative atomic sensitivity factor for the respective elements. This factor is relative to the intensity of the F1s signal and used to adjust the peak areas according to photoelectron cross-sections of each element. Polydimethylsiloxane (PDMS) could be used as a comparator to confirm the validity of the quantified data (Wagner *et al.* 1990, Briggs and Grant 2003).
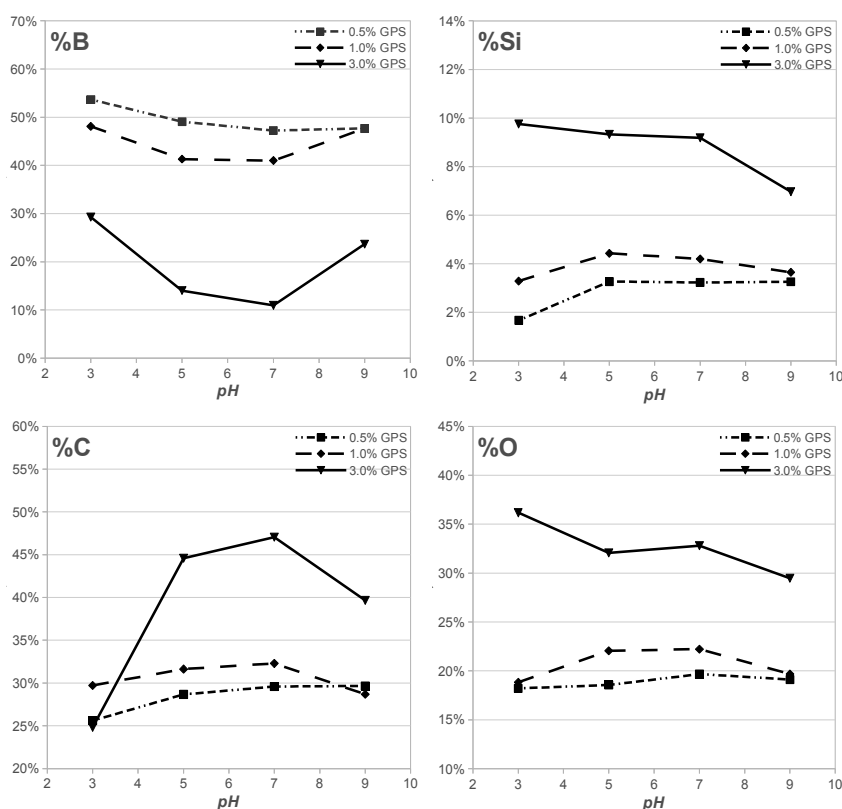
Figure 6.16 Elemental composition on BC surface according to the solution pH and GPS concentration.

6.2.4.2 Silane Layer

The thickness of the silane layers from the treatments with different solutions pH and GPS concentrations was determined using Eq. 5.5 and shown in Table 6.11. It was clear that higher concentrations led to a thicker siloxane structure on the BC. In the case of the solution pH, neutral solutions promoted thicker films in the full range of silane concentrations. Notably, the thickness of the silane layer (0.5 to 2.1 nm) did not match the length of the hydrolysed GPS molecule (~ 1.3 nm) (Brack *et al.* 2005, Kinloch *et al.* 2006].

Table 6.11 Thickness of silane layer according to the solution pH and GPS concentrations

Silane concentration	Thickness (nm)			
	pH3	**pH5**	**pH7**	**pH9**
0.5% GPS	0.5	0.8	0.7	0.8
1% GPS	0.7	0.6	0.9	0.6
3% GPS	1.3	1.5	2.1	1.2

The percentage of surface covered by the GPS layer (f_{GPS}) was determined using Eq. 5.6, followed by the calculation of the elemental concentration for the uncovered, $\%X_{BC}$, and silanised fractions, $\%X_{GPS}$ (Eq. 5.7), as shown in Table 6.12.

Table 6.12 Elemental percentage from the BC and from GPS layer on the surface.

Surface treatment	From the BC				From the GPS layer			
	%B/%B₀	*%B*	*%C_BC*	*%O_BC*	*f_GPS (%)*	*%Si*	*%C_GPS*	*%O_GPS*
Untreated	1.0	58.8	22.1	18.0	0.0	0.0	0.0	0.0
pH3, 0.5% GPS	0.9	53.7	20.2	16.4	8.8	1.7	5.4	1.8
pH3, 1% GPS	0.7	41.3	15.5	12.6	18.3	4.4	16.1	9.4
pH3, 3% GPS	0.5	29.3	11.0	8.9	50.3	9.8	13.8	27.2
pH5, 0.5% GPS	0.8	49.1	18.4	15.0	16.6	3.3	10.2	3.6
pH5, 1% GPS	0.8	48.1	18.1	14.7	29.8	3.3	11.6	4.1
pH5, 3% GPS	0.2	14.0	5.3	4.3	76.2	9.3	39.3	27.8
pH7, 0.5% GPS	0.8	47.2	17.8	14.4	19.7	3.2	11.8	5.2
pH7, 1% GPS	0.7	41.0	15.4	12.5	30.3	4.2	16.9	2.3
pH7, 3% GPS	0.2	11.0	4.1	3.4	81.4	9.2	42.9	29.5
pH9, 0.5% GPS	0.8	47.7	17.9	14.6	19.0	3.3	11.7	4.6
pH9, 1% GPS	0.8	47.6	17.9	14.6	19.0	3.7	10.8	5.1
pH9, 3% GPS	0.4	23.7	8.9	7.2	59.8	7.0	30.8	22.3

The elemental concentration from the silane structure on the BC surface was plotted as a function of f_{GPS} (Fig. 6.17). The composition of the fully silaned surface (f_{GPS} = 100%) using linear regression was found to be 11% of silicon, 39% of oxygen and 49% of carbon. These values were similar to the theoretical values determined from the stoichiometry of the fully crosslinked silane layer (Fig. 6.18), i.e., a Si:O:C ratio of 1:4:6 that corresponds to 9.1% for silicon, 36.4% for oxygen and 54.5% of carbon.

(a)   (b)   (c)
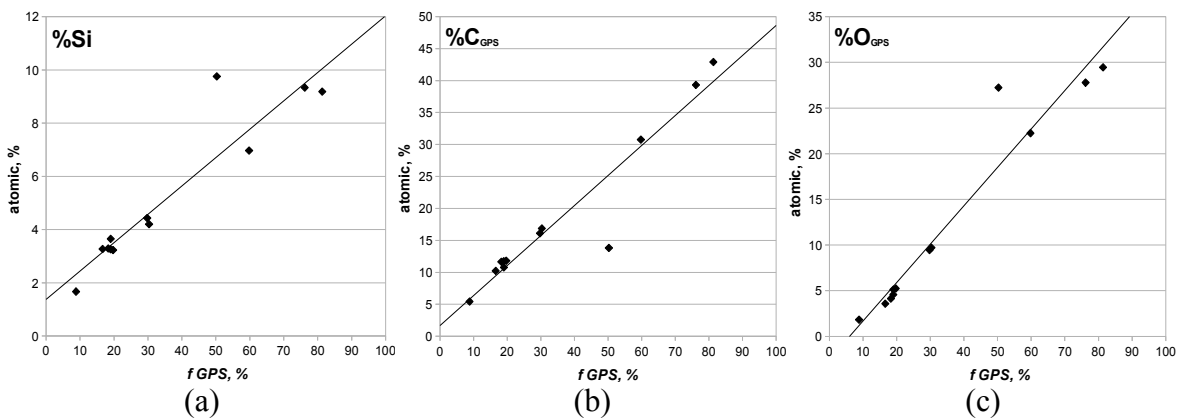
Figure 6.17 Elemental composition of (a) silicon, (b) carbon and (c) oxygen according to the GPS layer coverage percentage (f_{GPS}) on the BC surface.

The elemental percentages of the silane structures obtained for the GPS treatments are in agreement with the linear regressions, with the exception of 3%GPS in pH3 solution. This led to a higher %Si and %O, and a lower %C, when compared to that of similar f_{GPS}.
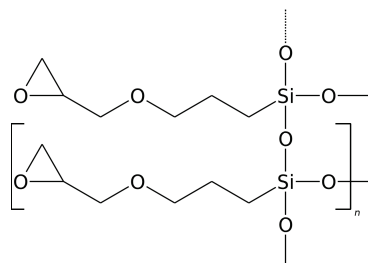
Figure 6.18 Structure of a fully condensed silane layer.

Furthermore, silicon composition on the BC surface for the various solution pH (Fig 6.19) was compared as a function of f_{GPS}. The silane coverage increased with GPS concentration, showing the highest values for pH5-7 solutions with 3%GPS. In contrast, less f_{GPS} was achieved by the more extreme acidic and basic solutions, specially when 0.5-1%GPS were used. The %Si increased with silane concentration, showing the highest values for pH3-7 with 3%GPS. The pH5-7 solutions generally provided similar behaviour for %Si and f_{GPS}, when the same silane concentration was used. In other solutions, the most acidic showed a wider range of %Si with a more limited f_{GPS}, whereas the most basic exhibited a smaller variation of the silicon content and silane coverage.
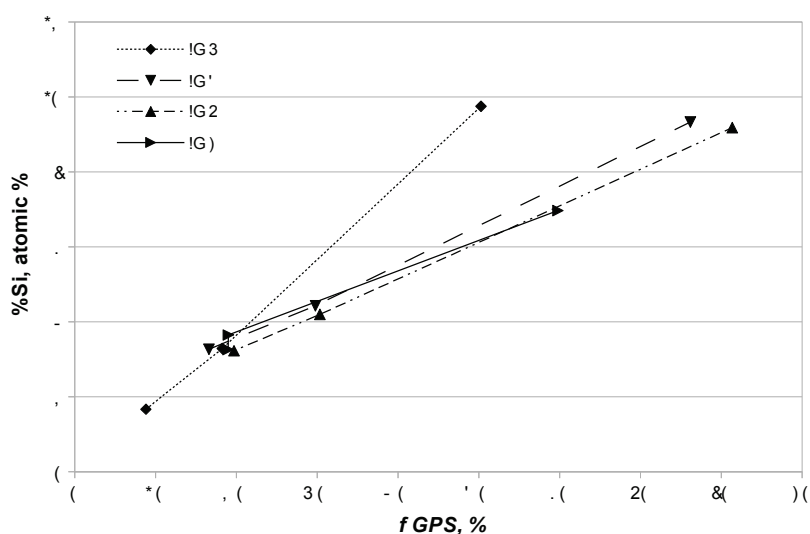
Figure 6.19 Silicon composition according to solution pH and GPS layer coverage percentage (f_{GPS}) on the BC surface.

6.2.4.3 Chemical analysis

Chemical analysis of the BC surfaces was attained by curve-fitting and assignment of the peaks in each high spectra (B1s, C1s, O1s and Si2p). The stoichiometry and full-width-at-half-maximum (FWHM) were considered in the fitting. The FWHM for the B-C and C-O/C=O peaks were defined according to that in literature (Jacobsohn *et al.* 2004), within a tolerance of 0.2 eV for best curve-fitting. Also, the same criteria was applied to the peaks in the O1s and Si2p spectra. The assignment of the peaks was conducted for the untreated and silane treated BC samples based on binding energies (BE) shown in Table 6.13.

Table 6.13 Peak assignments and fitting parameters for the high resolution XPS spectra.

Peak Assignment		Binding energy (eV)	FWHM (eV)	Gauss (%)	Reference[*]
B1s	B_0	186.9-188.6 / 189.5-190.1 ???			[1-4] / [5]
	B-C	187.9-190.6	1.9-2.0 [6]	70 [6]	[3, 4, 6-8]
	B-OH	189.2			[1]
	B-O	190.2-193.3 / 191.7-192.2 B-O(Si) / 193.3 B_2O_3, $B(OH)_3$ / 194.2 B-O-Si Glass network			[1, 3-5, 7-9] / [10] / [10] / [11]
C1s	C-B	281.3-282.9	1.6-1.7 [6]	70 [6]	[2-7]
	Oxy-BC	283.7-283.8	1.7 [6]	70 [6]	[6]
	C-Si	283.0-285.0			[12-15]
	C-H/C-C	284.3-285.3 / 284.4 Graphite	-	-	[1-5, 8, 13-16] / [17]
	C-O	286.0-286.7			[1-3, 5, 14, 15, 18]
	C=O	287.6-288.3			[1-3, 14, 15, 18]
	O=C-O	288.5-289.4			[13, 15, 18]
O1s	C=O	531.5-532.0	1.7 [6]	70 [6]	[6]
	O=C-O	531.6-532.1			[18]
	O-B	532.0-533.0 / 533.0 B_2O_3			[3, 5] / [10]
	O-Si	532.4-533.0 / 533.0 $Si-O_2$ / 532.5 Si-O			[1, 18] / [10] / [13]
	O-C	532.8-533.3 / 531.0??	1.7 [6]	70 [6]	[1, 6, 18] / [3]
Si2p	Si-C	100.4-100.7			[12, 19]
	Si-O	102.2-102.7 Si-O-Si Siloxane			[1, 20, 21]
		102.4-103.5 Si-O (Si, SiC), SiO_3C			[10, 12, 18, 21]
		102.4, Si-O 1 NBO, Si-O-B4			[11]
		103.9, B-O-Si Glass network			[11]
		101.7, $SiO_2Xn(X=Si,C;n=1,2)$			[10]
		102.4, Si			[14]

* [1] Brack *et al.* 2005; [2] Shi *et al.* 2003; [3] Velamakanni *et al.* 2009; [4] Kokai *et al.* 2001; [5] Mortensen e*t al.* 2006; [6] Jacobsohn *et al.* 2004; [7] Deshpande *et al.* 1994; [8] Ahn *et al.* 2005; [9] Zeng *et al.* 2001; [10] Pola *et al.* 2004; [11] Orhan *et al.* 2008; [12] Lee *et al.* 1991; [13] De Palma *et al.* 2007; [14] Van Ooij *et al.* 1991; [15] Ma *et al.* 2006; [16] Zhou *et al.* 2007; [17] Hong *et al.* 2010; [18] Wagner *et al.* 1979; [19] LaSurface 2012; [20] Vandenberg *et al.* 1991; [21] Xu 2004.

6.2.4.3.1 Untreated BC

Chemical analysis of the untreated surfaces was conducted through curve-fitting of high resolution spectra B1s, C1s and O1s (Fig. 6.20) to obtain the binding energy and intensity of each component (Table 6.14).

(a)

(b)

(c)
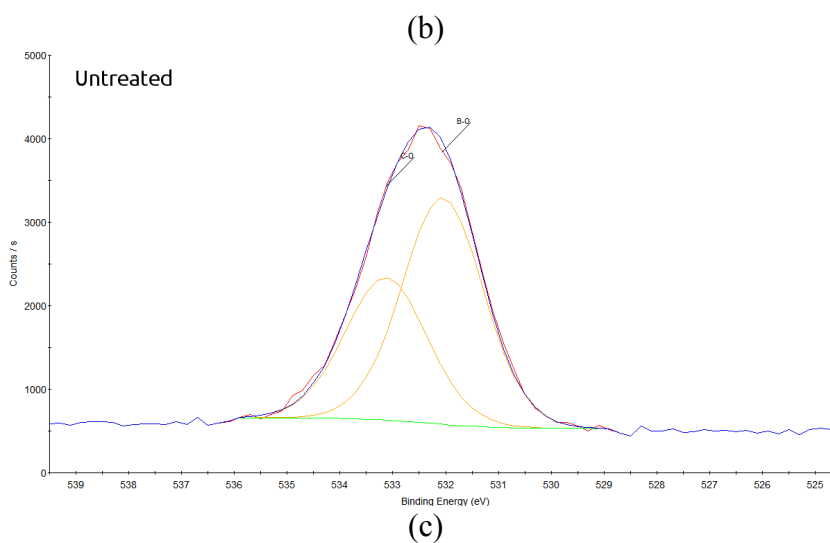
Figure 6.20 Curve-fit of the XPS high resolution B1s spectra of the untreated BC surface for (a) B1s, (b) C1s and (c) O1s.

Table 6.14 Peak assignments for the curve-fit of the high resolution XPS spectra for the untreated BC surface.

Spectra (% relative to all elements)	Peak assignment	Binding energy, eV	Atomic, % (relative to each element)
B1s (59%)	B-O	193.0	3.7
	B-OH	189.0	19.4
	B-C	187.6	76.9
C1s (22%)	O-C=O	289.1	4.7
	C=O	287.6	1.0
	C-O	286.5	11.0
	C-C / C-H	284.8	46.7
	C-B	282.2	36.6
O1s (18%)	C-O/C=O	533.2	40.0
	B-O/B-OH	532.0	60.0

The B1s signal was composed of three components. The primary peak at 187.6 eV was attributed to boron carbide (B-C, B_4C). The other two peaks found at 189.0 eV and 193.0 eV were assigned respectively to hydroxyl groups (B-OH) and oxides species (B_2O_3). No multiple B-C peaks were found as reported in some works resulting from different chemical environments, such as B–C bonds with C atoms in a graphitic state (188.5 eV) or in a sp^2 (C-B-C chain) / sp^3 ($B_{11}C$ icosahedra) hybridisation (187.9-188.5 eV / 189.5-190.6 eV) (Cermignani *et al.* 1995, Zhou *et al.* 2007).

In the case of the C1s, the spectra was fitted using four peaks. The primary and secondary peak were found at 282.2 and 284.8 eV and attributed to apolar components, i.e., BC (B-C) and adventitious carbon/graphitic bonds (C–C / C–H), respectively. Whereas, the high BE peaks associated with the presence of polar oxide and hydroxide-containing species, located at 286.5 and 287.6 eV were associated respectively to the C-OH/C-O-C and C=O. Again, no B-C peaks were distinguished from different chemical environments, i.e., C–B–C chain (281.0 - 282.5 eV) and icosahedra (282.2 - 283.6 eV) of the BC (Hong *et al.* 2010, Zhou *et al.* 2007). The native surface chemistry of the BC shows that most carbon was single bonded to carbon (C-C 46.7%) or to boron (C-B 36.6%). Also, C1s spectra confirms carbon element single and double bonded to oxygen (C-O 11.0%, C=O 4.7%), which were probably from ester or carboxylic acid species.

The O1s spectra were fitted with two peaks at 532.0 eV (60.0%) and 533.1 eV (40.0%). The former was assigned to B-O from boron hydroxides and oxides and the latter attributed to C-O, C=O and O=C-O functional groups observed in B1s and C1s spectra, respectively.

6.2.4.3.2 Silane treated BC

Chemical analysis of the silane treated BC was done through curve-fitting of high resolution spectra B1s, C1s, Si2p and O1s (Fig. 6.21-24) to obtain the BE and intensity of each contributions (Table 6.15-19).

The B1s spectra showed a broadened asymmetric profile centred at 187.7 eV which became less intense at lower BE values (187.1 eV), as solution pH (from 3 to 7) and %GPS increased (Fig. 6.21). The %B decreased from 59 to 11-54%, according to the parameters of the silane treatment. This was more evident using pH5-7 with medium and high GPS concentrations. Two peaks were assigned in high resolution B1s spectra which resulted from the boron element bonded to carbon (B-C) and hydroxyl group (B-OH) as shown in Table 6.15. The sum of all the curve fitting of the different boron peaks is equal to 100%, which corresponds to B1s total.

Table 6.15 Peak assignments for the curve-fit B1s spectra for untreated and silane treated BC surfaces.

Surface treatment (%B relative to all elements)	Binding energy, eV			Atomic, % (relative to B1s = 100%)		
	B-O	B-OH	B-C	B-O	B-OH	B-C
Untreated (59%)	193.0	189.0	187.6	3.7	19.4	76.9
pH3, 0.5% GPS (54%)	-	189.0	187.6	-	22.2	77.8
pH3, 1% GPS(48%)	-	189.1	187.6	-	24.6	75.4
pH3, 3% GPS (29%)	-	188.9	187.4	-	22.5	77.5
pH5, 0.5% GPS (49%)	-	189.2	187.7	-	19.1	80.9
pH5, 1% GPS(41%)	-	188.9	187.5	-	28.8	71.2
pH5, 3% GPS (14%)	-	188.7	187.2	-	26.8	73.2
pH7, 0.5% GPS (47%)	-	188.7	187.3	-	21.2	78.8
pH7, 1% GPS (41%)	-	189.1	187.4	-	19.3	80.7
pH7, 3% GPS (11%)	-	188.7	187.3	-	20.9	79.1
pH9, 0.5% GPS (48%)	-	188.9	187.3	-	19.4	80.6
pH9, 1% GPS (48%)	-	188.6	187.2	-	22.8	77.2
pH9, 3% GPS (24%)	-	188.8	187.1	-	19.0	81.0

The B1s was composed by two components with contributions of 71-81% for B-C and 19-29% for B-OH. The latter was located at a BE between 188.7 and 188.2 eV, showing higher percentage (23-26%) when pH3-5 solutions with medium and higher concentration of GPS were used. Whereas, smaller contributions were observed with the pH7-9 (19-23%)

pH9

pH7

pH5

pH3

0.5% GPS

1.0% GPS

3.0% GPS

Figure 6.21 High resolution B1s spectra of the silane treated BC surfaces with various GPS concentrations and solution pH.

solutions for the full range of concentrations. The peak assigned to the B-C bond was the major component (71-81%) for all silane treated BC surfaces, which exhibited the lowest contributions with 1-3%GPS in pH5 solution (71-73%). Generally, a small shift of the B-C peak to lower BE, from 187.6 to 187.1 eV, was observed as %GPS and solution pH increased.

The C1s spectra showed a more complex profile with various components, dominating the signal at 284.9 eV and 282.2 eV or at 286.4 eV and 284.7 eV, according to silane treatment (Fig. 6.22). Also, carbon concentration has increased from 22 to 26–47% depending on the solution pH and GPS concentration. The highest concentrations were observed with 3%GPS in pH5-9 solutions. Six chemical shifts in high resolution spectra were identified and the corresponding peaks were curve-fitted (Table 6.16). These peaks resulted from the carbon element being bonded to different functional groups with oxygen, carbon or hydrogen, silicon and boron. The sum of all the curve fitting of the different carbon peaks is equal to 100%, which corresponds to C1s total (Table 6.17).

Table 6.16 Peak assignments for the curve-fit C1s spectra for silanised BC surfaces.

Surface treatment	Binding energy, eV					
	O-C=O	C=O	C-O	C-C/C-H	C-Si	C-B
Untreated	289.1	287.6	286.5	284.8	-	282.2
pH3, 0.5% GPS	289.1	288.2	286.7	285.0	283.8	282.0
pH3, 1% GPS	289.6	288.1	286.6	284.9	283.6	281.
pH3, 3% GPS	289.4	288.2	286.8	285.1	283.9	281.9
pH5, 0.5% GPS	289.3	288.1	286.8	284.9	283.4	282.0
pH5, 1% GPS	289.3	287.8	286.6	284.9	283.5	282.0
pH5, 3% GPS	289.3	288.1	286.5	284.8	283.1	281.6
pH7, 0.5% GPS	289.3	288.0	286.6	284.8	283.7	281.7
pH7, 1% GPS	289.4	288.2	286.7	284.9	283.6	281.8
pH7, 3% GPS	289.2	287.6	286.4	284.8	283.9	281.6
pH9, 0.5% GPS	289.4	288.1	286.6	284.8	283.7	281.9
pH9, 1% GPS	289.0	287.8	286.5	284.7	283.5	281.6
pH9, 3% GPS	289.0	287.7	286.4	284.7	283.5	281.5

pH9

pH7

pH5

pH3

0.5% GPS

1.0% GPS

3.0% GPS

Figure 6.22 High resolution C1s spectra of the silane treated BC surfaces with various GPS concentrations and solution pH.

Table 6.17 Peak intensities for the curve-fit C1s spectra for silanised BC surfaces.

Surface treatment (%C relative to all elements)	Atomic, % (relative to C1s = 100%)					
	O-C=O	C=O	C-O	C-C/C-H	C-Si	C-B
Untreated (22%)	4.7	1.0	11.0	46.7	-	36.6
pH3, 0.5% GPS (26%)	4.2	2.4	24.1	32.1	9.6	27.6
pH3, 1% GPS (30%)	3.1	8.0	30.0	29.4	10.0	19.5
pH3, 3% GPS (25%)	5.2	3.7	47.7	33.1	3.4	6.9
pH5, 0.5% GPS (29%)	3.9	3.5	36.3	31.7	5.1	19.5
pH5, 1% GPS (32%)	4.7	7.2	35.5	31.6	4.4	16.5
pH5, 3% GPS (45%)	4.4	6.6	51.1	34.5	0.4	2.9
pH7, 0.5% GPS (30%)	4.3	3.7	34.1	29.2	9.3	19.4
pH7, 1% GPS (32%)	3.6	3.4	39.4	31.5	6.1	16.0
pH7, 3% GPS (47%)	5.0	7.6	44.2	37.1	3.3	2.8
pH9, 0.5% GPS (30%)	3.4	5.3	35.0	29.3	6.7	20.3
pH9, 1% GPS (29%)	2.9	2.7	33.2	32.3	8.7	19.3
pH9, 3% GPS (40%)	5.6	7.6	45.4	31.0	3.6	6.8

The high resolution spectra was composed by 3-6% for C-O=C, 2-8% for C=O, 29-37% for C-C/C-H, 0.4-10% for C-Si and 3-28% for C-B bonds. All spectra showed the existence of a C-Si peak from the GPS layer, specially when solutions with 0.5-1%GPS were used. Also, an increase in intensity of C-O component was found with the GPS concentration due to the higher presence of these bonds from the epoxy and ether groups of the silane structure. The slightly acidic solutions led to the lowest C-Si and greatest C-O component, as opposed to the most acidic solution. The C-B peak from the BC surface decreased as C-O to C-C/C-H ratio converged to values near that theoretically determined from the GPS stoichiometry (2:1), particularly as the silane concentration increased in pH5-7 solutions (Neyman 2003). Furthermore, silane treated BC showed a higher C=O component than that of the untreated material, in particular for the pH3-5 with 1%GPS and pH7-9 with 3%GPS. This indicates the presence of carbonyl groups within the silane structure.

The Si2p spectra showed a broadened asymmetric profile centred at 102.7 eV, which became more intense to lower BE (102.4 eV), as pH and silane concentration increased (Fig. 6.23). The silicon concentration ranged between 2 and 10% according to the silane layer present on the BC surface. Two chemical shifts in high resolution Si2p spectra were identified and respective peaks were curve-fitted (Table 6.18). The chemical states were assigned to the non-crosslinked (Si-O) and crosslinked (Si-O-Si) silane species. The latter results from the full or partial hydrolysis of the GPS and condensation of the hydrolysed form during the silane treatment. The sum of all the curve fitting of the two silicon peaks is equal to 100%, which corresponds to Si2p total.

Table 6.18 Peak assignments for the curve-fit Si2p spectra for the silanised BC surfaces.

Surface treatment (%Si relative to all elements)	**Binding energy, eV**		**Atomic, %** (relative to Si2p = 100%)	
	Si-O	Si-O-Si	Si-O	Si-O-Si
pH3, 0.5% GPS (2%)	103.1	102.3	53.5	46.5
pH3, 1% GPS (3%)	103.4	102.6	58.2	41.8
pH3, 3% GPS (10%)	103.4	102.6	27.6	72.4
pH5, 0.5% GPS (3%)	103.3	102.6	29.4	70.6
pH5, 1% GPS (4%)	103.3	102.4	43.2	56.8
pH5, 3% GPS (9%)	103.4	102.5	26.7	73.3
pH7, 0.5% GPS (3%)	103.4	102.4	19.5	80.5
pH7, 1% GPS (4%)	103.1	102.5	18.3	81.7
pH7, 3% GPS (9%)	103.3	102.5	21.1	78.9
pH9, 0.5% GPS (3%)	103.4	102.5	15.8	84.2
pH9, 1% GPS (4%)	103.2	102.4	17.3	82.7
pH9, 3% GPS (7%)	103.2	102.3	27.0	73.0

The peak assigned to the non-crosslinked GPS (~103.3 eV) was the major component for the most acidic solution, whereas, the smallest contributions were observed with the pH7-9 solutions using 0.5-1%GPS. An increase of the non-crosslinked species was confirmed from 0.5-1% of silane for pH3-5 and from 1-3%GPS for pH7-9 solutions. The second peak attributed to the crosslinked GPS layer (~102.4 eV) was always dominant on the BC surface, with the exception for pH3 with lower and medium concentration of silane. The intensity was generally higher for pH7-9, in particular for 0.5-1%GPS. Whereas, pH3-5 solutions showed the lowest Si-O-Si contributions. pH3-5 solutions showed an increase and pH7-9 a decrease in peak intensity from 1 to 3% GPS. Nevertheless, similar intensities were found with all solutions using the highest concentration of silane.

0.5% GPS

1.0% GPS

3.0% GPS

pH3

pH5

pH7

pH9
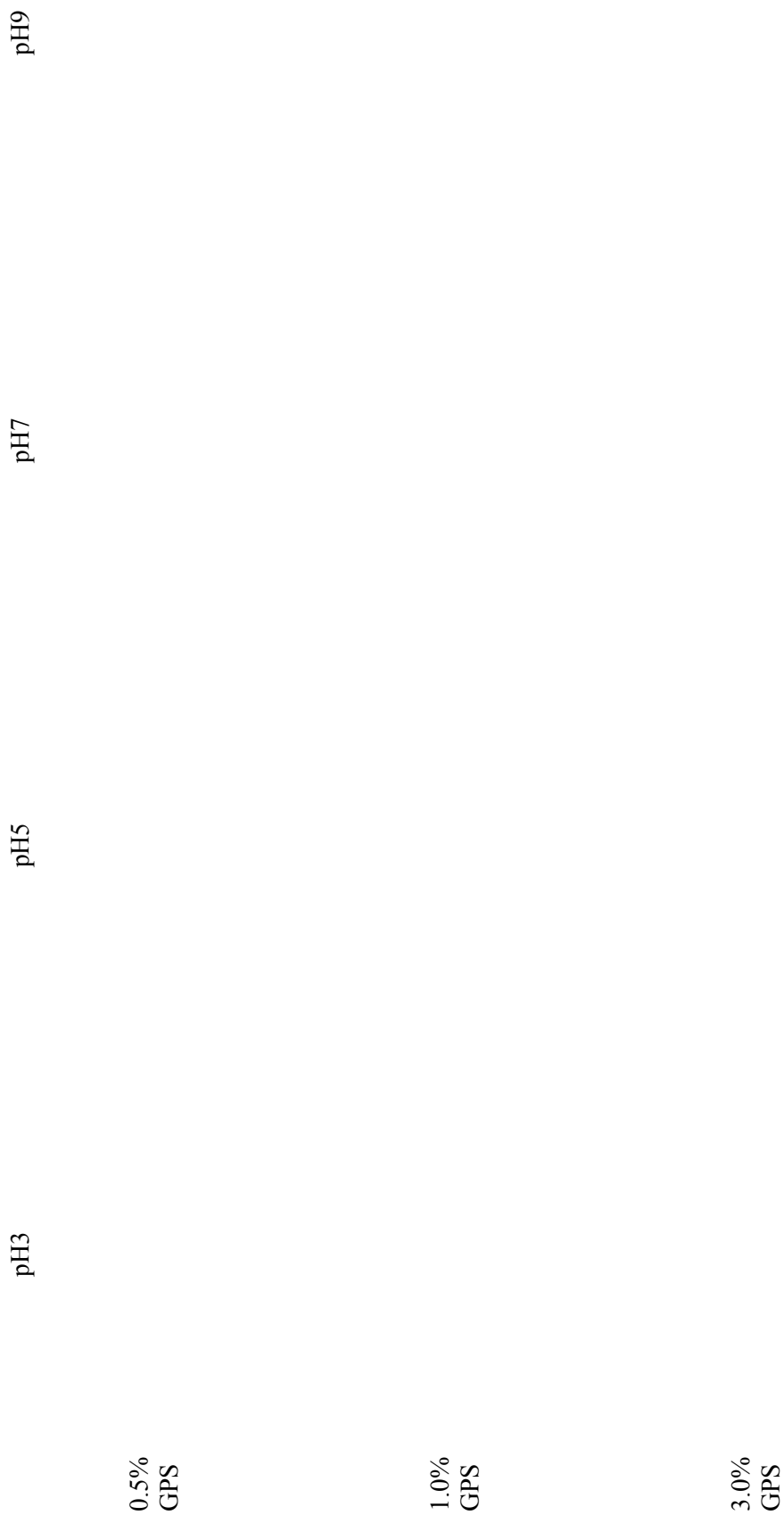
Figure 6.23 High resolution Si2p spectra of the silane treated BC surfaces with various GPS concentrations and solution pH.

The O1s spectra showed a broadened asymmetric profile centred at 532.3 eV with a higher contribution at lower BE, which became more intense and asymmetric at higher binding energies with the increase of solution pH and GPS concentration (Fig. 6.24). The oxygen content increased from 18% to 18-36% after silane modification. Generally, the oxygen element showed higher content when pH5-7 solutions were used in the full range of %GPS. The highest %O was exhibited by the pH3 solution with 3% of silane concentration. The chemical shifts in high resolution O1s spectra were identified and the corresponded peaks were curve-fitted. The sum of all the curve fitting of the different oxygen peaks is equal to 100%, which corresponds to O1s total.

Table 6.19 Peak assignments for the curve-fit O1s spectra for the silanised BC surfaces.

Surface treatment (%O relative to all elements)	Binding energy, eV			Atomic, % (relative to O1s = 100%)		
	Si-O	C-O	B-O	Si-O	C-O	B-O
Untreated (18%)	-	533.2	532.0	-	39.0	61.0
pH3, 0.5% GPS (18%)	533.8	532.8	531.7	7.4	65.3	27.3
pH3, 1% GPS (19%)	534.0	532.8	531.7	13.6	64.3	22.1
pH3, 3% GPS (36%)	533.9	532.8	531.9	15.1	74.3	10.6
pH5, 0.5% GPS (19%)	534.0	532.9	532.0	5.1	73.8	21.0
pH5, 1% GPS (22%)	533.9	532.7	531.7	14.7	73.6	11.7
pH5, 3% GPS (32%)	533.7	532.6	-	17.2	82.8	-
pH7, 0.5% GPS (20%)	534.0	532.6	531.4	5.4	77.7	16.9
pH7, 1% GPS (22%)	533.6	532.6	531.4	10.2	80.6	9.15
pH7, 3% GPS (33%)	533.6	532.6	-	16.2	83.8	-
pH9, 0.5% GPS (19%)	534.1	532.7	531.5	4.9	79.2	15.9
pH9, 1% GPS (20%)	533.6	532.5	531.5	5.9	76.1	18.0
pH9, 3% GPS (29%)	533.9	532.5	531.8	10.7	76.1	13.2

The O1s signal was generally composed by B-O (0-27%), C-O (65-84%) and Si-O (5-17%) contributions, as shown in Table 6.19. Also, a small shift to lower BE of the C-O (533.2 eV) and B-O (532.0 eV) bonds was observed after surface treatment to 532.5-532.9 eV and to 531.4-532.0 eV, respectively. The Si-O and B-O contributions were exclusively from the silane layer and BC surface, whereas, the C-O component resulted from both boron carbide and GPS. Hence, the Si-O component generally increased as B-O contribution decreased when higher silane concentration was used. The highest Si-O intensities were observed with 0.5-1%GPS in pH3-5 and 3%GPS in pH5-7 solutions. In the case of the latter, the B-C component was no longer noticed with the O1s signal being only composed by two strong signals from the Si-O and C-O bonds.

pH9

pH7

pH5

pH3

0.5% GPS

1.0% GPS

3.0% GPS
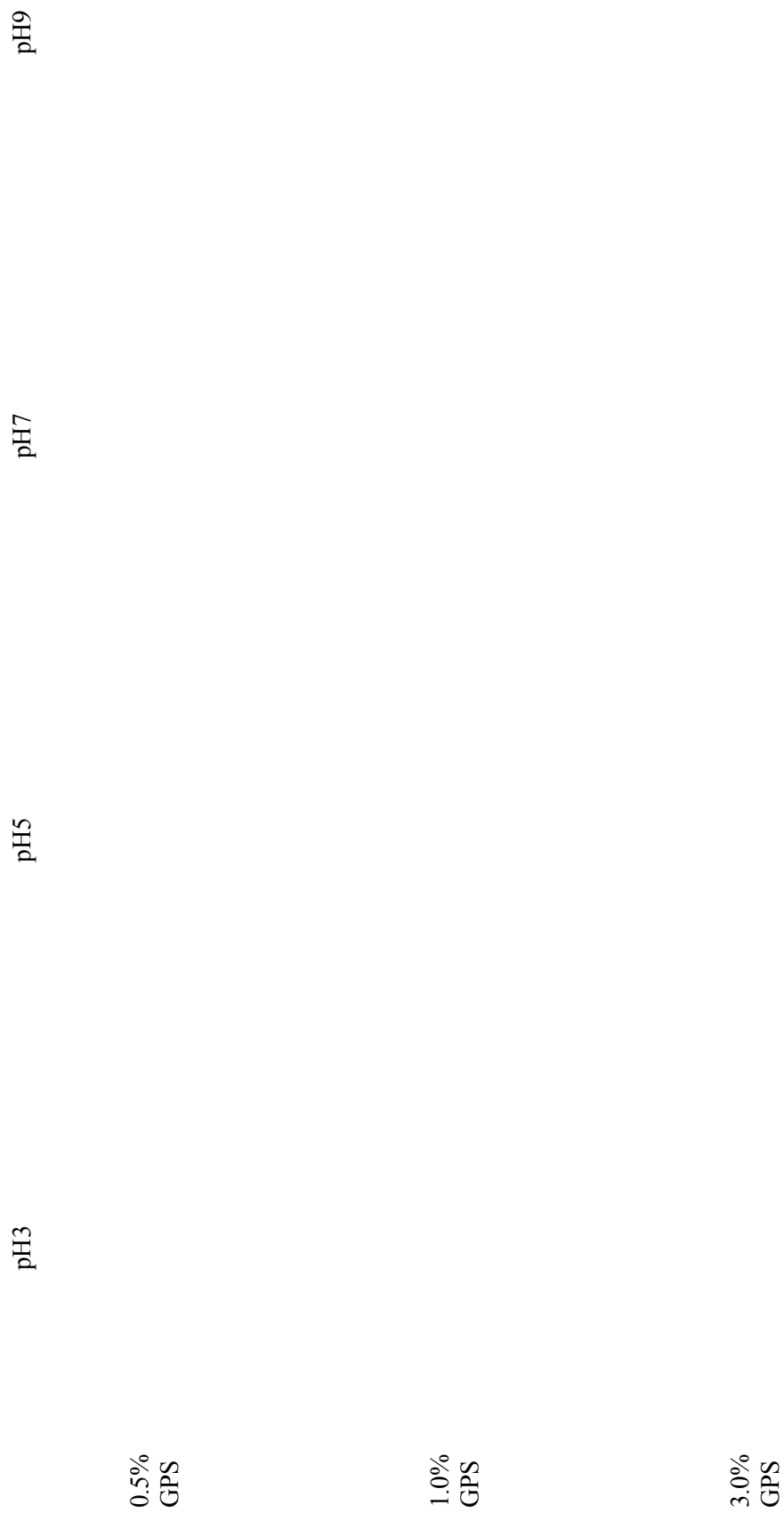
Figure 6.24 High resolution O1s spectra of the silane treated BC surfaces with various GPS concentrations and solution pH.

6.2.4.3 Summary

- Untreated BC surface was used as a baseline control, exhibiting a high %O as a result of a presence of hydroxyl and oxides species.

- %B decreased as %Si, %O and %C increased with %GPS, which was more evident from 1 to 3%GPS in pH5-7 solutions.

- An exception was observed with 3%GPS in pH3 solution that showed the highest %O and %Si, and lowest silane coverage on the BC surface.

- Silane thickness and coverage increased with %GPS, which were particularly higher with 1-3% in pH7 and pH5-7, respectively.

- More silane crosslinking was seen for the more basic solutions and lower %GPS (0.5-1.0%GPS in pH7-9).

6.3 BC-Epoxy PMC Characterisation

Physical-chemical analysis and mechanical testing of the BC-Epoxy PMC before and after ageing were conducted to evaluate the effect of the silane modification of the BC surface on the performance and durability of the PMC.

6.3.1 Physical-chemical properties

Physical-chemical studies were done by evaluating the bulk density, open porosity and water permeability of the composites. It is well known that the latter depends on: content, chemical nature and distribution size of the reinforcements; actual processing of the composite; polymer structure, water affinity and degradation processes of the matrix during immersion (Rodgers *et al.* 2005, Goettler *et al.* 2007, Lee *et al.* 2009, Abenojar *et al.* 2011). The BC reinforcement may also cause variations of cure process, such as, kinetics and degree of polymerisation or cross-linking (Abenojar *et al.* 2009b) which will affect the permeability of the composite. The other two factors considered in this study, were the porosity of the matrix and the hydrophobic nature of the ceramic additions (80%wt.) as a result of the surface treatments on the BC.

The first factor is related to a more effective wettability of the adhesive on the BC, which translates to (a) the adhesive's ability to replace the surrounding gas phase layer of the

particle during the mix process, (b) the mechanism by which a more uniform particle dispersion and reduced air entrapment is achieved after manufacturing, (c) the ability to minimise the void space through which the water can penetrate into the matrix of the composite during service lifetime. The second factor is related to adsorption of the silanes onto the BC leading to a more hydrophobic surface due to lower presence of hydrogen bonding sites across the surface. This is specially relevant when a large surface area is involved as a result of a very high content of BC particles with small grit size present in the composite. Both mechanisms have been observed in previous studies with composites and silanes (Lee *et al.* 2009). Therefore, a physical-chemical characterisation of the composite was conducted due to the change in both adhesive's wettability and hydrophobicity on the BC surface after silane or corona treatment, as confirmed in the previous sections.

6.3.1.1 Bulk density / Open porosity

The BC and epoxy exhibited a density of 2.52 g/cm^3 and 1.12 g/cm^3, respectively (Fig. 6.25). These values are in agreement with the data shown in literature of boron carbide and respective technical data sheets of the adhesive (Table 5.3 and 5.4). The theoretical density of the epoxy matrix composite with 80% wt. of BC was also calculated (2.24 g/cm^3) and compared with that of several PMCs.
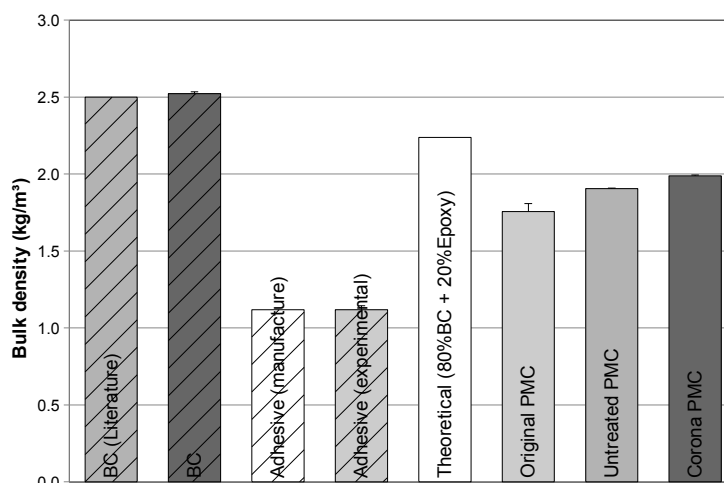
Figure 6.25 Bulk density obtained for the BC, epoxy adhesive, and for the original, untreated and corona treated PMCs.

The addition of BC into the epoxy adhesive led to a lower density than the expected theoretical value for the PMC. The experimental values ranged from 1.76 to 2.01 g/cm^3 (Fig. 6.25-26), with the lowest density being that of the original composite. The improved manufacturing process used in this work (high shear rate mix method and degassing), resulted in a small increase in density to 1.90 g/cm^3 (untreated PMC).
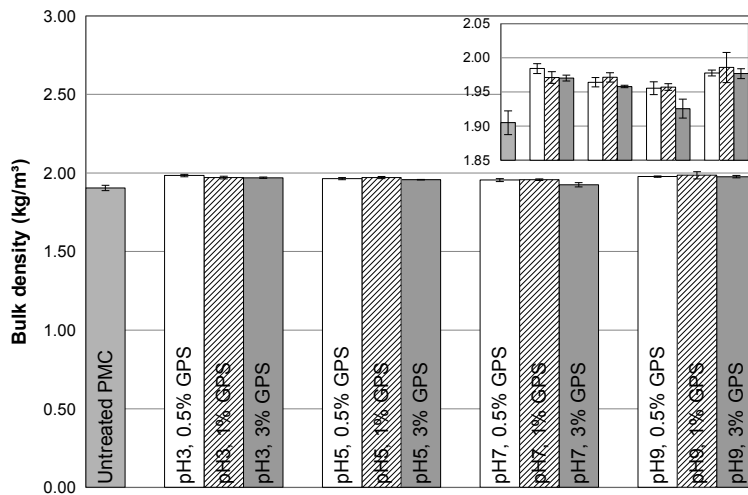
Figure 6.26 Bulk density for the untreated and silane treated PMCs with different solution pH and GPS concentrations.

The highest values were achieved with either the silane (1.93 to 1.99 g/cm^3) or corona (1.99 g/cm^3) treated BC particles as shown in the Fig. 6.25-26. The density for the silane treated PMCs was higher when lower concentrations in most- and mild- acidic solutions were used. The difference between the experimental and theoretical values suggests a porous structure, which was confirmed with the open porosity values (Fig. 6.27).
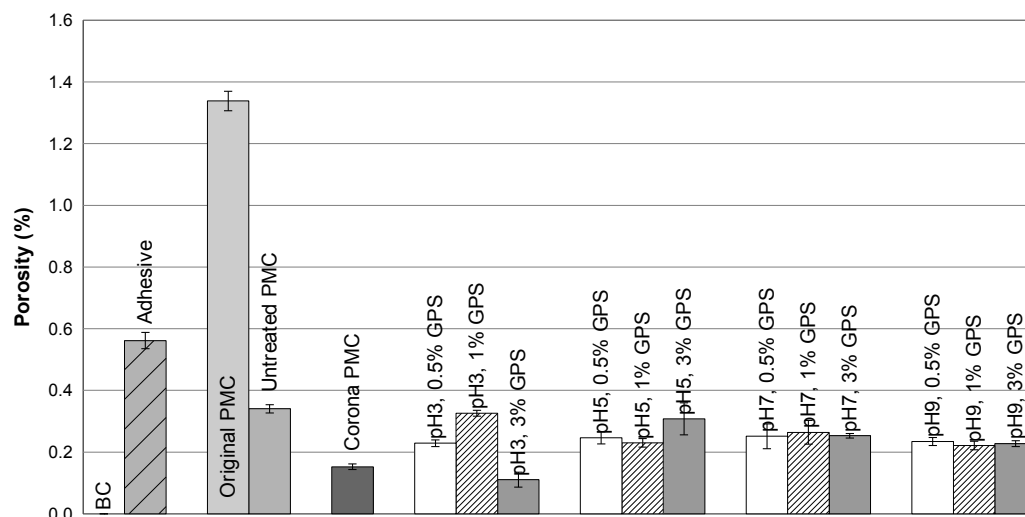
Figure 6.27 Porosity of the boron carbide, epoxy adhesive and the different PMCs.

As expected, the results for the sintered BC specimen displayed no porosity whilst the adhesive showed some "water absorption" as a result of possessing an open three-dimensional structure (0.56%). In the case of the PMC, the highest porosity was observed with the original (1.34%) composite. The use of the refined manufacturing process led to a steep decrease of the porosity from 1.34 to 0.34% (untreated). Notably, the lowest porosity was displayed by the treated PMCs, particularly the corona treated (0.15%). The majority of the silane treated PMCs exhibited porosities between 0.22 and 0.26%. The only exception was observed for BC treated with 3% GPS in a pH3 solution, exhibiting a porosity of 0.11%.

6.3.1.2 Water permeability

The water uptake of the immersed PMCs and constituent materials at 23ºC was measured with time as shown in the Fig. 6.28. The constituent materials showed differing behaviour (Fig. 6.28a), with the epoxy adhesive showing the highest absorption and the BC no water uptake at all. Thus, the composites exhibited a lower water uptake when compared to that of the pure epoxy as a result of the addition of BC (Fig. 6.28). In the case of the PMCs, the water uptake as a function of time can be divided in distinct stages: a faster or slower absorption (0 → 144 hours); followed by an increasing linear behaviour (144 → 2500 – 2800 hours), and finally by a progressively slower increase up to absorption values between 0.65% (pH5, 3%GPS) to 1.03% (untreated PMC) after 10200 hours of immersion.

The lowest and highest water uptakes in the initial stage were displayed by the corona discharged (0.06%) and untreated (0.14%) composite, respectively. In the case of the silane treated PMC, the absorption ranged between 0.09 and 0.13%, with higher uptakes being exhibited by 0.5-1%GPS at pH3 and 3%GPS at pH5 and pH9. In contrast, solution pH7 (0.5-3% GPS) and pH9 (0.5-1%GPS) led to composites with the lowest water absorption (.09-.10%).

In the second stage, the uptake behaviour of the various composites displayed a linear increase in water absorption up to 0.36-0.44%, which suggested a Fickian diffusion-controlled process.

The third stage showed a progressively slower rate as higher saturation levels were reached. An stepwise behaviour was observed during this stage, which may result from a complex combination of physical-chemical mechanisms. These can be related to the relaxation or degradation of the polymer structure from the swelling stress or chemical reactions with the water molecules, and to the formation of an interphase zone between BC particles and epoxy matrix (Ahmad *et al.* 2011).

The absorption rates were obtained in order to determine the water diffusion coefficient through the composites. The amount of water uptake is related to the gradient of the linear portion of the second stage of the absorption process, as shown in Fig. 6.29. Therefore, increase water uptake was observed for increasing silane concentration, except for pH3-5 solutions from 0.5-1% GPS. The greatest water uptakes were formed for pH9 solutions.
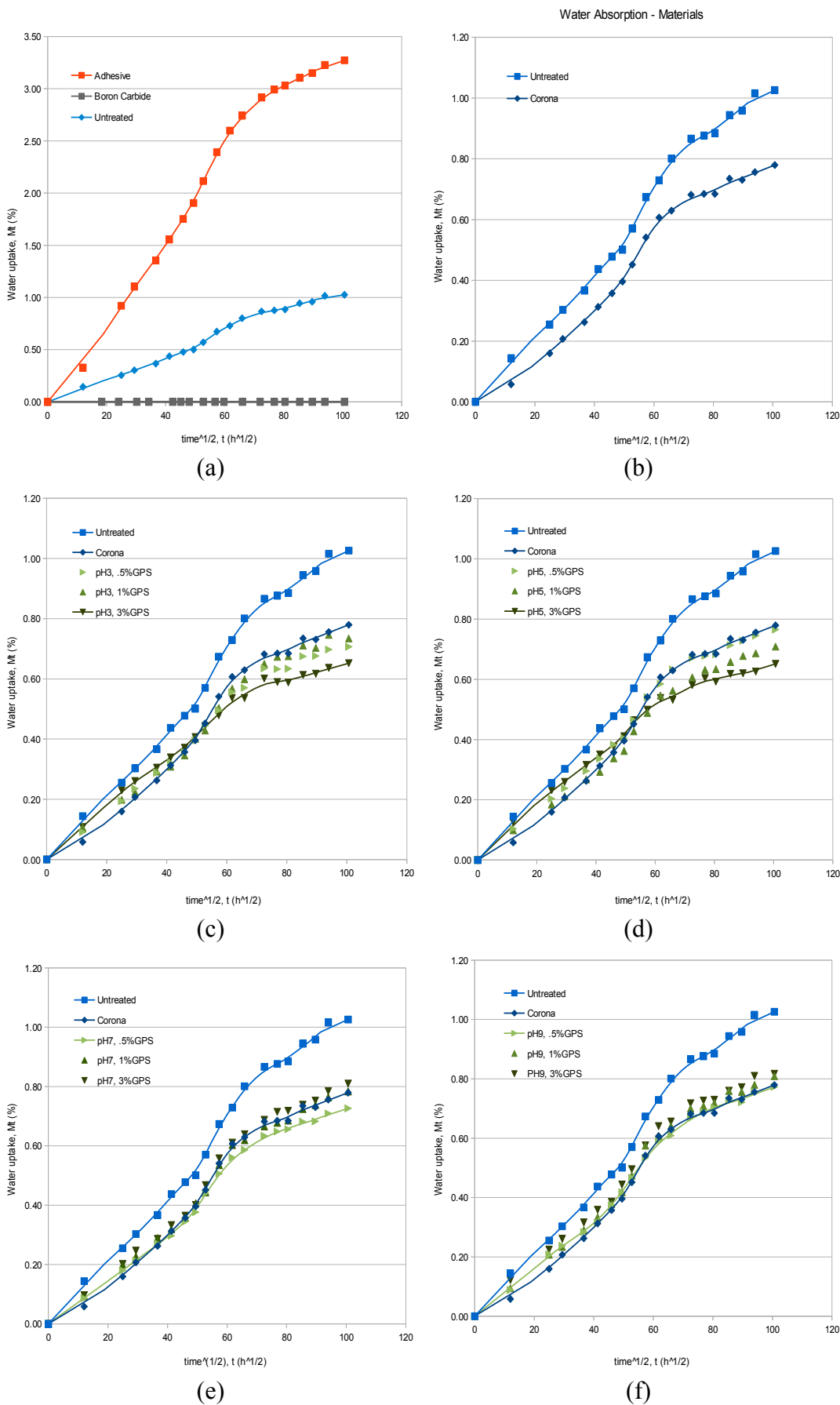
Figure 6.28 Water uptake as a function of the immersion time for the (a) constituent materials, (b) untreated and corona treated, and (c-f) silane treated PMCs.

(a)

(b)

(c)

(d)

(e)

(f)
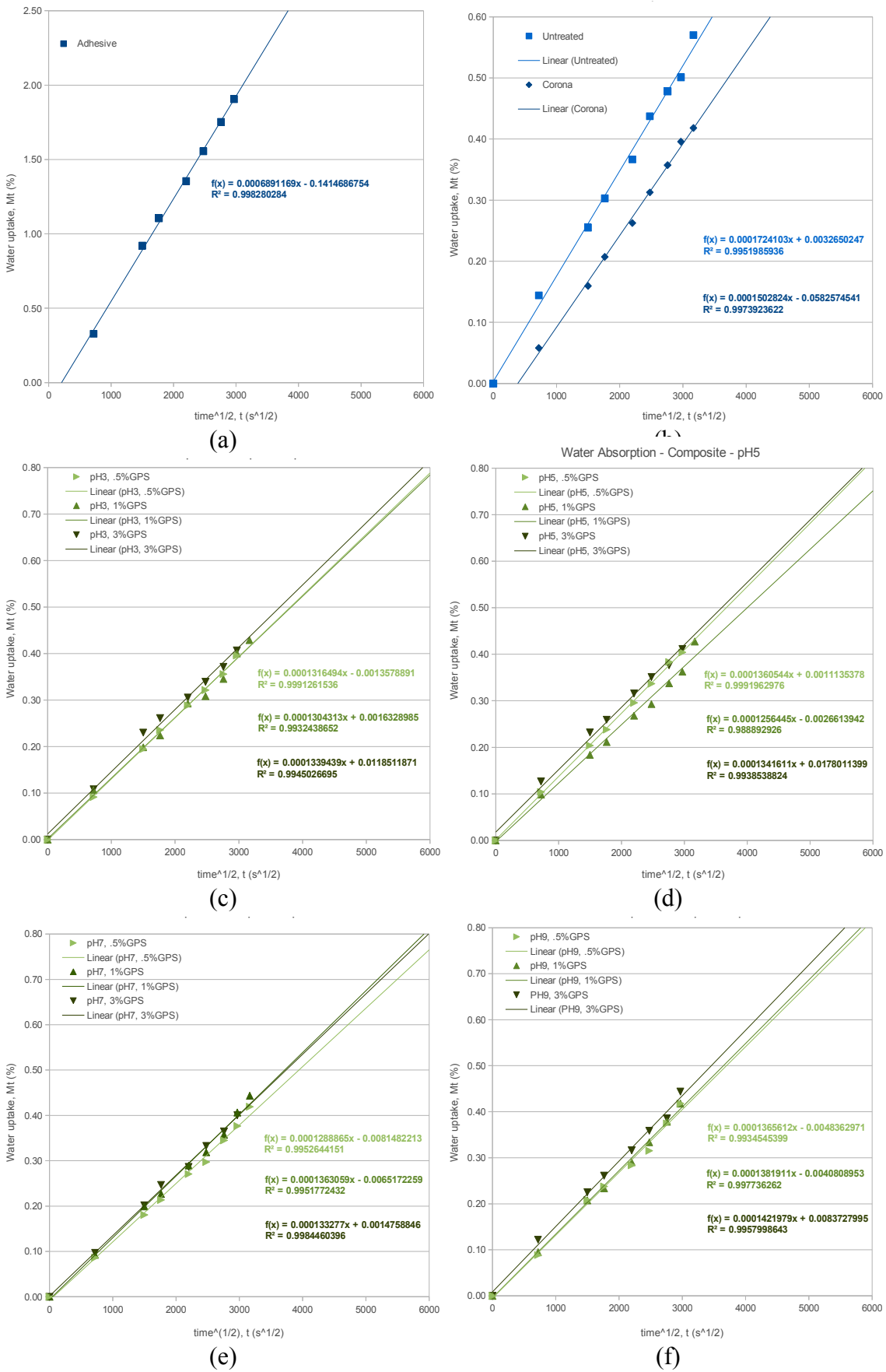
Figure 6.29 Slopes for the second stage of the water absorption process for the (a) adhesive, (b) corona and (c-f) silane treated PMCs.
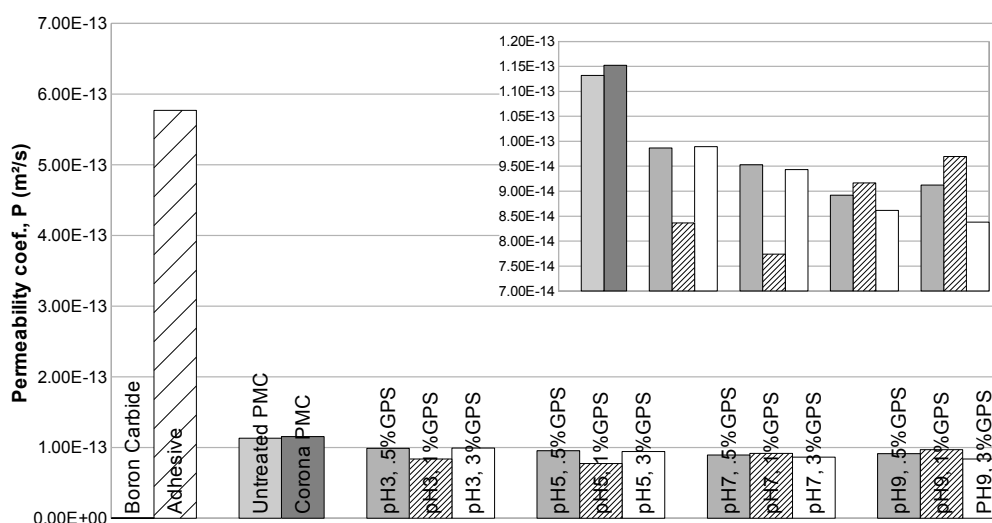
Figure 6.30 Water permeability coefficient for the constituent materials and PMCs.

The water absorption curves of the composites showed an linear behaviour for $M_t \leq 0.6 \times M_\infty$, followed by a deviation from Fickian diffusion. In order to determine the water diffusion and permeability coefficient for the PMCs, the linear portion of the absorption curves was used and the maximum uptake value at 10200 hours was considered as the moisture uptake at equilibrium saturation, M_∞ (Fig. 6.30, Table 6.20). The maximum uptake values for the PMC may be misleading due to the stepwise behaviour at final stage of the curves. In the case of the constituent materials, BC displayed no water permeability whereas the epoxy adhesive showed a coefficient of 5.77 x10^{-13} m^2/s. This value agrees with the permeability values reported in literature, ranging from 1.62 to 6.81 x10^{-13} m^2/s (Ahmad *et al.* 2010). The untreated and corona treated PMCs exhibited the highest water permeability coefficient of 1.15 x10^{-13} m^2/s. This value was 20% of that of the pure epoxy which can be related to the 1:4 ratio by weight of adhesive and BC used in the composition. On the other hand, the silane treated PMCs exhibited lower permeability coefficients, despite showing a higher porosity than the corona treated PMC (Fig. 6.27). Medium and lower GPS concentrations seemed to provide reduced permeability, with the exception for pH7 solutions. Also, pH3-5 showed higher sensitivity to the silane concentration, with a slight decrease from 0.5 to 1.0% but a steep increase from 1 to 3% of GPS. These variations in permeability due to the %GPS were less evident as pH increased.

Table 6.20 Moisture uptake at equilibrium saturation ($M_\infty = M_{t=10200h}$), water diffusion coefficient (D), and permeability coefficient (P) for all PMCs and respective constituent materials.

Material / Composite	M_∞ (%)	D (x10^{-13} m^2/s)	P (x10^{-13} m^2/s)
Boron carbide	-	-	-
Epoxy adhesive	3.27	1.76	5.77
Untreated	1.03	1.12	1.15
Corona	0.78	1.48	1.15
pH3, .5%GPS	0.71	1.38	0.98
pH3, 1%GPS	0.75	1.22	0.91
pH3, 3%GPS	0.65	1.68	1.09
pH5, .5%GPS	0.77	1.25	0.95
pH5, 1%GPS	0.71	1.25	0.89
pH5, 3%GPS	0.65	1.69	1.10
pH7, .5%GPS	0.73	1.25	0.91
pH7, 1%GPS	0.78	1.20	0.94
pH7, 3%GPS	0.81	1.08	0.87
pH9, .5%GPS	0.77	1.24	0.96
pH9, 1%GPS	0.81	1.16	0.94
pH9, 3%GPS	0.82	1.21	0.98

Summary

- In the case of the first stage, the order of the water uptake obtained for the PMCs was: untreated > 3% GPS > 0.5-1% GPS > corona treated

- Water permeability of the PMCs was determined from the second stage of the water uptake as a function of time (M_t vs $t^{1/2}$), which decreased according to the following order: corona treated , untreated > 3% GPS > 0.5-1% GPS.

6.3.2 Mechanical Properties

The following mechanical data was acquired to assess any improvements in shear, tensile and mix-mode performance as a result of the various surface treatment effects on the adhesion between the BC and epoxy adhesive. For comparison, the strength of pure epoxy resin was obtained using the same test methods to better understand the properties of the binder and the effect of adding the BC in the polymeric matrix. The following data does not provide sufficient information for statistical analysis but gives some indication about the relative influence of the surface treatments used in this study.

6.3.2.1 Rupture Strength (three-point bending test)

The rupture strength of the epoxy adhesive and composites at room temperature are shown in Fig. 6.31. The addition of 80% BC in the polymeric matrix led to a significant decrease in rupture strength, in comparison to the pure epoxy resin (i.e. from 93 to 52 MPa). The high shear rate mix method and degassing process used in the untreated composite resulted in a strength increase of 25% (65 MPa). The corona treatment demonstrated an improvement in strength of 8% as compared to the untreated. The silane treatment provided the most significant improvement, obtaining a rupture strength of 82 MPa (88% of the of the bulk resin strength). The rupture strength of the silane treated PMC is presented in Fig. 6.32, with respect to the solution pH and GPS concentration. The solution pH clearly demonstrated a significant influence on the mechanical properties of the composite. The most acidic solution was detrimental, whereas, strength improved with pH5-9 solutions. Beyond pH7 the improvements were lost with the highest GPS concentration. The silane concentration also had a marked effect on the strength according to solution pH, with the best performance resulting from the 0.5-1.0%GPS solutions. Beyond 1.0% the strength was reduced, this time with the exception of solution pH7. Together, these results showed a strong influence of the solution pH and concentration on the transverse rupture strength of the composite. The optimum treatment conditions to achieve the best mechanical properties for the composite were 0.5-1.0% of silane in pH5-7 solutions. The use of corona prior to the silane treatment resulted in a small decrease of the strength.
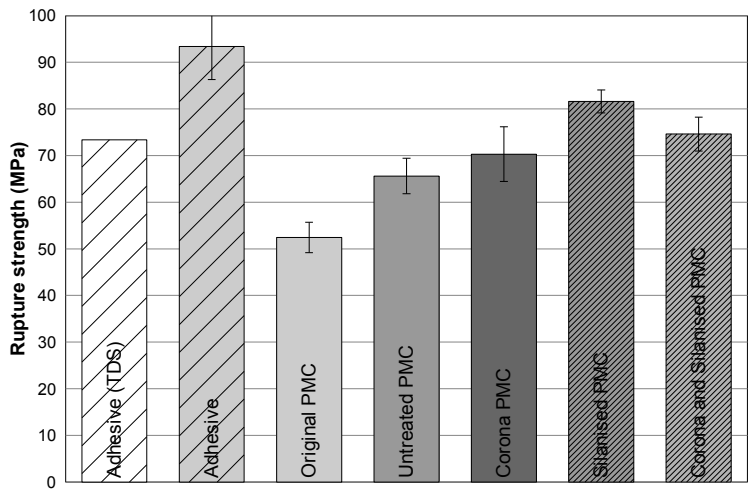
Figure 6.31 Rupture strength of epoxy adhesive and of the original, untreated, corona treated, silane treated (pH7, 0.5%GPS) and corona prior to silane treated PMCs.
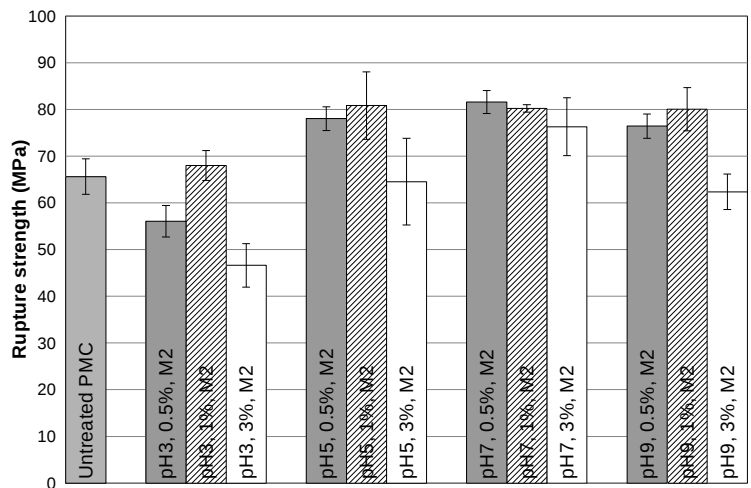
Figure 6.32 Rupture strength of silane treated PMC with various solution pH and GPS concentrations.

Tensile Strength (Isopescu test)

The tensile strength of the bulk epoxy resin and PMCs at room temperature are shown in Fig. 6.33. The addition of 80% BC in the resin led to a significant decrease in tensile strength of 57% (i.e. from 48 to 20 MPa). The untreated PMC developed a higher strength (39 MPa) as a result of the more refined manufacturing process. The corona treatment demonstrated a small improvement of 8% to 42MPa. The best of the silane treatments exhibited equivalent strength to that of the bulk epoxy resin. These improvements varied according to the particular silane treatment, as can be seen in Fig. 6.34. Most treatments provided some improvement in the tensile strength. The higher values were generally

observed with pH5 and pH7 solutions, following similar reasoning as reported in the previous section. Nevertheless, some exhibited lower strengths when formulated with pH3 and pH9 solutions. This was specifically observed for the 3% GPS solutions, highlighting a strong relationship with silane concentration. The better performances were formed using 0.5% and 1.0% GPS for a specific solution pH. The exception was solution pH7, which exhibited a more consistent strength through every concentration. Thus, the tensile strength was again affected by the solution pH and concentration, exhibiting optimal conditions when 0.5-1.0% GPS were used in pH5-7 solutions. The corona treatment applied onto the BC prior to the silane again resulted in a small decrease in strength.
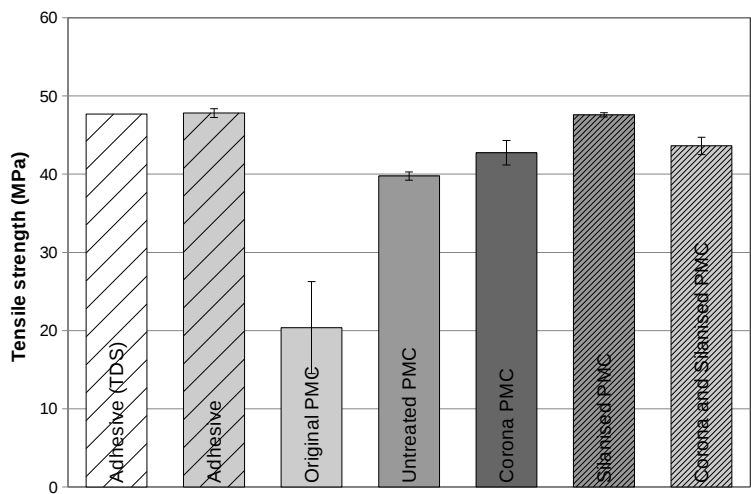
Figure 6.33 Tensile strength of epoxy adhesive and of the original, untreated, corona treated, silane treated (pH7, 0.5%GPS) and corona prior to silane treated PMCs.
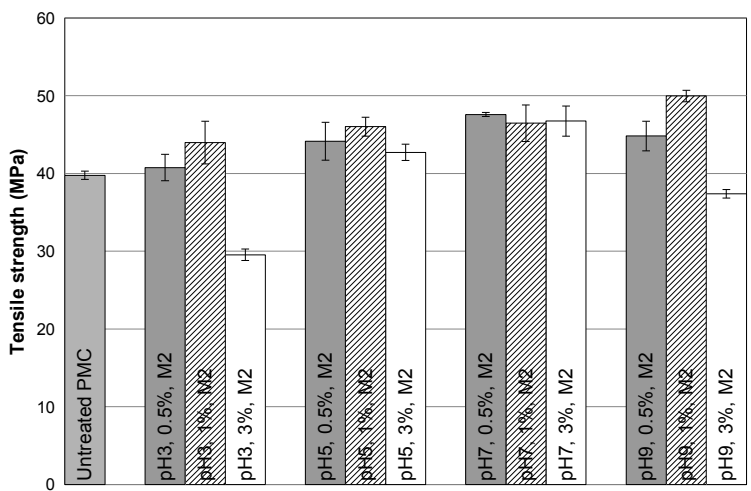
Figure 6.34 Tensile strength of silane treated PMC with different solution pH and GPS concentrations.

Shear Strength (double v-notch test)

The shear strength values of the epoxy adhesive and PMCs acquired through a non-standard test are shown in Fig.6.35. The addition of the BC particles led to a steep decrease in shear strength (71%) from 31 to 9 MPa (original). The use of the refined manufacturing process had no effect on the strength of the untreated PMC. An improvement of 25% and 56% was observed when corona (11 MPa) and GPS treatment (14 MPa) were applied to the BC particles respectively.

The evaluation of the shear strength was also conducted for the silane treated PMCs using different pH values and concentrations (Fig. 6.36). Although all the silane treatments led to an increase in the strength, the pH7-9 solutions showed the greatest improvements. The highest values for a specific pH were observed using 0.5-1.0%GPS, particularly between pH3-7 values. The best treatment conditions were 0.5-1.0% of silane in pH7 solutions. The corona treatment prior to silane treatment again demonstrated a small reduction in strength.
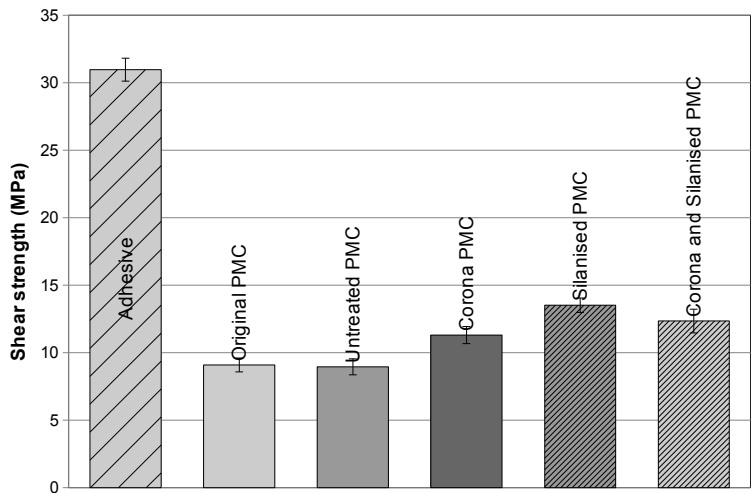
Figure 6.35 Shear strength of epoxy adhesive and of the original, untreated, corona treated, silane treated (pH7, 0.5%GPS) and corona prior to silane treated PMCs.
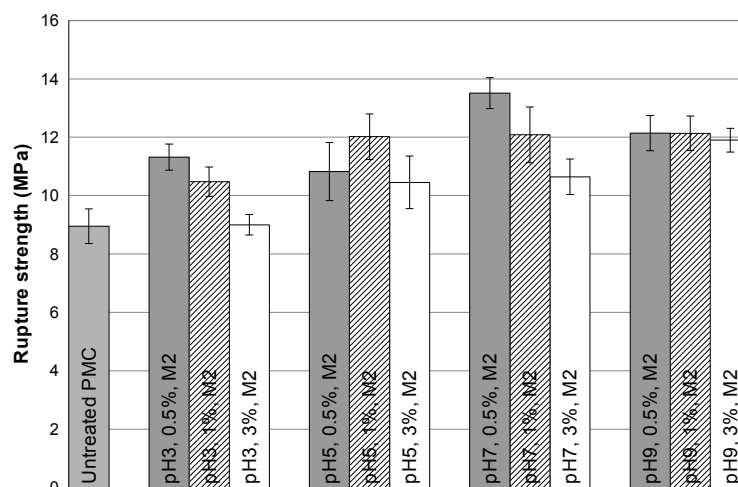
Figure 6.36 Shear strength of silane treated PMC with different solution pH and GPS concentrations.

6.3.3 Fracture Mechanism / Failure Surface (SEM)

In general the fracture surfaces of all the samples exhibited a rough topography typical of high filler content brittle polymeric matrix composite, possessing particles with angular shapes and sharp edges (Fig. 6.37). The high void content in the original and untreated PMCs was the result of entrapped air introduced during the mix and moulding stage of manufacture (Fig. 6.37a-b). The original PMC was prepared by using a z-blade mixer under conditions open to atmosphere. The poor strength of the original PMC was evident from the fracture surface, which showed a weak brittle failure due to the highly porous matrix (Fig. 6.37a). The improved but untreated composite exhibited lower porosity and SEM indicated crack branching and deflection around the particles (Fig. 6.37b), which resulted in a higher strength. In the case of the silane and corona treated PMCs, the treatments on BC led to a visible decrease in the amount of trapped air. Further evaluation was conducted to provide an indication of the failure modes on the surface of individual BC particles in the matrix of the treated PMC. The improved strength provided by the corona treatment appeared to be the result of better adhesion, indicated by traces of resin on the surface of some large particles (Fig. 6.37c). Even better adhesion resulted from the silane treated PMC, exhibiting distinct regions of epoxy and small BC particle clusters, again, remaining attached to surface of the larger particles (Fig. 6.37d).

x60   x470

x70   x470

x75   x350

x70   x350
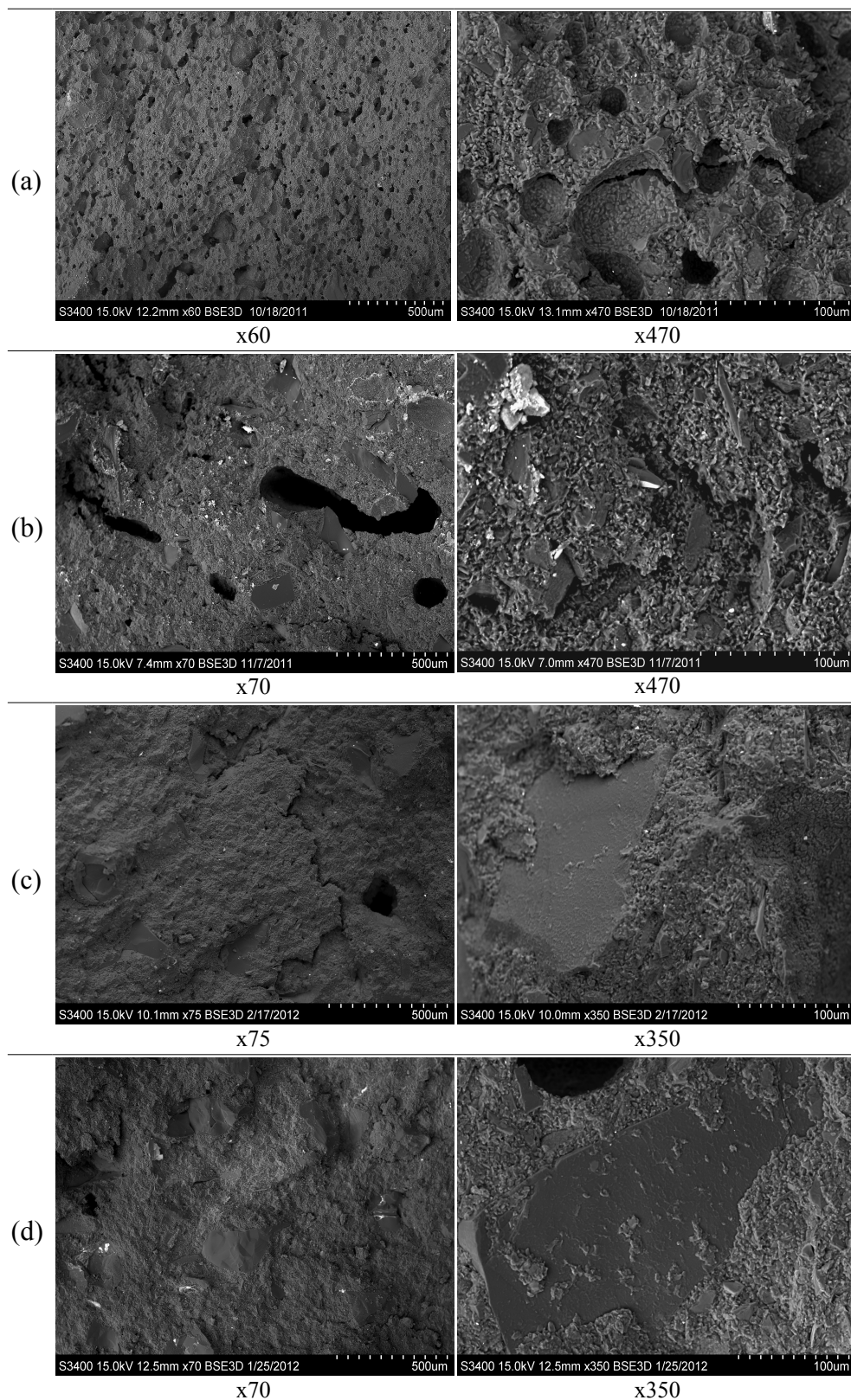
Figure 6.37 SEM micrographs using back scattering electrons on the failure surface of the a) original, (b) untreated, (c) corona treated and (d) silane treated PMCs.

6.3.4 Durability

The durability of aged adhesive and PMCs was evaluated through the determination of their mechanical strength by means of 3PB, Iosipescu and DVN tests (Fig. 6.38), and water uptake after immersion (Fig. 6.39).

6.3.4.1 Rupture Strength (three-point bending test)

An evaluation of the rupture strength data obtained from 3PB tests, before and after ageing, showed that the pure epoxy suffered a reduction in strength of 12% (Fig. 6.38a), as consequence of the degradation mechanisms described in section 5.3.2.2. In the case of the untreated PMC, a decrease of 16% was found. The greatest decrease was exhibited by the corona discharged (29%), which resulted in the lowest strength for the aged PMCs. In the case of the silane treatment, the majority led to a decrease between 1 and 25%. Exceptions were observed for 1% and 3%GPS in pH3 solution, showing no change and an increase in strength of 13% respectively. Generally, low concentration exhibited greater reductions in strength, whereas, higher %GPS showed similar performance to the unaged samples. In general the silane treated PMCs exhibited superior strength compared to the untreated and corona discharged PMC.

6.3.4.2 Tensile Strength (Isopescu test)

The investigation of the tensile strength obtained from Iosipescu tests, before and after ageing, showed that the adhesive exhibited a decrease in tensile strength of 23% (Fig. 6.38b). In respect to the PMCs, greatest reductions in strength were shown by untreated and corona discharged samples, 55% and 34% respectively. However, smaller reductions were displayed by the silane treated PMCs (8-30%), in particular for 3%GPS in pH3-5 solutions. The use of low %GPS led to a greater reduction in tensile strength, particularly as the solution pH increased. Finally, the combination of a high initial strength and smaller reductions led to PMCs with an superior strength of 52 to 120% compared to untreated PMC. This was in particular evident with the pH5 solutions.

(a)

(b)

(c)
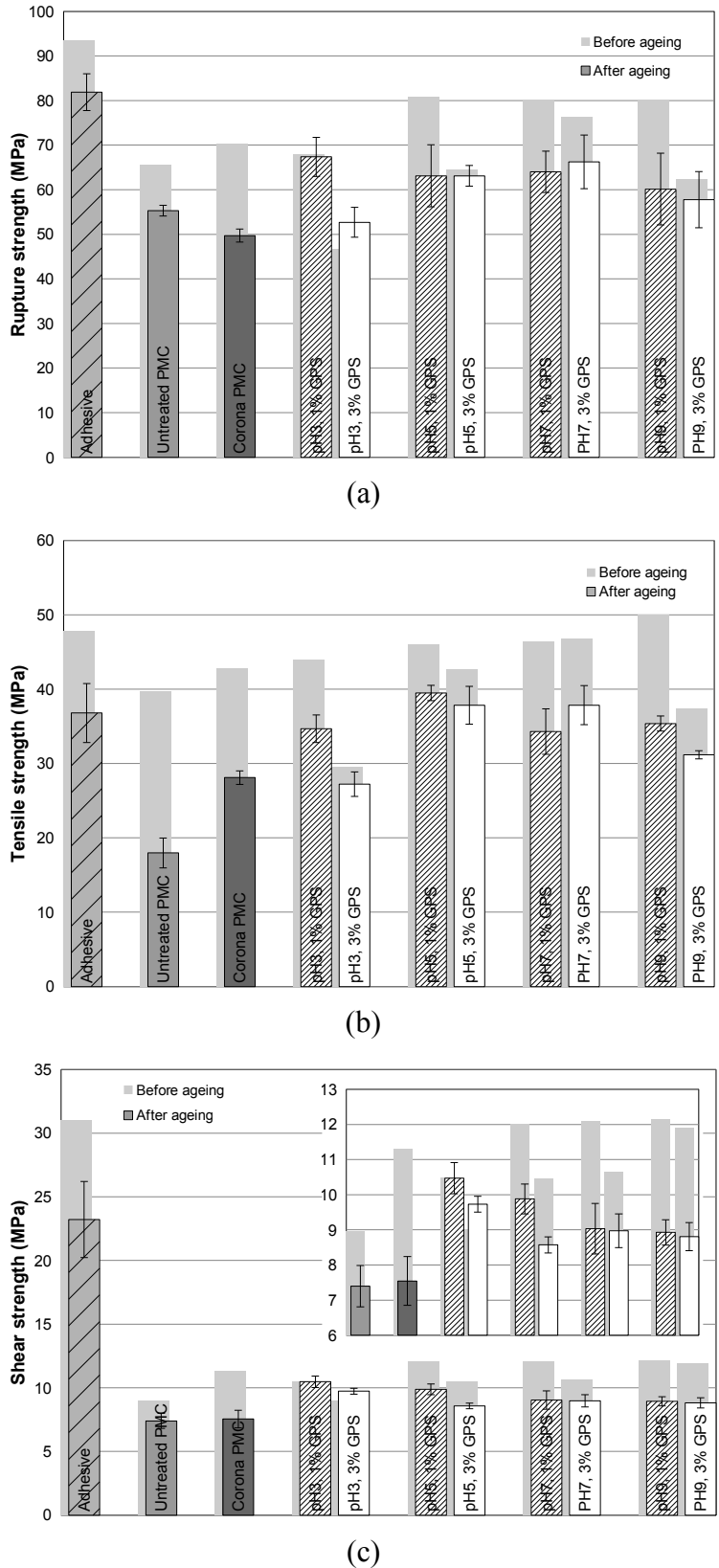
Figure 6.38 Mechanical strength by means of (a) 3PB, (b) Iosipescu and (c) DVN for the adhesive, and untreated, corona discharged and silane treated PMCs before and after water immersion.

6.3.4.3 Shear Strength (double v-notch test)

The shear strength data obtained from DVN tests, before and after ageing, showed that the pure resin suffered a steep reduction in shear strength of 25% (Fig. 6.38c). The highest loss in strength was exhibited by the corona discharged (33%) to similar values of the untreated PMC. All silane treated PMCs exhibited a higher strength (from 17 to 42%) compared to the untreated and corona treated as a result of smaller reductions in strength (8-30%). Exceptions were found for 1% and 3% GPS in pH3 solution, which showed no change and an increase in strength, respectively. Best mechanical properties were found with 1%GPS in pH3-5 solutions, despite lowest initial strength promoted by the most acidic solutions.

6.3.4.4 Water uptake

The water absorption values after 1500 hours of water immersion at 40ºC (Fig. 6.39) were obtained for assessment of the reduction in strength of the pure epoxy and PMCs. For all three sets of mechanical test samples, the epoxy adhesive showed the greatest water uptakes (3.5 – 3.6%). In the case of the PMCs, similar uptake values were found for the untreated and corona treated samples (0.74-0.76%). The silane treated PMCs exhibited slightly lower uptake values (0.66 to 0.73%) compared to that of the untreated and corona treated. For the 1%GPS treatments, a trend was observed with an increase in water uptake from the most acidic to basic solution (0.66% $\rightarrow$ 0.72 – 0.73%). Regarding the silane concentration, the use of 3%GPS led to a higher water uptake for a specific pH, with the exception of pH9 solution.

The water uptake was a strong indicator of the reduction in strength and durability of the PMCs. Generally, greatest water uptakes (corona, untreated > pH9 1%GPS > pH7 1-3%GPS) led to a higher losses in strength, with the exception of the 3%GPS in pH3 solution. This resulted in aged PMCs with higher mechanical properties when treated with pH3-5 solutions.

(a)

(b)

(c)
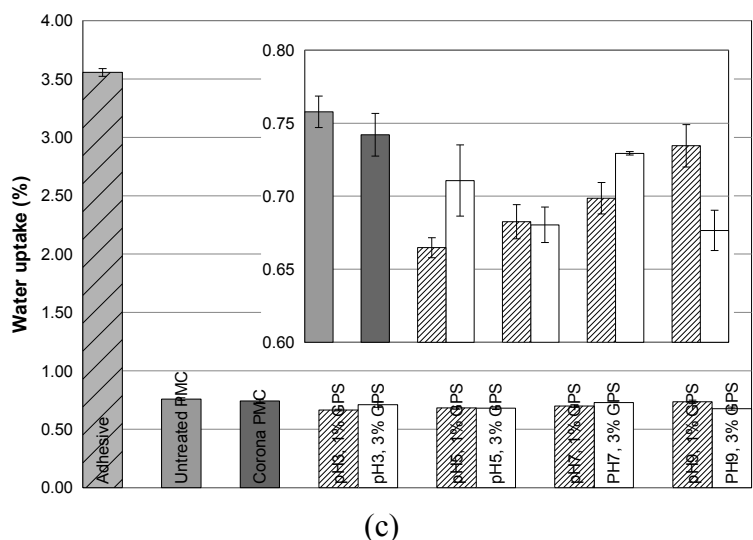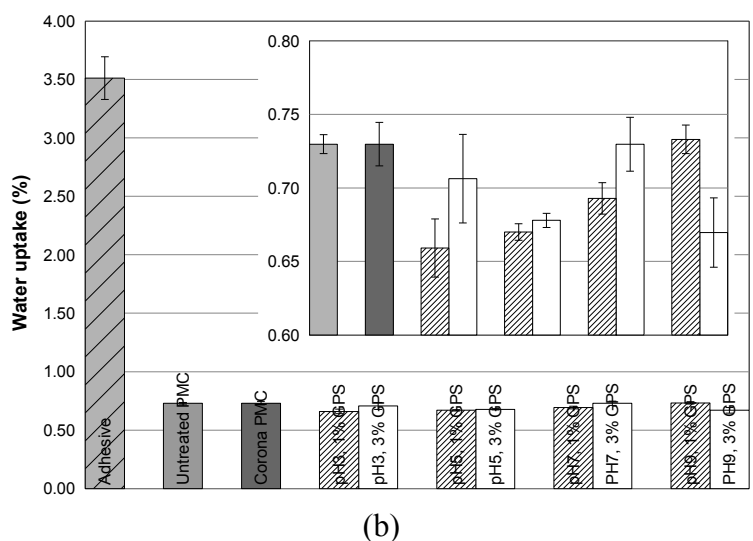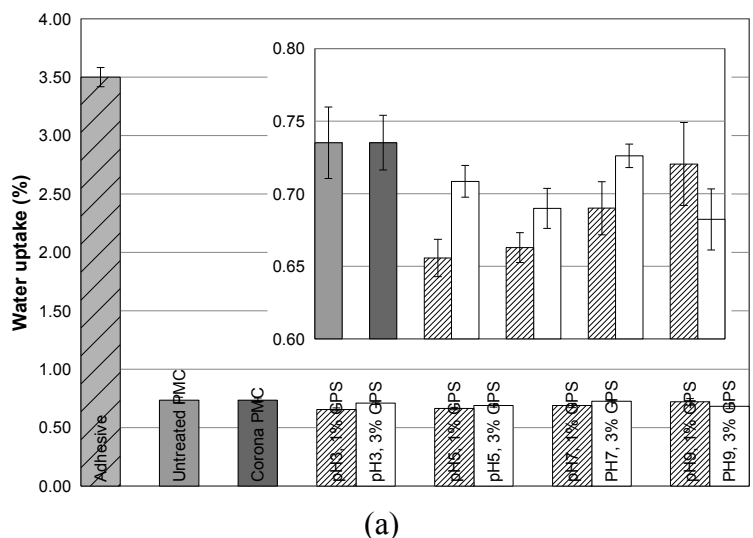
Figure 6.39 Water uptake for the (a) 3PB, (b) Iosipescu and (c) DVN samples of the adhesive, and untreated, corona discharged and silane treated PMCs after immersion.

CHAPTER 7 – DISCUSSION

In this chapter, the experimental findings from previous sections have been brought together to conduct an overall analysis in the context of the aims presented in Chapter 1. Thus, the discussion of the summarised results was conducted to evaluate the effect of the silane treatments and their parameters on the BC surface as well as on physical-chemical properties, mechanical performance and durability of the BC-epoxy PMC. Furthermore, the adhesion phenomena on the ceramic surface was analysed and consequently the optimal silane treatment conditions and mechanism for the BC were proposed.

7.1. Epoxy Adhesive

The chemistry, cure kinetics, viscoelastic behaviour and wettability of the adhesive is summarised in this section to better understand its behaviour as a liquid during the manufacture process and as a binder on mechanical properties of the PMC during service conditions.

7.1.1 Chemical Analysis / Cure Kinetics

Chemical analysis of the adhesive components (Fig. 6.1-2, Table 6.1-4) confirmed that the adhesive consisted of an unmodified basic liquid DGEBA resin and a mixture of a polyamine amide and dimer fatty acids as the curing agent. The adhesive, in conjunction with the use of a wetting additive, promoted lower viscosity and improved wettability. This helped achieve a better dispersion of the BC particles and consequently a reduction in the viscosity of the compound. Moreover, the resin was preheated at 40ºC, which effectively reduced the high viscosity resulting from the addition of BC. The working time of the compound was, however, compromised as discussed in the following sections. Monitoring the cure at 23ºC for 15 hours (Fig. 6.4-6.5, Table 6.5, Eq. 5.8) demonstrated a similar

degree of conversion to that obtained after 8 hours of cure at 40ºC, which corresponds to the process used in the manufacture of the PMC. Other studies have reported that BC particles can act as either an accelerator or a retardant in the first 60 minutes of the cure, as well as hinder the growth and crosslinking of the polymer chains, depending upon their size and concentration in the epoxy adhesive (Abenojar *et al.* 2009b).

7.1.2 Viscoelastic Properties

The viscoelastic properties of the pure adhesive were obtained (Fig. 6.6) to which were directly related to the molecular structure and cross-linking of the polymer matrix. This affected the mechanical properties and durability of the PMC which will be discussed later in this chapter. It was particularly evident that there was a higher water absorption from the aged PMCs as temperature increased from 20 to 40ºC. This was confirmed by the relaxation of the pure epoxy matrix, with a 40% decrease in storage modulus (E') or even greater loss if exposed to temperatures near the T_g (Fig. 6.6). In a study using a much lower concentration of BC (6 – 12 %wt.) in an epoxy resin showed that the particles hinder growth and crosslinking of the chains, and reduces molecular movements of the polymer network. This led to a material with a T_g and storage modulus in the glassy region slightly inferior to that of the pure adhesive, probably due to the stress created by the particles in the bulk (Abenojar *et al.* 2009b).

7.1.3 Surface Free Energy / Wettability

The surface free energy of the epoxy adhesive was determined to predict its wettability on the various BC surfaces during the manufacture of the PMC (Table 6.6-7, Fig. 6.7). The liquid epoxy exhibited mostly a dispersive nature, which reduced after cure with a small increase of the polar component. The SFE values of the cured resin were similar to those found in literature (Comyn 2006) and confirm that chemical changes during or after cure promote differences in the SFE.

The effect of the gelation process on the adhesive wettability was demonstrated by an increase in contact angle on the BC surface from 50 to 55°, specifically 15 minutes after mixing the resin with the curing agent. This correlates with the cure kinetics of the resin, which showed a faster reaction with a 30% degree of conversion during the first 30 minutes at 23°C (Fig. 6.5). Despite promoting better wettability during the mixing stage,

preheating the resin may lead to a faster cure process and therefore to a higher viscosity and poor mouldability of the PMC compound.

7.2. Silane Coupling Agent

A SCA was chosen for surface modification of BC since it presents various methods of application and chemical structures (organofunctionality, carbon chain length and alkoxy groups), which provide a high degree of flexibility and control to obtain different properties according to a particular resin or application. In this work, γ-glycidyloxypropyl-trimethoxysilane (GPS) was used for adhesion promotion and surface modification to the BC, which exhibits a short carbon chain structure with an epoxy functional group to ensure reaction with the adhesive (Kinloch *et al.* 2006). An amino functional group silane was not considered as it would act as a traditional curing agent for epoxy resins leading to changes in the kinetics of the cure (Davis *et al.* 2004, Johnsen *et al.* 2003), especially in this case where a large amount of silane treated BC particles was added to the adhesive. Furthermore, GPS aqueous solutions were exploited to form a monolayer of the silane on the BC, whereas, their incorporation into the adhesive formulation or use in sol-gel solutions are normally more suitable for general adhesive applications and thicker siloxane coatings, respectively.

7.2.1 Chemical Analysis

Chemical characterisation of the silane was performed to better understand any changes after hydrolysis and condensation (Fig. 6.10c,e, Table 6.8), and principally to evaluate the effect of the various silane treatments on the BC surface. Using FTIR, it was found that after 1 hour in pH5 aqueous solution, the GPS was fully hydrolysed due to the absence of Si–O–CH$_3$ stretching mode as well as by the presence of the silanol (Si-OH) vibration modes. After the drying stage at 104ºC for 8 hours, silane condensation was also confirmed by the presence of a strong band from the Si-O-Si stretching mode as a result of the high concentration of GPS used to obtain the gel (Johnsen *et al.* 2003). A degradation process was also identified, demonstrated by the presence of a weak band located at 1724 cm^{-1} from carbonyl (C=O) stretching mode and decrease in absorbance at 1252 cm^{-1} due to the degradation/opening of the epoxy ring (Bertelsen and Boerio 2001). This resulted in a

reduced number of oxirane groups available to react with the adhesive, which may have resulted in a lower effectiveness of the silane treatment (Abel *et al.* 2004). In contrast, the degradation of the epoxy group was not found on the silane treated BC particles. However, their surface chemistry was highly dependent on the solution pH and GPS concentration, as discussed in a later section.

7.2.2 Surface Free Energy / Wettability

Wettabilty tests on the gel were conducted to help interpret the properties promoted by the silane layer on the BC surface (Table 6.6). The GPS gel possessed a SFE of 51.46 mJ/m^2, which was composed of a high dispersive component (γ_S^{LW} = 45.0 mJ/m^2, γ_S^{AB} = 7.4 mJ/m^2). This was demonstrated by the lower contact angle for di-iodomethane (28 ± 2º). The Lewis acid component was the highest contributor to the polar component of the SFE, which can be partially due to the presence of the carbonyl groups resulting from the degradation of the epoxy ring (Cech *et al.* 2009, Kontárová 2011). The higher contact angles displayed by the most polar liquids, i.e., 64 ± 3º for water and 45 ± 2º for glycerol, demonstrated a hydrophobic surface. The epoxy adhesive exhibited high wettability on the gel surface (Table 6.9), providing with an experimental contact angle (38 ± 2º) slightly higher than that of the theoretical value (32º).

Thus, the hydrophobocity and wettability of the GPS gel promoted similar properties to those observed for the silane treated BC surface using similar methods (Table 6.9).

7.3 Boron Carbide

Surface analysis was conducted to evaluate the effect of the silane modification on the surface free energy, elemental/chemical composition and morphology of BC particles.

7.3.1 Untreated Surface

The SFE, chemistry and morphology of untreated BC was investigated prior to surface treatment using the sessile drop method, ATR-FTIR, XPS and OM/SEM.

7.3.1.1 Surface Free Energy / Wettability

The untreated BC surface showed a high dispersive component (γ_s^{LW} = 33.7 mJ/m^2, γ_s^{AB} = 18.8 mJ/m^2), which was in agreement with reported SFE values for BC coated materials (Maitz *et al.* 2006). It was found that the Lewis acid was the higher polar component due to the presence of boron oxide or hydroxyl species (Mortensen *et al.* 2006, Goldberg *et al.* 2000). The wettability of the adhesive on BC gave a contact angle of 52 ± 1º which agreed with the theoretical value (50º) from the SFE components of the uncured epoxy and untreated BC.

7.3.1.2 Chemical Analysis

The presence of hydroxyl groups and native oxide layer on the untreated BC surface was confirmed through FTIR (Fig. 6.10a, Table 6.8) and XPS (Fig. 6.14-15 and 6.20, Table 6.10 and 6.14). XPS elemental analysis has shown a surface composed of 59% boron, 22% carbon and 18% oxygen, which agreed with published work (Mortensen *et al.* 2006, Deshpande *et al.* 1994, Smeacetto *et al.* 2002). These findings gave a clear indication that the native BC surface has functional groups which can provide an attachment for the silane coupling agent to form a B–O–Si bond.

7.3.1.3 Morphology

The BC particles displayed a morphology typically representative of brittle materials (Fig. 6.8 and 6.9a,b,d). The grit sizes F60 and F360 showed a greater extent of fractures normally associated with brittle surfaces. In contrast, the F1200 tended to exhibit more rounded polygonal-type shapes, which was probably related to the milling process used to obtain the smaller particle size. Most of the particles possessed relatively sharp, thin edges that may act as crack promoters. BC particles exhibiting similar morphology have been shown to affect the mechanical properties of an epoxy PMC (Abenojar *et al.* 2009b).

7.3.2 Treated Surface

The effectiveness of various surface treatments on BC to promote mechanical strength and durability of the PMC was investigated using silane aqueous solutions with different solution pH and GPS concentrations. This was also compared with the corona discharge

treatment employed prior to the silane treatment.

7.3.2.1 Corona Discharge

The SFE and chemistry of the corona discharge treated BC were obtained by drop shape analysis using the sessile drop method and ATR-FTIR.

7.3.2.1.1 Surface Free Energy / Wettability

Corona discharge treatment of the BC led to an increase in the SFE (Fig. 6.12) from 52.5 to 64.6 mJ/m^2. This was associated with a steep decrease of the water contact angle from 47º to 7.5º, which was mainly related to the increase in the Lewis acid component ($\gamma_S^+ = 44.8$ mJ/m^2) due to the presence of negatively surface-charged boronic groups (Mortensen *et al.* 2006). Some species of boronic acids (R-B(OH)$_2$) have also been reported to accept a hydroxyl ion to form a tetrahedral borate ion (Goldberg *et al.* 2000, Siqueira *et al.* 2007). The improved wettability of the adhesive on the BC surface can not be completely attributed to a small increase in the dispersive component that resulted from the treatment. It can be partially a result of an increase in surface temperature, from 24 to 34ºC, due to the corona treatment. It is thought that an increase in temperature led to a reduction in viscosity of the adhesive and subsequently to improved wettability.

7.3.2.1.2 Chemical Analysis

FTIR confirmed the higher presence of boron hydroxyl and oxide groups (Fig. 6.10b) through an increase in absorbance of the characteristic bands from the O–H and B–O stretching and B–O–H deformation vibrations. These species can act as potential binding sites for the GPS, through a mode of attachment similar to that already supported for metal surfaces (Brack *et al.* 2005, Gutowski and Pankevicius 1993, Gutowski *et al.* 1999a, 1999b, 2000, 2002a, 2002b, 2003, 2005, Gutowski 2003). Also, bands from aliphatic C-H stretching were observed after corona treatment, which suggest a low concentration of hydrocarbon contamination on BC surface from the surrounding atmosphere.

7.3.2.2 Silane Coupling Agent

The effect of treatments on the SFE and chemistry of the BC was evaluated by sessile drop method, FTIR, SEM and XPS.

7.3.2.2.1 Surface Free Energy / Wettability

Surface modification on the BC through silane coupling agents and the effect of solution pH and GPS concentration were confirmed by the sessile drop method (Fig. 6.12). The silane treated material exhibited a lower SFE, mostly due to a steep decrease in the Lewis acid component. Thus, higher angles for the polar liquids were observed, in particular the water contact angle increased from 51º to 85°. This was more evident for the pH5-7 solutions with increased silane concentrations. This finding was in agreement with open literature (Almanza-Workman *et al.* 2002) which supported the hydrophobic nature of the organic functional groups present on the silane treated surface (Kinloch *et al.* 2006). On the other hand, the dispersive component increased when lower solution pH3-5 and 1-3%GPS were employed. This led to a decrease in contact angle for the uncured epoxy adhesive from 52º to 46º, which is in accordance with the theoretical contact angles (Eq. 5.10). Thus, the silane treated BC demonstrated evidence of an outward orientation of the epoxy functional groups from the BC surface (Fig. 7.1), leading to an increased hydrophobicity and improved adhesive wettability (Table 6.9).

∘ Epoxy functional group
● Silane backbone

(a)   (b)

Fig 7.1 Schematic illustration of the arrangement of the epoxy functional groups within a (a) multilayer and (b) monolayer silane structure on the surface.

An increase in the post-treatment time of the silane treated BC with 0.5-1%GPS in pH3 and pH7 solutions (Fig 6.13) led to a small increase in the polar component. This was more evident for the pH3 solution due to a reduction in silane coverage over the BC surface, as discussed in section 7.3.2.2.4. This can be associated with a reduced hydrophobic surface

allowing greater water absorption and/or oxidation to occur when exposed to the surrounding atmosphere (air). A similar study confirms this finding through mechanical testing (Abel *et al.* 2006), demonstrating greater losses of strength with longer post-treatment times. Nevertheless, the silane treatments continued to be active prior to bonding and particularly more stable for pH7 solutions, which remained active after 168 hours at 23ºC and 50%RH.

7.3.2.2.2 Morphology / Surface Topography

In a study by Abenojar *et al.* 2009a, improved mechanical strength of a silicon carbide (SiC) / epoxy PMC was attributed to the presence of the GPS layer and shape modification of the SiC particles. This was evident in the SEM morphological characterisation of the silane treated BC particles, which exhibited a lighter surface appearance and smoother edges as a result of the interaction of the electrons with the silane layer on the BC (Fig 6.9).

7.3.2.2.3 Chemical Analysis

The FTIR studies clearly showed an influence of the solution pH and silane concentration on the surface chemistry of the treated BC (Fig. 6.10-11, Table 6.8). These results support findings in the literature relating to the reaction mechanisms and kinetics of silane in aqueous solution, in particular the hydrolysis, condensation of the hydrolysed species and reactions with the hydroxyl groups from the surface.

In the case of the solution pH, the most acidic solution (pH3) led to the least chemical modification of the BC surface, due to the lower stability of the hydrolysed silane in these solutions. Similarly in the most basic solution (pH9), the surface chemistry changes were less obvious, which was due to both a higher concentration of dimers or larger oligomers, and a reduced number of silanol groups available to react with the hydroxyl groups on the BC surface. This was due to the rapid condensation of the silane in the more basic solutions. The pH5-7 solutions resulted in an increased modification of the BC surface due to a higher concentration of monomeric silanol in solution. This was a result of a faster hydrolysis and slower condensation of the silane in milder acidic conditions, promoting greater stability of the hydrolysed compound (Xue *et al.* 1991, Tesoro and Wu 1991, Parker and Maclachlan 2000, Johnsen *et al.* 2003).

The GPS concentration also affected the number of silanol groups available to both crosslink and react with the BC surface. This was supported by the increased intensity of the bands attributed to the silanol and Si–O–Si vibration modes with the increase of GPS concentration using pH5-7 solutions (Kurth *et al.* 1994, Rider 2006, Hanoosh and Abdelrazaq 2009). Identical bands were also found in the analysis of the GPS gel. The exception being the presence of a carbonyl characteristic band in the gel spectrum, which according to Bertelsen and Boerio 2001 is due to the oxidation of the epoxy group from the silane. Further multiple bands, found on the silane treated BC surface were attributed to the stretching and bending vibrations of the borosiloxane bond (B–O–Si) (Mansour *et al.* 2007, Wróblewska *et al.* 2010, Orhan *et al.* 2008). According to Siqueira *et al.* 2007, these bonds can be easily formed though condensation between B-OH and Si-OH/Si-OR groups.

XPS confirmed a reduction in boron concentration and the appearance of silicon on the silane treated BC surface (Table 6.10, Fig. 6.15-16). The boron contribution clearly decreased as %Si, %C and %O increased with the silane concentration. This implied that a silane layer was formed on the surface. Notably, the elemental variation relative to the untreated BC composition changed according to silane concentration (C > Si > O for 0.5-1% to C > O > Si for 3%). With the highest GPS concentration, there was more evidence of oxygen than silicon which suggests more silanol groups that have not undergone either water dehydration or alcohol condensation. This was particularly evident for the pH3 with 3%GPS, which exhibited a surface composition of oxygen as the major element, due to the faster silane hydrolysis and slower silanol condensation in the more acidic solutions (Xue *et al.* 1991, Tesoro and Wu 1991). XPS confirmed the increased surface modification at pH5-7 seen in FTIR results. A similar composition was obtained by Brack *et al.* 2005 using GPS on boron fibres.

The B1s spectra identified the presence of B-C and B-OH groups, which became less intense as solution pH (from 3 to 7) and %GPS increased (Fig. 6.21, Table 6.15). The boron hydroxide groups were more evident in pH3-5 which again may be related to a lower stability of silanol groups in more acidic solutions (Xue et al. 1991). A reduced presence of the silane layer was also evident at pH9 with an increase of the B-C peak. This was a result of the reaction of larger oligomers onto the BC surface due to a faster silanol condensation in more basic solutions. After silane treatment, there was no evidence of

boron oxides as a result of hydration to boric acid or borate ions (Duffin *et al.* 2011, Rybakov *et al.* 1995).

Evidence of GPS layer on surface was observed from the C1s spectra due to the presence of a C-Si peak (Fig. 6.22, Table 6.16-17). This was confirmed by the increase of the C-O component from the epoxy and ether groups and decrease in B-C/C-C peaks with the increase of silane concentration. However, higher C-O contribution were always accompanied by reduction in the C-Si peaks, which was probably related to a higher presence of epoxy groups aligned outward from the surface. This was particularly observed for pH5 as opposed to the most acidic solutions. Also, the C-O/C-C ratio was similar to the theoretical value (2:1) of the GPS stoichiometry (Neyman 2003), particularly when the silane concentration increased in pH5-7 solutions. The increase of the C-B peak from pH7 to pH9 again suggested limited presence of the silane layer. Compared with the untreated BC, higher C=O contribution (1%GPS in pH3-5, 3%GPS in pH5-9) could be associated with the degradation of the epoxy rings from the silane, which was also observed on the surface of the GPS gel by ATR-FTIR.

In the case of the Si2p spectra, the signal was exclusively from the silane layer (Fig. 6.23, Table 6.18). The signal was more intense as pH and GPS concentration increased, with the exception of 1-3%GPS from pH7 to pH9 due to a less presence of the silane layer (Xue *et al.* 1991, Tesoro and Wu 1991). This was also supported by a slight increase in the non-crosslinked silane peak, which is probably related to the limited accessibility of Si-OH groups to react with the surface as a result of the steric effects imposed by the larger oligomers formed in the most basic solution. Silane surface modification was more obvious for 0.5-1%GPS in pH5-9 and 3%GPS in pH3-7 solutions, with a signal dominated by the crosslinked silane component. An exception to this was the 0.5-1%GPS in pH3, which confirmed a limited crosslinking.

Regarding the O1s spectra, the signal became more intense with an increase in the GPS concentration and solution pH (Fig. 6.24, Table 6.19). However, the signal intensity decreased beyond pH7 due to a reduced presence of silane as a result of the formation of larger oligomers with fewer silanol groups (Xue *et al.* 1991, Tesoro and Wu 1991). Therefore, the oxygen concentration was generally higher for pH5-7, showing an increase of the Si-O component as B-O decreased with silane concentration. There was no B-O peak detected with these solutions when the highest %GPS was used. This supports the earlier findings which point to an increased presence of the GPS layer on the BC surface.

In contrast, the most acidic solution led to reduced presence and limited crosslinked silane layer as a result of the highest B-O and Si-O components from the BC and silanol groups, respectively.

7.3.2.2.4 Silane Layer

The silane layer thickness was strongly affected by the pH value and silane concentration (Table 6.11). This agreed with Abel *et al.* 2000 using GPS on aluminium substrates. Generally, thicker silane layers were found on the BC with higher %GPS in pH7 solutions due to the higher stability of the monomeric silanol in solution (Xue *et al.* 1991, Tesoro and Wu 1991). The thickness of the silane layer ranged between 0.5 to 2.1 nm. This suggests that layer varies from uncovered to a monolayer or a multilayer structure, given that the length of the hydrolysed GPS molecule is approximately 1.3 nm (Rider 2006, Kinlock *et al.* 2006). This agreed with the findings of Davis and Watts 1996 where the GPS layer seems to exists as a relatively disorganised structure with no dominant orientation or structuring.

A higher percentage of silane coverage on the BC was confirmed by an increase in GPS concentration for a specific pH (Table 6.12). This was particularly noticeable for pH5-7 solutions. In the case of a particular silane concentration, the coverage increased from pH3 to pH7 and reduced from pH7 to pH9. Hence, the largest silane coverage was obtained using pH7-9 with 0.5%GPS and pH5-7 with 1-3%GPS.

The elemental contribution of the silane layer as a function of coverage exhibited a linear behaviour (Fig. 6.17). From linear regression, the composition of a fully covered silane treated surface (f_{GPS} = 100%) should therefore be 11% of silicon, 39% of oxygen and 49% of carbon. This was indeed similar to that determined from the stoichiometry of the fully crosslinked silane layer (Fig. 6.18), i.e., a Si:O:C ratio of 1:4:6 which corresponded to 9.1% for silicon, 36.4% for oxygen and 54.5% of carbon. This composition therefore confirmed that the GPS had adsorbed onto the BC surface as a disordered multilayer siloxane structure with approximately half of the silanol groups oriented outward and the other half pointing inward (Kinloch *et al.* 2006). This linear behaviour was similar for both pH5 and pH7 solutions (Fig. 6.19), which resulted in a greater coverage and more crosslinked multilayer silane structure. In the case of the pH3, a wider range of silicon concentration and reduced coverage were observed as a result of the lower stability of the

silanol groups in solution. This led to limited crosslinking and/or changes in orientation (inwards or outwards) of the silicon or organofuntional groups in relation to the BC surface (van Ooij *et al.* 2006, Zhu and van Ooij 2004, Abel *et al.* 2000). pH9 exhibited both limited variation of silicon content and silane coverage. These results were likely to be due to the presence of more dimers, trimers or even larger oligomers with fewer silanol groups available for attachment to the BC surface (Xue *et al.* 1991, Tesoro and Wu 1991).

7.4 Proposed Mechanism of The Silane Attachment to BC Surface

An evaluation of the surface analysis suggests that the silane attaches to the BC by the following coupling mechanism. The untreated BC surface is composed of highly hygroscopic boron oxides, which result from the boron atoms on the surface reacting with oxygen in the atmosphere, leading to boric acids and derivatives (Mortensen *et al.* 2006, Steinbrück 2005, Rybakov 1995) as shown in Fig. 7.2a. These species can form hydrogen-bonding with the silanol group or, due to their Lewis acid nature, suffer a nucleophilic attack by the hydrolysed GPS to form a borosiloxane ($\equiv$B-O-Si$\equiv$) bond (Brinker and Scherer 1990). Despite boric acids species being hydroxides, they react with water molecules by releasing protons (Fig. 7.2b) rather than dissociate in aqueous solutions as typically observed with alkali and alkaline metal hydroxides. This mechanism is commonly found in the sol-gel process between hydrolysed ter- or tetra- alkoxysilanes and boron acid (Fig. 7.2c) to obtain borosilicate glass or ceramic precursors possessing crosslinked trigonal BO_3 units in the polysiloxane structure (Muralidharan *et al.* 2004, Peña-Alonso *et al.* 2005, Ivanova *et al.* 2006, Siqueira *et al.* 2006, Hunt *et al.* 2008, Schiavon *et al.* 2008). Although borosiloxane bonds are covalent in nature, they can be cleaved through hydrolysis in aqueous solution (Zha *et al.* 1998, Schiavon *et al.* 2008) in a similar way to that observed with Si-O-Si and Me-O-Si bonds (Plueddemann 1991, Abel *et al.* 2006). Heat must be provided during the drying stage in order to promote the formation of the B-O-Si bonds between the silane and BC surface (Fig. 7.2d). Moreover, work with GPS on boron fibres to improve bonding to epoxy adhesive has shown a water resistant silane layer covalently bonded to the surface. This was confirmed by water immersion and ToF-SIMS, with the latter detecting a weak peak which was attributed to a borosiloxane ion fragment (Brack *et al.* 2005). In the case of this study, the presence of a strong and hydrolytic resistant bond between the GPS layer and BC surface was confirmed through surface analysis on BC, and mechanical and durability tests conducted on the PMCs

detailed in the following sections. Therefore, an effective chemical bridge between the epoxy adhesive and BC has been attained.

(a)   (b)   (c)   (d)
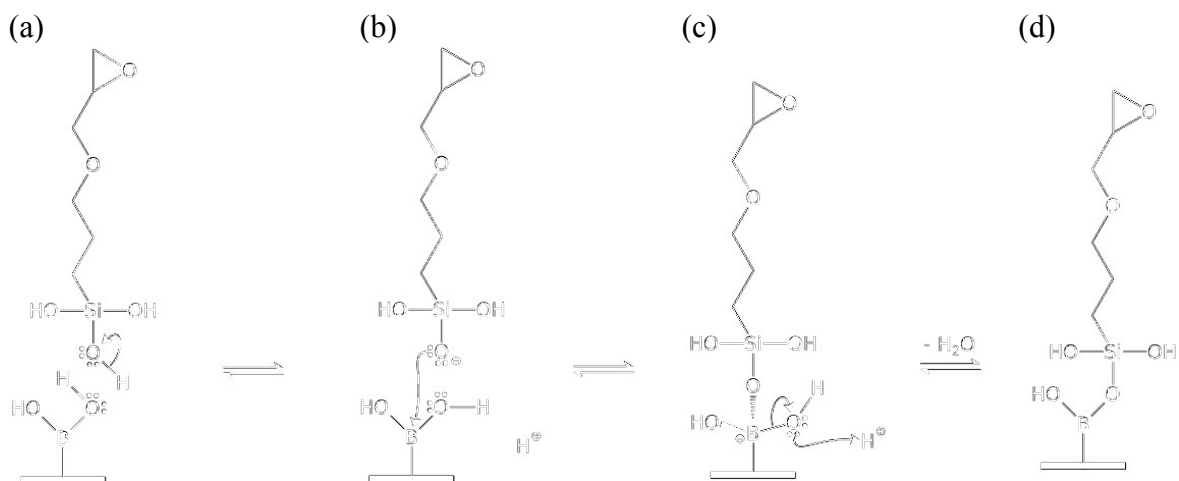
Figure 7.2 Reaction mechanism proposed for representation of the possible covalent bonding between GPS and BC surface, through hydrogen-bonding in solution and nucleophilic attack during the drying stage.

7.5 BC-Epoxy PMC

The silane surface modification also had a marked influence on physical-chemical and mechanical properties, and durability of PMCs. This includes the bulk density, open porosity and, water permeability, as well as rupture, tensile and shear strength before and after water immersion.

7.5.1 Physical-Chemical Properties

The bulk density, open porosity and water permeability of the PMCs depends on the adhesive's wettability and hydrophobicity on the BC surface, which according to the previous findings are strongly affect by the surface treatment.

7.5.1.1 Bulk Density / Open Porosity

Confirmation of the PMC's porosity was exhibited by a comparison of the experimental and theoretical bulk density values (Fig. 6.25-26). The lowest density was showed by the PMC produced using the original manufacturing process, which exhibited a large amount

of air trapped in the matrix. The refined manufacturing process led to an increase in density. The smaller standard deviation better dispersion/lower agglomeration of the particles and fewer air voids in the epoxy matrix. Previous investigations have demonstrated similar findings whereby better thermal conductivity was achieved with a silane treated SiC-epoxy PMC through the development of a more effective dispersion and chemical bridging between the particles and resin (Zhou *et al.* 2008, Kavitha *et al.* 2012). The highest densities were obtained with either the silane or corona treatment. Regarding the silane treated PMCs, the highest values were produced using 0.5-1.0%GPS in pH3-5 solutions. This was confirmed by the reduced porosity as shown in Fig. 6.27 and 6.37. Moreover, the least porous was displayed by the surface modified BC PMC in particular with corona (0.15%). This was likely to be the result of improved adhesive wettability due to the combination of a slight increase in the SFE dispersive component (Fig. 6.12) and higher surface temperature (34ºC). Generally, the silane treated PMC showed porosities between 0.22-0.26%. This was due to better adhesive wettability on the BC and reduced viscosity of the compound from the better dispersion of the particles in the resin (lower standard deviation, Fig. 6.26). Given the high BC content and relatively low viscosity of the resin used in previous findings, the displacement of the particles from the surface by entrapped air as a result of the high density of BC or agglomeration of the particles in the epoxy matrix (Abenojar *et al.* 2009b, Suresha *et al.* 2008) were not replicated in this study.

7.5.1.2 Water Uptake / Permeability

The water uptake of the PMCs was also influenced by surface treatments as shown in Fig. 6.28. Lower uptake compared to the epoxy resin was observed for the PMCs due to the addition of BC. The water uptake exhibited three distinct stages: initial by a step uptake, followed by a linear incremental behaviour and finally a progressively slower absorption rate as higher saturation levels were reached. The initial stage depended principally upon the open porosity (6.27). This mechanism is related to the effectiveness of the adhesive to wet the silane treated BC surface and minimise the air voids in the matrix, which otherwise provided a means for the water to penetrate into the PMC. Regarding the second stage (Fig. 6.29), an linear increase of water absorption was confirmed, which was affected by the hydrophobic nature of the silane treated BC particles. This was associated with the final structure of the silane layer on the BC, particularly when a high content of small grit size particles was present in the PMC. Hence, the absorption rate (obtained from the slope

of the linear regressions) was greatest when higher %GPS was used in pH9 solution. This was most probably related to the formation of limited coverage and a more open silane structure as pH and silane concentration increased (Xue *et al.* 1991, Tesoro and Wu 1991). In contrast, the slowest absorption rate was exhibited by pH3-7 solutions with 0.5-1%GPS. These findings correlate with the amount of porosity in the PMC and SFE of the BC, as previously discussed in the section 7.3.2.2.1 and 7.5.1.1. Hence, both porosity of the PMC and hydrophobic nature of the silane treated BC particles must be influential factors contributing to the degradation processes of the PMCs (Lee *et al.* 2009).

In the case of the water permeability of the PMCs (Fig. 6.30, Table 6.20), the untreated and corona discharged samples provided the highest values, despite exhibiting the highest and lowest values in porosity, respectively. The silane treated PMCs exhibited lower permeability, despite possessing higher porosities than that of the corona discharged. Therefore, the water permeability was found to be closely related to the hydrophobicity of the interface as a result of the silane treatments on the BC. Similar findings were found with silane treated BC in silicon coatings by providing improved corrosion resistance (Xu and Jia 2007). Low to medium concentrations appeared to provide reduced permeability, except for pH7 solutions. pH3-5 exhibited higher sensitivity to silane concentration, delivering a slight decrease from 0.5 to 1.0% and a steep increase from 1 to 3% GPS. The variations in permeability due to the silane concentration were less evident as pH increased.

7.5.2 Mechanical Properties

The mechanical strength of the PMCs and adhesion between the particles and epoxy were also influenced by the various surface treatments applied to the BC. For comparison purposes, the mechanical properties of the pure epoxy have been discussed.

The original PMC demonstrated the lowest strength as shown in Fig. 6.31, 6.33 and 6.35. This was due to poor particle dispersion and high porosity, which can be related to the high viscosity, and lack of adhesion between the BC and epoxy resin in the PMC (Suresha *et al.* 2009, Abenojar *et al.* 2009b). However, the use of the refined manufacturing process on the untreated PMC promoted a higher strength (25% in rupture, 95% in tensile) and no improvement in shear. The addition of the corona treatment provided a small increase in strength (8% in rupture and tensile, and 25% in shear strength). This is likely due to

improved adhesive wettability, which was the result of a small increase in SFE dispersive component and surface temperature increase from 24 to 34ºC.

Regarding the silane treatment, the PMCs demonstrated significant improvements in rupture, tensile and shear strength corresponding to 88%, 100% and 40% of that of the pure epoxy strength. This suggests enhanced adhesion due to the absorbed GPS layer containing outwardly orientated epoxy groups. Furthermore, solution pH and GPS concentration have clearly demonstrated a significant influence on the mechanical properties.

In case of the rupture strength (Fig. 6.32), the pH3 solution was detrimental, most likely due to the lower stability of the hydrolysed silane in more acidic solutions. Higher strength was generally achieved with pH7 solutions, again supporting earlier findings in the literature (Plueddemann 1991, Abel *et al.* 2006, Parker and Maclachlan 2000, Kim *et al.* 2010a). Beyond pH7 the improvements were lost with the highest silane concentration, thought to be due to the formation of larger oligomers with fewer silanol groups (Xue *et al.* 1991, Tesoro and Wu 1991). This suggests a more open and disorganised three-dimensional siloxane structure (Fig. 2.2b) with fewer covalent bonds available for attachment to the surface, which consequently led to reduced adhesion between the epoxy and BC particles. The best performance was observed using 0.5%GPS and 1%GPS, with the latter normally promoting highest strength. Beyond 1%GPS all but pH7 solution demonstrated significant reduction in strength. Together, solution pH and concentration show a strong influence on the rupture strength. Hence, optimal treatment conditions were 0.5-1.0%GPS in pH5-7 solutions which supported similar findings using GPS treatment on aluminium substrates (Kim *et al.* 2010A, Abel *et al.* 2006).

Similar behaviour was found in the tensile strength with most GPS solutions leading to some improvement (Fig. 6.34). The higher values were generally observed with pH5-7 solutions. Compared to the untreated PMC, lower strengths values were found when formulated with 3%GPS in pH3 and pH9 solutions, highlighting a strong relationship between solution pH and silane concentration. Better performances were produced using 0.5-1.0%GPS over the full pH range.

In regard to the shear strength, although all the silane treatments led to an increase (Fig. 6.36), the greatest improvements were exhibited by pH7-9 solutions. In the case of a particular solution pH, the highest strengths were obtained using low and medium silane concentrations. The best treatment conditions were found using 0.5-1.0%GPS in pH7

solution.

The use of corona prior to the silane treatment resulted in a small decrease in strength albeit slightly above that of the corona treated alone. This clearly disagreed with previous work, whereby a plasma treatment prior to GPS led to an improved bond strength between boron fibres and epoxy resin (Brack *et al.* 2005). The reduced strength in this study, was probably related to a higher contribution to the overall failure process of a thicker and weaker boron oxide layer formed during corona discharge. A similar observation was found with SiC-epoxy PMCs, whereby surface oxidisation prior to silane treatment led to lower thermal conductivity compared to that of the just silane treated particles, which was probably due to the thick overgrown oxides (Zhou *et al.* 2005).

7.5.3 Mechanical Strength Related to Type of Particle/Matrix Interface

Microscopic examination indicated that better adhesion in the corona treated PMC by traces of resin on the surface of some large particles, apparently as a consequence of cohesive adhesive failure near the interface (Fig. 6.37c). Even better adhesion resulted from the silane treated PMC, which exhibited distinct regions of epoxy and small BC particle clusters, again, remaining attached to the surface of the larger particles (Fig. 6.37d). The silane treatment appears to provide a stronger bond compared to that of the corona treated BC surface. This may be related to the chemical modification of the surface and consequent intermolecular interaction mechanisms between the BC particle and epoxy resin.

7.5.4 Durability

The durability of the PMCs and pure epoxy adhesive was evaluated by mechanical testing after water immersion. Their final strength showed a direct relationship to the amount of water absorbed by the matrix structure due to its diffusion into the free volume of the matrix and its ingress into the porous and interfacial region. This supports the work of Abenojar *et al.* 2011. These mechanisms were strongly influenced by the hydrophobicity of the BC surface. This supports the presence of a hydrophobic silane layer, providing a stronger and more water resistant bond between the BC and epoxy adhesive. Similar findings were confirmed in an earlier study with flax fibre PMCs (Wang 2004).

7.5.4.1 Effect of Water Immersion on Mechanical Strength

The pure epoxy demonstrated both a high uptake of water and reduction in strength (Fig. 6.38). The untreated and corona discharge treated PMCs showed the greatest loss in strength along with the highest water uptake values. Despite the improved adhesive wetting and reduced porosity of the corona PMC (Table 6.9, Fig. 6.27), its poor strength and high water ingression at the interfacial region may be due to the increased hydrophilic nature and weaker layer of boron oxides and hydroxides on the BC surface (Fig. 6.10b, Fig. 6.12). In the case of the silane treated PMCs, smaller losses in strength and water uptake were found, regardless of their porosity. In addition, these values were affected by solution pH and silane concentration. Strength losses were more evident with pH5-9, whereas, most acidic solutions led to little change in strength. In regard to the solution silane concentration, losses were more obvious with 1%GPS as pH increased, whereas, there was no discernible trend found with 3%GPS. Water uptake evaluation again confirmed a direct relationship to strength losses. Generally, higher silane concentration led to greater water absorption, despite exhibiting little reduction in strength. This may be associated with the formation of a more open and thicker GPS layer. This can reduce the stress across the interface as a result of the epoxy swelling and also increase water absorption during immersion (Vano 2008).

Generally, the corona discharged PMC demonstrated the poorest durability with strengths inferior to those of the silane treated PMCs and, in most cases, similar to that of the untreated PMCs. In the case of the silane treated PMCs, there was improved durability but this varied with solution pH and GPS concentration. The least losses or even slight improvements in strength resulted from pH3-5 solutions with the highest %GPS. Therefore, the optimal parameters for best durability were generally 1%GPS in pH3-5 solutions due to the combination of a higher initial strength and reduced loss when subjected to water immersion. These findings were in agreement with other work using GPS treatment on aluminium substrates, which showed the best durability when pH3-5 solutions were used (Abel *et al.* 2006).

7.5.4.2 Effect of Temperature on Water Uptake

No material leached out from the composites and the geometry of samples had no effect on the water uptake during immersion, the water uptakes of the pure adhesive and PMCs

subject to immersion for 1500 hours were compared at two different temperatures, 23ºC (M^{23}_{1500h}) and 40ºC (M^{40}_{1500h}) as shown in Table 7.1. The values at 23ºC were obtained from their water absorption curves, i.e., water uptake as a function of immersion time - M_t vs $t^{1/2}$ (Fig. 6.28). These curves were previously used to evaluate the effect of the silane treatments on the water permeability of the PMCs. In case of the water uptakes at 40ºC, they were acquired from environmental durability studies of the PMCs and constituent materials (Fig. 6.39). An increase in water uptake at 1500 hours was confirmed from 23 to 40ºC (Table 7.1). This appears to be related to an increase of the rate of water diffusion due to the relaxation of the epoxy matrix as temperature increase to values near to that of glass transition. It was found in this work, a decrease in the storage modulus of 33% from 23 to 40ºC (Fig. 6.6). Also, the diffusion rate is also affected by the addition of BC and the interaction of the water molecules with BC surface. The latter is highly dependent on interface resulted from various treatments and conditions used in this work. In addition, the immersion time at 23ºC (t^{23}) required to achieve the same water uptake values at 40ºC for 1500 hours (M^{40}_{1500h}) was obtained for the epoxy and PMCs through interpolation of their water absorption curves, by considering that similar degradation processes have occurred at both temperatures.

Table 7.1 Water uptake of the epoxy adhesive and PMCs, after 1500 hours of immersion at 23ºC (M^{23}_{1500h}) and 40ºC (M^{40}_{1500h}) and immersion time at 23ºC (t^{23}) required to obtain M^{40}_{1500h}.

Material	Water uptake, M_t (%), t = 1500 h			Immersion time at 23ºC, t^{23} (h) $M^{23}_t = M^{40}_{1500h}$
	23ºC, M^{23}_{1500h}	40ºC, M^{40}_{1500h}	ΔM (%)	
Adhesive	1.46	3.52	141.87	> 10100
Untreated	0.40	0.74	84.09	3800
Corona	0.29	0.74	157.30	6500
pH3, 1%GPS	0.30	0.66	119.69	5900
pH3, 3%GPS	0.32	0.72	123.46	> 10100
pH5, 1%GPS	0.28	0.67	139.04	8000
pH5, 3%GPS	0.33	0.68	103.98	> 10100
pH7, 1%GPS	0.30	0.70	130.24	6500 - 7300
pH7, 3%GPS	0.31	0.73	135.83	6500 - 7300
pH9, 1%GPS	0.31	0.73	134.08	6500
pH9, 3%GPS	0.34	0.67	98.52	4300-5300

Data from Table 7.1 confirmed that water uptake at 23ºC was less than that at 40ºC and a

longer immersion time was required to achieve the same saturation level at lower temperatures (t^{23}). The epoxy adhesive showed a 141% increase in water uptake at 40ºC. In the case of PMCs, the addition of BC in epoxy adhesive led to a reduction in water uptake, in particular when a high load of particles is used. The untreated composite showed the smallest increase (ΔM) and shortest immersion time (t^{23}) due to the highest water uptake at 23ºC as a result of its high porous nature. In contrast, the corona treated PMC exhibited the greatest ΔM due to the lowest and highest water uptake at 23ºC and 40ºC, respectively. This was probably related to the low porosity and weaker interface from the hydrophilic nature and weaker layer of boron oxides and hydroxides on the BC surface. Compared to the corona treatment, smaller ΔM was generally obtained by the silane treated PMCs due to the lower water uptake values at 40ºC. This was closely related to the hydrophobicity at the interface due to the presence of the silane layer on the BC. Regarding the solution pH, shorter immersion times were required for pH7-9. In contrast, pH3-5 solutions led to silane treated PMCs with higher hydrolytic stability due to the combination of a lower water uptake at 40ºC and longer immersion time, in particular when 3%GPS was used.

CHAPTER 8 – CONCLUSIONS AND FURTHER WORK

A new approach for surface modification of BC has been proposed in this work to obtain a PMC with superior performance and durability. This was achieved through the application of silane coupling agents, to improve adhesion to epoxy resin and hydrophobicity at the interface. The silane treatment was applied as a GPS aqueous solution on the BC surface using different solution parameters (concentrations and pH values). The experimental methodology was conducted to understand the mechanism behind silane treatment and to evaluate the effect of the parameters on the properties of the BC surface, in order to find the optimal treatment conditions. Hence, all the objectives initially defined in this study were achieved through wettability, chemical and morphological analysis on the BC as well as by physical-chemical, mechanical and durability studies on the PMCs. A summary of the research findings and future recommendations are provided.

8.1 Summary of Research Findings

The evaluation of the surface chemistry and free energy of untreated and modified BC was critical to fully understand the reliability of the silane treatment.

- The untreated surface was composed of boron oxide and hydroxyl groups which can either hydrogen-bond with the silanol group or, due to their Lewis acid nature, suffer a nucleophilic attack by the hydrolysed GPS to form a borosiloxane bond.

- Silane modification led to increased hydrophobicity and adhesive wettability due to the nature of the GPS layer formed on the BC. Surface treatment was most effective using pH5-7 solutions as a result of the greater stability of the hydrolysed silane and the presence of a more monomeric silanol aqueous solution.

- Surface analysis confirmed bands of medium and weak intensity which were similar to B-O-Si vibration modes typically found on borosilicate glass.

- The extent of crosslinked silane groups was found to be affected by the solution pH and GPS concentration. These were responsible for the structure of the layer

(cross-linking, density, thickness, coverage) and subsequently for the overall adhesion and hydrophobicity promoted by silane treatment.

- Silane thickness was strongly affected by pH value and GPS concentration (between 0.5 and 2.1 nm), exhibiting higher values with pH7 solution and higher %GPS. Lower values resulted from the extremes of the solution pH (pH3 and pH9) for the full range of silane concentrations.

- Corona discharge treatment provided better wettability of the dispersive epoxy adhesive on the BC, essentially as a result of an increase of surface temperature (34ºC). To a lesser extent, a higher polar SFE component also contributed due to the formation of more boron–oxygen species.

- Improved adhesive wettability led to PMCs with higher density and lower porosity, which resulted in a more effective dispersion of the particles in the epoxy matrix.

- Analysis of the GPS treated BC surface suggested that there was no dominant orientation or structuring of the silane on the surface.

- Manufacturing also had some influence on physical-chemical and mechanical properties of the PMC, suggesting the importance of various parameters (mix mode and degassing) that were used during this process to achieve optimised performance.

The enhanced adhesion of the epoxy adhesive on the treated BC was confirmed through mechanical testing and SEM. Both demonstrated correlation between strength improvement and the various surface modifications, and physical-chemical characterisation of the PMCs. In particular:

- Debonding was the dominant failure mechanism in the low strength untreated BC, which was illustrated by the lack of residual epoxy on the BC particles examined under SEM.

- Corona discharge, when applied as the only treatment, led to an increase in strength due to an improved adhesion. This was supported by the presence of increased traces of epoxy resin on the BC particles.

- The strength was, however, lower than that obtained with the silane treated PMCs when the corona was applied prior to GPS treatment. This was thought to be due to the further formation of boron oxide, which led to a thicker and (probably) weaker

layer on the BC. In summary, this showed that pretreatments can affect the surface chemistry and consequently the formation and performance of the GPS on BC.

- The highest improvements in PMC strength were supported by the formation of a GPS layer strongly attached to the BC surface. Optimal properties were generally obtained using low to medium silane concentrations in slightly acidic and neutral solutions (0.5-1.0%GPS, pH5-7). This led to a more extended GPS layer that promoted strength increases ranging between 24% and 56%. In some cases, similar rupture and tensile strengths to that of the pure epoxy were achieved, although at best only 40% of the adhesive's shear strength was obtained.

- Slight shape modification of the BC particles by the inclusion of the GPS layer also probably contributed to a reduction of stress concentrations, resulting from the morphology and sharp edges of the particles.

- The failure surfaces of the silane treated PMCs clearly showed distinct regions of epoxy and small BC particle clusters, again, remaining attached to surface of the larger particles.

The water permeability and ageing studies conducted on PMCs indicated a clear correlation between water uptake and strength loss. This confirmed that the durability of the PMCs was highly dependent on the hydrolytic stability of the GPS layer at the interfacial region, as promoted by the different treatments on the BC surface. In particular:

- PMCs that demonstrated better durability resulted from the combination of high initial mechanical properties and reduced loss in strength from the water immersion. The best results were obtained with lower silane concentration in a slightly acidic solution (1%GPS, pH3-5), due to the balance between the formation of a more compact structure and greater coverage of GPS layer.

- Strengths superior (122 to 220%) to those of the aged untreated PMC (100%) were obtained.

- In comparison to pure epoxy, the rupture and tensile strengths were found to be similar (82% and 107%). However, shear strength was only 45% of that of the pure epoxy.

- Optimal conditions for high initial strength (pH7) did not always lead to the best durability, suggesting that an extended and thicker but less compact layer was more

susceptible to water ingression.

- Corona discharge treatment, despite promoting enhanced initial strength, in most cases, did not provide any improved durability compared to the untreated PMC.

- Better durability was obtained by a hydrolytic resistant GPS layer on the BC, which points to the layer being covalently bonded at the surface, according to the mechanism proposed in this study.

The silane treatment proved to be an effective surface chemical modification of the BC which improved not only adhesion but also hydrophobicity, resulting in a PMC with superior strength and durability. In the case of BC, this study represents a baseline for future research with silanes since no work has been reported in the open literature. Moreover, this work provided an insight into the influence of some solution parameters and corona pretreatment on the GPS deposition. This thesis demonstrated the great potential of silane treatments to enhance adhesion in other resin systems and to improve other surface properties of BC, given the wide range of possible tailored silane structures available.

8.2 Further Recommendations

Despite the research work presented herein, new questions arise from the present experimental programme which require further investigation. Hence, a number of recommended topics for future research are proposed.

- Conduct a more rigorous approach on the thickness of the silane layer formed on the boron carbide through conventional angle resolved XPS (ARXPS). This method can determine concentration profiles by collecting a high spectra at different take-off angles, in particular for the silicon and boron elements.

- Study the interaction between oxidised BC and hydrolysed GPS by time-of-flight secondary ion mass spectroscopy (ToF-SIMS). This would enable depth profiles to be obtained and also to identify the B-O-Si ion fragments which could provide clear evidence of a covalent bond between ceramic material and GPS.

- Evaluate the effect of the untreated and silane treated particles on the cure process of the epoxy resin and consequently its viscolelastic properties, using similar

contents and size distribution to that used in this work. A recent study has demonstrated that small additions of untreated BC particles affected the kinetics, degree of conversion and crosslinking of an epoxy adhesive, according to their size and concentration (Abenojar *et al.* 2009b). This may result in a resin with different mechanical properties to that of the pure adhesive.

•   Although one of the main objectives during this study was to obtain a PMC with improved strength, the execution of additional mechanical testing with bonded joints could have provided a more sensitive evaluation of the promoted adhesion. This would remove factors related to the manufacturing of the PMC which affected its mechanical properties but were not related to the surface state of BC and consequently masked the overall effect of the silane treatment.

•   Study of the failure surfaces of a model epoxy/silane/BC before and after ageing by XPS could provide information about the thickness and interactions of GPS layer with epoxy and BC, which is related to the failure mode within the siloxane structure for the former or at the epoxy-silane or silane-BC interface for the latter. Previous work with silicon and silicon carbide has proved that a primary failure at epoxy-silane interface (Neyman 2003), whereas, cohesive failure was observed within the oxide/silane/adhesive diffusion zone on aluminium alloys (Abel *et al.* 2006).

•   In the case of the current work, only water immersion at 40ºC was conducted to investigate the interfacial stability of the PMCs from moisture ingression. Given that the PMC is to be used as a neutron shielding material, no information was obtained about their performance when exposed to radiation, particularly in regard to the degradation mechanisms of the epoxy polymeric systems to these conditions.

REFERENCES

- Abel, M. L., Digby, R. P., Fletcher, I. W., & Watts, J. F. (2000). Evidence of specific interaction between γ-glycidoxypropyltrimethoxysilane and oxidized aluminium using high-mass resolution ToF-SIMS. *Surface and interface analysis*, *29*(2), 115-125.

- Abel, M. L., Watts, J. F., & Digby, R. P. (2004). The influence of process parameters on the interfacial chemistry of γ-GPS on aluminium: A review. *Journal of Adhesion*, *80*(4), 291-312.

- Abel, M. L., Allington, R. D., Digby, R. P., Porritt, N., Shaw, S. J., & Watts, J. F. (2006). Understanding the relationship between silane application conditions, bond durability and locus of failure. *International journal of adhesion and adhesives*, *26*(1), 2-15.

- Abel, M. L. & Watts, J. F (2009). Examination of the interface of a model adhesive joint by surface analysis: a study by XPS and ToF-SIMS. *Surface and Interface Analysis* ,41(6), 508-516.

- Abenojar, J., Del Real, J. C., Martinez, M. A., & de Santayana, M. C. (2009a). Effect of silane treatment on SiC particles used as reinforcement in epoxy resins. *The Journal of Adhesion*, *85*(6), 287-301.301.

- Abenojar, J., Martínez, M. A., Velasco, F., Pascual-Sánchez, V., & Martín-Martínez, J. M. (2009b). Effect of boron carbide filler on the curing and mechanical properties of an epoxy resin. *The Journal of Adhesion*, *85*(4-5), 216-238.

- Abenojar, J., Martinez, M. A., Velasco, F., & del Real, J. C. (2011). Effect of moisture and temperature on the mechanical properties of an epoxy reinforced with boron carbide. *Journal of Adhesion Science and Technology*, *25*(18), 2445-2460.

- Adams, R. D. (Ed.). (2005). *Adhesive bonding: Science, technology and applications*. Cambridge, CRC Press, 84-111.

- Ahmad, Z., Ansell, M. P., & Smedley, D. (2010). Effect of nano-and micro-particle additions on moisture absorption in thixotropic room temperature cure epoxy-based adhesives for bonded-in timber connections. *International Journal of Adhesion and Adhesives*, *30*(6), 448-455.

- Ahmad, Z., Ansell, M. P., & Smedley, D. (2011). Moisture Absorption Characteristics of Epoxy Based Adhesive Reinforced with CTBN and Ceramic Particles for Bonded-in Timber Connection: Fickian or Non-Fickian Behaviour. In *IOP Conference Series: Materials Science and Engineering, 17*(1), 012011.

- Ahn, H. S., Cuong, P. D., Shin, K. H., & Lee, K. S. (2005). Tribological behavior of sputtered boron carbide coatings and the influence of processing gas. *Wear*, *259*(7), 807-813.

- Air Products (2001a). *Epoxy Additives for Civil Engineering*. Technical bulletin, Clayton Lane, Clayton, Manchester Mil 4SR.

- Air Products (2001b). *ANCAMIDE® 506 Curing Agent, Epoxy Curing Agents and Modifiers*. Pub. No. 125-9717.6.

- Air Products (2003). *Calculating Stoichiometry Ratios for Epoxy Curing Agents and Resins*.

- Air Products (2004). *Epoxy Curing Agents and Modifiers, Ancamide® 506 Hardeners*, Revision date: 7/22/04.

- Air Products (2008). *ANCAMIDE® 506 Curing Agent*. Material safety data sheet Version 2.2, MSDS Number 300000009039, Revision date: 04/27/2008.

- Alizadeh, A., Taheri-Nassaj, E., & Ehsani, N. (2004). Synthesis of boron carbide powder by a carbothermic reduction method. *Journal of the European Ceramic Society*, *24*(10), 3227-3234.

- Alizadeh, A., Taheri-Nassaj, E., & Baharvandi, H. (2011). Preparation and investigation of Al–4 wt% B4C nanocomposite powders using mechanical milling. *Bulletin of Materials Science*, *34*(5), 1039-1048.

- Allen, K. W. (2005). Adsorption theory of adhesion, in *Handbook of adhesion*, Packham, D. E. (Ed.), John Wiley & Sons.

- Ahmad, Z., Ansell, M. P., & Smedley, D. (2010). Effect of nano-and micro-particle additions on moisture absorption in thixotropic room temperature cure epoxy-based adhesives for bonded-in timber connections. *International Journal of Adhesion and Adhesives*, *30*(6), 448-455.

- Almanza-Workman, A. M., Raghavan, S., Deymier, P., Monk, D. J., & Roop, R. (2002). Water dispersible silanes for wettability modification of polysilicon. *Journal of The Electrochemical Society*, *149*(1), H6-H11.

- Aoqui, S. I., Miyata, H., Ohshima, T., Ikegami, T., & Ebihara, K. (2002). Preparation of boron carbide thin film by pulsed KrF excimer laser deposition process. *Thin Solid Films*, *407*(1), 126-131.

- Ash, M., Ash, I. (1993). *Chemical Tradename Dictionary*, John Wiley & Sons, New York, ISBN 1-56081-625-2.

- ATSDR (2012). *Toxicological Profile For Chromium*, U.S. Department Of Health And Human Services, Public Health Service, Agency for Toxic Substances and Disease Registry.

- ASTM Standard D5379-98 (1998). *Standard Test Method for Shear Properties of Composite Materials by the V-Notched Beam Method.* American Society for Testing and Materials, West Conshohocken, Pennsylvania (first published in May 1993).

- Avella, M., Errico, M. E., Martelli, S., & Martuscelli, E. (2001). Preparation methodologies of polymer matrix nanocomposites. *Applied organometallic chemistry*, *15*(5), 435-439.

- Awaja, F., Gilbert, M., Kelly, G., Fox, B., & Pigram, P. J. (2009). Adhesion of polymers. *Progress in polymer science*, *34*(9), 948-968.

- Baker, A. A., Rose, L. F., & Jones, R. (2003). Advances in the bonded composite repair of metallic aircraft structure (Vol. 1). Elsevier Science.

- Barraza, H. J., Aktas, L., Hamidi, Y. K., Long, J., Edgar, A. O., & Altan, M. C. (2003). Moisture absorption and wet-adhesion properties of resin transfer molded (RTM) composites containing elastomer-coated glass fibers. *Journal of adhesion science and technology*, 17(2), 217-242.

- BASF Chemical Company (2013). *Genamid®151*, Material Safety Data Sheet, v1.2.

- Berg, J. C. (1993). *Wettability*, in Surfactant Science, vol.49. Marcel Dekker

Incorporated.

- Bertelsen, C. M., & Boerio, F. J. (1999). Effect of Processing Variables on the Solution Characteristics of γ-Glycidoxypropyltrimethoxysilane (γ-GPS). *Journal of Adhesion*, 70(3-4), 259-279.

- Bertelsen, C. M., & Boerio, F. J. (2001). Linking mechanical properties of silanes to their chemical structure: an analytical study of γ-GPS solutions and films. Progress in Organic Coatings, 41(4), 239-246.

- Bexell, U., & Olsson, M. (2001). Characterization of a non-organofunctional silane film deposited on Al, Zn and Al–43.4 Zn–1.6 Si alloy-coated steel. *Surface and interface analysis*, *31*(3), 223-231.

- Bexell, U. (2003). *Surface characterisation using ToF-SIMS, AES and XPS of Silane films and organic coatings deposited on metal substrates* (Doctoral dissertation, Uppsala University).

- Bhattacharya, S. N., Gupta, R. K., Kamal, M. R. (2008). *Polymeric nanocomposites: theory and practice*. Carl Hanser Verlag, 233-268.

- Bieleman, J., Heilen, W., Silber, S., Ortelt, M., Scholz, W. (2008). Adhesion Promoters, in Additives for Coatings, Bieleman, J.(Ed.), Wiley-VCH GmbH.

- Bigdeloo, J. A., & Hadian, A. M. (2009). Synthesis of High Purity Micron Size Boron Carbide Powder from B_2O_3/C Precursor. *International Journal of Recent Trends in Engineering, 1*(5), 176-180.

- Biron, M., (2004). *Thermosets and Composites: Technical Information for Plastics Users*, Elsevier Science Ltd.

- Bitrez (2007). *Arapox 60–600. Technical Data Sheet, arapox high performance epoxy resins for the formulation of single and multi-component systems*, V01:01-07.

- Bitrez (2009). *Arapox 60–600*. Safety Data Sheet, Revision date: 01/05/09.

- Brack, N., Rider, A. N., Halstead, B., & Pigram, P. J. (2005). Surface modification of boron fibres for improved strength in composite materials. *Journal of adhesion science and technology*, *19*(10), 857-877.

- Briggs, D., & Grant, J. T. (Eds.). (2003). *Surface analysis by Auger and X-ray photoelectron spectroscopy* (p. 899). Chichester, UK: IM Publications

- Brinker, C. J. & Scherer, G. W. (1990). Sol-Gel Science: The Physics and Chemistry of Sol-Gel Processing. Gulf Professional Publishing, Technology & Engineering, Chapter 3, 223-226.

- BS EN 1389:2003, Advanced technical ceramics - Ceramic composites – Physical properties - Determination of density and apparent porosity, 2003.

- BS EN ISO 3325:1999, Sintered metal materials, excluding hardmetals – Determination of transverse rupture strength, 1999.

- BS EN 12289:2005, Advanced technical ceramics – Mechanical properties of ceramic composites at ambient temperature – Determination of in-plane shear properties, 2005.

- Butt, M. A., Chughtai, A., Ahmad, J., Ahmad, R., Majeed, U., & Khan, I. H. (2008). Theory of Adhesion and its Practical Implications. *Journal of Faculty of Engineering & Technology*, *2007*, 21-45.

- BYK (1998). *Wetting and Dispersing Additives for Solvent-Based and Solvent-*

Free Paint Systems, Data Sheet W5.

- BYK (2008). *BYK-W 920 / 966 / 980*, Data Sheet W503 Issue 05/08.

- BYK (2009). *Anti-Terra®-U*, Material Safety Data Sheet, v2.0, Revision Date 05/04/2009.

- BYK (2011a). *BYK-W 980 / 966, Wetting and Dispersing Additives with Viscosity Reducing and Anti-settling Properties in Adhesives*, Data Sheet ASW3, Issue 02/11.

- BYK (2011b). *BYK-W 980*, Material Safety Data Sheet, v5.0, SDB_GB, Revision Date 17.01.2011.

- Campbell, J., LaSalvia, J., Roy, W., Chin, E., Palicka, R., & Ashkin, D. (2008). *New Low-Cost Manufacturing Methods to Produce Silicon Carbide (SiC) for Lightweight Armor Systems*. Army Research Lab Aberdeen Proving Ground MD.

- Canfer, S., Robertson, S., (2007). *Method for Manufacturing Composite Articles Containing Boron Carbide*. United States Patent 3857744, *U.S. Patent* 2010/0041808 A1.

- Cech, V., Lichovnikova, S., Sova, J. & Studynka, J. (2009). Surface-Free Energy of Silicon-Based Plasma Polymer Films. In: *Silanes and Other Coupling Agents, Volume 5*, Mittal, K . L . (Ed.), CRC Press 333–348.

- Cermignani, W., Paulson, T. E., Onneby, C., & Pantano, C. G. (1995). Synthesis and characterization of boron-doped carbons. *Carbon*, *33*(4), 367-374.

- Chambers, R. C., Jones Jr, W. E., Haruvy, Y., Webber, S. E., & Fox, M. A. (1993). Influence of steric effects on the kinetics of ethyltrimethoxysilane hydrolysis in a fast sol-gel system. *Chemistry of materials*, *5*(10), 1481-1486.

- Chaudhari, P., Meshram, N., Singh, A., Topkar, A., & Dusane, R. (2011). Hot wire chemical vapour deposition (HWCVD) of boron carbide thin films from ortho-carborane for neutron detection application. *Thin Solid Films*, *519*(14), 4561-4564.

- Chehimi, M. M., Azioune, A., Cabet-Deliry, E. (2003). Acid-Base Interactions: Relevance to Adhesion and Adhesion Bonding, in *Handbook of adhesive technology*. 2nd Edition, Pizzi, A., Mittal, K. L., (Ed.), Marcel Dekker.

- Chen, X., Dam, M. A., Ono, K., Mal, A., Shen, H., Nutt, S. R., ... & Wudl, F. (2002). A thermally re-mendable cross-linked polymeric material. *Science*, *295*(5560), 1698-1702.

- Chen, M. W., McCauley, J. W., LaSalvia, J. C. & Hemker, K. J. (2005). Microstructural Characterization of Commercial Hot-Pressed Boron Carbide Ceramics. *Journal of the American Ceramic Society*, 88(7), 1935-1942.

- Chiang, M. Y., & Fernandez-Garcia, M. (2003). Relation of swelling and Tg depression to the apparent free volume of a particle-filled, epoxy-based adhesive. *Journal of applied polymer science*, *87*(9), 1436-1444.

- Chiao, L. (1990). Mechanistic reaction kinetics of 4, 4'-diaminodiphenyl, sulfone cured tetraglycidyl-4, 4'-diaminodiphenylmethane epoxy resins. *Macromolecules*, *23*(5), 1286-1290.

- Choudhury, A. R., Ezz, T., & Li, L. (2007). Synthesis of hard nano-structured metal matrix composite boride coatings using combined laser and sol–gel technology. *Materials Science and Engineering: A*, *445*, 193-202.

- Chow, C. P. L., Xing, X. S., & Li, R. K. Y. (2007). Moisture absorption studies of

sisal fibre reinforced polypropylene composites. *Composites science and technology*, *67*(2), 306-313.

- Cognard, P. (2006). *Handbook of Adhesives and Sealants: General Knowledge, Application of Adhesives, New Curing Techniques*. Elsevier Science.

- Comyn, J. (2006) Theories of Adhesion: in *Handbook of Adhesives and Sealants: General Knowledge, Application of Adhesives, New Curing Techniques*. Elsevier Science, Cognard, P. (Ed.), 1-45

- Comyn, J. (1997). *Adhesion Science* (Vol. 13). Royal Society of Chemistry, 1-43.

- Conde, O., Silvestre, A. J., & Oliveira, J. C. (2000). Influence of carbon content on the crystallographic structure of boron carbide films. *Surface and Coatings Technology*, *125*(1), 141-146.

- Crank, J. (1979). *The mathematics of diffusion*. Oxford university press, Chapter 4, 44-68.

- CRCWI (2002). Cooperative Research Centre for Wood Innovations. Annual Report 2001-2002, 15.

- CRCWI (2003). Cooperative Research Centre for Wood Innovations. Annual Report 2002-2003, 23-24.

- CRCWI (2004). Cooperative Research Centre for Wood Innovations. AnnualKontárová, S. (2012). *Nanolayered Composites* . (Doctoral dissertation, Brno Univerzity Of Technology). Report 2003-2004, 22-23.

- CRCWI (2005). Cooperative Research Centre for Wood Innovations. Annual Report 2004-2005, 21-22.

- Crosslink Tecnhology., (2012). Available from World Wide Web at http://www.crosslinktech.com/support/tips-and-tricks/epoxy-casting-tips.html, accessed on 11/2012.

- d'Almeida, J. R. M., Menezes, G. W. D., & Monteiro, S. N. (2003). Ageing of the DGEBA/TETA epoxy system with off-stoichiometric compositions. *Materials Research*, *6*(3), 415-420.

- Davis, G. D. (2003). Durability of Adhesive Joints, in *Handbook of Adhesive Technology, Revised and Expanded*. Pizzi, A., Mittal, K.L. (Ed.), Marcel Dekker, 273-292.

- Davis, S. R., Brough, A. R., & Atkinson, A. (2003). Formation of silica/epoxy hybrid network polymers. *Journal of non-crystalline solids*, *315*(1), 197-205.

- Davis, S. J., & Watts, J. F. (1996). Organization of methoxysilane molecules on iron. *International journal of adhesion and adhesives*, *16*(1), 5-15.

- Dandekar, D. P. (2001). *Shock response of boron carbide* (No. ARL-TR-2456). Army Research Lab Aberdeen Proving Ground MD.

- Dandekar, D. P., Ciezak, J. A., & Somayazulu, M. (2008). *Compression and Associated Properties of Boron Carbide*. Army Research Lab Aberdeen Proving Ground MD.

- Dawood, M., & Rizkalla, S. (2010). Environmental durability of a CFRP system for strengthening steel structures. *Construction and Building Materials*, *24*(9), 1682-1689.

- De Palma, R., Peeters, S., Van Bael, M. J., Van den Rul, H., Bonroy, K., Laureyn,

W., Mullens, J., Borghs, G., & Maes, G. (2007). Silane ligand exchange to make hydrophobic superparamagnetic nanoparticles water-dispersible. *Chemistry of Materials*, *19*(7), 1821-1831.

- Deflorian, F., Rossi, S., Fedrizzi, L., & Fedel, M. (2008). Integrated electrochemical approach for the investigation of silane pre-treatments for painting copper. *Progress in Organic Coatings, 63*(3), 338-344.

- Deshpande, S. V., Gulari, E., Harris, S. J., & Weiner, A. M. (1994). Filament activated chemical vapor deposition of boron carbide coatings. *Applied physics letters*, *65*(14), 1757-1759.

- Dhakal, H. N., Zhang, Z. Y., & Richardson, M. O. W. (2007). Effect of water absorption on the mechanical properties of hemp fibre reinforced unsaturated polyester composites. *Composites Science and Technology*, *67*(7), 1674-1683.

- Domnich, V., Reynaud, S., Haber, R. A., & Chhowalla, M. (2011). Boron carbide: structure, properties, and stability under stress. Journal of the American Ceramic Society, 94(11), 3605-3628.

- Dow Corning (2005). Product information organofunctional silanes: Dow Corning Z- 6040 silane. Ref. No. 22-1053E-01. Available from World Wide Web at http://www.dowcorning.com/applications/search/products/Details.aspx? prod=01011278&type=&country=GBR, accessed on 08/2012.

- Dow Chemical (2009). "D.E.H.™ 26, Epoxy Curing Agent." Technical data sheet, Form No. 296-01512-0109X-TD.

- Dow Chemical (2009). D.E.R. 331, Material Safety Data Sheet, No. 296-01408-0109X-TD.

- Duffin, A. M., Schwartz, C. P., England, A. H., Uejio, J. S., Prendergast, D., & Saykally, R. J. (2011). pH-dependent x-ray absorption spectra of aqueous boron oxides. The Journal of chemical physics, 134(15), 154503-154503

- Eaton, P., Holmes, P., & Yarwood, J. (2001). In situ and ex situ FTIR–ATR and Raman microscopic studies of organosilane hydrolysis and the effect of hydrolysis on silane diffusion through a polymeric film. Journal of applied polymer science, 82(8), 2016-2026.

- Ebnesajjad, S. (Ed.) (2008). 3 – Material Surface Preparation Techniques, in Adhesives Technology Handbook, William Andrew, 37-46.

- Efimenko, L. N., Lifshits, E. V., Ostapenko, I. T., Snezhko, I. A., & Shevyakova, E. P. (1987). Oxidation of hot-pressed boron carbide. *Powder Metallurgy and Metal Ceramics*, *26*(4), 318-321, cited by Li, Y. Q., & Qiu, T. (2007). Oxidation behaviour of boron carbide powder. *Materials Science and Engineering: A, 444*(1), 184-191.

- Elementis Specialities (2012). *Nonionic Surfactants*. Available from World Wide Web at http://www.elementisspecialties.com/esweb/esweb.nsf/pages/surfactants-nonionicsurfactants, accessed on 07/2012.

- Fernandez-García, M., & Chiang, M. Y. M. (2002). Effect of hygrothermal aging history on sorption process, swelling, and glass transition temperature in a particle-filled epoxy-based adhesive. *Journal of Applied Polymer Science*, *84*(8), 1581-1591.

- Ferreira, M. G. S., Duarte, R. G., Montemor, M. F., & Simões, A. M. P. (2004). Silanes and rare earth salts as chromate replacers for pre-treatments on galvanised steel. *Electrochimica Acta*, *49*(17), 2927-2935.

- Flick, E.W. (1993). *Epoxy Resins, Curing agents, Compounds, and Modifiers – A Industrial Guide*, 2nd Edition, Noyes Publications.

- Frazer, L. (2001). Cars and Environment: Forming Lasting Bonds , Environmental Health Perspectives , 109(9), A430-433.

- Friedrich, F., & Weidler, P. G. (2010). Contact pressure effects on vibrational bands of kaolinite during infrared spectroscopic measurements in a diamond attenuated total reflection cell. *Applied spectroscopy*, *64*(5), 500-506.

- Ghosh, D., Subhash, G., Lee, C. H., & Yap, Y. K. (2007). Strain-induced formation of carbon and boron clusters in boron carbide during dynamic indentation. *Applied Physics Letters*, *91*(6), 061910-061910.

- Gledhill, R.A., Shaw, S.J. and Tod. D.A. (1990). Durability of adhesive-bonded joints employing organosilane coupling agents. I*nternational Journal of Adhesion & Adhesives, 10*(3), 192-198.

- Global Industry Analysts (2012). *Boron Nitride and Boron Carbide: A Global Strategic Business Report*. Available in World Wide Web: http://www.researchandmarkets.com/reports/338568/boron_nitride_and_boron_car bide_global, accessed on 04/2012.

- Goettler, L. A., Lee, K. Y., & Thakkar, H. (2007). Layered silicate reinforced polymer nanocomposites: development and applications. *Polymer Reviews*, *47*(2), 291-317.

- Goldberg, S., Lesch, S. M., & Suarez, D. L. (2000). Predicting boron adsorption by soils using soil chemical parameters in the constant capacitance model. *Soil Science Society of America Journal*, *64*(4), 1356-1363.

- Good, R. J. (1993). Contact angle, wetting, and adhesion: a critical review. In: *Contact Angle, Wettability and Adhesion*. Mittal K. L. (Ed.). VSP, Utrecht, 3–36.

- Grady, D. E. (1994). Shock-wave strength properties of boron carbide and silicon carbide. *Le Journal de Physique IV*, *4*(C8), C8-385.

- Gopalani, D., Jodha, A. S., Das, M. K., Singh, R. K., & Baheti, G. L. (2009). Use of CR-39 films for nuclear radiation shielding efficacy evaluation of lining materials for combat vehicles. *Indian Journal of Physics*, *83*(6), 871-878.

- Gorshenkov, M. V., Kaloshkin, S. D., Tcherdyntsev, V. V., Danilov, V. D., & Gulbin, V. N. (2012). MV Gorshenkov, SD Kaloshkin, VV Tcherdyntsev, VD Danilov, VN Gulbin. *Journal of Alloys and Compounds*, *536*, S126-S129.

- Graf, R. T., Koenig, J. L., & Ishida, H. (1984). Characterization of silane-treated glass fibers by diffuse reflectance Fourier transform spectrometry. *Analytical Chemistry*, *56*(4), 773-778.

- Gutowski, W. S., & Pankevicius, E. R. (1993). A novel surface treatment process for enhanced adhesion of ultra-high modulus polyethylene fibres to epoxy resins. *Composite Interfaces*, *1*(2), 141-151.

- Gutowski, W. S., Wu, D. Y., & Li, S. (1993). Surface silanization of polyethylene for enhanced adhesion. *The Journal of Adhesion*, *43*(1-2), 139-155.

- Gutowski W.S., Wu D.Y., Li S., (1999a). Process improvements for treatment of

TPOs for enhanced adhesion of paints, sealants and adhesives. Society of Plastics Engineers Automotive TPO, Conference proceedings, Troy, Michigan., 20th-22nd Sept.1999, paper 37.

- Franquet, A., Le Pen, C., Terryn, H., & Vereecken, J. (2003). Effect of bath concentration and curing time on the structure of non-functional thin organosilane layers on aluminium. *Electrochimica Acta*, *48*(9), 1245-1255.

- Gutowsky, W.S., Wu, D.Y., Li, S., Cerra, A.P., Petinakis, S., Russell, L., Filippou, C. (1999b). Novel technology for more durable adhesion of structural sealants, self-adhesive tapes and adhesives. Pro 10: 3rd International RILEM Symposium on Durability of Building and Construction Sealants, Wolf, A.T. (Ed.), RILEM Publications SARL, 337-359.

- Gutowski, W.S., Russell, L., Hoobin, P., Filippou, C., Li, S., Bilyk, A. (2000). A novel technology for enhanced adhesion of paints and adhesives to automotive TPOs. In: Proceedings of TPOs in Automotive 2000, 23–25.

- Gutowsky, W.S., Li, S., Russel, L, Filippou, C., Spicer, M., Hoobin, P. (2002a). Molecular brush concepts in surface engineering of polymers for enhanced adhesion of adhesive and polymeric coatings. Mittal, K.L. (Ed.), Adhesive Joints: Formation, Characteristics and Testing, vol.2, 3-48.

- Gutowski, W. V., Li, S., Russell, L., Filippou, C., Hoobin, P., & Petinakis, S. (2002b). Effect of surface-grafted molecular brushes on the adhesion performance of bonded polymers and composite interfaces. *Composite Interfaces*, *9*(1), 89-133.

- Gutowski, W. V. S. (2003). Interface/interphase engineering of polymers for adhesion enhancement: Part I. Review of micromechanical aspects of polymer interface reinforcement through surface grafted molecular brushes. *The Journal of Adhesion*, *79*(5), 445-482.

- Gutowski, W. V. S., Li, S., Filippou, C., Hoobin, P., & Petinakis, S. (2003). Interface/interphase engineering of polymers for adhesion enhancement: Part II. Theoretical and technological aspects of surface-engineered interphase-interface systems for adhesion enhancement. *The Journal of Adhesion*, *79*(5), 483-519.

- Gutowski, W. S., Bilyk, A., Li, S., Espiritu, M., & Burgar, I. (2005). The influence of structure of the interface and interphase on paint adhesion. *Composite Interfaces*, *12*(8-9), 817-835.

- Halverson, D. C., Pyzik, A. J., Aksay, I. A., & Snowden, W. E. (1989). Processing of Boron Carbide-Aluminum Composites. Journal of the American Ceramic Society, 72(5), 775-780.

- Hanoosh, W. S., & Abdelrazaq, E. M. (2009). Polydimethyl Siloxane Toughened Epoxy Resins: Tensile Strength and Dynamic Mechanical Analysis. *Malaysian Polymer Journal*, *4*(2), 52-61.

- Harrison, C., Burgett, E., Hertel, N., & Grulke, E. (2008, January). Polyethylene⁄ Boron Composites for Radiation Shielding Applications. In *AIP Conference Proceedings* (Vol. 969, p. 484).

- Hara, O. (1990). Three Bond Technical News.,32. Available from World Wide Web at http://www.threebond.co.jp/en/technical/technicalnews/pdf/tech32.pdf accessed on 06/2012.

- Hartshorn, D. (2009). Surface Treatment, ChemQuest Group, The Adhesive and Sealant Council, Inc.

- Hayun, S., Rittel, D., Frage, N., & Dariel, M. P. (2008). Static and dynamic mechanical properties of infiltrated B$_4$C–Si composites. Materials Science and Engineering: A, 487(1), 405-409.

- Hearn, N. (2010). *Presentation of techniques for measurement of static surface and interfacial tensions*. In:A Short Course on Chemical Chemistry, Kruss GmbH, Bristol.

- Hoeben, W. F. L. M. (2000). *Pulsed corona-iduced degradation of organic materials in water*. Technische Universiteit Eindhoven.

- Hong, N., Langell, M. A., Liu, J., Kizilkaya, O., & Adenwalla, S. (2010). Ni doping of semiconducting boron carbide. *Journal of Applied Physics*, *107*(2), 024513-024513.

- Hong, N. (2012). An exploration of neutron detection in semiconducting boron carbide. (Doctoral dissertation, Department of Physics and Astronomy, University of Nebraska-Lincoln).

- Honkanen, M., Hoikkanen, M., Vippola, M., Vuorinen, J., Lepistö, T., Jussila, P., ... & Valden, M. (2011). Characterization of silane layers on modified stainless steel surfaces and related stainless steel–plastic hybrids. *Applied Surface Science*, *257*(22), 9335-9346.

- Hu, J. M., Liu, L., Zhang, J. Q., & Cao, C. N. (2006). Effects of electrodeposition potential on the corrosion properties of bis-1, 2-[triethoxysilyl] ethane films on aluminum alloy. *Electrochimica acta*, *51*(19), 3944-3949.

- Huang, G., & Sun, H. (2007). Effect of water absorption on the mechanical properties of glass/polyester composites. *Materials & design*, *28*(5), 1647-1650.

- Huang, Y. P., Feng, H. S., Liang, L., Xu, J., & Zhang, W. J. (2011). Boron Carbide Containing Paint Absorbing and Shielding Neutron Radiation. Journal of Tianjin University, 7, 016.

- Huang, Y., Liang, L., Xu, J., & Zhang, W. (2012). The design study of a new nuclear protection material. *Nuclear Engineering and Design*, 248, 22-27.

- Hudson, J. B. (1998). Atomic Structure of Surfaces, in *Surface Science: An Introduction*, John Wiley & Sons, 3-24.

- Hunt, J. R., Doonan, C. J., LeVangie, J. D., Côté, A. P., & Yaghi, O. M. (2008). Reticular synthesis of covalent organic borosilicate frameworks. *Journal of the American Chemical Society*, *130*(36), 11872-11873.

- Hunstman (2006). Araldite GY 6010, Material Safety Data Sheet, No. 3384.

- Huntsman (2009). *Amine Applications And Properties Data*. Technical Bulletin.

- Iglesias, J. G., González-Benito, J., Aznar, A. J., Bravo, J., & Baselga, J. (2002). Effect of glass fiber surface treatments on mechanical strength of epoxy based composite materials. *Journal of colloid and interface science*, *250*(1), 251-260.

- International Association of Plastics Distribution (2008). IAPD Property Tables - Epoxy Molding and Casting Resins. Available from World Wide Web at http://www.iapd.org/bookstore/property_tables/epoxy.pdf, accessed on 11/2013.

- Iosipescu, N. (1967). New accurate procedure for single shear testing of metals. *Journal of Materials, 2(3)*, 537-566.

- Irfan, M. H. (1998). Epoxies in the construction industry. In *Chemistry and*

Technology of Thermosetting Polymers in Construction Applications, Springer Netherlands, 78-122.

- Ishida, H., & Koenig, J. L. (1978). The reinforcement mechanism of fiber-glass reinforced plastics under wet conditions: A review. *Polymer Engineering & Science*, *18*(2), 128-145.

- Ishida, H., & Miller, J. D. (1984). Substrate effects on the chemisorbed and physisorbed layers of methacryl silane-modified particulate minerals. *Macromolecules*, *17*(9), 1659-1666.

- Ivanova, Y., Vueva, Y., & Fernandes, M. F. V. (2006). Si-OCB Amorphous Materials From Organic-Inorganic Hybrid Precursors. *Journal of the University of Chemical Technology and Metallurgy*, *41*(4), 417-422.

- Jacobsohn, L. G., Schulze, R. K., Maia da Costa, M. E. H., & Nastasi, M. (2004). X-ray photoelectron spectroscopy investigation of boron carbide films deposited by sputtering. *Surface science*, *572*(2), 418-424.

- Jiménez, I., Terminello, L. J., Himpsel, F. J., Grush, M., & Callcot, T. A. (1999). Photoemission, x-ray absorption and x-ray emission study of boron carbides. *Journal of electron spectroscopy and related phenomena*, *101*, 611-615.

- Johnsen, B. B., Olafsen, K., & Stori, A. (2003). Reflection-absorption FT-IR studies of the specific interaction of amines and an epoxy adhesive with GPS treated aluminium surfaces. International journal of adhesion and adhesives, 23(2), 155-163.

- Johnston, E. E., & Ratner, B. D. (1996). Surface characterization of plasma deposited organic thin films. *Journal of electron spectroscopy and related phenomena*, *81*(3), 303-317.

- Jun, J., Kim, J., Bae, Y., & Seo, Y. S. (2011). Enhancement of dispersion and adhesion of B_4C particles in epoxy resin using direct ultrasonic excitation. *Journal of Nuclear Materials*, *416*(3), 293-297.

- Jung, C. H., Lee, M. J., & Kim, C. J. (2004). Preparation of carbon-free B_4C powder from B_2O_3 oxide by carbothermal reduction process. *Materials letters*, *58*(5), 609-614.

- Jung, J., & Kang, S. (2004). Advances in Manufacturing Boron Carbide-Aluminum Composites. *Journal of the American Ceramic Society*, *87*(1), 47-54.

- Kakiage, M., Tominaga, Y., Yanase, I., & Kobayashi, H. (2012). Synthesis of boron carbide powder in relation to composition and structural homogeneity of precursor using condensed boric acid–polyol product. *Powder Technology*, *221*, 257-263.

- Kaloshkin, S. D., Tcherdyntsev, V. V., Gorshenkov, M. V., Gulbin, V. N., & Kuznetsov, S. A. (2012). Radiation-protective polymer-matrix nanostructured composites. *Journal of Alloys and Compounds*, *536*, S522-S526.

- Karaman, M., 2007, Chemical Vapor Deposition Of Boron Carbide, A Thesis Submitted To The Graduate School Of Natural And Applied Sciences Of The Middle East Technical University

- Kavitha, N., Balasubramanian, M., & Kennedy, A. X. (2012). Investigation of impact behavior of epoxy reinforced with nanometer-and micrometer-sized silicon carbide particles. *Journal of Composite Materials*.

- Kelly, E.G., Spottiswood, D.J., 1982, "Introduction to Mineral Processing.", Wiley,

New York;

- Khurmi, R. S., Sedha, R. S. (2008). Bonds in Solids. In: *Materials Science*. S Chand Limited, 91-105.

- Kim, J. G., Park, S. W., Yoon, S. H., & Lee, D. G. (2010a). Optimum silane treatment for the adhesively bonded aluminum adherends at the cryogenic temperature. *Journal of adhesion science and technology*, *24*(4), 775-787.

- Kim, K., Park, S. W., & Yang, S. S. (2010b). The optimization of PDMS-PMMA bonding process using silane primer. BioChip Journal, 4(2), 148-154.

- Kinloch, A. J. (1987). *Adhesion and adhesives: science and technology*. Kluwer Academic Pub.

- Kinloch, A. J., Tan, K. T., & Watts, J. F. (2006). Novel self-assembling silane for abhesive and adhesive applications. *The Journal of Adhesion*, *82*(12), 1117-1132.

- Kjellin, M., & Johansson, I. (Eds.). (2010). *Surfactants from renewable resources*. Wiley Series In Renewable Resources, John Wiley & Sons, Ltd., Part 3. Surface-Active Compounds as Forest-Industry By-Products, 47-49.

- Kokai, F., Taniwaki, M., Takahashi, K., Goto, A., Ishihara, M., Yamamoto, K., & Koga, Y. (2001). Laser ablation of boron carbide: thin-film deposition and plume analysis. *Diamond and related materials*, *10*(3), 1412-1416.

- Kommel, L., & Kimmari, E. (2003). Friction and Wear Changes of Boron Carbide Cermets Depending on the Structure. *Materials Science*, *9*(1), 51-53.

- Kommel, L., & Kimmari, E. (2006). Boron carbide based composites manufacturing and recycling features. *Materials Science*, *12*(1), 48-52.

- Kontárová, S. (2012). *Nanolayered Composites*. (Doctoral dissertation, Brno Univerzity Of Technology).

- Kouzeli, M., San Marchi, C., & Mortensen, A. (2002). Effect of reaction on the tensile behavior of infiltrated boron carbide–aluminum composites. *Materials Science and Engineering: A*, *337*(1), 264-273.

- Kudo, H., Suga, K., & Fujihira, M. (2008). Fabrication of substrates with various wettabilities for DNA molecular combing. *Colloids and Surfaces A: Physicochemical and Engineering Aspects*, *313*, 651-654.

- Kurth, D. G., Broeker, G. K., Kubiak, C. P., & Bein, T. (1994). Surface attachment and stability of cross-linked poly (ethylenimine)-epoxy networks on gold. *Chemistry of materials*, *6*(11), 2143-2150.

- LaSurface, ThermoFisher Scientific. Available from World Wide Web at http://www.lasurface.com/database/elementxps.php, accessed on 09/2012.

- Lazzari, R., Vast, N., Besson, J. M., Baroni, S., & Dal Corso, A. (1999). Atomic Structure and Vibrational Properties of Icosahedral B_ {4} C Boron Carbide. *Physical review letters*, *83*(16), 3230-3233.

- Lee, R. C., Aita, C. R., & Tran, N. C. (1991). The air-exposed surface of sputter deposited silicon carbide studied by x-ray photoelectron spectroscopy. *Journal of Vacuum Science & Technology A: Vacuum, Surfaces, and Films*, *9*(3), 1351-1354.

- Lee, M., & Yoo, Y. H. (2001). Analysis of ceramic/metal armour systems. *International Journal of Impact Engineering*, *25*(9), 819-829.

- Lee, H., & Speyer, R. F. (2003). Pressureless sintering of boron carbide. *Journal of*

the American Ceramic Society, *86*(9), 1468-1473.

- Lee, B. H., Kim, H. S., Lee, S., Kim, H. J., & Dorgan, J. R. (2009). Bio-composites of kenaf fibers in polylactide: Role of improved interfacial adhesion in the carding process. *Composites Science and Technology*, *69*(15), 2573-2579.

- Li, Y. Q., & Qiu, T. (2007). Oxidation behaviour of boron carbide powder. *Materials Science and Engineering: A*, *444*(1), 184-191.

- Lieberman, M. A., Lichtenberg, A. J. (2005). Principles of Plasma Discharges and Materials Processing, 2nd Ed., Wiley-Interscience, New York.

- Lipp, A., Roder, M., Anorg Z., Algemeine Chem, 343, 1, 1966

- Litz, L. M., & Mercuri, R. A. (1963). Oxidation of Boron Carbide by Air, Water, and Air-Water Mixtures at Elevated Temperatures. *Journal of The Electrochemical Society*, *110*(8), 921-925.cited by Li, Y. Q., & Qiu, T. (2007). Oxidation behaviour of boron carbide powder. *Materials Science and Engineering: A*, *444*(1), 184-191.

- Lu, J., Askeland, P., & Drzal, L. T. (2008). Surface modification of microfibrillated cellulose for epoxy composite applications. *Polymer*, *49*(5), 1285-1296.

- Ma, P. C., Kim, J. K., & Tang, B. Z. (2006). Functionalization of carbon nanotubes using a silane coupling agent. *Carbon*, *44*(15), 3232-3238.

- Mailvaganam, N. P. (1997). *Effective Use of Bonding Agents*. Update no.11, Institute for Research in Construction, National Research Council of Canada.

- Maitz, M. F., Gago, R., Abendroth, B., Camero, M., Caretti, I., & Kreissig, U. (2006). Hemocompatibility of low-friction boron–carbon–nitrogen containing coatings. *Journal of Biomedical Materials Research Part B: Applied Biomaterials*, *77*(1), 179-187.

- Manhani, L. G. B., Pardini, L. C., & Levy Neto, F. (2007). Assessment of tensile strength of graphites by the Iosipescu coupon test. *Materials Research*, *10*(3), 233-239.

- Mansour, R., Lafjah, M., Djafri, F., & Bengueddach, A. (2007). Synthesis of Borosilicate Zeotypes by Steam-assisted Conversion Method. *Journal of the Korean Chemical Society*, *51*(2), 178-185.

- Matje, P., Schwetz, K.A. (1988). *Surface oxygen pick up in submicron SiC and B_4C sintering powders at room temperature.* In Ceramic Powder Processing Science, Proceedings of the 2nd International Conference, Hausner, H., Messing,G. L., Hirano, S. (Eds.), Berchtesgaden (Bavaria) FRG, Deutsche Keramische Gesellschaft, 377–384.cited by Li, Y. Q., & Qiu, T. (2007). Oxidation behaviour of boron carbide powder. *Materials Science and Engineering: A*, *444*(1), 184-191.

- Makarenko, G., Kosolapova, T., & Marek, E. (1977). *Tugoplavkie boridi i silizidi*. AN USSR, Naukova dumka, Kiev.

- Markgraf, D. A. (2000). Corona Treatment: An Overview, Enercon Industries Corporation.

- Matisons, J.G. (2009). Silane coupling agents and Glass Fibre Surfaces: A perspective, *Silanes and Other Coupling Agents, Volume 5*, Mittal, K.L. (Ed), 3-22.

- Mauri, F., Vast, N., & Pickard, C. J. (2001). Atomic Structure of Icosahedral B_4C Boron Carbide from a First Principles Analysis of NMR Spectra. *Physical review letters*, *87*(8), 085506.

- May, P. W., Rosser, K. N., Fox, N. A., Younes, C. M., & Beardmore, G. (1997).

Deposition of CVD diamond onto boron carbide substrates. Diamond and Related Materials, 6(2), 450-455.

- Menczel, J. D., & Prime, R. B. (2009). *Thermal Analysis of Polymers, Fundamentals and Applications*. John Wiley & Sons, Inc.

- Miller, A. C., & Berg, J. C. (2003). Effect of silane coupling agent adsorbate structure on adhesion performance with a polymeric matrix. *Composites Part A: Applied Science and Manufacturing*, *34*(4), 327-332.

- Miller, J. D., & Ishida, H. (1986). Quantitative intermolecular reaction of hydrolyzed trialkoxysilanes at submonolayer, monolayer, and multilayer surface coverages. *Langmuir*, *2*(2), 127-131.

- Mittal K.L. (Ed.) (1993). *Contact Angle, Wettability and Adhesion*. VSP, Utrecht, 3–36.

- Mittal, K. L. (Ed.) (2000). *Silanes and Other Coupling Agents, Volume 2*. VSP, Utrecht.

- Mittal, K. L. (Ed.) (2003). *Silanes and Other Coupling Agents, Volume 3* VSP, Utrecht.

- Mondal, S., & Banthia, A. K. (2005). Low-temperature synthetic route for boron carbide. *Journal of the European Ceramic Society*, *25*(2), 287-291.

- Mortensen, M. W., Sørensen, P. G., Björkdahl, O., Jensen, M. R., Gundersen, H. J. G., & Bjørnholm, T. (2006). Preparation and characterization of Boron carbide nanoparticles for use as a novel agent in T cell-guided boron neutron capture therapy. *Applied radiation and isotopes*, *64*(3), 315-324.

- Muralidharan, P., Venkateswarlu, M., & Satyanarayana, N. (2004). Sol–gel synthesis, structural and ion transport studies of lithium borosilicate glasses. *Solid state ionics*, *166*(1), 27-38.

- Naebe, M., Sandlin, J., Crouch, I., & Fox, B. (2011). Novel light-weight Polymer-Ceramic Composites for Ballistic Protection, 16th International Conference on Composite Structures , ICCS 16 , FEUP, Porto.

- Naslain, R., Guette, A., Rebillat, F., Pailler, R., Langlais, F., & Bourrat, X. (2004). Boron-bearing species in ceramic matrix composites for long-term aerospace applications. *Journal of Solid State Chemistry*, *177*(2), 449-456.

- Naviroj, S., Culler, S. R., Koenig, J. L., & Ishida, H. (1984). Structure and adsorption characteristics of silane coupling agents on silica and E-glass fiber; dependence on pH. *Journal of colloid and interface science*, *97*(2), 308-317.

- Neyman, E. M. (2003). *Improvement in Adhesion for the Epoxy-SiC System via Plasma and Silane Surface Modification Techniques*. (Doctoral dissertation, Virginia Polytechnic Institute and State University).

- Nolan, M., Perova, T. S., Moore, R. A., Beitia, C. E., McGilp, J. F., & Gamble, H. S. (2000). Spectroscopic investigations of borosilicate glass and its application as a dopant source for shallow junctions. *Journal of The Electrochemical Society*, *147*(8), 3100-3105.

- O'Connor, D. J., Sexton, B. A., & Smart, R. S. (Eds.). (2003). Surface analysis methods in materials science (Vol. 23). Surface Science, 2nd Edition, Springer-Verlag Berlin Heidelberg, 91-99.

- O'Donoghue, M. W., Graham, R. G., Datta, V. W., Garrett, R. W., & Garrett, J. W.

(2003). Field Performance versus Laboratory Testing: A Study of Epoxy Tank and Vessel Linings Used in the Canadian Oil Patch. *Corrosion 2003*.

- Odegard, G., & Kumosa, M. (2000). Determination of shear strength of unidirectional composite materials with the Iosipescu and 10 off-axis shear tests. *Composites science and technology*, *60*(16), 2917-2943.

- Ohji, T., & Singh, M. (Eds.). (2009). *Advanced processing and manufacturing technologies for structural and multifunctional materials III*. Wiley-American Ceramic Society.

- Okuno, K. (2005). Neutron shielding material based on colemanite and epoxy resin. *Radiation protection dosimetry*, 115(1-4), 258-261.

- Orhan, J. B., Parashar, V. K., Flueckiger, J., & Gijs, M. A. M. (2008). Internal modification of poly (dimethylsiloxane) microchannels with a borosilicate glass coating. *Langmuir*, *24*(16), 9154-9161.

- Packham, D. E. (2005). Contact angles and interfacial tension, in *Handbook of adhesion*, Packham, D. E. (Ed.), John Wiley & Sons .

- Paint & Coating Industries, (2006). Available from World Wide Web at http://www.pcimag.com/articles/amine-curing-of-epoxy-resins-options-and-key-formulation-considerations, accessed on 01/2011.

- Palanivel, V., Zhu, D., & van Ooij, W. J. (2003). Nanoparticle-filled silane films as chromate replacements for aluminum alloys. *Progress in Organic Coatings*, *47*(3), 384-392.

- Palm, P. (2007). Corona treatment for any material thickness. Surface Finishing, Carl Hanser Verlag, Kunststoffe International, 40-42.

- Pantoja, M., Díaz-Benito, B., Velasco, F., Abenojar, J., & Del Real, J. C. (2009). Analysis of hydrolysis process of γ-methacryloxypropyltrimethoxysilane and its influence on the formation of silane coatings on 6063 aluminum alloy. Applied Surface Science, 255(12), 6386-6390.

- Parker, A. A., & Maclachlan, J. (2000). The relationship between silane hydrolysis and polymer adhesion to glass as studied by 13C solid state NMR. *Silanes and Other Coupling Agents, Volume 2*, Mittal, K. L. (Ed), 27.

- Parmenter, K. E., & Milstein, F. (1998). Mechanical properties of silica aerogels. *Journal of non-crystalline solids*, *223*(3), 179-189.

- Patnaik, P. (2003). *Handbook of inorganic chemicals* (Vol. 28). New York: McGraw-Hill.

- Pemble, M. (2009). Chapter 7. Vibrational spectroscopy from surfaces. In: *Surface Analysis – The principal techniques*. J.C. Vickerman, Ed. John Wiley & Sons Ltd, Chichester, England, 267-311.

- Peña-Alonso, R., Rubio Alonso, J., Rubio Alonso, F., & Oteo Mazo, J. L. (2005). Estudio por espectroscopía infrarroja de la reacción de obtención de geles de borosilicato con diferentes relaciones Si/B. *Boletin de la Sociedad Espanõla de Cerámica y Vidro, 44*(6), 387-392.

- Penn, L. S., Wang, H. (1998). Epoxy Resins in: *Handbook of Composites*, Lubin, G., (Ed.), Chapman & Hall, 48-74.

- Peterson, I. R. (2005). Towards a theory of adhesion with predictive power. *Surface Coatings International Part B: Coatings Transactions*, *88*(1), 1-8.

- Petrie, E. M. (2000). *Handbook of Adhesives and Sealants*. McGraw-Hill Professional, New York.

- Petrie, E. M. (2006a). Chapter 10: Adhesion Promoters And Primers. In: *Handbook of adhesives and sealants*, 2nd Ed. McGraw-Hill, New York.

- Petrie, E. M. (2006b). *Epoxy Adhesive Formulations*. McGraw-Hill Companies, Chapter 1-2, 1-42.

- PI-KEM (2011). Boron Carbide, B4C. Material Safety Data Sheet.

- Pierson, H. O. (1992). *Handbook of chemical vapor deposition (CVD): principles, technology, and applications*. Noyes Publications, New Jersey, 204-205.

- Pierson, H. O. (1996). *Handbook Of Refractory Carbides and Nitrides – Properties, Characteristics, Processing and Applications*. Noyes Publications, New Jersey.

- Plueddemann, E. P. (1991). *Silanes Coupling Agents*, 2nd Ed., Plenum Press, New York.

- Pocius, A. V. (2002). Adhesion and adhesives technology: an introduction. 2nd Ed., Hanser Gardner Publications, Cincinnati.

- Pola, J., Herlin-Boime, N., Brus, J., Bastl, Z., Vacek, K., Šubrt, J., & Vorlíček, V. (2005). IR laser production of nanostructured polyborocarbosiloxane powders with SiOB bonds. *Solid state sciences*, *7*(1), 123-131.

- Pugh, V. T. & Hendy, B. W., (1985). *Crispy Mix and Flexy Mix - high boron carbide content resin bonded neutron shielding materials*. ICANS VIII, 670.

- Ratner, B. D., Castner, D.G. (2009). Chapter 3. Electron spectroscopy for chemical analysis. In: Surface Analysis – The principal techniques. J.C. Vickerman, Ed. John Wiley & Sons Ltd, Chichester, England. 43-98.

- Rattana, A., Hermes, J. D., Abel, M. L., & Watts, J. F. (2002). The interaction of a commercial dry film adhesive with aluminium and organosilane treated aluminium surfaces: a study by XPS and ToF-SIMS. *International journal of adhesion and adhesives*, *22*(3), 205-218.

- Rattana, A., Abel, M. L., & Watts, J. F. (2006). ToF-SIMS studies of the adsorption of epoxy resin molecules on organosilane-treated aluminium: adsorption kinetics and adsorption isotherms. *International journal of adhesion and adhesives*, *26*(1), 28-39.

- Ray, B. C. (2006). Temperature effect during humid ageing on interfaces of glass and carbon fibers reinforced epoxy composites. *Journal of Colloid and Interface Science*, *298*(1), 111-117.

- Real, J. D., De Santayana, M. C., Abenojar, J., & Martinez, M. A. (2006). Adhesive bonding of aluminium with structural acrylic adhesives: durability in wet environments. *Journal of adhesion science and technology*, *20*(16), 1801-1818.

- Reichenbächer, M., Pop, J. (2012). Interpretation of Vibrational Spectra of Organic Molecules. In: *Challenges in Molecular Structure Determination*, Springer-Verlag Berlin Heidelberg, 123.

- Reynaud, S. (2010). *Fabrication and characterization of carbon and boron carbide nanostructured materials* (Doctoral dissertation, Rutgers University-Graduate School-New Brunswick).

- Richard P. W. (2005). Polymer diffusion: reptation and interdigitation, in *Handbook of adhesion*, Packham, D. E. (Ed.), John Wiley & Sons .

- Rider, A. N. (2006). Factors influencing the durability of epoxy adhesion to silane pretreated aluminium. *International journal of adhesion and adhesives, 26*(1), 67-78.

- Riekerink, M. O., Engbers, G. H. M., & Feijen, J. (2001). Gas plasma etching of adsorbed protein-gold colloids as a tool for surface nanostructuring: Surface preparation and chemical modification. *Structural And Chemical Modification Of Polymer Surfaces By Gas Plasma Etching*, 103.

- Roche, A., Dumas, J., Quinson, J. F., & Romand, M. (1991). in: D. Baptiste (Ed.), Mechanics and Mechanisms of Damage in Composite and Multimaterials", Mech. Eng. Publ., London, 1991, 269

- Rodgers, R. M., Mahfuz, H., Rangari, V. K., Chisholm, N., & Jeelani, S. (2005). Infusion of SiC Nanoparticles Into SC-15 Epoxy: An Investigation of Thermal and Mechanical Response. *Macromolecular Materials and Engineering, 290*(5), 423-429.

- Rodríguez, M. G., Kharissova, O. V., & Ortiz-Mendez, U. (2004). Formation of boron carbide nanofibers and nanobelts from heated by microwave. *Rev. Adv. Mater. Sci, 7*(1), 55-60.

- Roy, T. K., Subramanian, C., & Suri, A. K. (2006). Pressureless sintering of boron carbide. *Ceramics international, 32*(3), 227-233.

- Rybakov, S. Y., Sharapov, V. M., & Gavrilov, L. E. (1995). Oxygen effect on the stability of PECVD boron-carbon films. *Le Journal de Physique IV, 5*(C5), C5-921.

- Sandler, S. R., Karo, W., Bonesteel, J-A., Pearce, E. M. (1998). Dynamic Mechanical Analysis. In: *Polymer Synthesis and Characterization: A Laboratory Manual*. Academic Press, 189-206.

- Sano, T., Chin, E. S. C., Paliwal, B., & Chen, M. W. (2009). Comparison of Slip Cast to Hot Pressed Boron Carbide. *Processing and Properties of Advanced Ceramics and Composites: Ceramic Transactions*, 107.

- Sapieha, S., Cerny, J., Klemberg-Sapieha, J. E., & Martinu, L. (1993). Corona versus low pressure plasma treatment: effect on surface properties and adhesion of polymers. *The Journal of Adhesion, 42*(1-2), 91-102.

- Sato, T., Haryu, K., Endo, T., & Shimada, M. (1988). Oxidation of nonoxide ceramics by water vapor at high temperatures. *Japan Society of Materials Science, Journal, 37*, 77-82. cited by Steinbrück, 2005; Steiner, 2005.

- Savio, S. G., Ramanjaneyulu, K., Madhu, V., & Bhat, T. B. (2011). An experimental study on ballistic performance of boron carbide tiles. *International Journal of Impact Engineering, 38*(7), 535-541.

- Schiavon, M. A., Armelin, N. A., & Yoshida, I. V. P. (2008). Novel poly (borosiloxane) precursors to amorphous SiBCO ceramics. *Materials Chemistry and Physics, 112*(3), 1047-1054.

- Schultz, J., & Nardin, M. (2003). Theories and mechanisms of adhesion. *Handbook of adhesive technology*. 2nd Ed. Pizzi,. A., Mittal, K. L (Ed.), Marcel Dekker Inc, New York.

- Shi, L., Gu, Y., Chen, L., Qian, Y., Yang, Z., & Ma, J. (2003). A low temperature

synthesis of crystalline B$_4$C ultrafine powders. *Solid state communications*, *128*(1), 5-7.

- Shi, Q., Wang, L., Yu, H., Jiang, S., Zhao, Z., & Dong, X. (2006). A novel epoxy resin/CaCO3 nanocomposite and its mechanism of toughness improvement. *Macromolecular Materials and Engineering*, *291*(1), 53-58.

- Shorowordi, K. M., Laoui, T., Haseeb, A. S. M. A., Celis, J. P., & Froyen, L. (2003). Microstructure and interface characteristics of B$_4$C, SiC and A$_{12}$O$_3$ reinforced Al matrix composites: a comparative study. *Journal of Materials Processing Technology*, *142*(3), 738-743.

- Shukla, D. K., Kasisomayajula, S. V., & Parameswaran, V. (2008). Epoxy composites using functionalized alumina platelets as reinforcements. Composites Science and Technology, 68(14), 3055-3063.

- Sigma-Aldrich (2010). *440167 Aldrich*. Available from World Wide Web at (http://www.sigmaaldrich.com/catalog/product/aldrich/440167? lang=en&region=GB, accessed on 01/2011.

- Silva, L. F. M., & Ochsner, A. (Ed.) (2008). Adhesively bonded Joint composites, the Concept of the Interphase, in *Modeling of Adhesive Bonded Joints*, Springer-Verlag Berlin Heidelberg, 111-119.

- Singhal, S. K., & Singh, B. P. (2006). Sintering of boron carbide under high pressures and temperatures. *Indian Journal Of Engineering And Materials Sciences*, *13*(2), 129.

- Siqueira, R. L., Yoshida, I. V. P., Pardini, L. C., & Schiavon, M. A. (2007). Poly (borosiloxanes) as precursors for carbon fiber ceramic matrix composites. *Materials Research*, *10*(2), 147-151.

- Skorokhod, V., & Krstic, V. D. (2000). High strength-high toughness B4C-TiB2 composites. *Journal of materials science letters*, *19*(3), 237-239.

- Shorowordi, K. M., Laoui, T., Haseeb, A. S. M. A., Celis, J. P., & Froyen, L. (2003). Microstructure and interface characteristics of B$_4$C, SiC and Al$_2$O$_3$ reinforced Al matrix composites: a comparative study. *Journal of Materials Processing Technology*, *142*(3), 738-743.

- Smeacetto, F., Salvo, M., & Ferraris, M. (2002). Oxidation protective multilayer coatings for carbon–carbon composites. *Carbon*, *40*(4), 583-587.

- Smith, R. E. (2009). Surface Energy Data for Epoxies and epoxy resins. Diversified Enterprises . Available from World Wide Web at http://www.accudynetest.com/polymer_surface_data/epoxy.pdf accessed on 03/2012.

- Sreekala, M. S., Kumaran, M. G., & Thomas, S. (2002). Water sorption in oil palm fiber reinforced phenol formaldehyde composites. *Composites Part A: Applied science and manufacturing, 33*(6), 763-777.

- Steinbrück, M. (2005). Oxidation of boron carbide at high temperatures. *Journal of nuclear materials*, *336*(2), 185-193.

- Steiner, H. (2005). Modeling of boron carbide oxidation in steam. *Journal of nuclear materials*, *345*(1), 75-83.

- STFC (2009). *All about ISIS*. Available on World Wide Web at http://www.isis.stfc.ac.uk/about-isis/, accessed on 02/2012.

- Subramanian, C., Suri, A. K., & Murthy, T. C. (2010). Development of Boron-based materials for nuclear applications. *In the Forthcoming issue*, 312, 14-22.

- Summers, W. (1983). *Board scope particle size reduction by means of vibratory grinding*, J. Am. Ceram. Soc. Bull. 62 2, 212–215, cited by Yuan (2003).

- Sun, G., Li, Y. W., Hu, Q. K., Wu, Q. H., & Yu, D. L. (2009). Non-stoichiometric boron carbide synthesized in moderate temperature conditions. *Materials Science-Poland*, *27*(4/1).

- Suresha, B., Chandramohan, G., Jawahar, M. A., & Mohanraj, S. (2009). Three-body Abrasive Wear Behavior of Filled Epoxy Composite Systems. *Journal of Reinforced Plastics and Composites*, *28*(2), 225-233.

- Suri, A.K., Krishnamurthy, N., & Subramanian, C. (2009). Issues in the Synthesis and Fabrication of Refractory Carbides, Borides, Silicides and their Mixture. Advanced Processing and Manufacturing Technologies for Structural and Multifunctional Materials III, Ohji, T., Singh, M., Singh, D., Salem, J. (Ed.), *Ceramic Engineering and Science Proceedings, 30*(8), 69-71.

- Suryanarayana, C. (2001). Mechanical alloying and milling. *Progress in materials science*, *46*(1), 1-184.

- Tang, X., Whitcomb, J. D., Li, Y., & Sue, H. J. (2005). Micromechanics modeling of moisture diffusion in woven composites. Composites Science and Technology, 65(6), 817-826.

- Tesoro, G., & Wu, Y. (1991). Silane coupling agents: the role of the organofunctional group. *Journal of adhesion science and technology*, *5*(10), 771-784.

- Thévenot, F. (1990). Boron carbide—a comprehensive review. *Journal of the European Ceramic Society*, *6*(4), 205-225.

- Thwe, M. M., & Liao, K. (2002). Effects of environmental aging on the mechanical properties of bamboo–glass fiber reinforced polymer matrix hybrid composites. *Composites Part A: Applied Science and Manufacturing*, *33*(1), 43-52.

- Toumanov, I. N. (2003). *Plasma and high frequency processes for obtaining and processing materials in the nuclear fuel cycle*, Nova Publishers, New York, 247-316.

- Tsubota, T., Tanii, S., Ishida, T., Nagata, M., & Matsumoto, Y. (2005). Composite electroplating of Ni and surface-modified diamond particles with silane coupling regent. *Diamond and related materials*, *14*(3), 608-612.

- Tuominen, M., Lahti, J., Lavonen, J., Penttinen, T., Räsänen, J. P., & Kuusipalo, J. (2010). The influence of flame, corona and atmospheric plasma treatments on surface properties and digital print quality of extrusion coated paper. *Journal of Adhesion Science and Technology*, *24*(3), 471-492.

- Uehara, Tohru (1999). Chapter7 - Corona Discharge Treatment of Polymers. In: *Adhesion Promotion Techniques, Technological Applications*. Mittal, K.L., Pizzi, A. (Eds.), Marcel Dekker.

- ULIDES (2013). Epoxy (Epoxy) plastics - Typical Properties and Processing Information. Available from World Wide Web at http://plastics.ides.com/generics/13/epoxy-epoxy, accessed on 11/2013.

- Underhill, P. R., Goring, G., & DuQuesnay, D. L. (1998). A study of the deposition of 3-glycidoxypropyltrimethoxysilane on aluminum. International journal of adhesion and adhesives, 18(5), 307-311.

- Underhill, P. R., & DuQuesnay, D. L. (2006). The role of corrosion/oxidation in the failure of aluminum adhesive joints under hot, wet conditions. International journal of adhesion and adhesives, 26(1), 88-93.

- Van Ooij, W. J., & Sabata, A. (1991). Characterization of films of organofunctional silanes by TOFSIMS and XPS. *Journal of adhesion science and technology*, *5*(10), 843-863.

- Van Ooij, W. J., Zhu, D. Q., Prasad, G., Jayaseelan, S., Fu, Y., & Teredesai, N. (2000). Silane based chromate replacements for corrosion control, paint adhesion, and rubber bonding. *Surface Engineering*, *16*(5), 386-396.

- Van Ooij, W. J. (2004). Replacement of chromates by silanes–an overview. In *Proc. International Conference on Environmental Friendly Pre-treatments for Aluminium and other Metals ICEPAM 2004*.

- Van Ooij, W. J., Zhu, D., Palanivel, V., Lamar, J. A., & Stacy, M. (2006). Overview: The Potential of silanes for chromate replacement in metal finishing industries. *Silicon Chemistry*, *3*(1-2), 11-30.

- Van Schaftinghen, T., Le Pen, C., Terryn, H., & Hörzenberger, F. (2004). Investigation of the barrier properties of silanes on cold rolled steel. *Electrochimica acta*, *49*(17), 2997-3004.

- Vandenberg, E. T., Bertilsson, L. B., Kasjsa Uvdal, B. L., Erlandsson, R., Elwing, H. & Lungstrom, I. (1991). Structure of 3-aminopropyl triethoxy silane on silicon oxide. *Journal of Colloid and Interface Science*, 147(1), 103-118.

- Vano, M. (2008). *A study into the mechanical properties and clinical aspects*

- *of fiber posts*. (Doctoral dissertation, University of Siena).

- Velamakanni, A., Ganesh, K. J., Zhu, Y., Ferreira, P. J., & Ruoff, R. S. (2009). Catalyst-Free Synthesis and Characterization of Metastable Boron Carbide Nanowires. Advanced Functional Materials, 19(24), 3926-3933.

- Vogt, R. G., Zhang, Z., Topping, T. D., Lavernia, E. J., & Schoenung, J. M. (2009). Cryomilled aluminum alloy and boron carbide nano-composite plate. *Journal of Materials Processing Technology*, *209*(11), 5046-5053.

- Wagner, C. D., Riggs, W. M., Davis, L. E., Moulder, J. F., & Muilenburg, G. E. (1979). *Handbook of X-Ray Photoelectron Spectroscopy*, Perkin Elmer: Eden Prairie, Appendix 3.

- Wagner, C. D., Briggs, D., & Seah, M. P. (1990). Practical surface analysis. *Auger and X-ray Photoelectron Spectroscopy*, *1*, 595.

- Walker, P. (1991). Organosilanes as adhesion promoters. *Journal of Adhesion Science and Technology*, *5*(4), 279-305.

- Walrath, D. E., & Adams, D. F. (1983). The Iosipescu shear test as applied to composite materials. *Experimental Mechanics*, *23*(1), 105-110.

- Wang, Q., Xia, H., & Zhang, C. (2001). Preparation of polymer/inorganic nanoparticles composites through ultrasonic irradiation. *Journal of applied polymer science*, *80*(9), 1478-1488.

- Wang, B. (2004). *Pre-treatment of flax fibers for use in rotationally molded biocomposites* (Doctoral dissertation, University of Saskatchewan), 69.

- Wang, J., Guo, Q., Liu, L., & Song, J. (2005). The preparation and performance of high-temperature adhesives for graphite bonding. *International journal of adhesion and adhesives*, *25*(6), 495-501.

- Wang, J., Jiang, N., & Jiang, H. (2006a). The high-temperatures bonding of graphite/ceramics by organ resin matrix adhesive. *International journal of adhesion and adhesives*, *26*(7), 532-536.

- Wang, C., Huang, Y. D., & Wang, B. (2006b). Study on heat-resistant property of adhesive/carbon–carbon composites joints. *International journal of adhesion and adhesives*, *26*(4), 206-211.

- Warson, H., Finch, C. A. (2001). Applications of Synthetic Resin Latices, Volume 1, Fundamental Chemistry of Latices & Applications in Adhesives, John Wiley & Sons, 476.

- Watts, J. F., & Wolstenholme, J. (2003). *An Introduction to Surface Analysis by XPS and AES*, John Wiley & Sons, 79-86.

- Werheit, H. (2007). Are there bipolarons in icosahedral boron-rich solids?. *Journal of Physics: Condensed Matter*, *19*(18), 186207.

- Wentorf, R. H., DeVries, R. C., & Bundy, F. P. (1980). Sintered superhard materials. *Science*, *208*(4446), 873-880.

- White, S. R., Sottos, N. R., Geubelle, P. H., Moore, J. S., Kessler, M., Sriram, S. R., ... & Viswanathan, S. (2001). Autonomic healing of polymer composites. Nature, 409(6822), 794-797.

- Widsten, P., Gutowski, V. S., Li, S., Cerra, T., Molenaar, S., & Spicer, M. (2006). Factors influencing timber gluability with one-part polyurethanes–studied with nine Australian timber species. Holzforschung, 60(4), 423-428.

- Wróblewska, A., Fajdek, A., Milchert, E., & Grzmil, B. (2010). The Ti-MWW catalyst-its characteristic and catalytic properties in the epoxidation of allyl alcohol by hydrogen peroxide. *Polish Journal of Chemical Technology*, *12*(1), 29-34.

- Xie, Y., Hill, C. A., Xiao, Z., Militz, H., & Mai, C. (2010). Silane coupling agents used for natural fiber/polymer composites: A review. *Composites Part A: Applied Science and Manufacturing*, *41*(7), 806-819.

- Xu, D. (2004). *Durability and adhesion of a model epoxy adhesive bonded to modified silicon substrates* (Doctoral dissertation, Virginia Polytechnic Institute and State University).

- Xu, Z., Jia, M. (2007). Modification of boron carbide and its application in the silicone coating. Journal of Beijing University of Chemical Technology, Natural Science Edition, 34 (2), 52-56.

- Xue, G., Koenig, J. L., Ishida, H., & Wheeler, D. D. (1991). Chemical reactions of an epoxy-functional silane in aqueous solutions. *Rubber chemistry and technology*, *64*(2), 162-171.

- Yanase, I., Ogawara, R., & Kobayashi, H. (2009). Synthesis of boron carbide powder from polyvinyl borate precursor. *Materials Letters*, *63*(1), 91-93.

- Zakhariev, Z., Beshkova, M., Blaskov, V., Stambolova, I., & Perchemliev, C.

(2009). New superhard B12-nC3Men boride. *Journal of optoelectronics and adavnced materials*, *11*(10), 1533-1536.

- Zeng, Y., Ding, C., & Lee, S. W. (2001). Young's modulus and residual stress of plasma-sprayed boron carbide coatings. *Journal of the European Ceramic Society*, *21*(1), 87-91.

- Zha, C., Atkins, G. R., & Masters, A. F. (1998). A spectroscopic study of an anhydrous tetraethyl orthosilicate-boric acid-ethanol system. *Journal of sol-gel science and technology*, *13*(1-3), 103-107.

- Zhang, H., Huang, R. J., Li, L. F., & Evans, D. (2008, March). Properties of some toughened, radiation stable epoxy resins. In *AIP Conference Proceedings* (Vol. 986, p. 174).

- Zhou, M. J., Wong, S. F., Ong, C. W., & Li, Q. (2007). Microstructure and mechanical properties of B$_4$C films deposited by ion beam sputtering. *Thin Solid Films*, 516(2), 336-339.

- Zhou, T., Wang, X., Mingyuan, G. U., & Liu, X. (2008). Study of the thermal conduction mechanism of nano-SiC/DGEBA/EMI-2, 4 composites. *Polymer*, *49*(21), 4666-4672.

- Zhu, D., & Van Ooij, W. J. (2004). Corrosion protection of metals by water-based silane mixtures of bis-[trimethoxysilylpropyl] amine and vinyltriacetoxysilane. *Progress in Organic Coatings*, *49*(1), 42-53.

List of Journal Publications and Conference Papers by the Author

- Rodrigues, D.D., & Broughton, J.G. (2013). Silane Surface Modification Of Boron Carbide In Epoxy Composites. *International Journal of Adhesion and Adhesives 46*, 62–73.

- Rodrigues, D.D. , Broughton, J.G., Abel, M.-L., & Watts, J.F. (2013). The effect of silane treatment on the surface chemistry of boron carbide. Adhesion '13 - Twelfth International Conference on the Science and Technology of Adhesion and Adhesives, University of York, UK.

- Rodrigues, D.D., Winfield, P.H., & Morrey, D. (2013). Disbonding Technology for Adhesive Reversible Assembly in the Automotive Industry. *Materials Science Forum Volume 765*, 766–770.

- Rodrigues, D.D., & Broughton, J.G. (2011). Surface modification of boron carbide for improved adhesion in epoxy composites. Adhesion '11 - Eleventh International Conference on the Science and Technology of Adhesion and Adhesives, University of York, UK.

- Rodrigues, D.D., Custódio, J., Rosa, A., Ferreira, J., & Cruz, H. (2008). Thermal behavior of epoxy and polyurethane adhesives and bonded timber joints – preliminary results. COST ACTION E34, Final Conference on Bonding of Timber, Enhancing Bondline Performance, Sopron, Hungary.

- Custódio, J., Rodrigues, D.D. & Cruz, H. (2008). Can Tg be used as a service temperature indicator for the selection of a structural adhesive?, WCTE – World Conference on Timber Engineering, Miyazakyi, Japan.

- Rodrigues, D.D, Custódio, J., & Cruz, H. (2007). Selection of adhesives and quality control of structural repairs by bonding on site. COST ACTION E34 – 4th Workshop, Larnaka, Cyprus.

Table A.1 Appearance and physio-chemical properties of the adhesive components (Bitrez 2007, 2009; Air Products, 2001b, 2004, 2008; BYK 2008, 2011a, 2011b).

Properties	Component		
	Epoxy resin	**Curing agent**	**Wetting agent**
Colour	Amber	Amber	Brown
Form	Viscous liquid	Liquid	Liquid
Odour	Low resinous	Irritating	Alcohol
Refractive index (@20°C)	-	-	1.478
Viscosity (cP@25°C)	115-125	250	-
Amine value (mg KOH/g)	-	420	30
Acid value (mg KOH/g)	-	-	40
Volatile by volume (%)	0	-	20
Density (g/cm3)	1.16	0.95	0.99
pH	7.0	> 7	-
Boiling point (°C)	200	> 204.44	137
Flash point (°C)	>1 50	195, 160 (closed cup)	66
Explosion Limits (vol%)		-	1.0 - 10.6
Equivalent Wt/{H}	-	105	-
Recommended Use Level (phr, EEW = 190)	180 - 190	55	-
Water solubility	Insoluble	Slightly soluble	Insoluble

Table A.2 Boron carbide nomenclature, identifiers and properties (Pierson 1992, Thevenot 1990, Suri 2009, May 1997, Aoqui 2002).

Nomenclature	IUPAC	Boron carbide
	Others	Tetrabor, B4-C, B4C, Black Diamond
Identifiers	CAS number	12069-32-8
	PubChem (CID)	123279
	InChIKey	INAHAJYZKVIDIZ-UHFFFAOYSA-N
	ChemSpider ID	109889
General Properties	Molecular formula	B_4C
	Molar mass (g/mol)	55.25
	Acidity (pK_a)	6 – 7 (20ºC)
	Appearance	Dark gray-black, crystal/powder, odourless
	Melting point (ºC)	2350-2450
	Boiling point (ºC)	>3500
Chemical resistance	Acids (concentrated/dilute)	Fair/Good
	Alkalis	Fair
	Halogens	Fair
	Metals	Fair
Physical properties	Density (g/cm3)	2.48 - 2.52 (solid)
	Specific gravity	2.51
	Solubility in water	Insoluble
	Crystal structure	Rhombohedral / Orthorhombic
	Apparent porosity (%)	< 3
Mechanical properties	Hardness (Knoop/Vickers) (GPa)	27.5 – 34.3 / 31.4
	(Mohs)	9.5
	Modulus of Elasticity (GPa)	352 – 455
	Flexural strength (MPa)	330 – 400
	Compressive strength (MPa)	1400 – 3400
	Poisson's ratio	0.16 – 0.21
	Fracture toughness ($MPa.m^{1/2}$)	2.9 – 3.7
	Tensile modulus (GPa)	440 – 470
	Tensile strength (MPa)	350
Electrical properties	Volume resistivity (ohm.cm)	0.1 – 10 (25ºC)
	Conductivity (S)	140 (25°C)
Thermal properties	Coef. of thermal expansion (/ºC)	$5.0 – 5.6 \times 10^{-6}$ (20 – 1000ºC)
	Conductivity (W/m/K)	33 – 92 (20ºC)
	Specific heat ($J.K^{-1}.kg^{-1}$)	950 (25°C)
	Max. working temperature (ºC)	600 (oxidising atmosphere)
		2000 (reducing atmosphere)
	Neutron capture cross-section (barn)	600
	Upper continuous use temperature (ºC)	600 – 800

Table A.3 Instrumentation used for the surface polishing of the sintered BC.

Instrumentation		Description
Device	Buehler Metaserv	Motopol sample holder and 12" rotary grinder/polisher
	Olympus BX51M (BX2 series)	Optical microscope Binocular WH10X/22, Objectives x5, x10, x20, x50 and x100 JVC colour video digital camera, 800x600 resolution, grayscale a4i Docu v5.1.0.1766 build 20030220-SR1(030710) software, aquinto AG
	Decon 5200b	Heat and ultrasound bath for
Cloth	MD-Piano 600	Magnetic disc with diamond particles bonded in resin for fine grading of hard materials HV150-2000. Surface finish comparable to SiC-paper grit 600.
	MD-Allegro	Magnetic composite disc for one-set fine grinding for hard materials >HV 150
	MD-Dac	Self-adhesive polishing cloth made of satin woven acetate for polishing medium resilience and hard materials
	MD-Dur	Self-adhesive cloth of 100% pure silk thin textile, which give a very stiff support and high degree of planeness
Lubricant	DiaPro Allegro	Fine diamond suspension (9 μm) for 2nd stage of grinding
	DiaPro Dac	Fine diamond suspension (3 μm) for 1st stage of polishing
	DiaPro Nap B	Fine diamond suspension (1 μm) for 2nd stage of polishing

Table A.4 General information and physico-chemical properties of the silane coupling agent.

Nomenclature	IUPAC Others	Silane, trimethoxy[3-(oxiranylmethoxy)propyl]- 3-glycidyloxypropyl-trimethoxysilane Glycidyl 3-(trimethoxysilyl)propyl ether 3-(2,3-Epoxypropoxy)propyltrimethoxysilane
Identifiers	CAS number PubChem EC Number	2530-83-8 87570394 219-784-2
General Properties	Molecular formula Molar mass (g/mol) Purity (%) Appearance Odour Storage (ºC)	$C_9H_{20}O_5Si$ 236.34 ≥ 98 Colourless transparent liquid Mild 2 - 8
Physico-chemical Properties	Density (g/cm3) Specific gravity Refractive index n20/D Viscosity @25ºC (cP) Melting point (ºC) Boiling point (ºC) Flash point (ºC) Ignition temperature (ºC) Lower explosion limit Moisture resistance	1.07 1.07 1.429 3 - 4 -50 or <-70 20 at 3 hPa – lit. or 2 torr / 290 110, 135- close cup 400 0.43% (V) Sensitive

Table A.5 Surface energy and contact angles obtained for cured epoxy adhesives using various methods (Smith 2009).

Epoxy adhesive	Data[*]
Amine curing agent	$\gamma_C = 44$ mJ/m^2
DGEBA-amine	$\gamma_C = 43\text{-}47$ mJ/m^2
E11 cured 1h at 80°C	$\theta_W^Y = 54°$, $\theta_W^A = 90°$, $\theta_W^R = 18°$, $d\theta_W = 72°$
	$\theta_W^A = 85°$
DGEBA w/ 6%wt of N-N-diethylaminopropylamine	$\gamma_S = 46.8$ mJ/m^2
DGEBA w/ triethylenetetramine	$\gamma_S = 39.1$ mJ/m^2; $\gamma_s^D = 32.6$; $\gamma_s^P = 6.5$
Commercial 2k acid-cured epoxy	Various probe liquids. Geometric mean equation. $\gamma_S = 42.6$ mJ/m^2; $\gamma_s^D = 42.6$, $\gamma_s^P = 0.0$
E11 cured 1h at 80°C	$\gamma_S = 51.6$ mJ/m^2; $\gamma_s^D = 32.6$; $\gamma_s^P = 19.0$.
Rubber modified	$\gamma_S = 45.5$ mJ/m^2; $\gamma_s^d = 37.2$; $\gamma_s^p = 8.3$
Amine cured	$\gamma_S = 46.2$ mJ/m^2; $\gamma_s^d = 41.2$; $\gamma_s^p = 5.0$

[*] Symbols: γ – surface free energy; θ – contact angle; dθ – Contact angle hysteresis. Subscripts: C – critical, S – solid, W – water. Superscript: D – dispersive, P – polar, Y – Young's/Equilibrium, A – advancing, – R retreating.

Table A.6 Surface free energy of the silane treated BC using various solution pH and GPS concentrations.

BC surface	Surface free energy (mJ/m^2)				
	Total	γ_s^{LW}	γ_s^{AB}	γ_s^+	γ_s^-
Untreated	52.5	33.7	18.8	16.5	5.4
Corona	64.3	38.6	25.7	44.9	3.7
pH3, 0.5% GPS	38.2	34.1	4.1	2.3	1.8
pH3, 1.0% GPS	43.3	36.3	7.0	7.0	1.8
pH3, 3.0% GPS	42.7	37.9	4.8	2.8	2.1
pH5, 0.5% GPS	40.3	35.4	4.9	4.8	1.3
pH5, 1.0% GPS	40.6	37.5	3.1	13.2	0.2
pH5, 3.0% GPS	42.5	38.6	3.8	2.4	1.5
pH7, 0.5% GPS	37.0	33.9	3.1	2.1	1.1
pH7, 1.0% GPS	36.8	34.3	2.6	2.1	0.8
pH7, 3.0% GPS	42.6	38.0	4.7	3.9	1.4
pH9, 0.5% GPS	43.7	37.2	6.5	4.9	2.2
pH9, 1.0% GPS	40.5	33.7	6.8	4.9	2.3
pH9, 3.0% GPS	40.1	33.7	6.4	8.3	1.2

Table A.7 Contact angles of the probe liquids and surface free energy on silane treated BC using various solution pH and GPS concentrations.

BC surface	Contact angle (º, degrees)		
	H_2O	CH_2I_2	$C_3H_8O_3$
Untreated	51.0 ± 4.3	51.0 ± 3.9	31.0 ± 3.9
Corona	7.3 ±	42.0 ± 1.5	0.0 ±
pH3, 0.5% GPS	81.5 ± 1.2	50.4 ± 1.7	61.4 ± 1.5
pH3, 1.0% GPS	71.1 ± 2.7	46.3 ± 1.2	54.8 ± 2.1
pH3, 3.0% GPS	80.3 ± 0.6	45.1 ± 2.1	56.4 ± 1.1
pH5, 0.5% GPS	77.2 ± 3.0	48.0 ± 2.5	61.0 ± 2.0
pH5, 1.0% GPS	75.0 ± 2.9	44.1 ± 2.2	63.9 ± 0.6
pH5, 3.0% GPS	79.4 ± 0.6	41.9 ± 0.6	58.7 ± 1.2
pH7, 0.5% GPS	84.4 ± 0.4	50.7 ± 2.0	66.2 ± 2.1
pH7, 1.0% GPS	85.7 ± 2.2	50.0 ± 1.5	68.6 ± 0.9
pH7, 3.0% GPS	79.1 ± 1.9	44.1 ± 1.5	59.9 ± 1.0
pH9, 0.5% GPS	73.0 ± 4.0	44.7 ± 1.6	53.5 ± 1.4
pH9, 1.0% GPS	74.7 ± 1.8	51.0 ± 0.5	56.2 ± 0.5
pH9, 3.0% GPS	72.6 ± 2.0	51.1 ± 1.2	60.1 ± 1.7

pH9

pH7

pH5

pH3

0.5%
GPS

1.0%
GPS

3.0%
GPS

Figure A.1 Survey or wide spectra of the silanised BC surfaces treated with various GPS concentrations and pH solutions.